Radiosurgery
Editors: D. Kondziolka, M. McDermott,
J. Régis, R. Smee, J.C. Flickinger
Vol. 6

Radiosurgery

Editor
Douglas Kondziolka

KARGER

Radiosurgery

Radiosurgery

Vol. 6

KARGER

7th International Stereotactic Radiosurgery Society Meeting,
Brussels, September 11–15, 2005

Radiosurgery

Volume Editor

Douglas Kondziolka *Pittsburgh, Pa.*

99 figures, 24 in color, and 64 tables, 2006

KARGER

Basel · Freiburg · Paris · London · New York ·
Bangalore · Bangkok · Singapore · Tokyo · Sydney

Douglas Kondziolka, MD, MSc, FRCS(C), FACS
Departments of Neurological Surgery and Radiation Oncology
Center for Image-Guided Neurosurgery
UPMC Presbyterian Hospital
University of Pittsburgh
Pittsburgh, Pa., USA

Library of Congress Cataloging-in-Publication Data

International Stereotactic Radiosurgery Society. Meeting (7th : 2005 : Brussels, Belgium)
Radiosurgery / 7th International Stereotactic Radiosurgery Society Meeting, Brussels, September 11-15, 2005 ; volume editor, Douglas Kondziolka.
p. ; cm. – (Radiosurgery ; v. 6)
Includes bibliographical references and indexes.
ISBN 3-8055-8105-X (hard cover : alk. paper)
1. Radiosurgery–Congresses. I. Kondziolka, D. (Douglas), 1961- . II. Title. III. Series.
[DNLM: 1. Radiosurgery–Congresses. WL 368 I605r 2006]
RD594.15.R332 2006
617.4′81059–dc22

2006009471

Bibliographic Indices. This publication is listed in bibliographic services, including Current Contents® and Index Medicus.

www.karger.com
ISSN 1024–2651
ISBN 3–8055–8105–X

Contents

Preface

The International Stereotactic Radiosurgery Society represents a community of colleagues across the world. The 7th meeting of the society was held in Brussels, Belgium under the leadership of meeting chairman Dr. Marc Levivier and scientific program chairman, Dr. Jean Regis. Professor Jacques Brotchi served as the Honorary Chairman. I ended my two-year term as ISRS President. The meeting included attendees and companies from countries across the world. The disciplines of neurosurgery, radiation oncology, medical physics, radiology, oncology, neurology, and engineering provided scientific content across intracranial and extracranial radiosurgery topics. The elegant setting of Brussels, the European capital, provided a forum for collegiality, discussion, and debate. The 2007 meeting will be held in San Francisco, California.

This sixth volume of *Radiosurgery* includes evaluations of benign and malignant tumor radiosurgery, technology assessments, complication management, functional radiosurgery, and extracranial approaches. Radiosurgery and stereotactic fractionated radiotherapy papers were selected for publication by the editorial board. The ISRS remains the only society to embrace all of the different aspects of clinical and research radiosurgery. We remain indebted to our publisher, S. Karger AG, Basel, for their work on this volume and continued support of the society.

Douglas Kondziolka

The Jacob I. Fabrikant Award

ISRS Vice-President Dr. Robert Smee presents the 2005 Jacob Fabrikant Award for long-standing contributions to the field of radiosurgery to Professor Federico Colombo of Italy.

Kondziolka D (ed): Radiosurgery. Basel, Karger, 2006, vol 6, pp 1–11

Arteriovenous Malformation Radiosurgery: Evolution of the Technique

Federico Colombo[a], *Leopoldo Casentini*[a], *Carlo Cavedon*[b], *Joseph Stancanello*[b], *Paolo Francescon*[b], *Francesco Causin*[c], *Vittore Pinna*[c]

Departments of [a]Neurosurgery, [b]Medical Physics, and [c]Neuroradiology, City Hospital, Vicenza, Italy

Abstract

Object: In our department, radiosurgery as been employed for managing arteriovenous malformations (AVMs) since 1984. An original, LINAC based, isocentric, multiple converging arcs technique has been utilized for treating 642 patients until December 2002. Since January 2003, an image-guided robotic radiosurgery apparatus (the Cyberknife) has been utilized in clinical practice. A modification of the treatment planning procedure was developed in order to include angiography in target volume definition. **Technique:** The technique is based on image fusion between CT and 3D rotational angiography. The image fusion procedure employs a mutual information maximization algorithm, the maximization of entropy correlation coefficient, to take into account translation, rotation, linear scaling and angular deformation. **Results:** The new procedure allowed the employ of the Cyberknife in a series of 113 patients affected by AVMs. In large (>10 ml) and spinal AVMs, prescribed radiation dose has been delivered in 2 fractions. One patient suffered for adverse effects due to irradiation. Two bleeding occurrences have been observed so far in treated patients. In small sized (<2.5 ml) AVM (26 patients) one-year complete obliteration rate is 46%. **Conclusions:** In small AVMs the Cyberknife frameless radiosurgery procedure seems to afford the same good results obtained with frame-based isocentric techniques. Since, in large AVMs, target volume dose homogeneity may influence the tendency to bleed, the employ of the new radiosurgery robotic apparatus, with its highly homogeneous irradiation distribution into the target, might decrease the risk of bleeding after radiosurgery.

In Vicenza Neurosurgery Department cerebral arteriovenous malformations (AVMs) radiosurgery was introduced in 1984. A linear accelerator (LINAC)-based, multiple converging arc technique was employed for treating 642 AVM

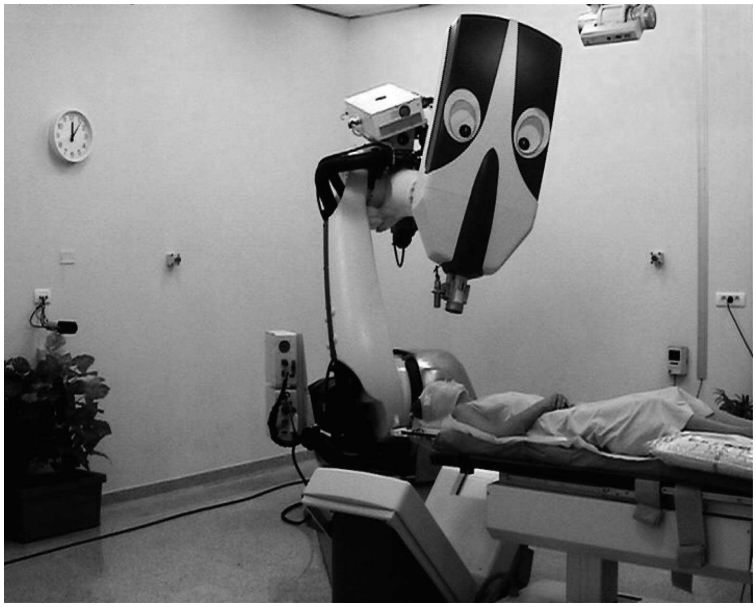

Fig. 1. Radiosurgical procedure with the Cyberknife.

patients with good results [1, 2]. From a statistic evaluation of treated patient population, we found that bleeding recurrence in the latency period – the main shortcoming of AVMs radiosurgery – might be related to poor dose homogeneity inside the nidus of large volume AVMs, a characteristic feature of isocentric procedures [3]. Since January 2003, a frameless, image-guided robotic radiosurgery apparatus, the Cyberknife (Accuray Inc., Sunnyvale, Calif., USA) [4] has been utilized for treating AVMs (fig. 1). This system works with a non-isocentric radiation geometry.

The aim of this paper is to describe the evolution of the AVM radiosurgery technique, to present our early clinical results with the Cyberknife, and to discuss possible advantages connected to the peculiar features of the robotic radiosurgery apparatus.

Prior Data

Our first patient affected by a cerebral AVM was treated on November 1984. Until December 2002, 642 patients were treated with our LINAC-based converging arc technique [1]. Median follow-up in this series is over 120 months.

Out of these patients we were able to perform and/or collect and verify 351 control angiographies undertaken at least 24 months after treatment. Complete obliteration rate was 62% (258 patients). As reported in previous papers, results were strongly influenced by AVM dimensions [1, 2]. If subdivided AVMs in small (S) – less than 15 mm in diameter, medium (M) – between 15 and 25 mm and large (L) – over 25 mm in diameter – total obliteration rate at 24 months follow-up angiography ranged from 96% in small to 33% in large AVMs.

We did not observe any bleeding recurrence after angiographic 'cure'.

As regard to complications, 28 patients suffered from morbidity due to radiation, ranging from mild transitory neurological complaints (14 patients) to permanent disabling ones (hemiparesis, visual field reduction, diencephalic syndrome, trigeminal dysesthesia: 13 patients). One patient developed a radio-induced tumor (pathology: gliosarcoma) in the site of her previous AVM, 13 years after successful treatment and died from it.

The most frequent untoward effects indirectly related to treatment were, however, determined by bleeding occurrences during the latency period before complete obliteration. Forty-eight cerebral hemorrhages were observed. Bleeding took place from 6 days to 48 months after radiosurgery in 43 patients (defined 'latency period', after which re-treatment should be considered). Five patients bled from 48 to 170 months after irradiation. 9 patients died as a consequence of their AVMs rupture (1.4%). Emergency surgery was performed on 9 patients. Fifteen patients suffered from stabilized neurological symptoms (2.3%).

During this long period, significant hardware changes were introduced in the procedure. The first 4 MV LINAC was substituted, after 213 patients, by a 6 MV employed up to 2002. Head frames were initially fixed to the treatment couch while, after 1990, we used a stable, rigid floor mounted stand for head fixation. However, the most important evolution regards the treatment planning system. Stereotactic biplanar angiography was the only morphological database for target determination up to early 1990. Three dimensional data (contrast enhanced CT in stereotactic conditions) were after introduced with an original custom made software (Radioplan). Subsequently we moved to commercially available treatment planning systems for combining stereotactic angiography information with the CT and/or MRI. At the end of our LINAC experience the 3D angiography was implemented to the treatment planning. Originally, the 3D angiography – stereotactic CT image fusion process was iterative and manual, nevertheless, the procedure allowed improved spatial representation of the target with respect to biplanar stereotactic angiography [5]. Notwithstanding these improvements gradually introduced in a 20 years time span, clinical results in terms of total obliteration and complications rate did not change significantly.

Since January 2003, a frameless, image-guided robotic radiosurgery apparatus, the Cyberknife [4] has been utilized in clinical practice. This apparatus recur to a conformal, non-isocentric, irradiation geometry. In its basic conformation, the Cyberknife is unable to implement angiography into the treatment planning system. In order to employ the new technique for AVM, a modification of the treatment planning procedure had to be developed to include angiographic data in target definition.

Materials and Methods

AVMs Radiosurgery Treatment Planning

In a first step contrast-enhanced CT images of the intended target are acquired. The imaging modality that has to be fused to CT is three-dimensional rotational angiography (3DRA). Morphological and functional information are very different from each other.

The maximization of entropy correlation coefficient, a mutual information maximization algorithm [6, 7], is employed to calculate the parameters of a spatial transformation that takes into account rotation, translation, linear scaling and angular deformation. This method allows also precise estimation of registration accuracy [8, 9].

When 3DRA secondary datasets are fused to CT, immediate visualization of anatomy, target outline and critical structures on both modalities is allowed. The image fusion procedure takes 20 min, including pre- and post-processing steps that are required in order to make the datasets readable by the treatment planning system.

Registered data sets can be imported into the Cyberknife treatment planning system for evaluation of the best-suited irradiation procedure (either isocentric or conformal) and for adequate computation of irradiation parameters. The operator can evaluate 3D rendering of isodose surfaces on the preferred modality (fig. 2a–c).

Clinical Experience

Among 500 patients treated with the Cyberknife from January 30, 2003 to August 1, 2005, 113 (55 males and 58 females) were affected by cerebral AVMs and 1 by a spinal AVM.

At treatment, age ranged from 13 to 70 years (mean 36 years). Symptoms of appearance were bleeding in 56, epilepsy in 25, neurological deterioration in 16, headache in 12. In 4 patients the AVM was revealed by examinations made for non-related diseases or trauma.

Before radiosurgery, 4 patient underwent unsuccessful attempts of surgical removal; 57 patients underwent incomplete AVM embolization. Twenty patients were re-treated for patent nidus remnant after a first radiosurgery.

AVM irradiated volume varied from 0.1 ml to 42 ml (mean 4.4 ml). Maximum radiation doses from 23 to 30 Gy (mean 25.2 Gy) were delivered. The borders of target volume were encompassed by isodose surfaces from 70 to 85%.

In cerebral AVMs with target volumes smaller than 10 ml radiation was delivered in single session. In 14 patients with target volumes larger than 10 ml, in 2 patient with brain stem AVMs and in the single patient with a spinal AVM, radiation dose was delivered in 2 fractions, 8–30 days apart.

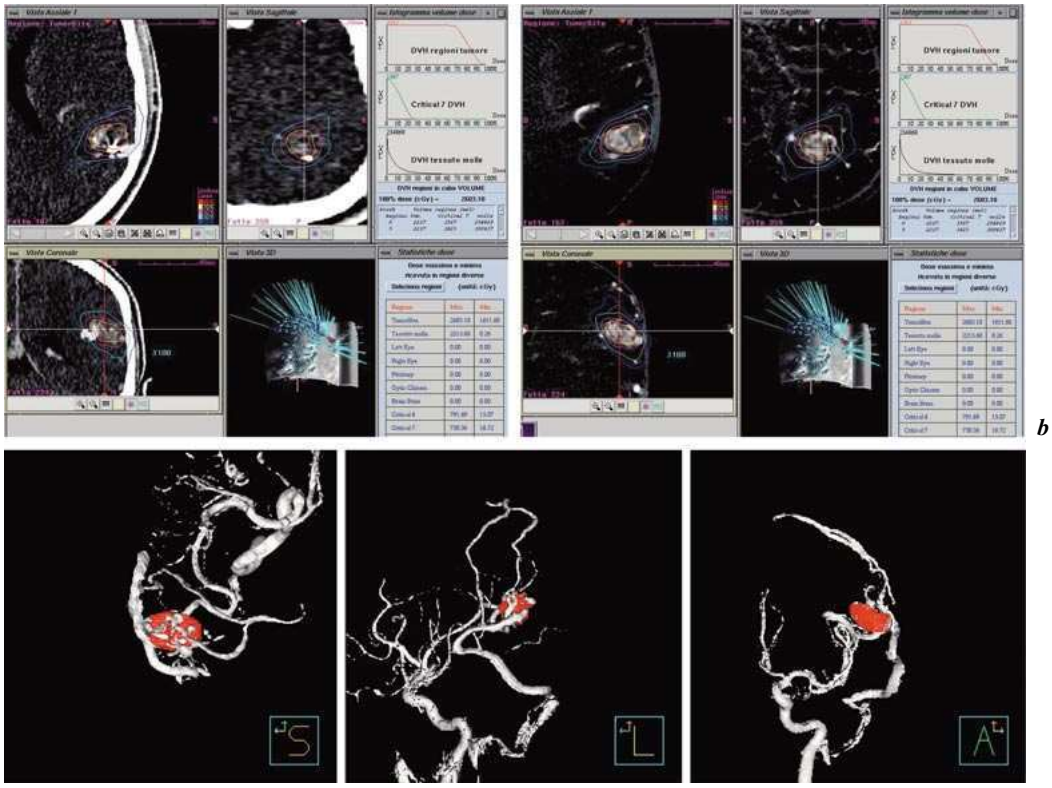

Fig. 2. C.G., 40-years-old male. Epilepsy due to a left temporal AVM fed by middle cerebral branches. Target volume 2.7 ml. Conformal treatment planning, collimator 10 mm, 26 Gy Dmax. ***a*** Treatment planning on Cyberknife console, displaying isodoses lines on a CT, (***b***) 3DRA on axial, sagittal and frontal plane and (***c***) 3DRA reconstructed images, showing the AVM nidus, treatment target volume, covered by 70% isodose surface.

Results

Follow-up ranged from 1 to 26 months. Up to date (July 2005) clinical data are available for 110 out of 113 patients. One patient suffered from a transient complication after irradiation, requiring temporary corticosteroid medication (fig. 3a, b). Two bleeding recurrences were observed and one patient died from it.

Follow-up is too short for evaluation of success rate in terms of AVM complete obliteration. However, 14 of 26 patients with small to medium size (<2.5 ml) AVMs and follow-up longer than one year underwent MR angiography that suggested complete or subtotal obliteration. In these patients control angiography confirmed complete obliteration of the malformation in 12 out of 14

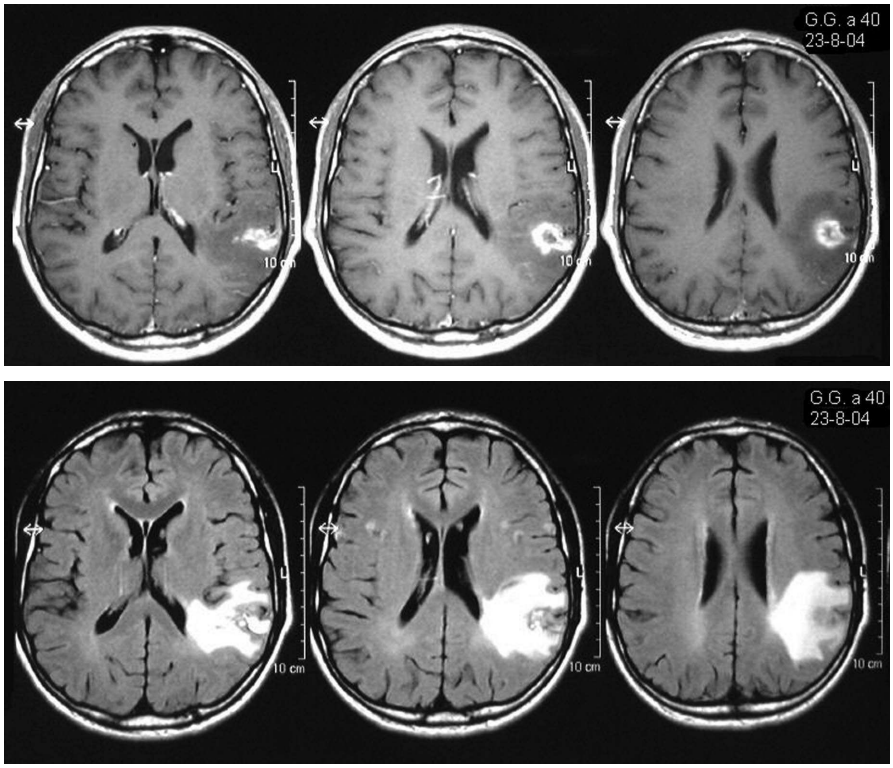

a

b

Fig. 3. ***a***, ***b*** Same patient of figure 2. Eight months after radiosurgery. Dysphasia and difficulty with calculation. MRI imaging showing contrast enhanced area, surrounded by edema. Clinical picture normalized after 15 days corticoid medication.

(in 2 persisted very tiny AVM remnants, to be verified at later follow-up). One-year complete obliteration rate is 46% (fig. 4a–d).

In all patients treatment planning was performed with the aid of 3D reconstruction of the AVM nidus based on angiographic data. In 47 patients the target volume originally defined on CT was significantly modified (≥20%) after the introduction of angiographic data, usually in the direction of target volume reduction.

The Cyberknife treatment planning system has the possibility to simulate different beam geometries, isocentric or non-isocentric. Dose distribution with the isocentric technique is similar to that obtained in more conventional radiosurgery approaches, such as the LINAC-based procedure we employed until

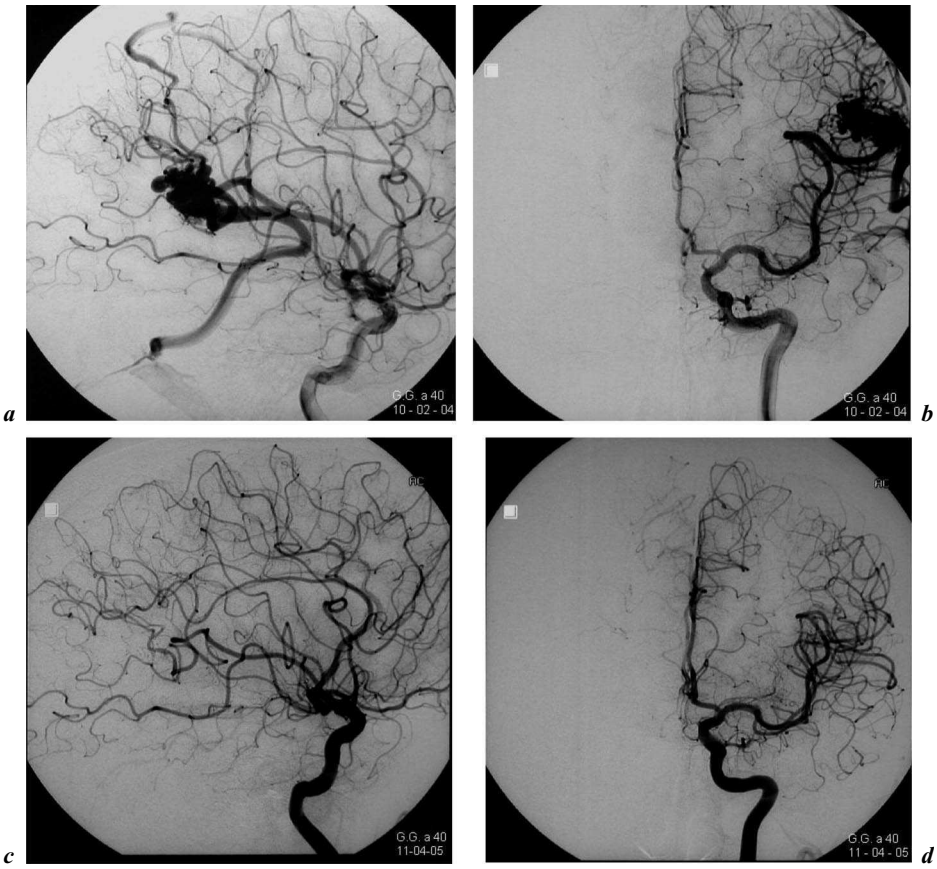

Fig. 4. Same patient of figures 2 and 3. Follow-up angiography (***a***, ***b***) before and (***c***, ***d***) 15 months after treatment, showing complete obliteration.

2003. We compared these two different solutions in 5 patients with large (>10 ml) and/or irregular AVMs. Target volume was delineated first; treatment-planning options – same dose prescription to the same target volume – were then studied employing (a) multiple isocenters (from two to four) and (b) non-isocentric inverse planning. Results were evaluated in terms of standard radiobiological indicators for quality assurance in radiosurgery, conformity and homogeneity indexes [10]. Results are shown in table 1. They seem to suggest that, at least in 3D irregular niduses, an higher dose homogeneity (lower homogeneity indexes) can be attained into the target volume with the conformal, non-isocentric approach.

Table 1. Comparison between treatment plans of 5 AVMs with the Cyberknife in conformal shape and multiple isocenters modality in terms of dosimetric indexes

Patient	Target volume cc	Maximum dose, Gy	Modality of treatment	Mean dose, %	Minimum dose, %	Volume of the target receiving dose ≥ 70%	Homogeneity index	Conformity index
1	1.23	27	Conformal	83.8	56	92.3	1.79	1.82
			3 isocenters	79.0	51	84.3	1.96	2.31
			2 isocenters	73.9	41	71.9	2.44	2.77
2	9.74	25	Conformal	79.9	35	88.7	2.86	4.45
			4 isocenters	78.4	24	79.1	4.17	5.57
3	6.83	25	Conformal	84.5	50	96.7	2.00	2.40
			3 isocenters	75.4	34	73.6	2.94	4.06
4	5.28	27	Conformal	76.7	42	76.2	2.44	2.41
			3 isocenters	76.5	26	73.8	3.85	5.29
5	6.37	25	Conformal	10.5	54	98.0	1.85	2.17
			2 isocenters	9.3	31	69.7	3.23	1.70

Homogeneity and conformity indexes are calculated following Shaw et al. [10].

Discussion

Image Fusion Procedure

Angiographic data are necessary for adequate AVM radiosurgery treatment planning. We recur to an image fusion to implement 3D angiography into Cyberknife treatment planning. Image fusion is a technique that combines complementary information from two separate imaging modalities into a single imaging study [9, 11]. Most image fusion techniques are completely automatic, based on chamfer matching [9, 12].

The first iterative and manual image fusion we introduced in 2002 already allowed improved spatial representation of the target with respect to biplanar stereotactic angiography [5]. The main advantage of utilizing 3DRA for treatment planning is the possibility to reconstruct three-dimensionally not only the target volume but also any selected isodose surface, and to verify it immediately by moving the viewpoint at operator's choice. Isodoses reconstruction affords an immediate check of the adequacy of the treatment planning to spare nearby critical structures. In the present experience, modifications induced by critical evaluation of angiographic data were mostly in the direction of a decrease of target volume. A possible explanation is that 3DRA permit better discrimination between nidus shunt vessels and large draining veins, often obscuring the target outline.

With regard to clinical validation, follow-up is too short to allow any definitive conclusion about the efficacy of AVMs Cyberknife radiosurgery in general: nevertheless early successful results obtained in small AVM – the only ones that could be verified in this short time span – confirm the high spatial accuracy afforded by the procedure.

Risk of Bleeding in Relation to Radiosurgery Treatment Planning

Hemorrhages in the latency period before effective obliteration represents the main drawback in AVMs radiosurgery. Risk of bleeding in treated patients still represents a subject of strong debate. Frequency of bleedings after radiosurgery has been evaluated and found to be equal [13–16], inferior [17–19] or – at least in particular situations – superior [2, 3] to natural history of untreated AVMs.

We studied bleeding risk after radiosurgery on our series of 565 patients affected by cerebral AVMs [3]. Patients were considered at risk of hemorrhage from irradiation to the time of obliteration estimated as the midpoint between the last radiological evidence of AVM flow and the first evidence of complete obliteration or to the time of last evidence of AVM flow where complete obliteration was not attained. Poisson regression was used to estimate hemorrhage rates per 100 person-years of follow-up. A commercially available software package was used to compute the influence of different variables with respect to a baseline bleeding risk – considered 2 per 100 person years – with 95% confidence intervals. Variables related to a significant higher bleeding risk in the latency period were dose homogeneity into target volume ($p < 0.05$) and – less important, $p \approx 0.05$ – target volume.

Our data suggest that in patients treated with partial volume irradiation (poor dose homogeneity) radiosurgical treatment might induce an increased tendency to bleed before complete obliteration is attained. In these cases part of the AVM absorbs a radiation dose below optimal. This part is more likely to remain unobstructed when the part fully irradiated is already obliterated. Toward unobstructed portion a blood stream rerouting can be suspected. Spetzler states that risk of hemorrhage increases with the partial embolization of large AVMs [20]: a similar effect could be expected in cases of incomplete obliteration obtained by radiosurgery [2, 3]. Han confirmed this prediction in a publication dealing with grades IV and V AVMs: an increase of annual risk of hemorrhage from 1 to 10.4% was reported in 14 patients who had undergone partial treatment (5 of them with radiosurgery) [21]. According to these observations, Miyamoto et al. [22] found an annual risk of hemorrhages of 14.6% in 46 patients who underwent palliative treatments of AVMs: 24 of these patients – 19 grades IV and V – were treated by radiosurgery. Most of these patients harbored large (over 3 cm diameter) AVMs. In the meanwhile this point of view has been confirmed by other authors [18, 23, 24].

The hypothesis that an increase of bleeding risk can be related to a non-homogeneous dose distribution inside the AVM nidus leaded a shift in our irradiation strategy for large volume AVMs in which the Cyberknife played an important role. We started to use routinely the homogeneity index and conformality index [10], with the aim of improving treatment planning in large AVMs. We tried to achieve the highest dose homogeneity by avoiding partial volume – high dose irradiation and to deliver to the whole malformation a uniform radiation dose, recurring to dose fractionation schedules for improving healthy tissues radiation tolerance, a critical feature when dealing with large target volumes. This double-edged strategy – highest dose homogeneity, dose fractionation – has been made possible by the introduction of the Cyberknife.

Conclusion

We have described early results obtained in AVMs radiosurgery with the Cyberknife. Since, in large and/or irregular AVMs, according to our 20 years LINAC experience, target volume dose homogeneity may influence the tendency to bleed, the employ of the new radiosurgery robotic apparatus – with its peculiar capabilities of non-isocentric irradiation geometry with homogeneous dose distribution – might decrease the risk of bleeding in the latency period. With respect to frame-based radiosurgery techniques, the Cyberknife has the possibility to exploit fractionated regimens, allowing safe radiosurgery also in large volume AVMs.

References

1 Colombo F, Benedetti A, Pozza F, Marchetti C, Chierego G: Linear accelerator radiosurgery of cerebral arteriovenous malformations. Neurosurgery 1989;24:833–844.

2 Colombo F, Pozza F, Chierego G, Casentini L, De Luca GP, Francescon P: Linear accelerator radiosurgery of cerebral arteriovenous malformations: an update. Neurosurgery 1994;34:14–21.

3 Colombo F: Linear accelerator radiosurgery of arteriovenous malformations: Vicenza experience; in Smee R (ed): Proceedings of the 4th Congress of International Stereotactic Radiosurgery Society. The Price of Wales Hospital Press, Sidney, 1999, p 47 (abs).

4 Adler JR, Murphy MJ, Chang SD, Hancock SL: Image-guided robotic radiosurgery. Neurosurgery 1999;44:1299–1307.

5 Colombo F, Cavedon C, Francescon P, Casentini L, Fornezza U, Castellan L, Causin F, Perini S: Three-dimensional angiography for radiosurgical treatment planning for arteriovenous malformations. J Neurosurg 2003;98:536–543.

6 Maes F, Collignon A, Vandermeulen D, Marchal G, Suetens P: Multimodality image registration by maximization of mutual information. IEEE Trans Med Imaging 1997;16:187–198.

7 Meeks SL, Bova FJ, Friedman WA: Technical aspects of radiation physics; in Gildenberg PL, Tasker RR (eds): Textbook of Stereotactic and Functional Neurosurgery. New York, McGraw-Hill, 1998, pp 649–668.

8 Stancanello J, Cavedon C, Francescon P, Cerveri P, Ferrigno G, Colombo F, Perini S: Development and validation of a CT-3D rotational angiography registration method for AVM radiosurgery. Med Phys 2004;31:1363–1371.
9 Van Herk M, de Munck JC, Lebesque JV, Muller S, Rasch C, Touw A: Automatic registration of pelvic tomography data and magnetic resonance scans including a full circle method for quantitative accuracy evaluation. Med Phys 1998;25:2054–2066.
10 Shaw E, Kline R, Gillin M, Souhami L, Hirschfeld A, Dinapoli R, Martin L: Radiation therapy oncology group: radiosurgery quality assurance guidelines. Int J Radiat Oncol Biol Phys 1993;27: 1231–1239.
11 Holupta EJ, Kooy HM: A geometrical algorithm for medical image correlations. Med Phys 1992;19:433–438.
12 Alexander E, Kooy HM, Van Herk M, Schwartz M, Schwartz M, Barnes PD, Tarbell N, Mulkern RV, Holupta EJ, Loeffler JS: Magnetic resonance image directed stereotactic neurosurgery: use of image fusion with computerized tomography to enhance spatial accuracy. J Neurosurg 1995;83: 271–276.
13 Friedman WA, Blatt DL, Bova FJ, Blatt JM, Mendenhall WM, Kubilis PS: The risk of hemorrhage after radiosurgery for arteriovenous malformations. J Neurosurg 1996;84:912–919.
14 Pollock BE, Flickinger JC, Lunsford LD, Bissonette DJ, Kondziolka D: Hemorrhage risk after stereotactic radiosurgery of cerebral arteriovenous malformations. Neurosurgery 1996;38:652–661.
15 Steiner L, Lindquist C, Adler JR, Torner JC, Alves W, Steiner M: Clinical outcome of radiosurgery for cerebral arteriovenous malformations J Neurosurg 1992;77:1–8.
16 Steiner L, Prasad D, Lindquist C, Steiner M: Clinical aspects of gamma knife stereotactic radiosurgery; in Gildenberg PL, Tasker RR (eds): Textbook of Stereotactic and Functional Neurosurgery. New York, McGraw-Hill, 1998, pp 763–803.
17 Karlsson B, Lindquist C, Steiner L: Effect of gamma knife surgery on the risk of rupture prior to AVM obliteration. Minim Invasive Neurosurg 1996;39:21–27.
18 Karlsson B, Lax I, Soderman M: Risk of hemorrhage during the 2-year latency period following gamma knife radiosurgery for arteriovenous malformations. Int J Radiat Oncol Biol Phys 2001;49:1045–1051.
19 Kjellberg RN: Proton beam therapy for arteriovenous malformations of the brain; in Schmideck HH, Sweet WH (eds): Operative Neurosurgical Techniques. New York, Grune & Stratton, 1988, pp 911–915.
20 Spetzler RF, Hargraves RW, McCormick PW, Zabramski JM, Flom RA, Zimmerman RS: Relationship of perfusion pressure and size and risk of hemorrhage from arteriovenous malformations. J Neurosurg 1992;76:918–923.
21 Han PP, Ponce FA, Spetzler RF: Intention to treat analysis of Spetzler-Martin grades IV and V arteriovenous malformations: natural history and treatment paradigm. J Neurosurg 2003;98:3–7.
22 Miyamoto S, Hashimoto N, Nagata I, Nozaki K, Morimoto M, Taki W, Kikuchi H: Posttreatment sequelae of palliatively treated cerebral arteriovenous malformations. Neurosurgery 2000;46: 589–593.
23 Friedman WA, Bova FJ, Bollampally S, Bradshaw P: Analysis of factors predictive of success or complications in arteriovenous malformations radiosurgery. Neurosurgery 2003;52:296–308.
24 Nataf F, Moussa R, Merienne I, Ghossoub M, Schlienger M: Hémorragie après radiochirurgie des malformations artério-veineuses cérébrales [in French]. Neurochirurgie 2001;47:336–343.

Federico Colombo
Divisione di Neurochirurgia, Ospedale Civile
viale Rodolfi 37
IT–36100 Vicenza (Italy)
Tel. +39 0444 993826, Fax +39 0444 927590
E-Mail federico.colombo@ulssvicenza.it

Kondziolka D (ed): Radiosurgery. Basel, Karger, 2006, vol 6, pp 12–25

Quality Assurance in Stereotactic Imaging using the Known Target Point Method

Stefan G. Scheib[a], *Stefano Gianolini*[a], *Nicoletta Lomax*[a], *Andreas Mack*[b]

[a]Klinik Im Park, Department of Medical Radiation Physics, Zürich, Switzerland;
[b]Gamma Knife Centre Frankfurt, Frankfurt, Germany

Abstract

A high degree of geometrical accuracy is of utmost importance in stereotactic treatment modalities. Because of possible image distortions in stereotactic imaging, dedicated quality assurance procedures, based on the known target point method, have been introduced. Three different phantoms with known target points have been designed to determine the geometrical accuracy of stereotactic imaging modalities. Two phantoms are made of 8 PMMA plates, which fit into the stereotactic frame and are imaged together with the appropriate fiducial marker box. The CT/DSA phantom holds 45 steel spheres (diameter = 1 mm), the MR phantom 21 three-dimensional cross hairs, positioned at known coordinates with a precision better than 0.1 mm. The third phantom is a water filled cylinder (outer diameter = 17.5 cm, height = 13.5 cm) with 145 embedded rods of 1 mm in diameter and 10 mm distance. After imaging, data import into the treatment planning system and stereotactic coordinate transformation, the coordinates of the visible markers are determined and compared with the known ones. Additionally, calculated image studies for each phantom have been generated in order to get a quick overview using the image fusion option of the treatment planning system. The mean (max) value of the determined deviation in MR images tested here, is between 0.67 (1.18) and 1.04 (1.91) mm. Usually CT images are not susceptible to image distortions and the maximal deviation is less than 0.6 mm. A maximum deviation of 2.8 mm was found in image intensifier based angiographic images. Special attention must be paid to the geometrical accuracy of stereotactic imaging modalities. Using the commercially available phantoms described here, facilitates this task considerably. However, patient related artefacts, leading to geometrical targeting uncertainties, cannot be monitored using this method.

In stereotactic radiosurgery (SRS) small (volume typically less than 25 cm^3) and clearly circumscribed, lesions are treated using highly conformal three-dimensional (3D) dose distributions applied with a high degree of geometrical accuracy [1, 2]. The irradiation techniques used, usually produce small fields (full width at half maximum – FWHM – down to 4 mm) and steep dose gradients (up to 40% per mm), thus dedicated quality assurance protocols must be available in order to guarantee an accurate treatment in terms of target and dose localization, dose conformity and absolute dose. In the literature several publications can be found addressing these issues [3–9].

One of the prerequisites for SRS, independent of the irradiation technique used, is the precise, 3D localization of anatomical structures (within the brain) using diagnostic imaging modalities such as computed tomography (CT), magnetic resonance imaging (MR) and angiography (Angio). It is well known and documented in the literature that geometrical uncertainties and/or systematic image distortions in stereotactic MR and image intensifier based angiographic images of up to 5 mm and even more have been observed [10–21]. Quality assurance in stereotactic imaging is, therefore, of utmost importance and is also clearly addressed in published recommendations concerning SRS [3–5]. Uncertainties introduced in this stage of the radiosurgical or neurosurgical treatment cannot be compensated for by subsequent treatment steps [1].

The aim of this study was to set up a quality assurance procedure for stereotactic imaging modalities using the so called known target point method [4] which is able to determine the geometrical accuracy of the imaging modalities used. Analyses of the quantitative results will help to optimize image acquisition parameters in order to decrease the target localization error as much as possible while taking into account the diagnostic quality of the images used for treatment planning. Additionally, the image data transfer, the stereotactic coordinate transformation and image fusion implemented in the treatment planning system (TPS) is being checked simultaneously. The known target point phantoms fulfil the demands of the recently published German DIN-6875–1 [3] which covers acceptance tests for intracranial stereotactic radiation treatments using linear accelerators and gamma knifes.

Materials and Methods

The known target point method applied at our site enables the geometrical localization accuracy of MR, CT and Angio images to be determined. For this purpose we have developed two different phantoms. Each phantom, which fits exactly into the stereotactic frame is made of 8 lucite plates ($20 \times 18 \times 1.5\,cm^3$) and is imaged together with the appropriate fiducial marker box in the typical patient set up using the same imaging protocols for patients undergoing the stereotactic procedure. The 8 lucite plates are aligned with the help of two adjustment

Fig. 1. Known target point phantom used in MR imaging, consisting of 8 lucite plates with 21 imbedded 3D cross hairs, mounted in the stereotactic Leksell frame.

pins and kept together with two plastic screws. The phantoms are screwed into the stereotactic frame and the geometrical alignment is based on the fit of the base plate into the stereotactic frame (see figs. 1, 3). Together with the tight mechanical tolerances for the known target points, this set-up guarantees a mechanical overall precision of less than 0.1 mm.

The MR phantom holds 21 3D cross hairs at known target positions distributed throughout the whole stereotactic space, including in particular the peripheral region, which is most susceptible to geometrical uncertainties due to inhomogeneities in the base magnetic field. Each cross hair ($32 \times 23 \times 24$ mm) consist of 5 individual glass vials (outer diameter = 3 mm, inner diameter = 2 mm) filled with a copper sulfate solution and positioned with its center at a known stereotactic coordinate. The 5 glass vials which form a single 3D cross hair are 23, 14 and 7 mm long. In figure 1, the MR phantom mounted in the stereotactic Leksell frame is shown. Figure 2 shows a close up of the MR phantom showing the cross hairs in the superior region of the phantom. Also the recesses ($40 \times 40 \times 1$ mm) parallel with the base plane of the frame, in which radiochromic films can be placed for testing the dose localization accuracy, can be seen.

The CT/Angio phantom holds 45 steel spheres of 1 mm in diameter positioned at known coordinates, again distributed throughout the whole stereotactic space. Figure 3 shows this phantom mounted in the stereotactic Leksell frame. Due to the one-to-one positioning of

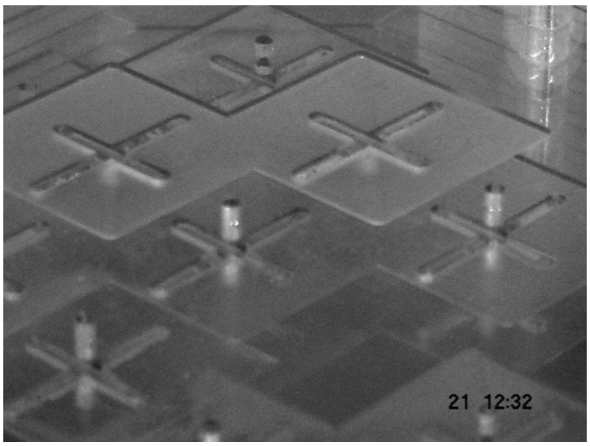

2

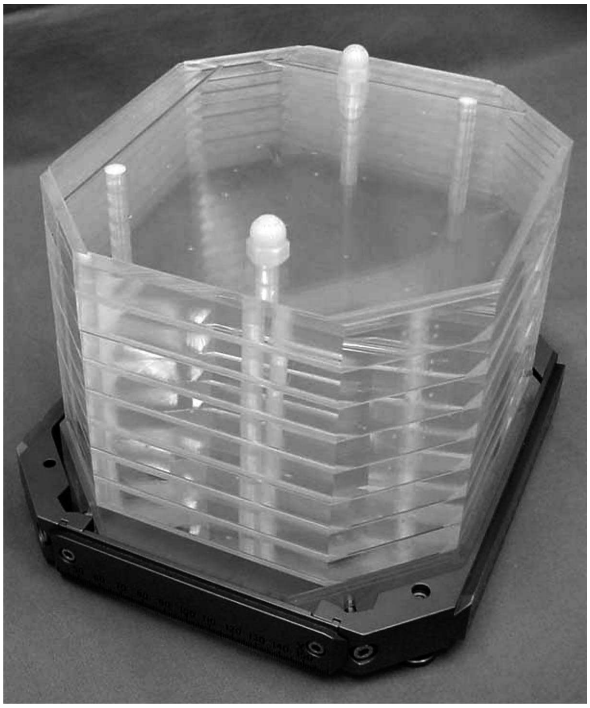

3

Fig. 2. Close up of upper region of the MR phantom indicating the 3D cross hairs ($32 \times 23 \times 24$ mm) made of glass vials (outer diameter = 3 mm, inner diameter = 2 mm) and filled with copper sulfate solution. The recesses, in which radiochromic films could be placed for dose localization measurements, are also visible.

Fig. 3. Known target point phantom used in CT and angiographic imaging, consisting of 8 lucite plates with 45 imbedded steel spheres (1 mm in diameter), mounted in the stereotactic Leksell frame.

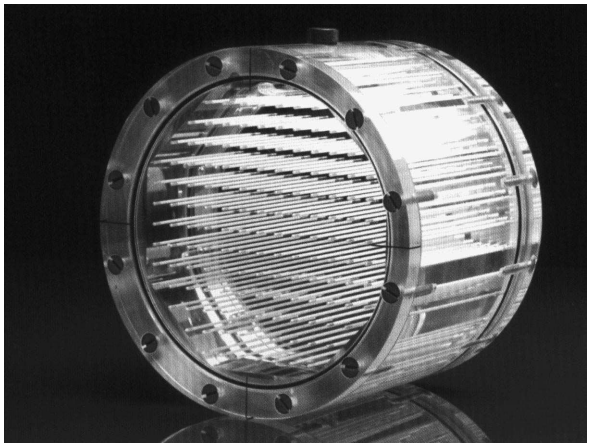

Fig. 4. Cylindrical rod phantom (outer diameter = 17.5 cm, height = 13.5 cm) with 145 embedded rods (1 mm in diameter). The rods are located on a 2D grid with a grid constant of 10 mm. With the help of a dedicated adapter, the central rod can be positioned at a known coordinate in planes parallel to the stereotactic frame.

the steel spheres, the stereotactic coordinates of each sphere visible in ap and lateral X-ray projection images can be unambiguously defined.

Figure 4 shows a complementary phantom which is made of a water filled cylinder (outer diameter = 17.5 cm, height = 13.5 cm) with 145 embedded rods of 1 mm in diameter. The rod spacing is 10 mm and with the help of a dedicated adapter, the central rod of the phantom can be positioned in the center of planes parallel to the stereotactic frame. In contrast to the phantoms shown in figures 1 and 3 this phantom is highly sensitive to systematic image distortions like pincushion distortions in MRI.

For phantom imaging the same imaging protocols are used as for stereotactic patients. For MR imaging a GE Signa 1.5T Echospeed LFX, for CT imaging a GE Lightspeed plus with four detector rings and for angiography a Siemens, HICOR system was used. After imaging, the data are imported into the TPS (Leksell GammaPlan® release 5.32), where the images are being stereotactically defined. As a result of this stereotactic definition a mean and maximal fiducial error is given, which is calculated by the TPS based on a fit of the fiducial marker positions found in each image of the study. Then the images are displayed and the known target positions are found with the help of the TPS, by positioning the cursor's cross hair in the axial, sagittal and coronal views at each of the glass cross hair, steel sphere or rod position. This is illustrated in figure 5 showing a snapshot of the screen layout for a MRI study and the 3D cross hair phantom. The measured stereotactic coordinate is displayed at the top right corner of the screen and is manually transferred to a spread sheet (see table 1). In order to check the image fusion algorithm and to get a quick overview, a calculated image study, showing the known target points, is imported into the TPS and fused with the measured MRI study. Figure 6 shows an axial, coronal and sagittal view of the fused images for a single 3D cross hair. The target point in the calculated image study is visualized by the bright voxels in figure 6.

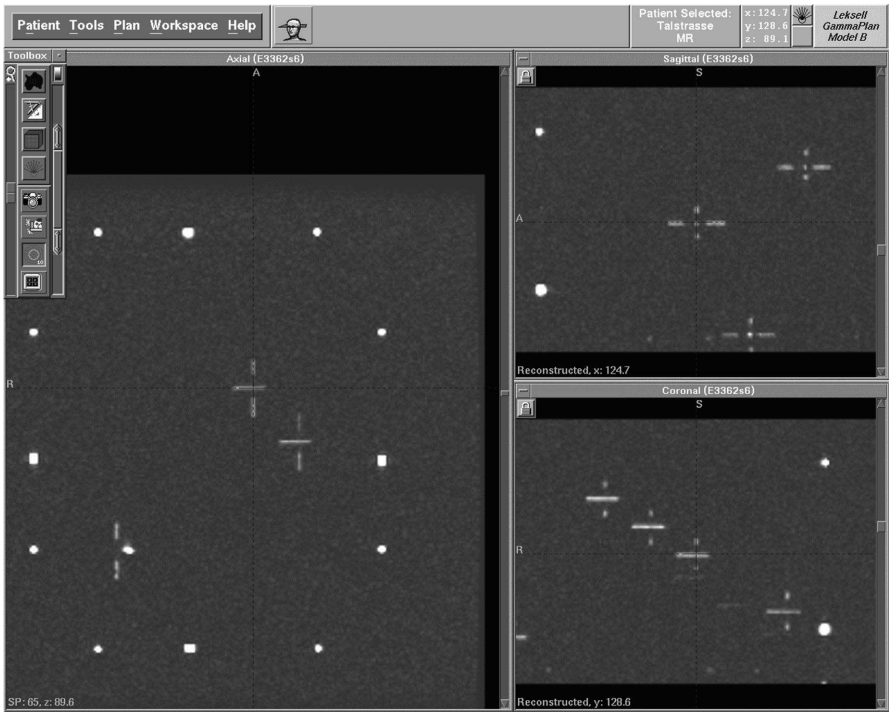

Fig. 5. Screenshot of the treatment planning software (Leksell GammaPlan® – LGP release 5.32) showing an axial (left), sagittal (right top) and coronal (right bottom) view of the stereotactic MR images of the known MR target point phantom. The cross hair provided by the TPS is positioned on one of the glass cross hairs, resulting in a measured stereotactic coordinate (x, y, z) displayed in the top right corner of the screen.

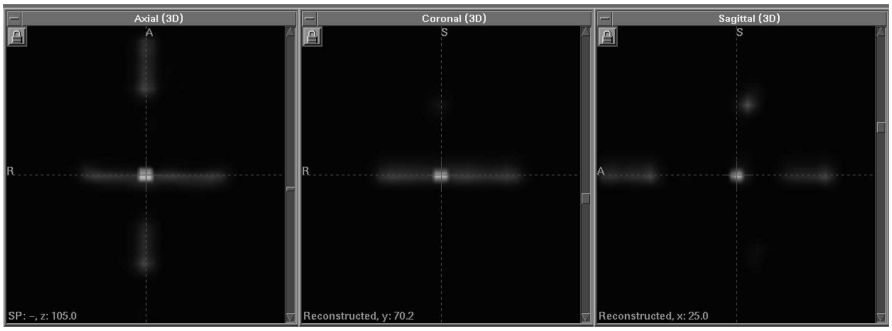

Fig. 6. Axial, coronal and sagittal view of a single 3D cross hair. The images displayed are fused images of the measured MRI study and the calculated image study representing the known target points (bright voxel in the center of the images).

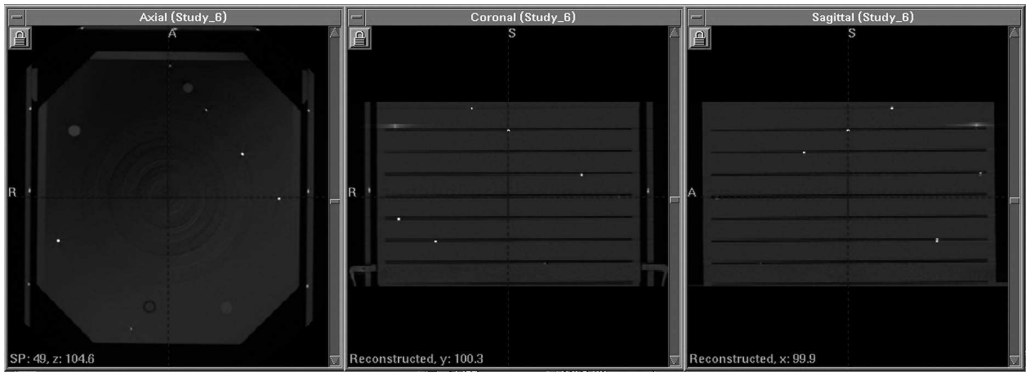

Fig. 7. Axial, coronal and sagittal view of stereotactic CT images of the known CT/Angio target point phantom. The steel spheres are clearly visible and the stereotactic coordinates can be determined by identifying each steel sphere with the cross hair provided by the TPS.

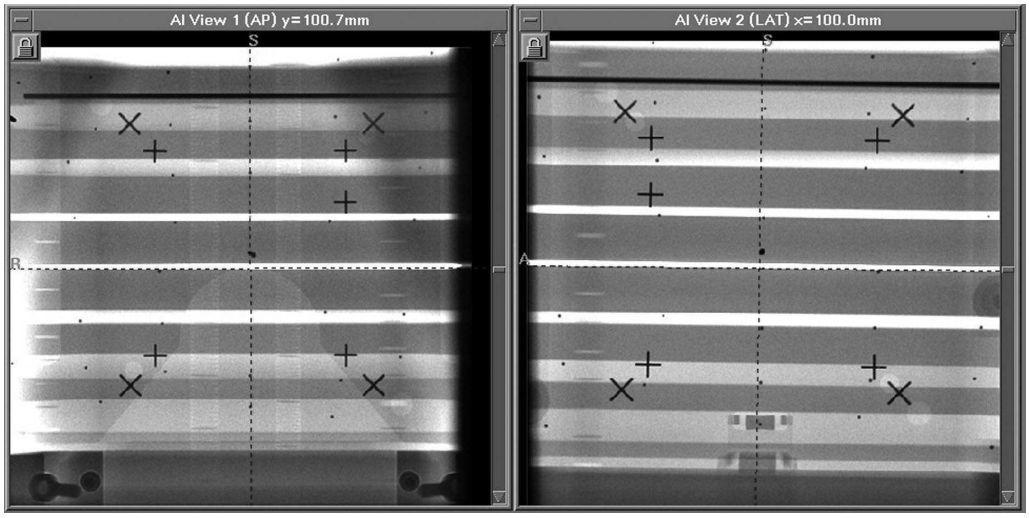

Fig. 8. Lateral (left) and ap (right) view of X-ray images taken of the known CT/Angio target point phantom together with the fiducial box using an image intensifier based angiography unit. The stereotactic coordinates of the steel spheres can be unambiguously identified in both projection images due to their one-to-one positioning.

Figure 7 shows an axial, sagittal and coronal view of a CT data set for the corresponding phantom. Again the cursor position is set to the visible steel sphere and the corresponding measured coordinate is read off. As for the 3D cross hair phantom the corresponding calculated image study can be fused to the acquired image study for a quick

Table 1. Data analyses spread sheet for the MR phantom

Marker number	Target coordinates			Measured coordinates			Absolute errors				Distance
	x/mm	y/mm	z/mm	x/mm	y/mm	z/mm	dx/mm	dy/mm	dz/mm	dr/mm	D/mm
1	100.0	70.0	45.0	100.3	68.9	44.7	0.3	1.1	0.3	1.18	62.6
2	75.0	100.0	45.0	75.4	98.9	44.9	0.4	1.1	0.1	1.17	60.4
3	150.0	40.0	60.0	150.3	39.5	59.2	0.3	0.5	0.8	0.99	87.7
4	125.0	70.0	60.0	125.3	69.0	59.5	0.3	1.0	0.5	1.16	55.9
5	100.0	100.0	60.0	100.0	99.5	59.7	0.0	0.5	0.3	0.58	40.0
6	75.0	130.0	60.0	75.2	130.7	59.6	0.2	0.7	0.4	0.83	55.9
7	50.0	160.0	60.0	50.0	159.2	60.1	0.0	0.8	0.1	0.81	87.7
8	100.0	130.0	75.0	100.1	129.6	75.0	0.1	0.4	0.0	0.41	39.1
9	50.0	40.0	90.0	50.0	39.5	89.8	0.0	0.5	0.2	0.54	78.7
10	150.0	100.0	90.0	150.3	99.3	89.7	0.3	0.7	0.3	0.82	51.0
11	125.0	130.0	90.0	125.1	129.6	90.0	0.1	0.4	0.0	0.41	40.3
12	25.0	70.0	105.0	25.3	69.6	104.7	0.3	0.4	0.3	0.58	80.9
13	175.0	130.0	120.0	175.1	129.8	119.8	0.1	0.2	0.2	0.30	83.2
14	150.0	160.0	120.0	150.0	159.8	120.0	0.0	0.2	0.0	0.20	80.6
15	100.0	40.0	135.0	100.2	39.7	134.7	0.2	0.3	0.3	0.47	69.5
16	75.0	70.0	135.0	75.3	69.6	134.8	0.3	0.4	0.2	0.54	52.4
17	50.0	100.0	135.0	50.1	99.6	134.5	0.1	0.4	0.5	0.65	61.0
18	25.0	130.0	135.0	25.0	129.4	134.7	0.0	0.6	0.3	0.67	88.0
19	175.0	70.0	150.0	175.1	69.5	149.8	0.1	0.5	0.2	0.55	95.0
20	125.0	100.0	150.0	124.9	99.7	149.4	0.1	0.3	0.6	0.68	55.9
21	100.0	160.0	150.0	99.6	160.2	149.6	0.4	0.2	0.4	0.60	78.1

For all 21 known 3D cross hair positions (target coordinates) the measured positions (measured coordinates) are used to calculate the absolute errors in x, y and z-direction and the resultant distance dr between the known and measured target point (absolute errors). In the last column the distance of the known target point from the center of the phantom is calculated.

overview. In figure 8 a lateral (left) and an ap view (right) using an image intensifier angiography unit of the CT/Angio phantom is shown. Again, by positioning the cursor on a visible steel sphere in the ap and lateral image the target coordinate can be unambiguously defined.

Figure 9 shows a MR image of the rod phantom, the corresponding calculated image and the fused image using the TPS. The image fusion allows to quickly examine the whole MR study because systematic image deviations like pin cushion distortions can easily be recognized in fused images. For quantitative analyses of deviations between imaged and real rod positions a dedicated analyses software can be used [22–24].

Table 1 shows an example spread sheet for the 3D cross hair MR phantom. For all 21 known target coordinates the x, y and z values are given. Each measured target point is

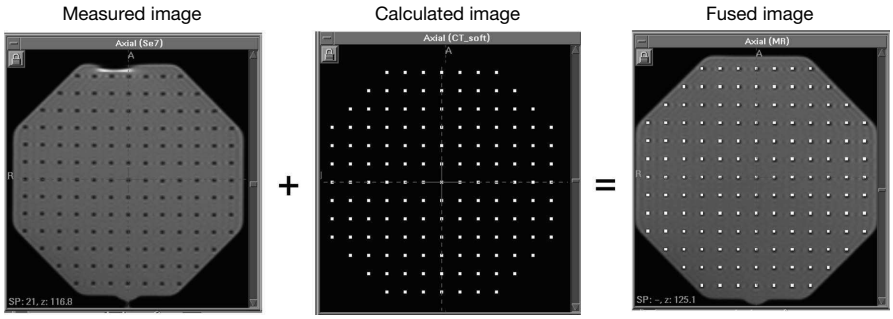

Fig. 9. Qualitative analyses of MR image distortions using the cylindrical rod phantom and the image fusion with the corresponding calculated image.

copied from the TPS with its x, y and z value to the corresponding line and columns and the absolute errors dx, dy, dz and dr are calculated. In the last column of the spread sheet the distance of the target coordinate from the central position, which in Leksell coordinates is $x = y = z = 100.0$ mm is given. The mean absolute error and the standard deviation is calculated based on the 21 individual measurements (see table 1) and shown together with the minimal and maximal error in table 2. These values are compared to the mean and maximal fiducial errors given by the TPS shown in table 2.

Results

Depending on the MR imaging protocol applied, increased deviations between measured and known coordinates are found near the stereotactic frame. This is also recognized by the maximal fiducial error found in the stereotactic image definition, which is always found in the slice next to the frame and rapidly decreases for superior slices. For example axial T2-weighted 3D fast spin echo images with an image resolution of 512×256 pixel and a slice thickness of 1 mm show a mean error of 0.67 ± 0.28 mm and a maximal error of 1.18 mm. These values are compared to a mean error of 1.04 ± 0.51 mm and a maximal error of 1.91 mm for an axial T1-weighted 2D fast spin echo sequence with an image resolution of 256×256 pixel and a slice thickness of 2 mm. Comparing these results with the mean fiducial errors given by the TPS (0.3 and 0.4 mm) it can be seen that the mean absolute error found is approximately twice the mean fiducial error.

In order to more systematically analyze potentially existent image distortions in MRI the cylindrical rod phantom can be used. In figure 10 two MRI studies using axial T1-weighted 2D fast spin echo sequences but different

Table 2. For each image study analyses the mean and maximal fiducial error noted by the TPS is compared to the minimal, maximal and mean (± standard deviation) error of table 1 derived from the measured target points

	Absolute errors			
	dx/mm	dy/mm	dz/mm	dr/mm
Mean absolute error	0.2	0.5	0.3	0.67
Standard deviation	0.1	0.3	0.2	0.28
Minimal error	0.0	0.2	0.0	0.20
Maximal error	0.4	1.1	0.8	1.18
	Fiducial errors (mm)			
Mean	0.3			
Max	1.3			

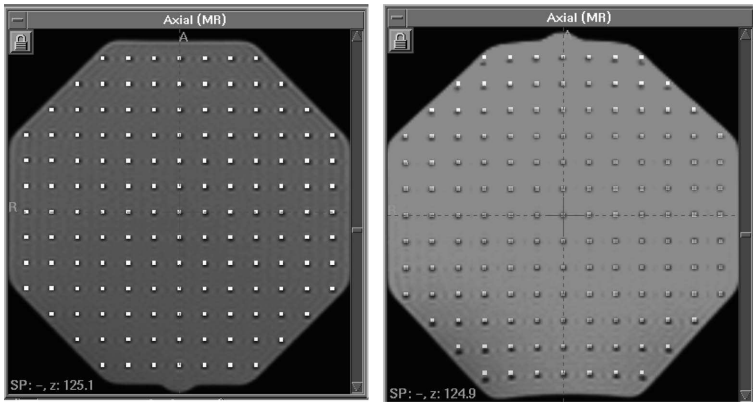

Fig. 10. Qualitative analyses of pin cushion distortions in MR images using image fusion and the cylindrical rod phantom. The right image taken with a rather old MR scanner shows systematic deviations of the imaged rods (dark dots) from the real rod positions (bright dots) in the upper and lower part of the image in contrast to the left image, where almost no pin cushion distortion is recognized.

MR-scanners are shown. Due to the limited homogeneity of our old MR scanner (right image in figure 10) an increased pin cushion distortion can be recognized comparing the measured rod positions (dark dots) with the known positions (bright dots) in the lower and upper part of the fused image.

Images acquired with a more homogeneous base magnetic field result in significantly reduced image distortions, which is qualitatively illustrated by the left image in figure 10, where calculated and measured rod positions almost coincide.

Dependent on the CT image acquisition mode (axial/helical), reconstruction algorithm and slice thickness the geometrical accuracy changes. Again, the measured mean error found by analysing the 45 known target points is more than double the mean fiducial error given by the TPS. In contrast to the MR measurements the mean absolute error corresponds to the maximum fiducial error found by the TPS, emphasizing that no systematic spatial variations are present in the CT images analyzed. We found that an increased slice thickness will increase the mean error and helical data acquisition does not compromise the geometrical localization accuracy.

The image intensifier based angiographic images showed a systematic increase of the localization error with increasing distance from the phantom center, because we do not use any correction algorithms prior to stereotactic image definition. A maximum deviation of 2.8 mm and a mean error of 0.78 mm was found as a typical error for this imaging modality. Due to systematic image distortions present in our image intensifier based system, the localization error increases with increasing distance from the center of the image intensifier screen [22]. Therefore, we used only the central part of the image intensifier screen which kept the maximal error less than 1.3 mm.

The time spend for extracting the stereotactic coordinates of the known target points exclusive imaging, varies with the imaging modality from around 15 min for the MR phantom to 30 min for the CT/Angio phantom. The resultant target point localization accuracy takes into account not only the imaging modality, but also the stereotactic definition process (data transfer, orientation, scaling, stereotactic coordinate transformation) using the TPS. Therefore, the procedure described here can also be used as a quality assurance tool for stereotactic coordinate transformations based on the fiducial markers and for image fusions performed by the corresponding software tool. By repeated stereotactic definition using the TPS with different window and level settings, we found different values for the mean and maximal fiducial error varying within 0.3 mm. In order to check the observers accuracy in defining the target positions, we repeated the analyses for the same data set. For the CT/Angio phantom this spatial uncertainty was 0.15 mm and for the MR phantom 0.5 mm considering a single 3D glass cross hair. The mean errors calculated for identical imaging parameters, but for images acquired at different dates (without any maintenance intervention), do not significantly change and are within an uncertainty of 0.2 mm.

Discussion

The localization accuracy found in stereotactic CT images is typically less than 0.6 mm in our institution, depending on the slice thickness and the maximum fiducial error found, which itself is dependent on the window and level setting during stereotactic image definition. Due to the non-existent systematic image distortions, the maximum fiducial error found is similar to the mean error found using the known target point method. Possible mechanical problems within the CT gantry or the table movement could result in increased target point localization errors, which give reason to check the CT imaging protocol during acceptance and regular constancy checks.

In contrast, MR imaging, the most important imaging modality in SRS, needs special attention, because MR images often show systematic geometrical distortions, which could limit their use in SRS. Image distortions and artefacts are present in all MR images. Artefacts are mostly patient related, such as chemical shift or susceptibility artefacts and change the local geometry of selected structures within the patient. These patient related artefacts are difficult to correct for and in principle limit the geometrical accuracy of MR images [12]. In contrast, image distortions deriving from the MR scanner itself (static field inhomogeneities, gradient field non-linearities, eddy currents produced by switching gradients) often affect all images within an imaging study. These systematic distortions, dependent on the imaging sequence applied, also limit the localization accuracy, but can be measured and optimized using dedicated commercially available phantoms [7, 9, 13, 14, 17, 22–24].

Different imaging protocols like 2D spin echo protocols or 3D volume acquisitions can be analyzed and optimized in terms of target point localization accuracy. In addition, it is possible to monitor changes occurring over a period of time, due to changes in MR scanner components (head coil, shim and gradient coils) [22]. Further systematic changes in the MR sequences under consideration for stereotactic imaging, like slice thickness, slice selection (axial, sagittal, coronal), pulse sequence, etc. can be tested in terms of localization accuracy.

In order to analyze and if necessary correct systematic pin cushion distortions in angiographic images, a plane grid phantom in front of the image intensifier has to be used [22]. If no image distortion correction is applied, or after such a correction has been performed, the localization accuracy of angiographic images can be tested using the known target point phantom. Due to the introduction of flat panel detectors in angiographic imaging systematic image distortions, mainly due to the curvature of the input phosphor of the image intensifiers, no longer occur, therefore improving the localization accuracy of this imaging modality significantly. Even so, with the help of the known target

point phantom not only the localization accuracy, but also the correct image transfer and image orientation within the TPS is automatically tested.

In general, special attention must be paid to the geometrical accuracy of stereotactic imaging modalities, because their geometrical uncertainties usually dominate the overall geometrical accuracy of the treatment [1], compared to the high mechanical accuracy and stability e.g. the Leksell Gamma Knife® which is less than 0.5 mm. Detailed analyses of all links in the chain of uncertainties guarantee a geometrical and dosimetrical accuracy of the treatment, which is well within clinical based and standardized tolerances. This accuracy can be monitored using the described and clinically validated phantoms for routine quality assurance which are in agreement with published technical standards [3–5].

Also the geometrical accuracy of CT images, dependent on the image acquisition mode, should be determinded before using this imaging modality as a reference data set in (frameless) image fusion with MR and PET [7, 9, 18].

These findings are also important for image based stereotactic interventions based on MR imaging. Apart from image intensifier based angiographic imaging, which is being currently replaced by flat panel detector based systems, MR images show significant target point localization errors dependent on the imaging sequence used. This is unlike to change in the near future, because modern MR scanners are often optimized for fast imaging, higher base magnetic field strength, shorter and wider magnet bores, which may compromise the geometric target point localization accuracy. It has also been noticed that optimized imaging sequences transferred to another MR scanner, do not result in comparable localization errors, thus emphasizing the rather complex interplay of the individual imaging parameters, making in house testing indispensable. With the introduction of flat panel imaging detectors in angiographic imaging, the major source of geometrical uncertainty in the near future will be the MR scanner.

Regular constancy checks of all imaging modalities used for stereotactic interventions are highly recommended because planned or unplanned maintenance may significantly change the localization accuracy and the time spent for regular constancy checks on the imaging modalities is not prohibitive.

References

1 Mack A, Czempiel H, Kreiner HJ, Dürr G, Wowra B: Quality assurance in stereotactic space, a system test for verifying the accuracy of aim in radiosurgery. Med Phys 2002;29:561–568.

2 Lomax NJ, Scheib SG: Quantifiying the degree of conformity in radiosurgery treatment planning. Int J Radiat Oncol Biol Phys 2003;55:1409–1419.

3 DIN 6875–1: Special radiotherapy equipments – Part 1: Percutaneous stereotactic radiotherapy, basic performance characteristics and essential test methods. 2004 DIN Deutsches Institut für Normung e.V., Beuth Verlag, Berlin.

4 Hartmann GH: Quality Assurance Program on Stereotactic Radiosurgery. Berlin/Heidelberg/New York, Springer, 1995.

5 Schell MC, Bova FJ, Larson DA, Leavitt DD, Lutz WR, Podgorsak, Wu A: AAPM Report No. 54, Stereotactic Radiosurgery, Report of Task Group 42, 1995, New York, NY, American Institute of Physics.
6 Yeung D, Palta J, Fontanesi J, Kun L: Systematic analysis of errors in target localisation and treatment delivery in stereotactic radiosurgery (SRS). Int J Radiat Oncol Biol Phys 1994;28: 493–498.
7 Karger CP, Hipp P, Henze M, Echner G, Hoess A, Schad L, Hartmann GH: Stereotactic imaging for radiotherapy: accuracy of CT, MRI, PET and SPECT. Phys Med Biol 2003;48:211–221.
8 Choi DR, Ahn YC, Kim DY, Huh SJ, Lee JI: Accuracy in target localization in stereotactic radiosurgery. Med Dosim 1997;22:53–58.
9 Ekstrand KE, Olds WW, Branch CL: A simple test phantom for stereotactic computed tomography. Med Phys 1993;20:391–393.
10 Bednarz G, Downes MB, Corn BW, Curran WJ, Goldman HW: Evaluation of the spatial accuracy of magnetic resonance imaging-based stereotactic target localization for gamma knife radiosurgery of functional disorders. Neurosurgery 1999;45:1156–1163.
11 Ertl A, Saringer W, Heimberger K, et al: Quality assurance for the Leksell gamma unit: considering magnetic resonance image-distortion and delineation failure in the targeting of the internal auditory canal. Med Phys 1999;26:166–170.
12 Michiels J, Bosmans H, Pelgrims P, Vandermeulen D, Gybels J, Marchal G, Suetens P: On the problem of geometric distortion in magnetic resoncance images for stereotactic neurosurgery. Magn Reson Imaging 1994;12:749–765.
13 Orth RC, Sinha P, Madsen EL, Frank G, Korosec FR, Mackie TR, Metha MP: Development of a unique phantom to assess the geometric accuracy of magnetic resonance imaging for stereotactic localization. Neurosurgery 1999;45:1423–1429.
14 Prott FJ, Haverkamp U, Willich N, Resch N, Stöber U, Pötter R: Comparison of imaging accuracy at different MRI units based on phantom measurements. Radiother Oncol 1995;37:221–224.
15 Schad LR, Ehricke HH, Wowra B, et al: Correction of spatial distortion in magnetic resonance angiography for radiosurgical treatment planning of cerebral arteriovenous malformations. Magn Reson Imaging 1992;10:609–621.
16 Sumanaweera TS, Adler JR, Napel S, Glover GH: Characterization of spatial distortion in magnetic resonance imaging and its implications for stereotactic surgery. Neurosurgery 1994;35:696–704.
17 Walton L, Hampshire A, Forster DM, Kemeny AA: A phantom study to assess the accuracy of stereotactic localization, using T1-weighted magnetic resonance imaging with the Leksell stereotactic system. Neurosurgery 1996;38:170–176.
18 Yu C, Petrovich Z, Apuzzo ML, Luxton G: An image fusion study of the geometric accuracy of magnetic resonace imaging with the Leksell stereotactic localization system. J Appl Clin Med Phys 2001;2:42–50.
19 Boone JM, Seibert JA, Barrett WA, Blood EA: Analysis and correction of imperfections in the image intensifier-TV-digitizer imaging chain. Med Phys 1991;18:236–242.
20 Chakraborty DP: Image intensifier distortion correction. Med Phys 1987;14:249–252.
21 Rudin S, Bednarek DR, Wong R: Accurate characterization of image intensifier distortion. Med Phys 1991;18:1145–1151.
22 Scheib SG, Gianolini S, Lomax NJ, Mack A: High precision radiosurgery and technical standards. Acta Neurochir Suppl 2004;91:9–23.
23 Mack A, Mack G, Scheib S, et al: Quality assurance in stereotactic radiosurgery/radiotherapy according to DIN 6875–1. Stereotact Funct Neurosurg 2004;82:235–243.
24 www.ptgr.de

Stefan G. Scheib, PhD
Department of Medical Radiation Physics, Klinik Im Park
Seestrasse 220
CH–8027 Zürich (Switzerland)
Tel. +41 44 209 22 16, Fax +41 44 209 20 11
E-Mail stefan.scheib@hirslanden.ch

Kondziolka D (ed): Radiosurgery. Basel, Karger, 2006, vol 6, pp 26–35

Monte Carlo Simulation for Gamma Knife Radiosurgery using the Grid

Vasu Ganesan, Rami Mehrem, John Fenner, Lee Walton

National Centre for Stereotactic Radiosurgery, Royal Hallamshire Hospital, Sheffield, Department of Medical Physics and Clinical Engineering, University of Sheffield, UK

Abstract

Gamma Knife radiosurgery is an established technique for the treatment of intracranial lesions and vascular malformations in the brain. In this study, dose distributions in a phantom calculated by GammaPlan have been compared with dose distributions computed by a Monte Carlo code (RAPT) assuming the phantom as a homogenous medium. Comparisons have considered both single shot plans and treatment plans. Approximately 200 radiosurgery treatment plans have been simulated using the Monte Carlo method and the initial results are discussed in this paper. The features and application of the GEMSS Grid (cluster of powerful computers) used for our computational work is described here. Analysis of the number of photons required for adequate simulation is also presented. A preliminary study of the effects of in-homogeneity has also been carried out by incorporating a 5 mm thin bone shell into the water phantom and the observed differences in the dose distribution are presented here. MATLAB software has been used to view, overlay and compare the dose distributions. A classical method of visualization of isodose lines and conformity indices has been used to compare and quantify differences.

Several authors have attempted simulating the dose distribution produced by four of the available collimators of the Gamma Knife radiation unit using Monte Carlo simulation [1, 2]. However, long computation times have limited previous studies to the simulation of single field treatments. We have investigated the use of a Grid offering up to 80 processors for Monte Carlo simulations of actual multiple field treatment plans. These simulations represent one aspect of the 'Grid Enabled Medical Simulation Services (GEMSS)' project to validate the suitability of a Grid environment for the solution of computationally intensive health applications.

Leksell GammaPlan, the propriety Gamma Knife treatment planning system, uses a simple semi-empirical algorithm and computes dose distribution in real time in response to beam placement. However, it does not account for the heterogeneity within the brain and assumes the skull is a homogeneous medium of water [3, 4]. Monte Carlo techniques provide a more robust calculation algorithm with the potential to correct for tissue in-homogeneity. This report describes our use of Monte Carlo techniques to simulate treatment plans, initially using the same assumptions as GammaPlan i.e. within a homogeneous water equivalent medium. We also present preliminary results in which a thin bone shell was introduced to study in-homogeneity effects.

Materials and Methods

GEMSS and RAPT

Grid Enabled Medical Simulation Services, is the European Union funded project, that provided the high performance-computing platform for running our computationally intensive Monte Carlo applications. One such application was Monte Carlo simulation of radiosurgery treatment plans. The Grid consisted of two large PC clusters placed in University of Vienna, Austria (16 CPUs) and NEC, Germany (64 CPUs) using an interface built around web services that addresses issues specific to the health sector [5]. This provided a suitable environment for simulation of Gamma Knife treatment plans.

The treatment plans for our routine patients were constructed using Leksell GammaPlan version 5.34 (Elekta, Crawley, UK). The Monte Carlo code called RAPT (Radiotherapy Application for Parallel Technology) based on EGS4 modified to run and distribute work within a multi processor environment was used for simulations. RAPT treats photon propagation rigorously, following the path of every photon and calculates the energies of their interactions. Unlike other Monte Carlo codes RAPT does not repeatedly model the interactions of photons as they leave the source and pass through the collimation system. RAPT uses a beam profile data from previously calculated simulations to produce an energy and intensity profile at a point beyond the collimation system [1, 2]. Monte Carlo is used to simulate the photon interactions as they leave this point and enter the patient. The computed dose distribution is currently limited to 1 mm resolution within the high dose volume. In regions where there is heterogeneity in tissue, RAPT is expected to produce a more accurate dose distribution [6].

A graphical user interface was developed using MATLAB, version 6.5.1 (Math works, Inc., USA) to transfer the treatment data, number of photons, no of isocentres, skull geometry, their corresponding X, Y, Z co-ordinate values, gamma angles, weight of the shot, and the plugging pattern to the Monte Carlo code on the Grid. Facilities to view the dose distributions in the axial, coronal and sagittal sections were also incorporated. A utility called MetriX (developed by S. Riley) was developed to display two dose distributions side by side and provides facilities for the comparison of GammaPlan and RAPT solutions. This facilitates measurement of full width at half maximum, beam profiles, point of maximum dose, similarity (conformity) index, percentage coverage of one distribution over another.

Plans simulated by RAPT were derived from actual treatments performed in radiosurgery centre at Sheffield. The treatment parameters were obtained from GammaPlan and forwarded to the Grid using the Input GUI for RAPT calculations. Once the Monte Carlo computations were completed the results were downloaded on the client computer for subsequent analysis and comparison with GammaPlan solution.

Results and Discussion

Initially, a spherical water equivalent homogeneous medium was used to quantify simulation performances. Single shots of 4, 8, 14, and 18 mm collimators were placed at the centre of phantom of radius 80 mm. The dose distribution obtained by Monte Carlo simulation were compared with those of GammaPlan for each of the four collimators.

Figure 1 shows a typical dose distribution for a single 18 mm shot placed at isocentre (100, 100, 100) in the centre of the spherical phantom. (a) by gamma plan, (b) by RAPT Monte Carlo simulation, (c) superposing isodose lines of one distribution over the other in the axial plane, (d) superposing in the sagittal plane. Only 90, 50, 20 and 10% isodose lines are shown here for clarity. All four collimator helmets showed excellent correlation. It was also demonstrated that dose distributions with a number of the sources 'plugged' using template plugging patterns were found to correlate well. Whereas in an extreme situation, we placed a shot at the periphery of the phantom and found the differences in dose distribution between GammaPlan and RAPT distribution, as illustrated in figure 2.

In order to determine the number of photons required for adequate Monte Carlo simulation, a photon statistics study was undertaken, investigating the effect of photon statistics over the range from 0.1 million photons per beam to 60 million photons per beam. Repeating one Monte Carlo study several times with a different starting seed number and comparing the results, enabled an estimate of percentage error (i.e. maximum absolute value of percentage differences of normalized distributions) in a solution to be obtained as a function of number of photons. Figure 3 shows a plot of percentage error against number of photons used. We found 1.0–3.0 million photons per beam were satisfactory for our studies typically resulting in error of less than 2%.

Approximately 200 Gamma Knife radiosurgery plans with multiple shots were compared with the RAPT simulated dose distributions. The homogeneous medium assumption used by GammaPlan was imposed on the Monte Carlo simulation at this stage. Examples of a typical, acoustic neuroma plan and a meningioma plan are shown in figures 4 and 5 respectively, showing the dose distribution in axial, coronal and sagittal section. Column-1 in the figures 4 and 5 illustrates GammaPlan distribution superimposed on MR images, Column-2

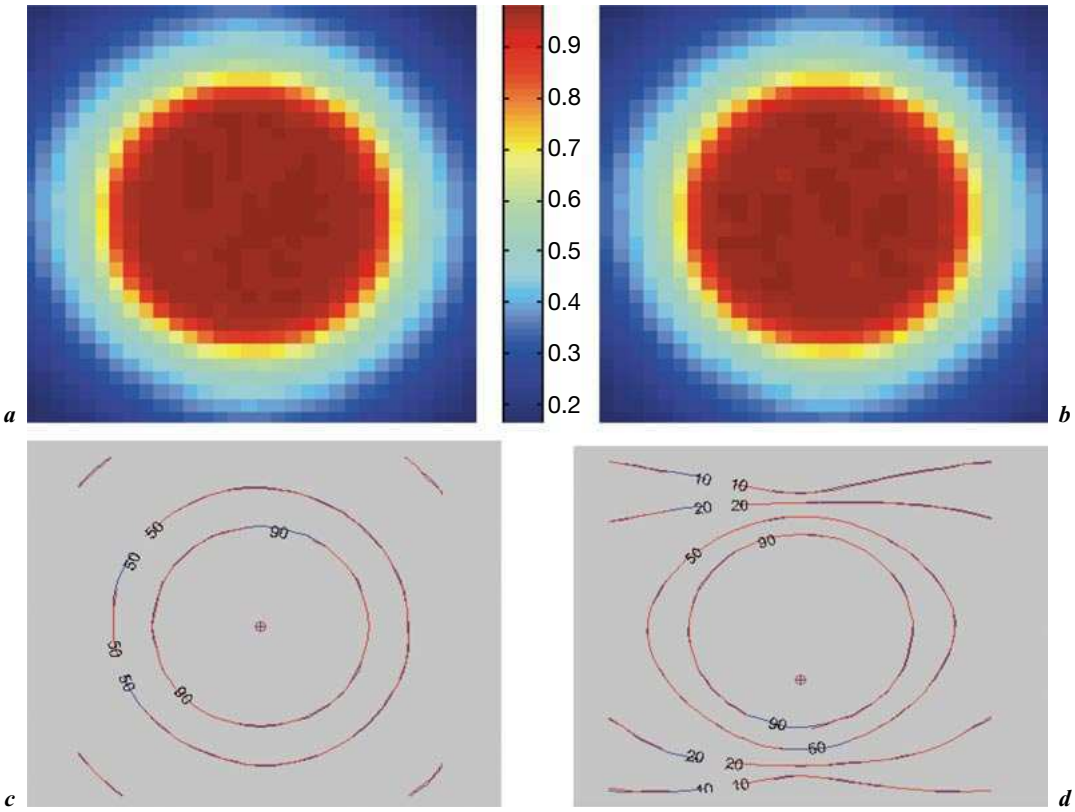

Fig. 1. Distribution of dose at the centre of a spherical phantom produced by an 18 mm field as predicted by (***a***) GammaPlan, (***b***) Monte Carlo simulations, (***c***) overlaying 90, 50, 20 and 10% isocontours produced by RAPT (Red) over GammaPlan (blue) in axial view and (***d***) overlaying in sagittal view.

shows the GammaPlan distribution without images and column-3 shows the Monte Carlo solutions.

Figure 4 shows good correlation between the GammaPlan and RAPT solutions and is typical of the correlation in the cases that we have observed. Figure 5 shows an example of a case in which slightly poorer correlation was apparent with small but visible differences in the isodose distributions. It is evident that this is probably as a result of differences in the maximum point value used for normalization.

Satisfactory results with the dose distributions obtained by RAPT encouraged us to investigate the effects of tissue in-homogeneity. This was incorporated by

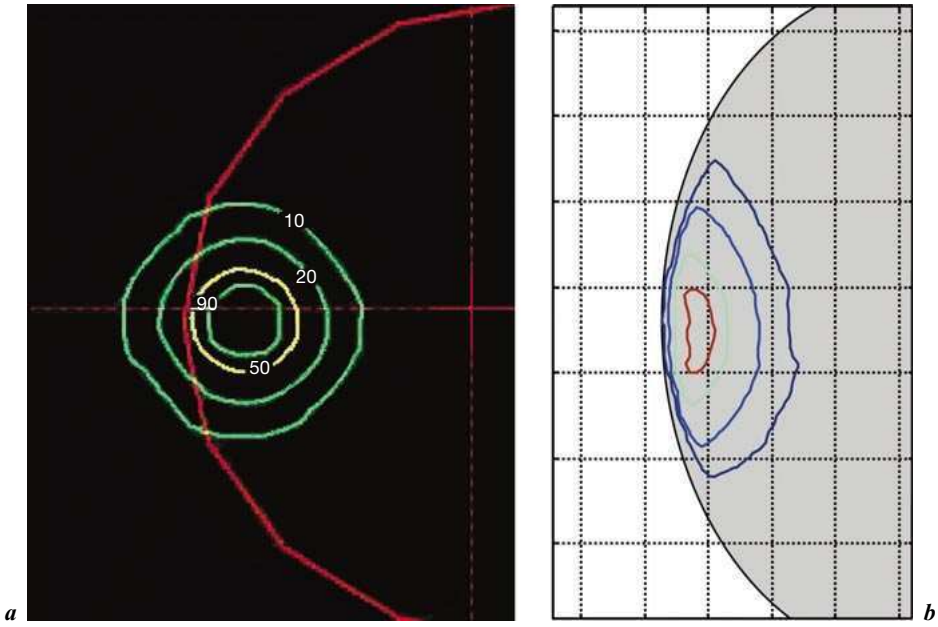

Fig. 2. Dose distribution by GammaPlan (***a***) and RAPT (***b***) when shot placed near phantom surface.

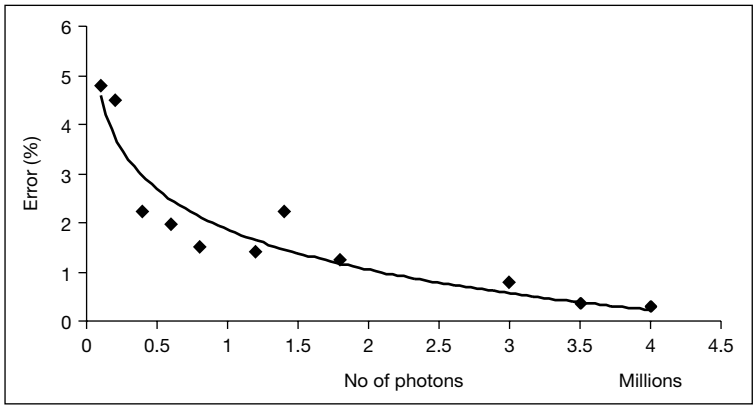

Fig. 3. Graph showing the variation of the percentage error in the Monte Carlo solution with number of photons simulated.

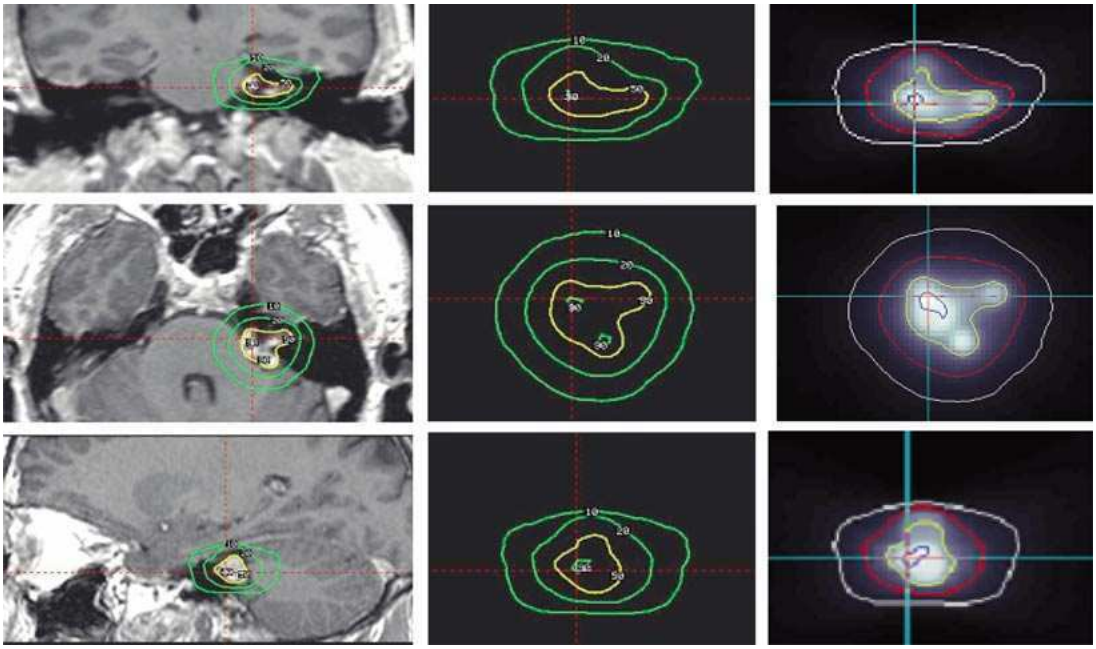

Fig. 4. An example of an acoustic neuroma plan with dose distribution simulated by GammaPlan and Monte Carlo.

introducing 5 mm bone shell in to the water phantom of radius 80 mm, with the bone shell at 5 mm from the surface of the phantom. A 18 mm shot was placed at varying distances from the centre of the phantom to the surface and simulated in each case using RAPT. The dose distributions were compared with the homogeneous situation. Figure 6 shows a dose distribution in a homogenous situation and with bone shell. The variation in distribution is apparent when the shot is placed near the bony interface. When the phantom is assumed homogenous, the dose distribution is not affected, but when the in-homogeneity is considered, there is large deviation in the distribution.

Figure 7 shows profiles of the dose distribution along a radial through the phantom with one curve assuming the medium as homogenous and the other curve incorporating a 5 mm concentric bone shell at a depth of 5 mm from the surface of phantom. When a shot of 18 mm diameter is placed at 5 mm from the inner surface of bone shell within the phantom, the second curve shows a 40% increase in dose compared to the first curve, with the increase confined to the bone. Adjacent to bone shell, the dose decreases rapidly and is reduced (by up

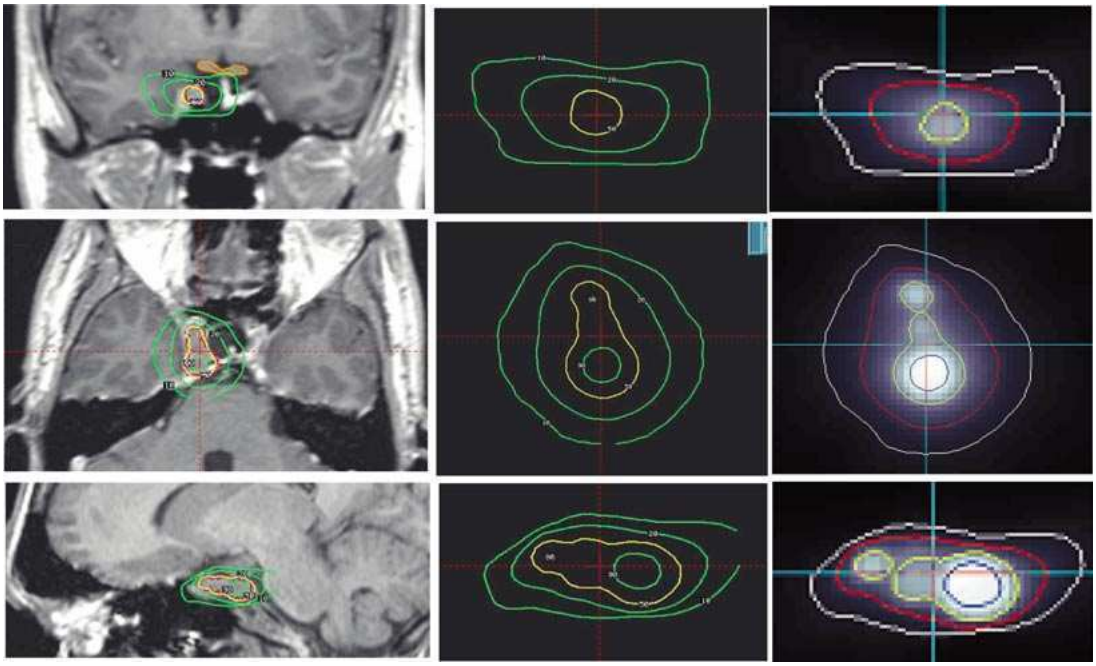

Fig. 5. An example of a meningioma plan with dose distribution simulated by GammaPlan and Monte Carlo.

to 6%) by the presence of the bone. In a clinical situation this would be directly over the target tissues of interest.

A conformity index (comparing the 50% isocontours for both situations) was used to quantify the changes in the distribution [7]. Figure 8 shows the variation in conformity index as the isocentre moves from the centre of the phantom closer to the bone shell. When the isocentre is placed near to centre of the phantom, little variation in dose shape is evident, but significant changes occur when isocentre is within 15 mm of the bone shell. Further studies on the effect will form the focus of future work.

It should be noted that in order to perform these RAPT Monte Carlo simulations, the Grid has been essential for our studies. Table 1 presents the computational times involved in the simulation process. The table shows a comparison of a normal office PC, a powerful PC and the GEMSS Grid. With the computational burden reduced to less than a hour for our multiple shot radio surgery plans the Grid has enabled us to perform the simulations in a realistic time frame. In addition the RAPT software has proved to be very robust.

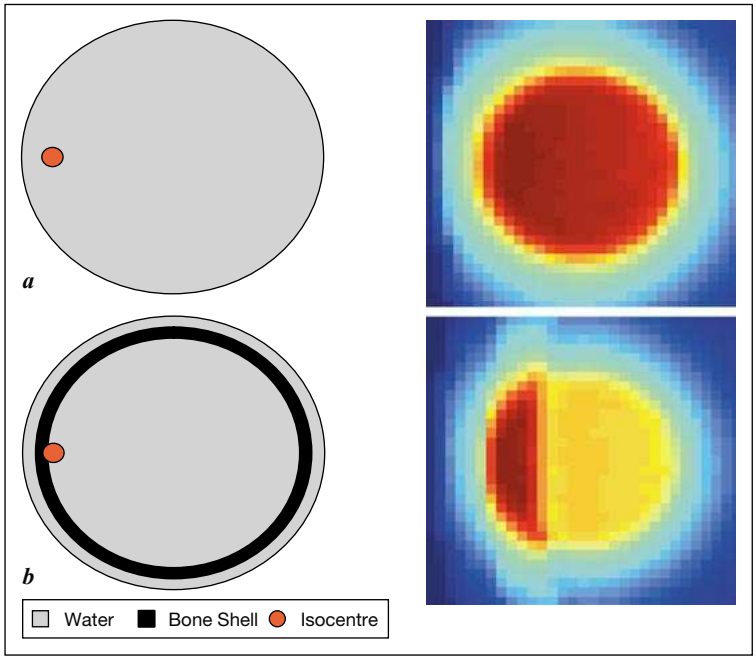

Fig. 6. Monte Carlo simulated dose distributions (***a***) in a homogeneous medium at the position shown within a spherical phantom (***b***) adjacent to a bone shell.

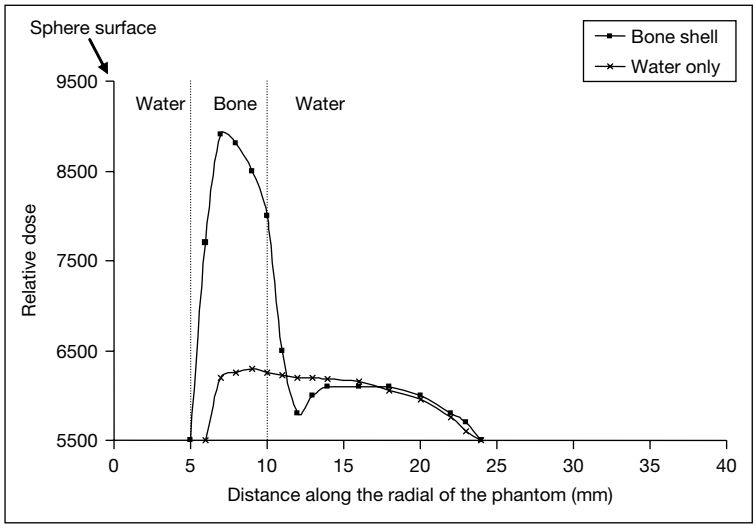

Fig. 7. Monte Carlo simulated dose profiles in a spherical homogeneous phantom medium and with 5 mm bone shell added.

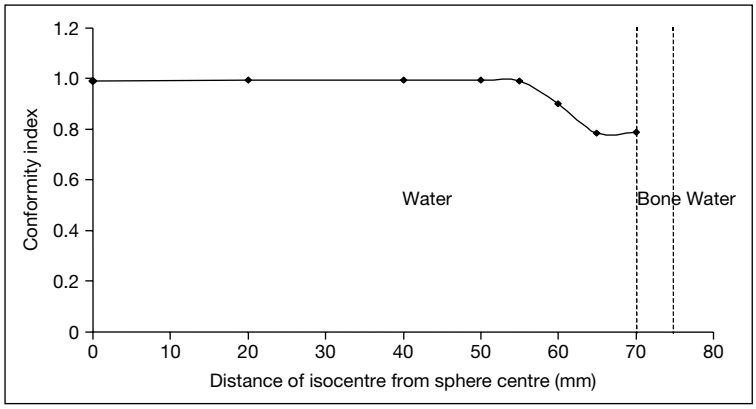

Fig. 8. Graph to show how the conformity index varies between water with bone shell and water-only medium as a function of distance of isocentre from centre of the phantom.

Table 1. Monte Carlo computation times

Computer used	Time for 3.0 million photons per beam	
	single shot	multiple shot
Office PC	72 h	Crashed
Powerful PC	20–25 h	Several days
GRID	15–20 min	1 h

Conclusion

Monte Carlo simulation for single shots of collimator sizes of 4, 8, 14 and 18 mm of the Gamma Knife showed an excellent correlation with the GammaPlan dose distributions. Also the dose distributions of multiple shot treatment plans demonstrated a good agreement with the Monte Carlo simulated ones when the medium is assumed a homogeneous. However the improved physics of the RAPT Monte Carlo method is particularly apparent at boundaries between materials with different linear attenuation coefficients within the head and indicates significant deviation from solutions obtained using GammaPlan. The use of a Grid computing resource offers a promising platform for the Monte Carlo simulation of radiosurgery treatment plans.

Acknowledgements

We would like to express our sincere thanks to S. Riley, C. Ferris, and K. Potter for their valuable contribution to this work. J. Cheung (Gamma Knife Centre, Canossa Hospital, Honk Kong) and Al-Dweri (Departmento de Fisica Moderna, Universidad de Granada, Granada, Spain) for sharing their results of single field simulations with us. P. Melas, M. Surridge and S. Middleton (IT-Innovation, University of Southampton, UK) for their valuable assistance with the RAPT code. Elekta Instrument AB, Sweden for help with extracting GammaPlan data.

GEMSS was a European Union FP5 funded project (IST-2001–37153).

References

1 Al-Dweri FMO, Lallena AM, Vitches M: A simplified model of the source channel of the Leksell Gamma Knife tested with PENELOPE. Phys Med Biol 2004;49:2687–2703.
2 Cheung JYC, Yu KN, Ho RTK, Yu CP: Monte Carlo calculations of single beam dose profiles used in gamma knife treatment planning system. Med Phys 1998;25:1673–1675.
3 Walton L, Bomford CK, Ramsden D: The Sheffield Stereotactic Radiosurgery Unit, physical characteristics and principles of operation. Br J Radiol 1987;60:897–906.
4 Wu A, Lindner G, Maitz A, Lunsford LD, Flickinger JC, Bloomer WD: Physics of Gamma Knife approach on convergent beams in stereotactic radiosurgery. Int J Radiat Oncol Biol Phys 1990;18:941–949.
5 Fenner JW, Mehrem RA, Ganesan V, Riley S, Middleton SE, Potter K, Walton L: Radiosurgery planning supported by the GEMSS Grid; in Solomonides T, et al. (eds): From Grid to Healthgrid. IOS Press, 2005, pp 190–197.
6 Gill A, Surridge M, Scielzo G, Felici R, Modesti M, Sardu G: RAPT: A parallel radiotherapy treatment planning code; in Liddel H, Colbrook A, Hertzberger B, Sloot P (eds): Proceedings of High Performance Computing and Networking. Brussels, Belgium, 1996, Vol 1067, pp 183–193.
7 Paddick I: A simple scoring ratio to index the conformity of radiosurgical treatment plans. J Neurosurg 2000;93(suppl 3):219–222.

Mr Vasu Ganesan, Senior Medical Physicist
Stereotactic Radiosurgery, Floor-C, Royal Hallamshire Hospital
Glossop Road
Sheffield S10 2JF (UK)
Tel. +44 114 2713576, Fax +44 114 2754930
E-Mail vasu.ganesan@sth.nhs.uk

Kondziolka D (ed): Radiosurgery. Basel, Karger, 2006, vol 6, pp 36–49

In vivo Estimation of Extracranial Doses in Stereotactic Radiosurgery with the Gamma Knife and Novalis Systems

Thierry Gevaert[a,c], *Françoise Desmedt*[a,c], *Bruno Vanderlinden*[a,c], *Bob Schaeken*[d], *Christel Van Ranst*[e], *Guy Storme*[b], *Marc Levivier*[a], *Stéphane Simon*[a,c], *Dirk Verellen*[b]

[a]Gamma Knife Center, ULB, Hôpital Erasme, [b]Department of Radiotherapy, Oncology Center, AZ VUB, [c]Department of Radiation Therapy and Laboratory of Physics, Institut Jules Bordet, Brussels, [d]XIOS, Diepenbeek, [e]ULB, Science Soc., Pol. et Eco., Brussels, Belgium

Abstract

Objective: The purpose of this work is to investigate the extracranial doses in vivo during intracranial treatments comparing the Gamma Knife system with the Novalis system for identical pathologies. The analysis is limited to single fraction stereotactic radiosurgeries. **Methods:** Measurements were performed with TL dosimeters positioned on the lateral canthus, thyroid, breasts and gonads to obtain the dose received to these anatomical regions. Based on these observations, an estimate of the risk for cancer induction and detriment will be proposed. The measured doses were normalized to 24 Gy, and the influence of target maximum dose, reference isodose volume, equivalent treatment time (which is related to the activity of the ^{60}Co sources for the Gamma Knife) and distance on extracranial doses are analyzed. **Results:** The average extracranial dose with a normalized prescription dose of 24 Gy is comparable for both machines. Gamma Knife: For the lateral canthus, thyroid, breast and gonads the median doses were 435, 103, 48, and 6 mGy, respectively. Novalis: For the lateral canthus, thyroid, breast and gonads the median doses were 234, 79, 45, and 3 mGy, respectively. For the Gamma Knife system as well as the Novalis system no correlation could be found between maximum dose, reference isodose volume and extracranial doses. On the other hand, for the Gamma Knife system the equivalent treatment time and distance have a significant influence on doses received on extracranial sites. For the Novalis system only the distance and the geographical placement of the arcs will influence the extracranial dose. **Conclusions:** Doses to extracranial sites are small, ranging from 1.4% of the prescribed dose (24 Gy) for the lateral canthus to 0.02% for the gonads for the Gamma Knife and in the range of 0.97% of the prescribed dose (24 Gy) for the lateral canthus, to 0.01% for the gonads for the Novalis. According to ICRP-60, the risk for cancer induction after a radiosurgical treatment

is estimated to about 0.2% for both the Gamma Knife and Novalis systems; the risk for detriment is estimated at 0.3% for both systems. Although these risks are very small, they must be kept to a minimum value for long life expectancy patients, by choosing the appropriate treatment strategy.

The purpose of this work is to investigate the extracranial doses in vivo during intracranial treatments by comparing the Gamma Knife system with the Novalis system for identical pathologies. The treatments studied are limited to stereotactic radiosurgeries. The aim was to investigate the dose the other organs (lateral canthus, thyroid, breast, and gonads) will receive during a treatment for an intracranial lesion. Also the influences of target maximum dose, reference isodose volume, equivalent treatment time, and distance on extracranial doses are analyzed.

The Gamma Knife is designed to focally irradiate targeted volumes within the brain in a stereotactic, highly conformal manner. It employs frame fixation for head immobilization during imaging and treatment, 3D imaging and computer simulation during treatment planning and target-focused beams from 201 ^{60}Co radiation sources during treatment.

The Gamma Knife model C is a device which includes several new technologies, most notably an automatic positioning system (APS) that allows robotic movement of stereotactic frame between two irradiation shots. This unit includes an updated planning software (GammaPlan v5.34) consistent with the APS hardware, a computerized control console and a couch that is compatible with the APS. This positioning system includes robotic positioners that attach the stereotactic frame to the collimator helmet. A special stereotactic frame is required for attachment to the APS. This frame has a hole in the middle of the lateral bar that the bevelled peg of the APS fits into and a slot on the right side of the base ring for attaching the gamma angle. The model C unit can be used with or without the APS (using the standard trunnions) [1]. With these evolutions of the Gamma Knife, the model C will now automatically go to another shot without any intervention of the physicist. This means that there will be another distribution of extracranial dose.

The Novalis system, which is an integrated system consisting of a single-energy of 6 MV coupled to the Brainscan (v5.2) treatment planning system (TPS), is a device originally designed for stereotactic radiosurgery. It is also equipped with stereotactic frames which can be attached on the treatment couch. Moreover, the Novalis is equipped with a micro-multileaf collimator (mMLC). This mMLC consists of 52 leaf pairs of varying width: the central leaves are 3 mm wide, while the outer leaves are 4.5 mm and 5.5 mm. The maximal

field size at isocenter distance is 10×10 cm. This is the major difference between the common LINAC (use of macro-multileaf collimator) and the Novalis (use of mMLC) and replaces one of the secondary collimators. The fine 3 mm central leaves allow the Novalis to accurately mirror the contour of the tumor from any angle. This innovative and effective treatment is called 'Shaped Beam Surgery'. The system is capable of performing several conformal radiotherapy techniques including conformal beam treatment, arc-therapy using circular collimators, dynamic conformal arc and intensity modulated radiotherapy using dynamic multileaf collimation. Because of the different conformal radiotherapy techniques, the Novalis is also able to treat extracranial lesions such as lung, liver, and prostate. For this device, the extracranial doses were not measured before, so it was interesting to do such a study [2].

The aim of radiosurgery is to cover most of the lesions with prescribed radiation and sharp dose fall-off and to avoid any secondary effects on critical tissues. Intracranial tissues are obviously the most critical but extracranial doses to healthy tissues must also be evaluated. The international Commission on Radiological Protection (ICRP) recommends in its publication 60 to take 5%/Sv as risk factor for an induced lethal cancer and 7.5%/Sv as risk factor of total detriment occurrence after a low dose and low dose rate population exposure. Several studies on extracranial doses have already been published [3, 4]. We propose here a study of 228 unselected patients treated with the LGK model C and 40 unselected patients treated with the Novalis.

Material and Methods

The extracranial doses were measured in vivo with TL dosimeters at the lateral canthus, the thyroid, the breast, and the gonads. The TLD's used for this research are LiF:Mg, Ti and $Li_2B_4O_7$:Mn, with a dimension of $3.2 \times 3.2 \times 0.9$ mm. Their effective atomic number ($Z_{eff} = 8.2$ and 7.4, respectively) makes them close to tissue equivalence ($Z_{eff} = 7.42$) for the photoelectric effect. The Compton effect component of the mass attenuation coefficient is proportional to the Z/M ratio, here M is the molar mass. This ratio is approximately similar to the tissue equivalence.

Once they were placed and irradiated during a patient's treatment, the reading was obtained by heating the TLD's with the Harshaw QS 3500. The TLD's are first placed into a drawer. Once the drawer is closed, the TLD's are preheated at a temperature of 135°C during 12 s, then acquired at a temperature of 270°C during 16 s and finally annealed at a temperature of 305°C during 20 s. This procedure has been done for the Gamma Knife treatments as well as for the Novalis treatments. The TL-reading is translated to the dose with the correction factors calculated after irradiation under known reference conditions. For the Gamma Knife, the TL dosimeters were calibrated in a ^{60}Co beam and irradiated to 1 Gy and positioned at a depth of 5 mm in a phantom made of several plates (PMMA) of 20×20 cm^2. For the Novalis, the TLD's were calibrated with the Novalis itself by using the 6 MV photon beam at 5 cm depth in a 10×10 cm field and an SSD of 100 cm, for a prescribed dose of

1 Gy. The calibration was not performed at maximum depth, the reason of this is the occurrence of a slight dip in the profile of the beam at d_{max}. So if we calibrate at d_{max}, this would result in an underdosage of up to 3% for some TLD's in the center of the field. The TLD's were placed into specially drilled holes in a plate of White-Water-Phantom, which is a solid material with absorption properties similar to water.

The acquired dose for each organ was a result of the average of two dosimeter readings.

To have a better view on the extracranial doses for both machines, it is advisable to normalize them to a given dose. Otherwise, we always have to take the received dose to the lesion into account to compare the extracranial doses for the Gamma Knife and Novalis systems. The reason is that the prescribed dose to the lesion ranges from 12 (Acousticus Neurinoma) to 90 Gy (Trigeminal Neuralgia) and without normalization this dose will also have its importance for the comparison of the extracranial doses. Due to this normalization all the pathologies can simply be compared. The level of the normalization dose is arbitrary chosen at 24 Gy, because this is a common dose used in most stereotactic radio surgery cases. The normalization was performed in function of the prescription dose, because this is the common dose used for both the Gamma Knife and the Novalis and not at the maximum dose, because the TPS calculates the maximum dose differently for the Gamma Knife and Novalis systems.

Results

The simplest way to compare the extracranial doses is to take the average doses for the normalized data for each organ without any analysis. Table 1 summarizes the average, maximum and minimum doses for all patients and sites of measurements for the Gamma Knife and Novalis systems. As expected, the largest doses are delivered to the lateral canthus and the smallest ones to the gonads. The doses are generally small, which means a small chance to have stochastic effects, and deterministic effects will not occur.

It can be observed that the normalized dose for the lateral canthus is much higher for the Gamma Knife system (435 mGy) than for the Novalis system (234 mGy).

The doses for the three remaining organs are in the same order of magnitude. For the Gamma Knife, the average normalized doses on the thyroid, breast and gonads were 103, 48, and 6 mGy, respectively. For the Novalis, the average normalized doses on the thyroid, breast, and gonads were 79, 45, and 3 mGy, respectively. The Gamma Knife uses usually a prescription dose at the 50% isodose line, which will double for the maximum dose. The Novalis uses usually a prescription dose at the 80% isodose line, which will not double for the maximum dose.

Analysis of the Target Maximum Dose Influence

The first parameter to analyze is the prescribed dose which can be found in the calculation of the brainscan (v5.2) for the Novalis system or the Gammaplan (v5.34) for the Gamma Knife system. The range of the maximum

Table 1. In vivo measurements for the Gamma Knife and Novalis systems with a 24 Gy isocenter dose normalization

	Gamma Knife system, mGy (N = 288)			Novalis system, mGy (N = 40)		
	average dose	maximum dose	minimum dose	average dose	maximum dose	minimum dose
Lateral canthus	435.7 ± 87.2	3,158.9	48.8	233.7 ± 46.8	863.4	6.6
Thyroid	103.2 ± 20.6	365.5	30	79.4 ± 16	242.3	20.6
Breast	47.8 ± 9.6	173.9	10	45.4 ± 9	236.6	14.1
Gonads	5.9 ± 1.2	242.4	0.9	2.8 ± 0.6	8.8	0.44

prescribed dose in this comparison is from 15 to 90 Gy. Sometimes the prescribed dose can reach 140 Gy for functional lesions for the Gamma Knife. No direct correlation could be determined between the maximum target dose and the extracranial (lateral canthus, thyroid, breast, and gonad) normalized delivered doses. The conclusion is that a maximum dose of 90 Gy does not necessarily involve a higher extracranial dose than the 45 Gy maximum prescribed doses.

Analysis of the Reference Isodose Volume Influence

Another interesting parameter to analyze is the reference isodose volume which is defined as the volume receiving the therapeutic prescribed dose. The volume depends on the size of the target or the lesion. With this parameter too, the influence of the target size in function of the extracranial doses is given. The reference isodose volume is defined as the volume of a 80% isodose line for the Novalis. For the Gamma Knife, the reference isodose volume is usually defined as the 50% isodose line and sometimes other isodose lines depending on the size and the matching of the lesion. The lateral canthus, thyroid, breast, and gonad doses, which are normalized to 24 Gy as a function of the reference isodose volume which had first to be calculated manually, show no direct correlation.

Analysis of the Treatment Time Influence

Treatment time is defined as the total time of irradiation or, in other words, the time spent in the Novalis or Gamma Knife at the treatment position.

The Novalis system will rather use monitor units (MU) than time. One monitor unit describes the dose delivered by a LINAC. Generally the LINAC is calibrated to deliver 1 cGy under reference conditions (SSD 100 cm, depth of

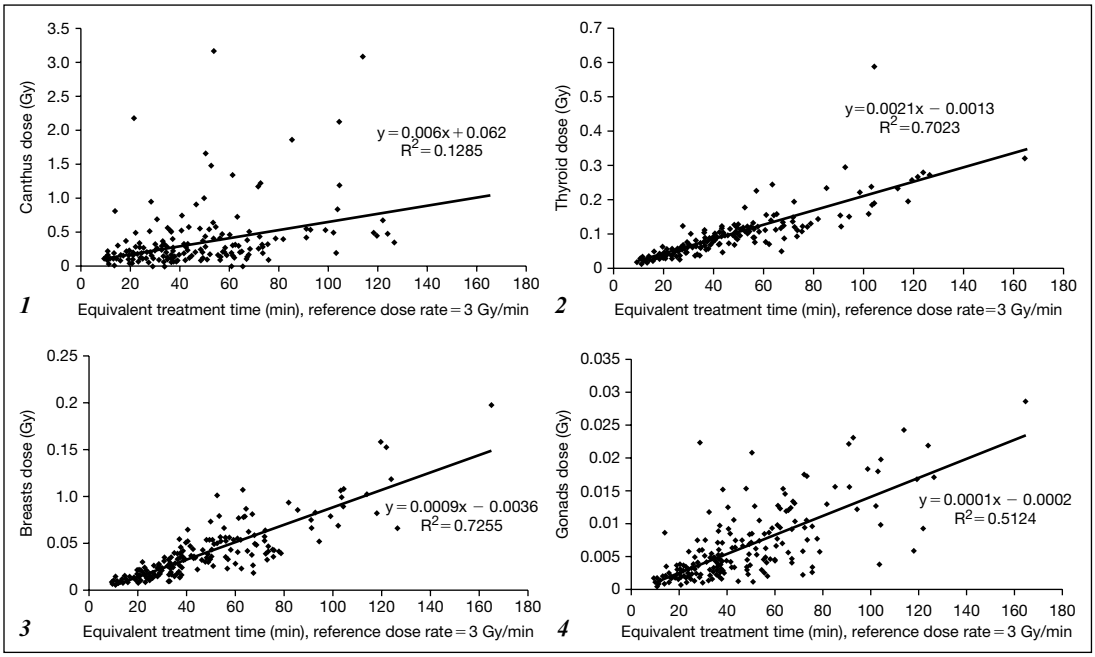

Figs. 1–4. Normalized lateral canthus, thyroid, breast and gonad doses in function of time for the Gamma Knife.

maximum dose for a $10 \times 10\,cm^2$ field for 1 MU). The Novalis system generates a dose rate of 800 MU/min for every stereotactic treatment.

For the Gamma Knife system there is no fixed dose rate. As ^{60}Co is decreasing with time, results are normalized to a given dose rate and presented in figures 1–4. The choice of the normalization is at random and for this study we took 3 Gy/min as the normalization dose rate.

Without normalization, the dose rate of every treatment day will differ and the results will also depend on the decreasing dose rate. With this normalization it is as if we had done all the treatments in one day and that is why the decreasing dose rate must not be taken into account. The treatment time depends amongst other things on the numbers of isocenters used.

No correlation could be found between the MU and the extracranial doses for the Novalis system. For the gonads, there may be a linear relation, but to reach this conclusion more measurements are needed and could be part of further investigations.

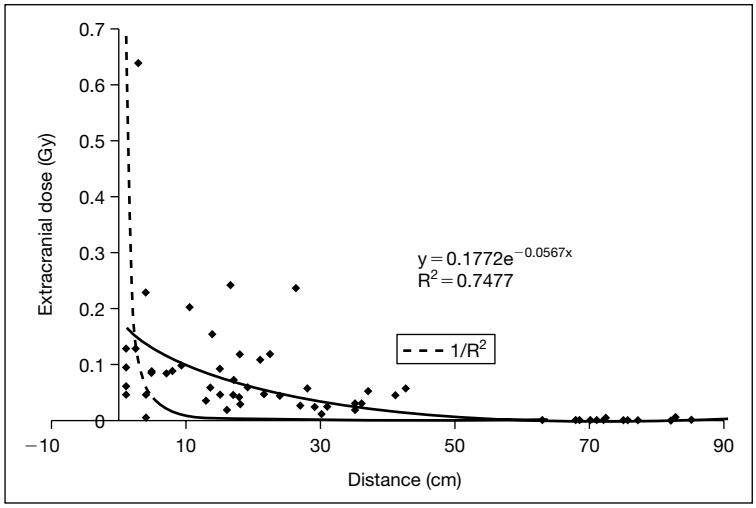

Fig. 5. Normalized organ doses in function of distance, with exponential regression and inverse square law for the Novalis.

For the Gamma Knife system we found a correlation between the equivalent treatment time and the extracranial doses. On the four graphs for the Gamma Knife (figures 1–4) linear regression was performed. For thyroid and breasts, a linear correlation was found with an R^2 value of respectively 0.7023 and 0.7255. For gonads, a linear relation is also found but with a smaller R^2 value than for the thyroid and breasts, being 0.5124. The lateral canthus doses are almost not correlated with the equivalent treatment time, with an R^2 value of 0.1285.

Analysis of the Distance Influence

Another possible parameter to analyze is the distance between the source and extracranial sites.

For the Novalis system the distance is from the isocenter to the sites of interest (lateral canthus, thyroid, breast and gonads) and is shown in figure 5.

The distance measured for the Gamma Knife system is a little different. Because the lateral canthus is most of the time in the helmet, the measurements start from the thyroid. The measured distance is from the helmet to the sites of interests (thyroid, breast and gonads). These results are shown in figure 6.

For both the Gamma Knife and the Novalis, a correlation has been found between the distance and the organ doses. A decreasing exponential equation was fit to the data. We found for the Novalis and Gamma Knife an R^2 of respectively

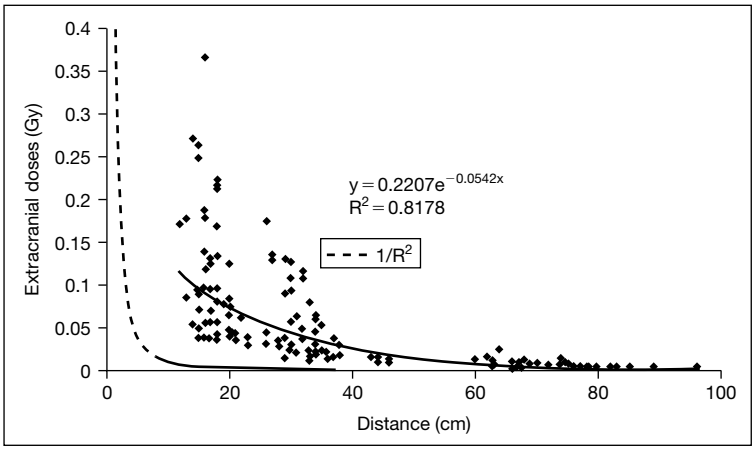

Fig. 6. Normalized organ doses in function of distance, with exponential regression and inverse square law for the Gamma Knife.

0.7477 and 0.8178. On these figures, the inverse square law was also included. The results on the graph do not exactly match with this law.

Analysis of Other Possible Influences

The most important influences of the extracranial doses for the Gamma Knife system have been dealt with.

For the Novalis system, there is still no parameter which will give a correlation with the extracranial doses. The parameter which might give a contribution is the geographical placement of the arcs. Because the Novalis is a machine that uses a gantry, which is not fixed to the treatment couch like the Gamma Knife, the way the arcs (gantry) turn around the patient might give a contribution to the extracranial doses. The only problem with this parameter is that it cannot be shown in a graph. To have the certainty that the geographical placement of the arcs will contribute to the extracranial doses for this work, some tests on a phantom (Alderson Rando Phantom for Radiotherapy, Berthold) will be done. For every treatment arc, new TLD's are placed only on the thyroid. The thyroid was chosen because it is the most sensitive organ for arc placement (qua distance isocenter – extracranial sites). The test was performed by simulating two different lesion sizes at two different locations in the brain. The first location was in the center of the head situated in the sagittal midplane area at a 5 cm depth and the second one was 3 cm off-center left of the first location and also at a 5 cm depth. The two sizes of the lesions were 0.9 and 5.9 cm respectively. The prescription dose for all lesions was 20 Gy. The 0.9 cm lesion was irradiated

Table 2. Results of the test on geographical placement of the arcs for the Novalis system

	Dose, Gy
1 cm diameter in sagittal area	0.19 ± 0.01
6 cm diameter in sagittal area	0.18 ± 0.01
1 cm diameter, 3 cm of the sagittal area	0.03 ± 0.002
6 cm diameter, 3 cm of the sagittal area	0.01 ± 0.001

with a circular mMLC shape of 1 cm diameter and the 5.9 cm with a 6 cm diameter. The table was at an angle of 90° and the gantry was rotating from 30° to 130°. Table 2 shows the results of this test. A higher contribution was observed in the central lesion with a sagittal arc compared to the one observed at the off-center lesion. Outside the central area the higher the field size, the higher the dose to the thyroid.

Risk Estimation

In table 1, the average normalized doses for every site of interest can be found, expressed in the unit gray. To give a risk estimation of the received dose, the doses must be converted to sievert (Sv), which is an SI derived unit of equivalent dose or effective dose (of radiation) and is dependent upon the biological effects of radiation as opposed to the physical aspects, characterized by the absorbed dose (measured in gray). The equivalent dose $H_{T,R}$ to a tissue is found by multiplying the absorbed dose (in gray) $D_{T,R}$ by a 'radiation weighting factor' w_R, dependent upon radiation type. The radiation weighting factor w_R can be found in ICRP 60 and is 1 for photons of all energies. This means that gray = sievert for this work, because the Gamma Knife and the Novalis use this kind of radiation.

The effective dose E to an individual can then be found by multiplying the effective dose $H_{T,R}$ by a factor dependent upon the part of the body irradiated, the 'tissue weighting factor' w_T, which can also be found in the ICRP 60. The basic idea is to express the risk from an exposure of a single organ or tissue in terms of the equivalent risk from an exposure of the whole body. The bone surface, skin and other organs (remainder) are excluded from the weighted sum and in order to be consistent with the estimation of the effective dose, there must be a normalization factor equal to the sum of w_T. Their dose equivalents are probably not negligible but not very different from the effective dose and in these circumstances, the effective dose will remain the same, whether we take these organs into account or not. In the article of 'Measurements of extracranial

doses in patients treated with Leksell Gamma Knife C' [5], De Smedt et al. found from anthropomorphic phantom measurements that the dose in depth or at the surface of the same slice of the phantom was roughly the same, which means from a radiobiological point of view that the esophagus and the thyroid, the breast and the lung, the colon, the liver and the stomach, the gonads and the bladder, are receiving the same dose. The bone marrow is a little bit more complicated, because this structure is at different placements in the body. That is why the relative contribution of the bone marrow, also based on a radiobiological point of view, will be equal to 25% to the head region, 25% for the breast region and 50% to the gonads region. The extracranial equivalent doses related to the different organs can be seen as followed: Lateral canthus dose: 25% of the bone marrow, thyroid dose: the esophagus and the thyroid itself, breast dose: the breast itself, the lung and 25% of the bone marrow, gonads dose: the gonads, the bladder and 50% of the bone marrow. The equivalent extracranial dose related to the colon, the liver and the stomach was not measured in this experiment, but these organs are located in the abdomen region, which is also situated between the breast and the gonads. The abdomen dose was calculated by taking an approximation of the dose between the one given for both the breast and the gonads. This results in an effective dose of 37 mSv and 29 mSv for the Gamma Knife and the Novalis, respectively. With the effective dose, an estimation of fatal cancer and the detriment can be done. ICRP 60 shows the occurrence of fatal cancer for every organ. The total occurrence of fatal cancer is 5%/Sv. This results in a risk estimation of a fatal cancer of 0.19% and 0.15% for the Gamma Knife and Novalis, respectively. The total detriment is then assessed by multiplying the contribution of fatal cancer probability with the contribution of severe genetic disorders, the relative length of life lost for each fatal cancer and for genetic effects, and the relative non-fatal contribution. ICRP60 shows the detrimental occurrence for every organ. The total detrimental occurrence without taking the bone surface, the remainder and the skin into account is 7.5%/Sv. This results in a percentage of detriment of 0.28 for the Gamma Knife and 0.22 for the Novalis.

Discussion

We observe from table 1 that the normalized doses for the lateral canthus are much higher for the Gamma Knife than for the Novalis. This can probably be explained because this part of the body is most of the time within the helmet and supposed to be exposed to scatter, leakage and sometimes primary direct gamma beams. Another explanation is that this organ is also supposed to be closer to the isocenter than the other sites of measurement, because of the use of

201 sources, which are placed in a hemispherical structure and only plugged when necessary for a better shape of the dose-volume histograms. The Novalis uses arcs to generate the dose to the lesion. This means that the dose to the canthus will be random and only dependent on the position of the arc. If it passes through the canthus, it will generate a higher dose. The three remaining organs in table 1 are similar in dose, a patient treated with the Gamma Knife will have almost the same dose as a patient treated with Novalis. The biggest difference will be in the way the organ dose generates from the machines.

The target maximum dose does not influence the normalized extracranial doses for both the Gamma Knife and Novalis systems.

No correlation can be made between extracranial doses and reference isodose volume for the Gamma Knife and Novalis systems. Reference isodose volume is dependent on target size. A larger size of the target does not involve a higher extracranial dose. For the Gamma Knife, there could be an explanation. Larger volumes are treated with 14 mm or 18 mm collimator helmets. The total number of shots or the total number of isocenters with such collimators is smaller, which means a shorter total treatment time.

The total amount of MU does not influence the normalized extracranial doses.

On the other hand, figures 1–4 show that the equivalent treatment time normalized at 3 Gy/min is well correlated with the extracranial doses for the Gamma knife. For the lateral canthus and gonads, correlation is not as significant as for thyroid and breast. Direct beam on the TLD's for lateral canthus can of course explain a higher variance in results. Gonad doses are usually small, so the variance can also be larger because of the uncertainties with TLD's and the lack of events. The different positioning on the patient can also influence extracranial doses because placing on gonads is not always at the same position. Another reason is that the lateral canthus is sometimes located in the helmet itself. Before discussing the next parameter, please note the following observation. When we take a close look at figures 1–4, the values on the X-axis are normalized to 3 Gy/min. The numbers of the X-axis range from 9 to 164 min, which means a target dose comparable with 27 (9 min, 3 Gy/min) and 492 Gy (164 min, 3 Gy/min). This is of course senseless and these graphs have to be interpreted as follows: First, the prescription dose is not proportional to the treatment time. The notion is, because of the multiple isocenters, the relation between the given dose to the volume and the time to get this dose varies. Finally, the given dose rate is valid for one shot of the collimator helmet of 18 mm. If we use the other three collimators (4, 8, or 14 mm), the rate will be lower and the treatment time longer.

For the Novalis (fig. 5) and the Gamma Knife systems (fig. 6), a correlation can be found between the distance and the normalized extracranial doses.

This correlation means, as can be expected, the farther the organs are situated from the source, the smaller the dose the organs receive. Also on figures 5 and 6, the inverse square law was included to the graphs, to see if both machines can be seen as a point source. The conclusion is that the Gamma Knife as well as the Novalis cannot be seen as a point source. The reason is that the Gamma Knife uses 201 collimated sources at a distance of about 40 cm between the source and the isocenter, and that the Novalis uses collimated beams at a distance of about 100 cm between the source and the isocenter. These two distances are too short to have the occurrence of the inverse square law, which can originate at a larger distance, which, on a clinical view, can of course never occur.

The results in table 2 show that there is some relation between the thyroid dose and the target size and the location. When a lesion is situated in the center (midplane sagittally), the thyroid will receive a higher dose compared to lesions situated off-center from a sagittal arc (i.e. table at 90°, gantry 30°–130°). Another fact, which can be observed, is that for these centrally located lesions the field size will not influence the dose contribution to the thyroid. If we take a look at the off-center lesion, there is an influence of the field size and of course also of the size of the lesion on the thyroid dose. This can be observed in table 2, where the thyroid receives a higher dose with the use of a larger field, because of overlapping with the thyroid.

The general conclusion is that there is a small chance of cancer induction and detriment for the patient, but it is practically non-existent. Furthermore, the benefits of such a treatment are much higher than the risk of a cancer induction. This is also a justification of the practice, which is needed to continue such a treatment [6]. Compared with the risk estimation of death due to smoking, which is 33.3% [7], the risk of cancer or detriment due to the irradiation is negligible.

Conclusion

Although there is no correlation between the extracranial dose and the prescribed dose, it might be interesting to compare the delivered prescribed dose to the intracranial lesion with the received extracranial dose. The conclusion of this study is that for the patient the received extracranial dose is little and ranges from 1.5% of the prescribed dose (24 Gy) for the lateral canthus to 0.02% for the gonads for the Gamma Knife and in the range of 0.97% of the prescribed dose (24 Gy) for the lateral canthus to 0.01% for the gonads for the Novalis. Despite these low doses, the principle of ALARA (as low as reasonably achievable) should be applied where practical [6].

The risk for a cancer induction after a radiosurgical treatment is about 0.2% for both the Gamma Knife and Novalis systems and the risk for detriment

is 0.3% for both the Gamma Knife and Novalis systems. This is of course practically non-existent, but the chance of a cancer and/or detriment because of the radiation is very small. The biggest danger remains around the lesion itself, which might receive a toxic dose when it is located in a functional region such as near the brainstem, the optical nerve, chiasm, . . . But with the TPS, the neurosurgeons try to stay under the tolerance level.

The general conclusion for the patient is that the benefit of a radiosurgical treatment is much higher than the possible cancer induction due to radiation for the patient.

The conclusion of the comparison of the extracranial doses between the Gamma Knife-system and the Novalis-system is that the received extracranial doses are comparable and in the same order of magnitude. Only at the lateral canthus a big difference can be observed.

As shown in the results, for the Gamma Knife as well as the Novalis, no correlation could be shown between maximum dose, reference isodose volume and extracranial doses. On the other hand, for the Gamma Knife the equivalent treatment time and distance have a significant influence on doses received on extracranial sites. For the equivalent treatment time the meaning is, the longer the patient stays on the treatment couch, the more doses he/she will receive on the extracranial sites (lateral canthus, thyroid, breast and gonads). The distance has less meaning, because it depends on the height of the patient. For the Novalis it is only the distance that will influence the dose and the geographical placement of the arcs. The distance is also less meaningful, as for the Gamma Knife.

References

1 Kondziolka D, Lunsford LD: Instrumentation, technique and technology. Neurosurgery 2002;50:429–432.
2 Germano IM: LINAC and Gamma Knife Radiosurgery. AANS Publication Committee, Neurosurgical Topics, 1998, pp 24–25.
3 Cheng Y, Gabor J, Apuzzo MLJ, MacPherson DN, Petrovich Z: Radiation doses for Model C Gamma Knife radiosurgery. Neurosurgery 2003;50–55.
4 Stepherd SF, Childs PJ, Graham JD, Warrington AP, Brada M: Whole body doses from linear accelerator-based stereotactic radiotherapy. Int J Radiat Oncol Biol Phy 1997;38.
5 De Smedt F, Vanderlinden B, Simon S, Paesmans M, Devriendt D, Massager N, Ruiz S, Lorenzoni J, Van Houtte P, Brotchi J, Levivier M: Measurements of extracranial doses in patients treated with Leksell Gamma Knife C. Kondziolka D (ed): Radiosurgery. Basel, Karger, 2004, vol 5, pp 197–212.
6 ICRP Publication 60: The 1990 Recommendations of the ICRP, Annals of the ICRP. Pergamon Press, 1991.
7 Bonneux LGA: Roken en kanker, Instituut voor maatschappelijke gezondheidszorg, Rotterdam, 2001.
8 Bova F, Goetsch SJ: Modern linac stereotactic radiosurgery systems have rendered the Gamma Knife obsolete. Med Phys 2001;28:1839–1841.

9 Goetsch SJ: Risk analysis of Leksell Gamma Knife model C with automatic positioning system. Int J Radiat Oncol Biol Phys 2002;52:869–877.
10 Luxton G, Petrovich Z, Jozsef G, Nedzi LA, Apuzzo ML: Stereotactic radiosurgery: Principles and comparison of treatment methods. Neurosurgery 1993;32:241–259.

Thierry Gevaert
Institut J. Bordet, Nuclear Medicine Department
121, Bd de Waterloo
BE–1000 Brussels (Belgium)
Tel. +32 254 132 59, Fax +32 253 862 84
E-Mail Thierry.gevaert@bordet.be

Kondziolka D (ed): Radiosurgery. Basel, Karger, 2006, vol 6, pp 50–59

Image-Guided Target Localization for Stereotactic Radiosurgery: Accuracy of 6D versus 3D Image Fusion

Jian-Yue Jin[a], *Samuel Ryu*[a,b], *Jack Rock*[b], *Kathleen Faber*[a], *Marilyn Gates*[b], *Shidong Li*[a], *Benjamin Movsas*[a]

Departments of [a]Radiation Oncology and [b]Neurosurgery, Henry Ford Hospital, Detroit, Mich., USA

Abstract

Purpose: This study was aimed to demonstrate the accuracy of an image-guided target localization system with 6D image fusion in a dedicated linear accelerator radiosurgery unit, and compared to that with the 3D fusion. **Materials and Methods:** An anthropomorphic phantom implanted with multiple 2 mm metal spheres was used for the study. The phantom was CT scanned with 2 mm and 3 mm slice thicknesses. Experiments were performed to evaluate the localization accuracy at 10 separate isocenters in various regions of cranium and body in the phantom. Isocenters were placed at the center of the implanted markers. Translational and rotational deviations were intentionally created at the initial setup for each isocenter. Following localization with 6D image fusion, a set of kV X-rays and MV portal images were taken to verify the isocenter position. 3D image fusion was also performed for comparison. **Results:** The accuracy of 6D fusion localization was consistently less than 1 mm for all 10 isocenters. There was no significant difference in localization accuracy (average 0.7 mm) by the thickness of CT slices between 2 mm and 3 mm. For various translational and rotational deviations in the initial setup, the accuracy of 6D fusion method was less than 1 mm, compared to that of 3D fusion where the accuracy margin could be 2–10 mm depending on the degree of initial positioning. **Conclusion:** The 6D image fusion method achieved the accuracy of target localization within 1 mm for radiosurgery of cranium and body sites. This can lead to a step forward to the non-invasive positioning for radiosurgery.

Accurate targeting is essential for intra-cranial and extra-cranial stereotactic radiosurgery and for most of the modern radiotherapy. Image guided

target localization is often employed to achieve such accurate positioning [1–6]. BrainLab Novalis unit is one of the dedicated radiosurgery systems employing such image guided localization devices. It uses a combination of the optical tracking system with the external infrared markers (ExacTrac system) and the X-ray image guidance system with the internal bony anatomy to localize the target. The external marker based ExacTrac system has a precision of 0.3 mm to identify an external marker in a phantom test [7]. However, the infrared markers are placed on the skin surface which could potentially change the relative position to the target due to skin mobility. Weiss et al. [8] reported a position variation of up to 2 cm using the ExacTrac system to setup the gynecologic cancer patients, which is similar to the uncertainty of traditional setup method using the room laser aligned to the skin tattoo.

The X-ray image guidance system directly matches the projections of internal bony structures on the X-ray images and on the digitally reconstructed radiographys (DRRs). This could greatly improve the localization accuracy for targets that is rigidly fixed to the bony structures. Unlike most of the other X-ray image guidance systems, which use either a manual match or an implanted marker based match, the earlier version of the Novalis system used an auto-fusion algorithm with 3 degrees of freedom (3D fusion) along the X, Y, and Z axes. A set of two DRRs was calculated in a fixed direction, and position deviations in three translational dimensions (X, Y, Z) were taken into consideration during the image fusion process to find the best match between the corresponding X-ray image and DRR. Because rotational deviations could exist after the patient was initially setup with the ExacTrac system, the bony structures projected to the X-ray image in a different direction would appear differently from the corresponding DRR. Therefore, this may not be, in reality, the best match between the X-ray image and DRR. This would lead the auto-fusion process to either an arbitrary position or a deviated position to the true isocenter. An image fusion algorithm with 6 degrees of freedom (6D fusion) was recently developed to address this issue. This algorithm calculates DRRs with various rotational and translational deviations and compares them with the corresponding X-ray image to find the set of DRRs with the best similarity to the set of X-ray images. The 3 rotational and 3 translational deviations used for calculating the best matching set of DRRs are then considered to be the position deviations between the setup treatment position and the simulation position.

Although the 6D fusion algorithm was expected to improve the localization accuracy, a systematic evaluation of its performance has not been published. The purpose of this study is (1) to evaluate the performance of the new

6D fusion-based image guidance system, (2) to compare the 6D fusion with the earlier 3D fusion system.

Materials and Methods

Radiosurgery and Positioning Equipment

BrainLab Novalis radiosurgery unit and ExacTrac/Novalis Body image guidance system (Version 3.5, BrainLab, AG, Heimstetten, Germany) were used in this study. The ExacTrac/Novalis Body system is the integration of the infrared optical system and the X-ray image system. The Infrared optical system is mainly composed of two infrared cameras securely mounted on the ceiling, emitting low infrared signals and monitoring the positions of infrared reflective markers placed on the patient's skin. The infrared system is not only used for initial patient setup with external infrared markers on the patient skin, but also for precise control of the treatment table by attaching the table with a 'reference star', which is consisted of 4 infrared reflective markers. The X-ray system is composed of two floor-mounted X-ray tubes projecting stereotactic beams to the corresponding flat-panel amorphous-Si detectors mounted on the ceiling. Two X-ray images are taken and fused with the 3D simulation CT images to determine the setup position deviations. The new image guidance software provides both the 6D fusion and the 3D fusion options. In addition, it provides a manual fusion option, in which the three translational dimensions can be varied by the user manually to find the best match between the X-ray images and corresponding DRRs, and an implanted marker match option, in which images are matched with the points defined by the implanted makers.

Experimental Procedure

An anthropomorphic phantom implanted with 10 metal spheres of 2 mm diameter in different regions (both cranial and thoracic regions) was used for this study. Five infrared markers were placed on the surface of the phantom. CT scan was performed with slice thicknesses of 2 and 3 mm. The CT images were imported into the BrainScan treatment planning system. The first set of experiments was to evaluate the localization accuracy of the 6D fusion-based image guidance system. Each implanted metal sphere served as an isocenter in different locations. The phantom was first setup with the external infrared markers, and then was intentionally moved to a position with deviations of 1–5 cm in translational directions, and 1–2 degrees in rotational directions. Localization X-ray images were taken and the 6D fusion was performed. The phantom's position was then adjusted in three translational directions to the isocenter according to the fusion result. A set of verification kV X-ray images and MV portal images were taken to verify the isocenter position. The localization error was determined by comparing the position of the isocenter to the center of the metal sphere. The second set of experiments was to compare the 6D fusion with the 3D fusion for various initial setup positions. An isocenter was selected at the center of a metal sphere in the thoracic vertebrae region. The phantom was setup with either a fixed rotational deviation (1–2 degrees in each rotational direction) with various translational (−5 to 5 cm in the longitudinal direction), or a fixed translational deviation (1–5 mm in each translational direction) with various rotational deviations along the AP direction (−5 to 5 degree). Localization X-ray images were taken for each deviated setup, and image fusions were performed with algorithms of 3D fusion, 6D fusion and implanted marker match for each deviated position.

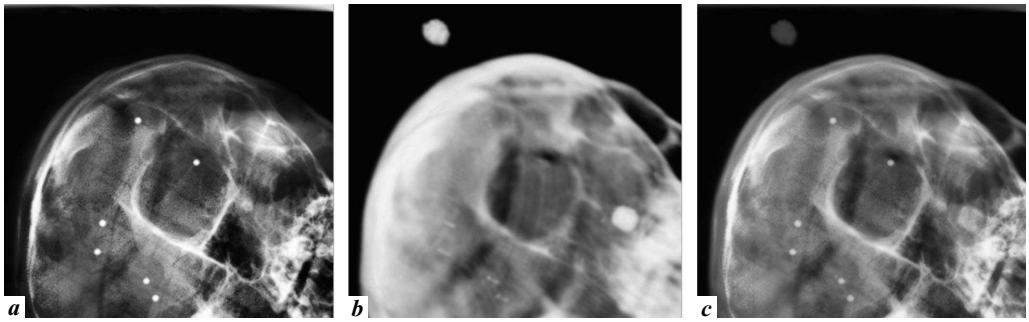

Fig. 1. 6D fusion of X-ray images with corresponding DRR. ***a*** X-ray image, (***b***) DRR, and (**c**) fusion (mixed) image of (***a***) and (***b***).

During 3D and 6D fusion processes, the areas where the metal spheres were located were excluded to ensure that only the phantom structures were used for the fusion. The deviations detected by each fusion method were recorded and compared. The implanted marker match method was used as the standard in this experiment.

Results

The kV X-ray image had a high spatial and contrast resolution. The detailed bony structures as well as the metal spheres were clearly distinguishable. The DRR appeared to have relatively low resolution. Due to CT artifacts for metal material, the metal spheres appeared to be distorted into elongated objects. Figure 1 shows a kV localization X-ray image of an isocenter at the cranial region (a), the corresponding DRR (b), and the fusion (mixture) image after 6D fusion (c). The corresponding anatomic structures appeared to be well matched in this image. However, quantitative match results were difficult to obtain purely based on anatomic land markers.

Figure 2a and b show a pair of kV X-ray images after the table position was readjusted according to the 6D fusion guided localization. The cross at the center of image represents the isocenter position of the X-ray system. The distance between the center of the sphere and the cross in an image represents the isocenter deviation in the image plane. The overall spatial deviation (3D vector D) could be approximately calculated as

$$D = \sqrt{(d^2_{\text{image 1}} + d^2_{\text{image 2}}) * 3/4}, \quad (1)$$

by assuming that the deviations were equally distributed in three main orthogonal coordinates, where $d_{\text{image 1}}$ and $d_{\text{image 2}}$ are the deviations in image 1 and

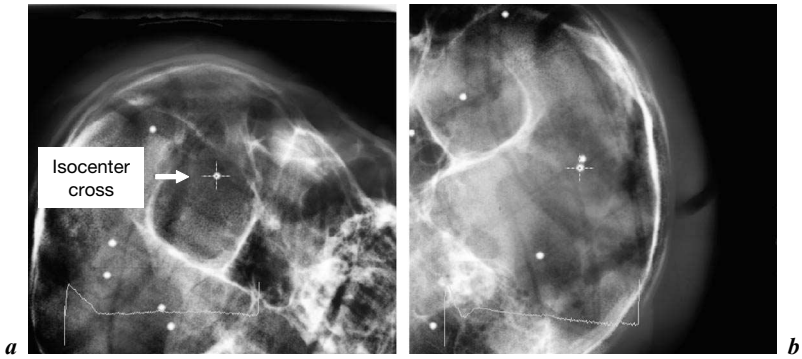

Fig. 2. Two verification X-ray images for evaluation of deviation between the X-ray isocenter (cross) and the planned isocenter (center of the metal sphere). The cross mark (arrow) at the center of image represents the isocenter position of the X-ray system.

Table 1. Target localization errors of the 6D image fusion method in 10 different isocenters evaluated by kV X-rays and MV portal films in an anthropomorphic phantom

CT slice thickness mm	By kV X-rays			By MV portal film		
	Image 1 mm	Image 2 mm	Overall	Image 1 mm	Image 2 mm	Overall
2	0.52 ± 0.25	0.59 ± 0.21	0.68 ± 0.28	0.58 ± 0.19	0.61 ± 0.14	0.73 ± 0.20
3	0.61 ± 0.23	0.67 ± 0.19	0.78 ± 0.26	0.62 ± 0.17	0.59 ± 0.24	0.74 ± 0.25

image 2, respectively. However, this spatial deviation only represents the localization position related to the X-ray system's isocenter. To determine the repositioning accuracy for the actual treatment isocenter (the Linac's isocenter), orthogonal MV portal films were taken on the radiosurgery treatment table after repositioning. The spatial deviation between the planned isocenter (the center of the metal sphere) and the actual treatment isocenter (the center of the portal film) was calculated similarly as Equation (1), where $d_{\text{image 1}}$ and $d_{\text{image 2}}$ are the deviations in two portal films, film 1 and film 2, respectively.

First, we tested the effect of slice thickness of the CT scan because DRRs are reconstructed from these images. There was no significant difference of accuracy between 2 mm and 3 mm thickness slices. The 6D fusion method was able to localize each isocenter within a 1-mm-radius circle defined by the corresponding metal sphere on each projected image plane. The average accuracy was in the order of 0.7 mm. The results are shown in table 1 as the mean of the

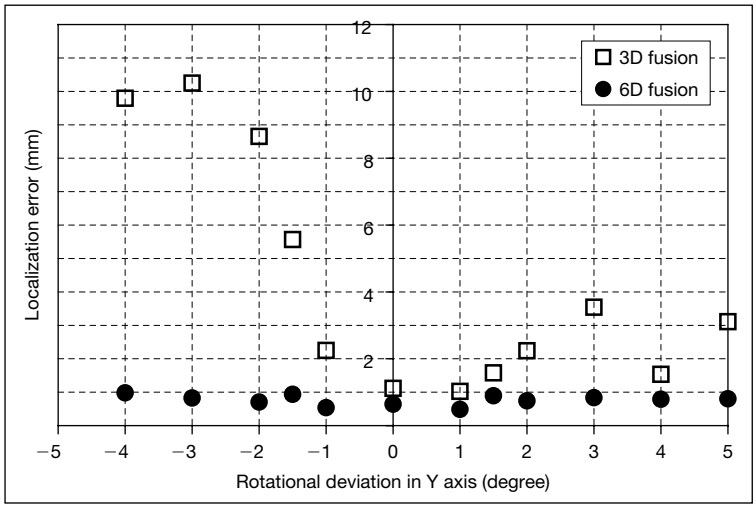

Fig. 3. Accuracy of localization according to the rotational deviation created in the initial setup for the 3D and 6D fusion methods. The variation of isocenter was drawn as a function of rotational deviation created along the anterior-posterior (Y) axis.

localization errors and their standard deviation for 10 isocenters determined by the kV X-ray images and by the MV portal films. The localization accuracy determined by the kV X-ray images was consistent with that determined by the MV portal image, indicating that the isocenter of the X-ray system coincided with the isocenter of the Linac. We have also tested the implanted-marker-match method with verification X-ray images and portal films, and confirmed that implanted marker match was a reliable and accurate localization method.

Then, we tested the importance of rotational deviation in localization accuracy. Based on the previous result, 3 mm thickness CT images were used in this test. The localization error was calculated using the implanted marker method as the standard. Overall spatial deviation for the isocenter was calculated as

$$D = \sqrt{(x_f - x_i)^2 + (y_f - y_i)^2 + (z_f - z_i)^2}, \tag{2}$$

where x_i, y_i, z_i were the three translational deviations obtained from the implanted markers method, and x_f, y_f, z_f were the three translational deviations from the 3D or 6D fusion method. For each initial setup position, the three translational dimensions were fixed with deviations of about 1–5 mm. Only one rotational angle (table rotation) was varied for different setup position. The other two rotation dimensions were fixed with small deviations from 0.5–1.0 degree. Figure 3 shows the localization error secondary to rotational deviation

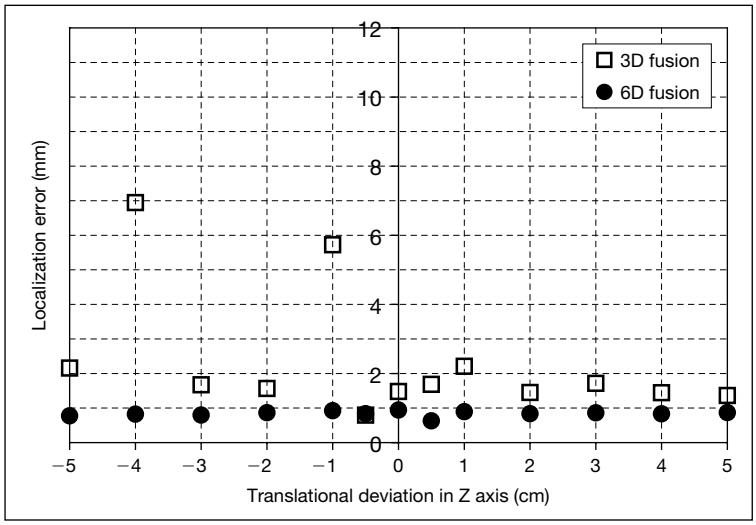

Fig. 4. Accuracy of localization according to the translational deviation created in the initial setup for the 3D and 6D fusion methods. The variation of isocenter was drawn as a function of translational deviation created along the superior-inferior (Z) axis.

by using 3D fusion and 6D fusion methods for the same isocenter. The results of 3D fusion method showed a large variation of localization accuracy particularly when the rotational deviation was greater than 2 degrees. The localization error reached up to about 2 mm at smaller rotational angles. In sharp contrast, the overall localization error was less than 1 mm by 6D fusion method for all different initial setup positions. This accuracy level was not changed by large rotational angle created at the initial setup.

To determine the accuracy by 6D fusion method in regards to the translational deviation, three rotational dimensions were fixed with deviations of 0.5–2 degrees at each angle. For the translational dimensions, only the longitudinal direction was varied for different setup position. The other two dimensions were fixed with small deviations from 2 to 5 mm. For 3D fusion method, the localization error was generally within 1.4–2.2 mm for most of the initial setup positions, with a large variation of 6–7 mm at certain setup positions. However, the overall localization accuracy for 6D fusion was within 1 mm for all different initial setup positions, and there was little variation with the longitudinal deviation created at the initial setup. These results are shown in figure 4. The results indicate that the 6D fusion method consistently improved the localization accuracy and reliability than the 3D fusion method. Table 2 summarizes the statistical results of the mean localization errors and their standard deviations in three

Table 2. Target localization errors for the 3D and 6D fusion methods at different initial setup positions evaluated by the implanted marker method

Fusion method	Localization error for initial setup positions with various rotational deviations, mm			Localization error for initial setup positions with various translational deviations, mm		
	X	Y	Z	X	Y	Z
3D	−1.07 ± 1.93	−2.93 ± 2.63	1.61 ± 2.71	0.54 ± 0.92	−0.65 ± 1.13	0.52 ± 2.45
6D	0.56 ± 0.18	−0.51 ± 0.20	0.03 ± 0.21	0.61 ± 0.10	−0.52 ± 0.16	0.02 ± 0.19

translational dimensions for different setup positions. The mean localization error was 0.56 mm, −0.51 mm and 0.03 mm in X (lateral), Y (AP) and Z (longitudinal) axes for setup positions with different rotational angles, and 0.61 mm, –0.52 mm and 0.02 mm in three axes for setup positions with different translational deviations. There was a systematic difference about 0.6 mm in the lateral direction, and −0.5 mm in the AP direction, between the 6D fusion method and the implanted marker method for this isocenter.

Discussion

From phantom studies, we have demonstrated that the 6D fusion method could achieve sub-millimeter accuracy for various isocenter positions in the cranial and thoracic regions, and for various initial setup positions with different translational and rotational deviations. Substantial improvement was observed for the 6D fusion method compared to the 3D fusion, when significant rotational deviation existed at the initial setup positions.

The mean of the localization errors usually represents the systematic error, or the accuracy of the localization method. Because the evaluation techniques would have a component of inherent inaccuracy, the mean of the localization errors should represent the systematic difference of the isocenter positions determined by the 6D fusion method and by the measurement technique here. The standard deviation represents the random error, the precision, or the uncertainty of the localization method. As shown in table 2, the standard deviation for the 6D fusion method in each direction was ranging from 0.1 mm to 0.21 mm for different initial setup positions. For various initial setup variations up to ±5 cm in a translational direction, or up to ±5 degrees in a rotational direction, the 6D fusion method was able to localize the isocenter to the same position with about 0.2 mm standard deviation in each main orthogonal

direction. This suggests that 6D fusion has a superior precision to localize the target. However, there was a systematic difference about 0.6 mm in the lateral direction, and −0.5 mm in the AP direction, between the 6D fusion method and the implanted marker match method. This systematic error seemed to vary slightly from isocenter to isocenter in the same CT image set, and seemed to be relatively larger for isocenters between the different CT image sets. We speculate that this systematic error could potentially come from the following sources: (1) image artifacts for the metal sphere in the CT image, (2) limited spatial resolution of the CT image, and (3) the uncertainty of reconstructing the DRR in the fusion software. Nevertheless, this systematic error is less than 1 mm, indicating that the 6D fusion method is a reliable and accurate target localization technique.

Our results indicate that accurate localization can be achieved by 6D image fusion guidance for both cranium and body sites. This level of accuracy is suitable for radiosurgery, and provides a good basis to use for non-invasive radiosurgery of the brain and body sites such as spine. It should be pointed out that the study was carried out in an anthropomorphic phantom. The application of this technique to real patients could have different implications. In a cranial case, because the bony structure is usually rigid, the relative positions of all the bony anatomic details should be same between simulation and treatment. However, in extra-cranial cases, such as spinal radiosurgery, the bony structure (mainly the vertebrae) of a patient could have slightly different curvatures between the simulation and treatment due to potential setup position difference and breathing motion. We are testing the accuracy and performance of 6D image fusion in the patients who receive radiosurgery to the spine or the cord. Our preliminary experience shows that more than 95% of the patients have satisfactory accuracy for radiosurgery using the 6D image fusion. The factors that seem to create any difficulty include poor image quality of large patients, organ motion of the ribs, and the bony structures that obscure the image fusion process by overlap of shoulder or pelvic bones, as well as variation of spine curvature. We think these factors may contribute inconsistency of simulation and treatment positions. This clinical study is in progress for non-invasive radiosurgery of the brain and the spine.

References

1 Murphy MJ: An automatic six-degree-of-freedom image registration algorithm for image-guided frameless stereotaxic radiosurgery. Med Phys 1997;24:857–866.

2 Ryu S, Fang Yin F, Rock J, Zhu J, Chu A, Kagan E, Rogers L, Ajlouni M, Rosenblum M, Kim JH: Image-guided and intensity-modulated radiosurgery for patients with spinal metastasis. Cancer 2003;97:2013–2018.

3 Yin FF, Ryu S, Ajlouni M, Yan H, Jin JY, Lee SW, Kim J, Rock J, Rosenblum M, Kim JH: Image-guided procedures for intensity-modulated spinal radiosurgery. Technical note. J Neurosurg 2004;101(suppl 3):419–424.
4 Jaffray DA, Siewerdsen JH, Wong JW, Martinez AA: Flat-panel cone-beam computed tomography for image-guided radiation therapy. Int J Radiat Oncol Biol Phys 2002;53:1337–1349.
5 Cheng CW, Wong J, Grimm L, Chow M, Uematsu M, Fung A: Commissioning and clinical implementation of a sliding gantry CT scanner installed in an existing treatment room and early clinical experience for precise tumor localization. Am J Clin Oncol 2003;26:e28–e36.
6 Pouliot J, Bani-Hashemi A, Chen J, Svatos M, Ghelmansarai F, Mitschke M, Aubin M, Xia P, Morin O, Bucci K, Roach M 3rd, Hernandez P, Zheng Z, Hristov D, Verhey L: Low-dose mega-voltage cone-beam CT for radiation therapy. Int J Radiat Oncol Biol Phys 2005;61:552–560.
7 Wang LT, Solberg TD, Medin PM, et al: Infrared patient positioning for stereotactic radiosurgery of extracranial tumors. Comput Biol Med 2001;31:101–111.
8 Weiss E, Vorwerk H, Richter S, Hess CF: Interfractional and intrafractional accuracy during radiotherapy of gynecologic carcinomas: a comprehensive evaluation using the ExacTrac system. Int J Radiat Oncol Biol Phys 2003;56:69–79.

Jian-Yue Jin, PhD
Department of Radiation Oncology, Henry Ford Hospital
2799 W. Grand Blvd
Detroit, MI 48202 (USA)
Tel. +1 313 916 0234, Fax +1 313 916 3235
E-Mail jjin1@hfhs.org

Kondziolka D (ed): Radiosurgery. Basel, Karger, 2006, vol 6, pp 60–70

Analyzing 3.0 T MRI-Scanners for Implementation in Radiosurgery

Andreas Mack[a], *Robert Wolff*[a], *Stefan G. Scheib*[f], *Marcus Rieker*[b], *Dirk Weltz*[b], *Guenther Mack*[b], *Hans-Jürg Kreiner*[c], *Ulrich Pilatus*[d], *Friedhelm E. Zanella*[d], *Heinz D. Böttcher*[e], *Volker Seifert*[d]

[a]Gamma Knife Centre, Frankfurt, [b]PTGR-GmbH, Tübingen, [c]GKS/GKF GmbH, München, Departments of [d]Neuroradiology and [e]Radiotherapy, University Hospital, Frankfurt, Germany; [f]Department of Medical Radiation Physics, Klinik Im Park, Zürich, Switzerland

Abstract

Introduction: Given the high mechanical accuracy of the Leksell Gamma Knife®, the most sensitive technical factor having an influence on the overall precision of radiosurgery is the imaging (mainly magnetic resonance imaging (MRI)) study. The new generation of MRI-Scanners with field strength up to 3.0 T deliver promising image quality concerning anatomical resolution and contrast but critical features are the sensitivity to susceptibility and chemical shift effects both creating artefacts. **Methods:** The 3.0 T MRI-Scanner (Siemens 'Trio') was analyzed and compared to a Siemens Magnetom 'Expert' 1.0 T and to a Philips 'Gyroscan' 1.5 T. The analyses was performed in three steps: (1) The evaluation of the magnitude of error was performed within transversal slices in two orientations (axial/coronal) by using a cylindrical phantom with an embedded grid. (2) The deviations were determined for 21 targets in a slab phantom with known geometrical positions within the stereotactic frame. (3) Distortions caused by chemical shift and/or susceptibility effects were analyzed in a head-phantom. An in-house developed software was used for data analyses. **Results:** The 3.0 T MRI-Scanner was analyzed using sequences in axial and coronal orientations. The mean deviation was <0.3 mm in axial and <0.4 mm in coronal orientation. For the known targets the maximum deviation came up to 1.16 mm (far from the center). Due to inhomogeneities a shift in z-direction up to 1.5 mm was observed for a data set which was shown compressed by 1.2 mm. By optimizing these parameters in the protocol these inaccuracies could be reduced to <1.1 mm. **Conclusions:** The scanner showed up with sophisticating anatomical contrast and resolution in comparison to the established 1.0 T and 1.5 T scanners. However, due to the high-field strength the field within the head coil is very sensitive to inhomogeneities and therefore 3.0 T imaging data still have to be handled with care.

The use of magnetic resonance imaging (MRI) as the primary imaging modality in radiosurgery has become increasingly attractive because of its excellent depiction of the brain's normal anatomy and demonstration of lesions not seen with other imaging modalities [1–7]. However, this technique is plagued by image distortion, a problem not seen with the earlier X-ray of ventriculography and computed tomography.

The problem of MRI distortion for stereotactic radiosurgery is multifactorial, complex, variable and just beginning to be understood [8–11]. It can produce significant errors in localization [3]. This is important for small lesions and functional stereotactic targets. There is not yet any commercial system which reliably circumvents all such distortions. Accurate target localization in any facility must rely on rigorous 'in house' testing, problem solving and ongoing accuracy assessment to ensure appropriate precision [12–22].

Our interest in this issue began after we noted errors and a shift in target localization when searching on suitable parameters for a 3D-sequence for a 3.0 T MRI-Scanner (Siemens 'Trio').

Here we quantitatively compare the coordinates of phantom rods arranged in an embedded grid, targets (cross hairs) and edges (interfaces) defined using the mentioned MRI-scanner with geometrically known positions.

Further on we compare and discuss these findings with the results from a 1.0 T MRI-Scanner (Siemens 'Magnetom') and of a 1.5 T MRI-Scanner (Philips 'Gyroscan').

Materials and Methods

The study was carried out using a 3.0 T MRI-Scanner (Siemens 'Trio'). A Leksell frame made of aluminum together with carbon posts and titanium screws and the corresponding fiducial box filled with copper sulphate served as the stereotactic coordinate system.

Three different phantoms, manufactured by PTGR Germany, were used in this process of optimizing sequence parameters (see fig. 1). A cylindrical phantom (Ø175 mm) with an embedded grid of 145 rods made of fiber glass (see fig. 2a) served as the basis in evaluating the magnitude of error within transversal slices in two orientations (axial/coronal). The 'known target phantom' (developed by S. Scheib, Switzerland) consisting of slabs with embedded targets (glass vials Ø3 mm (outside), Ø1.5 mm (inside)) at geometrically exactly known positions within the stereotactic coordinate system (see fig. 2b) was used to determine the deviations in stereotactic space. A head phantom, developed by PTGR Germany, was used to analyze distortions caused by chemical shift and susceptibility effects. This phantom consists of two hemispheres (Ø150 mm) made of plastic (PMMA) which can be enclosed by a shell of PTFE (Ø160 mm) to simulate the structure of the skull (see fig. 3b). The two hemispheres have a cubic clearance of (72 mm^3) which can be filled with slabs of different materials (see fig. 2c). The phantom is mounted to the stereotactic frame by specially developed adapters (see fig. 3c). To guarantee a defined geometrical position, the

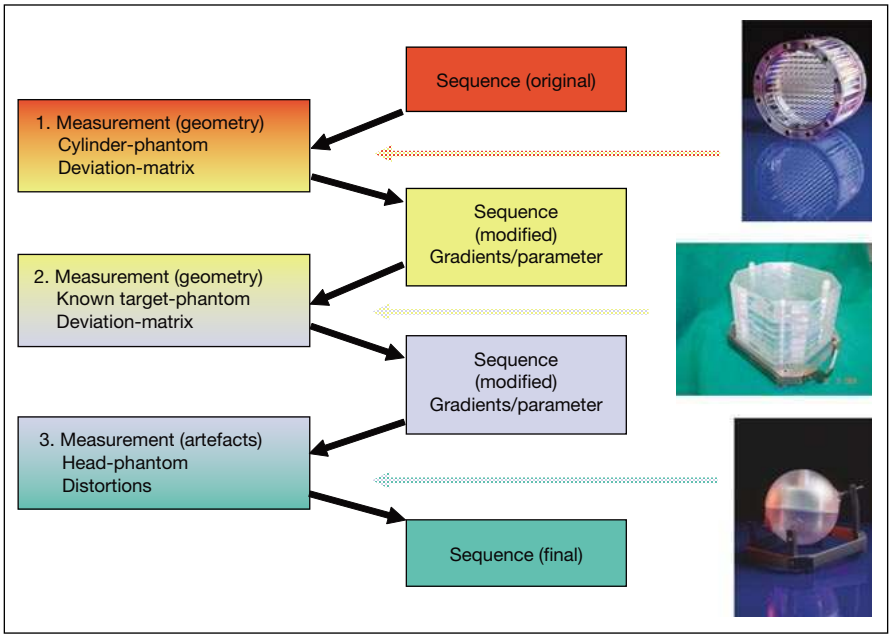
Sequence (original)
1. Measurement (geometry)
Cylinder-phantom
Deviation-matrix
Sequence
(modified)
Gradients/parameter
2. Measurement (geometry)
Known target-phantom
Deviation-matrix
Sequence
(modified)
Gradients/parameter
3. Measurement (artefacts)
Head-phantom
Distortions
Sequence (final)

1

2a

b

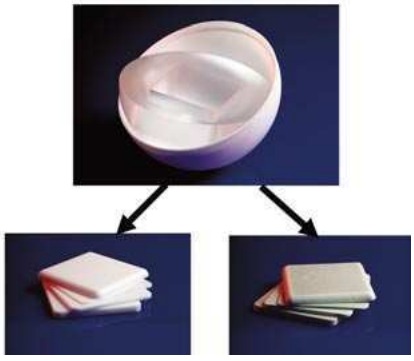

c

3a

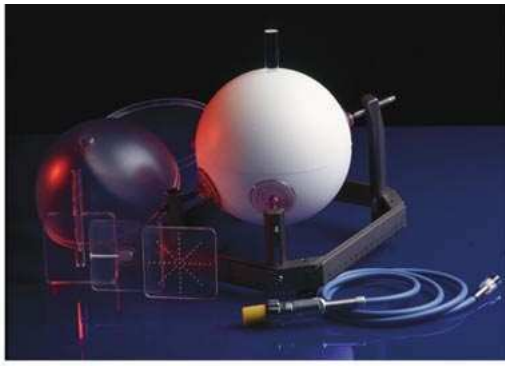

b

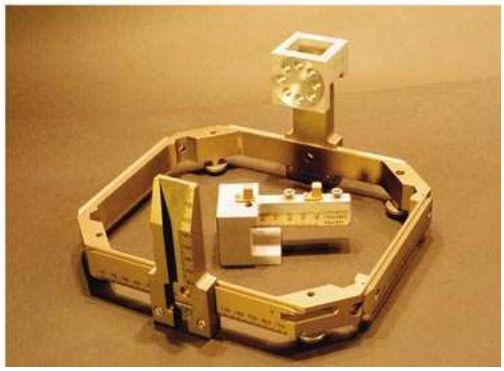

c

phantom can be positioned and adjusted by these adapters fitting the slides of the Leksell frame (see fig. 3a).

The quantitative analysis was performed by using a software, developed by PTGR Germany. The deviations in location were measured for every rod in the cylinder phantom and compared to the position in the corresponding reference grid. The errors in location for

Fig. 1. Protocol for optimizing the parameters of a MRI sequence. In a first step the deviation matrix is determined with a cylindric grid phantom. After adjusting the parameters of the sequence the deviations are determined with the 'known target phantom'. After further modification of the parameters, distortions due to chemical shift and susceptibility effects are analyzed with a head phantom leading to the final optimized parameters.

Fig. 2. Phantoms for quality assurance (QA) in stereotactic radiosurgery: (***a***) precise cylinder phantom containing a grid of 145 rods; (***b***) known target phantom consisting of slabs with 21 embedded known targets (cross hairs with glass vials); (***c***) head phantom consisting of spheres and shells and a cubic clearance for inserts (slabs of different materials, detectors of all kind).

Fig. 3. Positioning device for head phantom: (***a***) the phantom is fixed to adapters by plastic pins; (***b***) the head phantom can be enclosed by shells of PTFE to represent the bony structure of the skull. Furtheron the cubic clearance can be filled with different materials and can take a variety of detectors as well, (***c***) adapters which fit into the slides of the Leksell frame system.

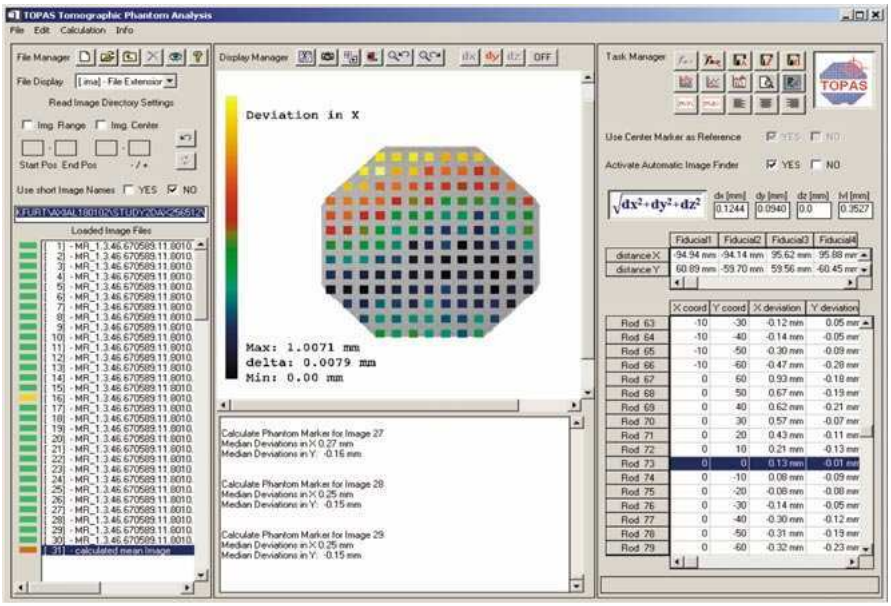
TOPAS Tomographic Phantom Analysis
File Edit Calculation Info
File Manager
Display Manager
Task Manager
Deviation in X
Max: 1.0071 mm
delta: 0.0079 mm
Min: 0.00 mm
Loaded Image Files
Use Center Marker as Reference
Activate Automatic Image Finder
Calculate Phantom Marker for Image 27
Median Deviations in X 0.27 mm
Median Deviations in Y: -0.16 mm
Calculate Phantom Marker for Image 28
Median Deviations in X 0.25 mm
Median Deviations in Y: -0.15 mm
Calculate Phantom Marker for Image 29
Median Deviations in X 0.25 mm
Median Deviations in Y: -0.15 mm

4

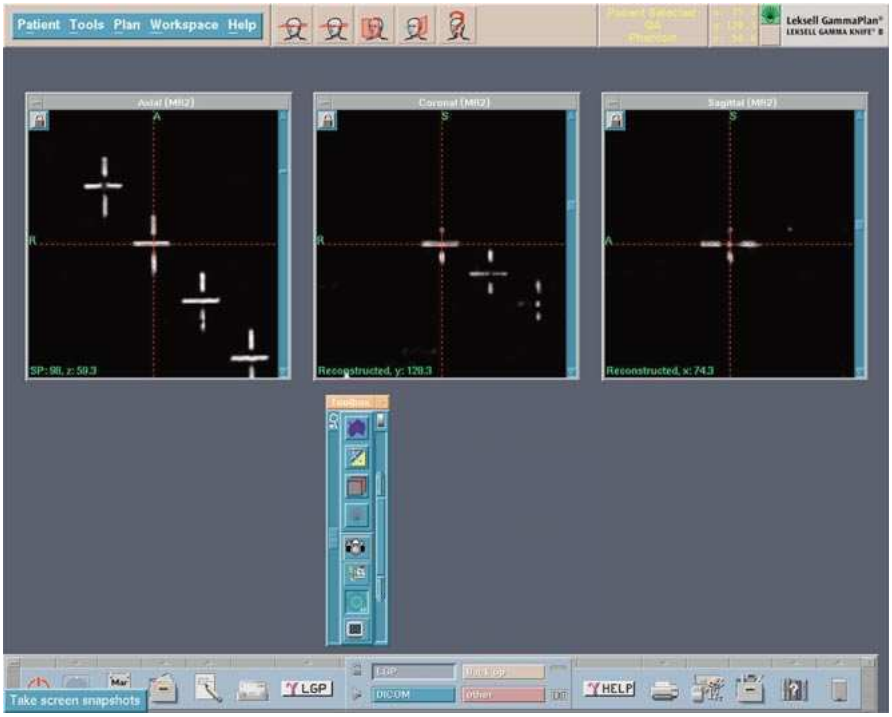
Patient Tools Plan Workspace Help
Leksell GammaPlan
Axial (MR2)
Coronal (MR2)
Sagittal (MR2)
Reconstructed, y: 128.3
Reconstructed, x: 74.3
Take screen snapshots
LGP
HELP

5

the cross hairs (targets) and the interfaces of the inhomogeneous layer in the head phantom were determined by Gamma Plan 5.34 after definition of the images.

Results

A 3.0 T MRI-Scanner (Siemens 'Trio') was analyzed in this investigation, subdivided into three categories.

In a *first step* the magnitude of error was determined using the cylindrical grid phantom delivering a deviation matrix for transversal scans in axial and coronal orientations (fig. 4). The mean deviation for all images in this example was < 0.3 mm in axial and < 0.4 mm in coronal orientation. The maximum displacement error came up to 1 mm (represented in red color) the minimal error was 0 mm.

In the *second step* the 'known target' phantom was used coming up with a maximum absolute error of 1.16 mm being in good accordance to the results from measurement taken with the cylinder phantom (see fig. 5 and table 1). However, we have to keep in mind that these images were defined and analyzed by LGP so that the displacement error is a combination of the true displacement caused by the imaging modality itself and a superimposed additional intrinsic error within the definition process (transformation etc.).

In the *last step* the head phantom was used to determine sensitivities to chemical shift and susceptibility phenomena due to inhomogeneities in the phantom. For an embedded layer of PTFE ($\rho = 2.2$ g/cm^3) a general shift of the interface could be observed (see fig. 6) with a maximum deviation of 1.5 mm mainly at low z-values. After definition of the images the data set was compressed by 1.2 mm.

The complete procedure of all three measurements was performed several times always after having changed the corresponding sensitive parameters of the sequence ending up with the setups shown in table 2.

Discussion and Conclusion

Distortions of MR images for stereotactic localization arise from a number of sources, but some of these problems are being solved with the advances in scanner

Fig. 4. Evaluation after the first step of optimization. Determination of the geometrical accuracy in axial orientation. The deviations for every rod are represented in the lower right table.

Fig. 5. Evaluation after the second step of optimization. Determination of the geometrical accuracy of 21 targets with known geometrical positions and coordinates in stereotactic space. The cross hairs are represented in LGP in all orientations.

Table 1. Siemens 3.0 T ('Trio'): Example of results for the verification of the 21 geometrically known positions (targets) in stereotactic space. The right column shows the distance to position 100/100/100 in the Leksell stereotactic coordinate system

Marker number	Target coordinates			Measured coordinates			Absolute errors				Distance
	x/mm	y/mm	z/mm	x/mm	y/mm	z/mm	dx/mm	dy/mm	dz/mm	dr/mm	D/mm
1	100.0	70.0	45.0	100.3	68.9	44.7	0.3	1.1	0.3	1.18	62.6
2	75.0	100.0	45.0	75.4	98.9	44.9	0.4	1.1	0.1	1.17	60.4
3	150.0	40.0	60.0	150.3	39.5	59.2	0.3	0.5	0.8	0.99	87.7
4	125.0	70.0	60.0	125.3	69.0	59.5	0.3	1.0	0.5	1.16	55.9
5	100.0	100.0	60.0	100.0	99.5	59.7	0.0	0.5	0.3	0.58	40.0
6	75.0	130.0	60.0	75.2	130.7	59.6	0.2	0.7	0.4	0.83	55.9
7	50.0	160.0	60.0	50.0	159.2	60.1	0.0	0.8	0.1	0.81	87.7
8	100.0	130.0	75.0	100.1	129.6	75.0	0.1	0.4	0.0	0.41	39.1
9	50.0	40.0	90.0	50.0	39.5	89.8	0.0	0.5	0.2	0.54	78.7
10	150.0	100.0	90.0	150.3	99.3	89.7	0.3	0.7	0.3	0.82	51.0
11	125.0	130.0	90.0	125.1	129.6	90.0	0.1	0.4	0.0	0.41	40.3
12	25.0	70.0	105.0	25.3	69.6	104.7	0.3	0.4	0.3	0.58	80.9
13	175.0	130.0	120.0	175.1	129.8	119.8	0.1	0.2	0.2	0.30	83.2
14	150.0	160.0	120.0	150.0	159.8	120.0	0.0	0.2	0.0	0.20	80.6
15	100.0	40.0	135.0	100.2	39.7	134.7	0.2	0.3	0.3	0.47	69.5
16	75.0	70.0	135.0	75.3	69.6	134.8	0.3	0.4	0.2	0.54	52.4
17	50.0	100.0	135.0	50.1	99.6	134.5	0.1	0.4	0.5	0.65	61.0
18	25.0	130.0	135.0	25.0	129.4	134.7	0.0	0.6	0.3	0.67	88.0
19	175.0	70.0	150.0	175.1	69.5	149.8	0.1	0.5	0.2	0.55	95.0
20	125.0	100.0	150.0	124.9	99.7	149.4	0.1	0.3	0.6	0.68	55.9
21	100.0	160.0	150.0	99.6	160.2	149.6	0.4	0.2	0.4	0.60	78.1

technology available in most centers [23–25]. For example most nonlinearities in the magnetic gradient field are now been corrected by a combination of MRI internal mathematical corrections (compensation circuits – routinely used in current scanners) and the use of volume as opposed to slice acquisition [26, 27]. Chemical shifts can occur at fatty interfaces and necessitate avoidance of this material in fiducials and consideration in certain scanning protocols, when this material is in the patient and near the target. Magnetic field inhomogeneities which arose from variations in the main magnetic field have been largely obviated in current scanners with routine 'shimming' [11]. One proposed solution to the distortion problem is fusion of MR with computed tomography images [22, 28]. Image fusion, however, is not without its own potential for error and may introduce localization inaccuracies as large as, or greater than, those obtained with stereotactic imaging. On the other hand, object-induced inaccuracies remain a concern. Differences in magnetic susceptibility (e.g. between tissue and air) can produce local distortions which need

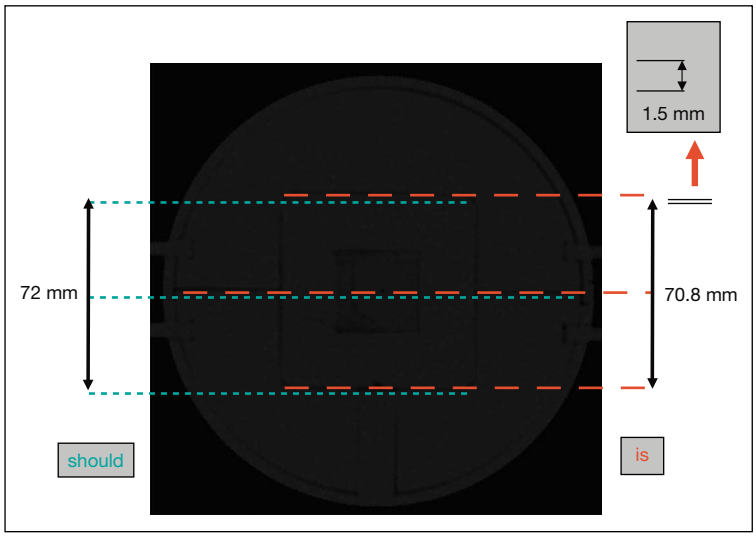

Fig. 6. Evaluation after the final step of optimization. The impact of chemical shift and susceptibility artefacts on the accuracy of MR imaging is shown. The set of images is compressed (in this example by 1.2 mm) and a shift in z-direction can be observed (1.5 mm).

to be recognized. Metal in the field produces artefacts [3]. Although methods for automatic distortion correction, which would rectify these latter two types of distortion, are being developed, they are not generally available at present [29, 30].

In this paper, we describe observed inaccuracies mainly due to chemical shifts and susceptibility artefacts. Because of the high field strength, these artefacts are dominant compared to the always apparent artefacts mentioned above. After adjusting the corresponding sensitive parameters in the protocol the error resulted in the order of <1.1 mm.

A variety of methods have been used to assess image and target distortions for stereotactic localization [31–35]. However only a few authors compare the deviations to given coordinates of a 'known target phantom' which we used in addition to a cylindrical grid phantom. By using different phantoms (e.g. head phantom with embedded inhomogeneities) we could distinguish between deviations and general shift phenomena. The derivation of this shift and also the fact that the data sets are compressed is still not clear. The shift itself is probably an effect caused by the high field strength overlaying the common distortions already mentioned (e.g. stereotactic frame), whereas the compression of the data set in z-direction is still in discussion. The values for slice thickness and z-positions strongly depend on the usage of the routine for defining images in the planning system (LGP 5.34) which could be an explanation.

Table 2. Optimized sequence parameters for different MRI-Scanners derived from the measurements of the optimization process

Specification	Gyroscan Philips 1.5 T	Magnetom-expert Siemens 1.0 T	Magnetom-Trio Siemens 3.0 T
Sequence	T1-3D	T1-3D-mpr	T1-3D-mpr
FOV	210	250	260
ROV	100	80	
Foldover suppression	No	No	
Matrix	256	256	256
Reconstruction	256	256	256
Scan %	65	100	100
Overcontinuous slices	No		
Slices	100	128	160
Slice thickness	1.5	1.5	1.0
Foldover direction	RL	PA	RL
Interactive positioning	N/A	0	0
Scan mode	3D	3D	3D
Technique	FFE	TFE	TFE
Fast imaging mode	None		Yes
Gradient mode	Default		
SAR mode	High		
Echos	Yes	1	
Partial echo	No		
Shifted echo	No		
TE, ms	Shortest	4.4 ms	2.6 ms
Flip angle	30	10	15
TR, ms	25	11.4	1240
Water fat shift	User defined		
Contrast enhancement		T1	T1
Shim	No	No	No
SPIR		No	No
Zoom imaging		No	No
Diffusion mode		No	No
NSA	1	1	2

Whereas the grid phantom is convincing in the representation of displacement errors in one plane (at a time (axial/coronal)) with a fine resolution (every 10 mm), the 'know target' phantom can demonstrate inaccuracies for 21 targets, spread out in stereotactic space in one measurement only with the disadvantage of having a spoarse spatial resolution. Both phantoms, however, can be used to determine deviations to a given reference. The head phantom can be used for several purposes and besides serves as an ideal tool for modelling dose distributions.

We used our set of phantoms not only to determine the spatial inaccuracies but also to optimize the sensitive parameters of the corresponding sequence. In this content it was interesting to see that although the automatic shimming was turned off (see table 1), the results could even be improved. This again proves the very complex interplay of many parameters which all have to be taken into consideration when optimizing the sequence protocol.

References

1 Alexander E, Kooy HM, van Herk M, Schwartz M, Barnes PD, Tarbell N, Mulkern RV, Holupka EJ, Loeffler JS: Magnetic resonance image-directed stereotactic neurosurgery: use of image fusion with computerized tomography to enhance spatial accuracy. J Neurosurg 1995;83:271–276.
2 Carter DA, Parsai EI, Ayyangar KM: Accuracy of magnetic resonance imaging stereotactic coordinates with the Cosman-Roberts-Wells frame. Stereotact Funct Neurosurg 1999;72:35–46.
3 Condon B, Hadley D: Errors in MR stereotaxy due to undetected extraneous metal objects. Phys Med Biol 1997;42:1779–1789.
4 Ehricke HH, Schad LR, Gademann G, Wowra B, Engenhart R, Lorenz WJ: Use of MR angiography for stereotactic planning. J Comput Assist Tomogr 1992;16:35–40.
5 Kondziolka D, Lunsford LD, Kanal E, Talagala L: Stereotactic magnetic resonance angiography for targeting in arteriovenous malformation radiosurgery. Neurosurgery 1994;35:585–590; discussions 590–591.
6 Schulder M, Holodny A, Liu WC, Gray A, Lange G, Carmel PW: Functional magnetic resonance image-guided surgery of tumors in or near the primary visual cortex. Stereotact Funct Neurosurg 1999;73:31–36.
7 St George EJ, Butler P, Plowman PN: Can magnetic resonance imaging alone accurately define the arteriovenous nidus for gamma knife radiosurgery? J Neurosurg 2002;97(5 suppl):464–470.
8 Choi DR, Ahn YC, Kim DY, Huh SJ, Lee JI: Accuracy in target localization in stereotactic radiosurgery. Med Dosim 1997;22:53–58.
9 Ertl A, Saringer W, Heimberger K, Kindl P: Quality assurance for the Leksell gamma unit: considering magnetic resonance image-distortion and delineation failure in the targeting of the internal auditory canal. Med Phys 1999;26:166–170.
10 Guo WY, Chu WC, Wu MC, Chung WY, Gwan WP, Lee YL, Pan HC, Chang CY: An evaluation of the accuracy of magnetic-resonance-guided Gamma Knife surgery. Stereotact Funct Neurosurg 1996;66(suppl 1):85–92.
11 Jursinic P, Prost R, Schultz C: A new magnetic resonance head coil and head immobilization device for gamma knife radiosurgery: an analysis of geometric distortion and signal/noise characteristics. J Neurosurg 2002; 97(suppl 5):563–568.
12 Barker GJ, Tofts PS: Semiautomatic quality assurance for quantitative magnetic resonance imaging. Magn Reson Imaging 1992;10:585–595.
13 Bell RA: Quality assurance for MRI. Part one. Adm Radiol 1988;7:18–19, 21–22, 24.
14 Bell RA: Quality assurance for MRI. Part two. Adm Radiol 1988;7:22–25.
15 Berardi P, Bergamini C, Gavelli G, Lembo C, Pavlica P, Pierotti L, Vianello Vos C: Development and use of quality control program in magnetic resonance. Radiol Med (Torino) 1995;89:310–318.
16 Firbank MJ, Harrison RM, Williams ED, Coulthard A: Quality assurance for MRI: practical experience. Br J Radiol 2000;73:376–383.
17 Pollock BE, Kondziolka D, Flickinger JC, Patel AK, Bissonette DJ, Lunsford LD: Magnetic resonance imaging: an accurate method to evaluate arteriovenous malformations after stereotactic radiosurgery. J Neurosurg 1996;85:1044–1049.
18 Schad LR: Improved target volume characterization in stereotactic treatment planning of brain lesions by using high-resolution BOLD MR-venography. NMR Biomed 2001;14:478–483.

19 Scheib SG, Gianolini S, Haller D, Wellis GN, Siegfried J: Volumeseries: a software tool for target volume follow-up studies with computerized tomography and magnetic resonance imaging. Technical note. J Neurosurg 2000;93(suppl 3):203–207.
20 Walton L, Hampshire A, Forster DM, Kemeny AA: A phantom study to assess the accuracy of stereotactic localization, using T1-weighted magnetic resonance imaging with the Leksell stereotactic system. Neurosurgery 1996;38:170–176; discussions 176–178.
21 Yu C, Apuzzo ML, Zee CS, Petrovich Z: A phantom study of the geometric accuracy of computed tomographic and magnetic resonance imaging stereotactic localization with the Leksell stereotactic system. Neurosurgery 2001;48:1092–1098; discussions 1098–1099.
22 Yu C, Petrovich Z, Apuzzo ML, Luxton G: An image fusion study of the geometric accuracy of magnetic resonance imaging with the Leksell stereotactic localization system. J Appl Clin Med Phys 2001;2:42–50.
23 Drzymala RE, Mutic S: Stereotactic imaging quality assurance using an anthropomorphic phantom. Comput Aided Surg 1999;4:248–255.
24 Landi A, Marina R, DeGrandi C, Crespi A, Montanari G, Sganzerla EP, Gaini SM: Accuracy of stereotactic localisation with magnetic resonance compared to CT scan: experimental findings. Acta Neurochir (Wien) 2001;143:593–601.
25 Orth RC, Sinha P, Madsen EL, Frank G, Korosec FR, Mackie TR, Mehta MP: Development of a unique phantom to assess the geometric accuracy of magnetic resonance imaging for stereotactic localization. Neurosurgery 1999;45:1423–1429; discussions 1429–1431.
26 Guo WY: Application of MR in stereotactic radiosurgery. J Magn Reson Imaging 1998;8: 415–420.
27 Wu TH, Lee JS, Wu HM, Chu WF, Guo WY: Evaluating geometric accuracy of multi-platform stereotactic neuroimaging in radiosurgery. Stereotact Funct Neurosurg 2002;78:39–48.
28 Kooy HM, van Herk M, Barnes PD, Alexander E 3rd, Dunbar SF, Tarbell NJ, Mulkern RV, Holupka EJ, Loeffler JS: Image fusion for stereotactic radiotherapy and radiosurgery treatment planning. Int J Radiat Oncol Biol Phys 1994;28:1229–1234.
29 Schad LR, Bock M, Baudendistel K, Essig M, Debus J, Knopp MV, Engenhart R, Lorenz WJ: Improved target volume definition in radiosurgery of arteriovenous malformations by stereotactic correlation of MRA, MRI, blood bolus tagging, and functional MRI. J Radiol 1996;6:38–45.
30 Schad LR, Ehricke HH, Wowra B, Layer G, Engenhart R, Kauczor HU, Zabel HJ, Brix G, Lorenz WJ: Correction of spatial distortion in magnetic resonance angiography for radiosurgical treatment planning of cerebral arteriovenous malformations. Magn Reson Imaging 1992;10:609–621.
31 Bednarz G, Downes MB, Corn BW, Curran WJ, Goldman HW: Evaluation of the spatial accuracy of magnetic resonance imaging-based stereotactic target localization for gamma knife radiosurgery of functional disorders. Neurosurgery 1999;45:1156–1161; discussions 1161–1163.
32 Caudrelier JM, Vial S, Gibon D, Kulik C, Fournier C, Castelain B, Coche-Dequeant B, Rousseau J: MRI definition of target volumes using fuzzy logic method for three-dimensional conformal radiation therapy. Int J Radiat Oncol Biol Phys 2003;55:225–233.
33 Kondziolka D, Dempsey PK, Lunsford LD, Kestle JR, Dolan EJ, Kanal E, Tasker RR: A comparison between magnetic resonance imaging and computed tomography for stereotactic coordinate determination. Neurosurgery 1992;30:402–406; discussions 406–407.
34 Mack A, Czempiel H, Kreiner HJ, Durr G, Wowra B: Quality assurance in stereotactic space. A system test for verifying the accuracy of aim in radiosurgery. Med Phys 2002;29:561–568.
35 Piovan E, Zampieri PG, Alessandrini F, Gerosa MA, Nicolato A, Pasoli A, Foroni R, Giri MG, Bricolo A, Benati A: Quality assessment of magnetic resonance stereotactic localization for Gamma Knife radiosurgery. Stereotact Funct Neurosurg 1995;64(suppl 1):228–232.

Andreas Mack, PhD
Gamma Knife Centre
Schleusenweg 2–16, NG 95
DE–60528 Frankfurt (Germany)
Tel. +49 0 69 677 359 14, Fax +49 0 69 677 359 11
E-Mail a.mack@gkfrankfurt.de

Kondziolka D (ed): Radiosurgery. Basel, Karger, 2006, vol 6, pp 71–85

Assessment of the Accuracy in Ophthalmic Radiosurgery

Josef Novotný, Jr.[a], *Josef Novotný*[a], *Roman Liščák*[a], *Václav Spěváček*[b], *Jan Hrbáček*[b], *Pavel Dvořák*[b], *Tomáš Čechák*[b], *Jaroslav Tintěra*[a], *Josef Vymazal*[a], *Vilibald Vladyka*[a]

[a]Hospital Na Homolce, Department of Medical Physics, Department of Stereotactic and Radiation Neurosurgery, [b]CTU in Prague, Faculty of Nuclear Sciences and Physical Engineering, Prague, Czech Republic

Abstract

Purpose of this study was to assess different aspects of ophthalmic radiosurgery accuracy performed on the Leksell Gamma Knife (ELEKTA Instrument, Sweden): (1) accuracy of magnetic resonance imaging (MRI) for the eye, (2) stability and rigidity of eye fixation, (3) accuracy of the Leksell GammaPlan (ELEKTA Instrument, Sweden) treatment planning system calculations and (4) treatment delivery by the Leksell Gamma Knife. It was demonstrated in this study that Leksell Gamma Knife can be used for ophthalmic radiosurgery with sufficient accuracy. Stability of eye fixation and geometric accuracy of MRI can be achieved with careful quality control. Siemens EXPERT (Siemens, Germany) 1T MRI scanner was found to be better for eye imaging compared to Siemens SYMPHONY (Siemens, Germany) 1.5 T in terms of geometric accuracy. Coronal MRI slices demonstrated higher image distortion and were not accepted for eye imaging. Three-dimensional gradient echo image sequence with 1.3 mm slice thickness was selected for a standard imaging procedure for eye lesions. Eye fixation technique used in this study was achieved by retrobulbar local anesthesia and applying two sutures in the rectus muscles and attaching these sutures to the Leksell stereotactic frame. This eye fixation technique showed very good stability and rigidity in time, patient prone versus supine position had no effect on stereotactic target and eye structures localization. Treatment planning system calculations for relative doses demonstrated good agreement with measured data. Absolute doses measured by pinpoint ion chamber at depths of 10 mm and deeply showed relatively good agreement with the treatment planning system calculated data (delivered doses were systematically lower than calculated ones usually within 3–5%). Absolute doses measured by pinpoint ion chamber in depths less than 10 mm showed relatively large deviation compare to the treatment planning system calculated data (delivered doses were systematically lower than calculated ones of about 15–20%). One should be aware of this, especially when reporting doses for structures as eye lid, eye lens and etc. Calculation errors can be probably reduced by a sufficient volume of a proper built-up material fixed on a patient eye.

Stereotactic radiosurgery (SR) or stereotactic radiotherapy (SRT) was originally designed for the treatment of rigid centrally or almost centrally located intracranial targets [1, 2]. SR or SRT of ophthalmic lesions is relatively far from these standard treatment conditions mainly due to very eccentric target location and motion of an eye. These aspects specific to the treatment of ophthalmic lesions should be taken into account. First of all proper eye fixation or eye motion monitoring system is required since eye can move during the treatment procedure. Very eccentric target volume location can also cause some inaccuracies in the treatment planning calculations including relative dose distribution as well as absolute dose calculations (calculation of treatment time or monitor units). Finally, there may be also some technical inconveniences to treat patients due to limitations in the range of coordinate system in this very eccentric target locations. Despite of all these difficulties SR or SRT is tempting alternative for ophthalmic lesions treatment mainly due to its very high accuracy and delivery of high conformal dose distribution to small volume of the treatment target.

For all kinds of SR or SRT it is imperative to employ a patient fixation system that is highly reproducible and meets the accuracy requirements for high precision treatments. Additionally, for treatments of ocular lesions it is not sufficient to fixate the patient's head but the eye itself has to be fixated in the same position during imaging for treatment planning and during delivery of all treatments. Several different eye-immobilization systems and techniques have been described in the literature [3–11]. In principle eye-immobilization techniques can be divided into two groups: (1) passive immobilization techniques when the eye is immobilized by different mechanical means from outside and (2) active immobilization techniques when the patient controls the eye position, e.g. by fixation of a light source.

Tokuuye et al. [3] described a mask fixation technique with a plastic mould gently pressed down over the orbit to restrict ocular movements. Zehetmayer et al. [4] reported on a suction immobilization technique for SR of intracranial malignancies at the Leksell Gamma Knife. Langmann et al. [5] used an invasive fixation method of the globe by means of retrobulbar anesthetic blocking for eye treatments at the Leksell Gamma knife. Šimonová et al. [6] and Vladyka et al. [7] reported series of patients with uveal melanomas and glaucomas treated at the Leksell Gamma Knife (ELEKTA Instrument, Sweden) when an eye fixation was achieved by retrobulbar local anesthesia and applying two sutures in the rectus muscles and attaching these sutures to the Leksell stereotactic frame.

Active eye-immobilization techniques, where the patient controls the eye position, e.g. by fixation of a light source, have been described in literature for proton/helium ion beam therapy and recently also for linear accelerator

(LINAC) based SRT of malignant tumors [8, 9]. For proton/helium ion beam therapy a surgical intervention is performed to position tantalum clips at the border of the visible tumor under diaphanoscopical control. These clips are used during treatment planning to define the target volume and to verify the position of the tumor during treatment delivery by using X-rays [10]. Recently Petersch et al. [11] described a new noninvasive eye fixation system for the application of LINAC-based image guided/gated SRT of uveal melanoma. The system is attached to commercially available thermoplast mask system and is based on patient's fixation of a light point. Computer controlled eye monitoring provides quantitative information about the quality of the patient repositioning, both about the repositioning of the patient's head within the mask and about the eye's rotational state with respect to the reference position as determined during imaging for treatment planning prior the actual treatment. When eye position exceeds preset geometrical limits the system is able to automatically initiate interruption of patient irradiation.

Prerequisite for correct treatment planning is a good imaging of the target and surrounding structures, especially organs at risk. Typical imaging modality for ophthalmic lesions is magnetic resonance imaging (MRI) that can be supplemented by computer tomography (CT). Generally MRI brings better contrast compare to CT when imaging intracranial and intraocular areas. However, while CT is supposed to be free of geometric distortions MRI may produce some geometric image distortions (sometimes a few millimeters) that are not acceptable for SR or SRT treatment planning. Generally, MRI geometric distortion is mainly function of: MRI scanner employed, MRI sequence used, image slice orientation, position in imaged volume, material and geometric parameters of the stereotactic frame [12–14]. The issue of image geometric distortion is even more crucial in the case of eye imaging when a target and other structures of interest are in very frontal location. It is essential to check extent of geometric distortions for each MRI scanner and sequence employed for eye imaging.

Due to very frontal location of eye volume some mechanical difficulties can occur when treating patient on the Leksell Gamma Knife while this issue is not a problem when treating patient on the stereotactically adapted LINAC. Depending on patient's head shape and volume it might be difficult to adjust properly frame position to reach all Leksell stereotactic coordinates. Specifically Y (posterior–anterior) Leksell stereotactic coordinate can exceed sometimes limits engraved on the Leksell stereotactic frame. Due to this a special Y coordinate extender was developed at Na Homolce Hospital to be able to treat also Y coordinates exceeding limits of commercially available Leksell stereotactic frame (see fig. 1a). Treatment of eye lesions on the Leksell Gamma Knife requires typically extremely large patient's neck rake (when supine position is used) that can be hardly tolerated or even impossible to perform for some

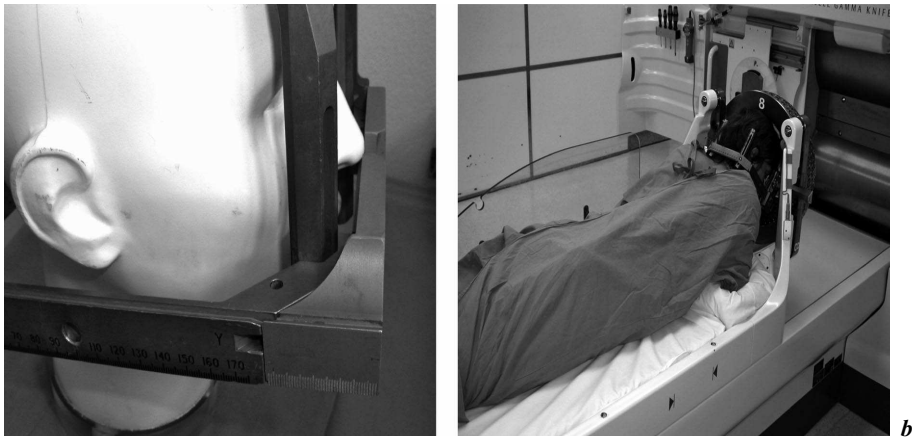

Fig. 1. ***a*** Special Y coordinate extender developed at Na Homolce Hospital used for the treatment of eye lesion when Y coordinate exceeds limits of commercially available Leksell stereotactic frame. ***b*** Typical treatment of eye lesion on the Leksell Gamma Knife in patient prone position.

patients. Consequently, for patient's better comfort the treatment is typically done in prone patient position (see fig. 1b).

Due to very eccentric target volume location some inaccuracies in the treatment planning calculations including relative dose distributions as well as absolute dose calculations (calculation of treatment time or monitor units) can be expected. This issue is even more important for surface structures of eye, e.g. eye lens, eye lid, cornea and etc. than for target volumes itself since these structures are located in depths smaller than built-up of employed photon energies.

Petersch et al. [11] reported excellent agreement between measurements and treatment planning sytem calculations for uveal melanomas at depth 15–20 mm. However, at small depths ($<$10 mm) the treatment planning system cannot model the influence of absorption in eye motion monitoring device accurately if beam passed perpendicularly through it. Consequently, Petersch et al. suggested to avoid frontal beams when doing treatment planning as solution to reduce significantly dosimetric errors.

Purpose of this study was to assess different aspects of ophthalmic radiosurgery accuracy performed on the Leksell Gamma Knife. Following questions were addressed in this study: (1) How accurate is MRI of eye?, (2) How stable is eye fixation?, (3) How accurate are Leksell GammaPlan (ELEKTA Instrument, Sweden) treatment planning system calculations? and (4) How accurate is treatment delivery by the Leksell Gamma Knife (ELEKTA Instrument, Sweden)?

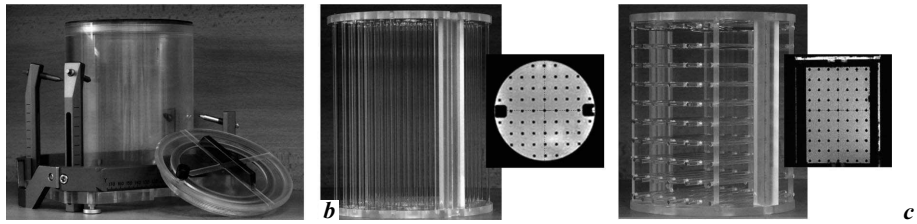

Fig. 2. Special cylindrical phantom (***a***) with axial (***b***) and coronal (***c***) inserts was constructed to assess the accuracy of MRI in this study. MRI of axial and coronal inserts are also displayed.

Methods and Materials

MRI Geometric Accuracy

Special cylindrical phantom with two inserts (axial and coronal) was constructed to assess the accuracy of MRI (fig. 2). The phantom was fixed in the Leksell stereotactic frame and underwent stereotactic MRI under routine clinical conditions. More information about the phantom can be found in [12]. Phantom measurements were performed on both available Siemens MRI scanners: 1 T EXPERT (Siemens, Germany) and 1.5 T SYMPHONY (Siemens, Germany). Following MRI sequences were tested on both scanners: T_1-weighted spin-echo (T1 SE), T_2-weighted turbo-spin-echo (T2 SE), proton density-weighted turbo-spin-echo (PD SE), three-dimensional T_1-weighted gradient-echo (3D GE). More details regarding the sequence parameters can be found in [12]. The images were transferred into the Leksell GammaPlan treatment planning system and the stereotactic coordinates of the rods were determined. The deviations between stereotactic coordinates based on MRI and estimated real geometrical position given by the construction of the phantom insert were evaluated for each study. The deviations were further investigated as a function of: (a) MRI scanner employed, (b) MRI sequence, (c) image orientation.

Stability and Rigidity of Eye Fixation

Fixation of the eye by retrobulbar local anesthesia and two sutures of rectus muscles to the frontal posts of stereotactic frame is routinely used in our department. Since patient is for better comfort usually treated in a prone position but imaged in supine position, additional evaluation of eye fixation rigidity and assessment of potential discrepancies between prone and supine imaging were evaluated. Two subsequent MRIs in different positions (supine and prone) of a patient with fixed eye were done. To assess also the stability of eye fixation in time these two subsequent imaging were done in at least 2 h interval (that is typical time interval for the whole treatment procedure). Three volumes including eye, tumor and eye lens were outlined on MRI done in patient supine position and then projected to MRI done in prone patient position (fig. 3). Maximal deviations in outlined volume structures in X, Y, Z stereotactic coordinates were measured using the Leksell GammaPlan treatment planning system altogether for ten different patients.

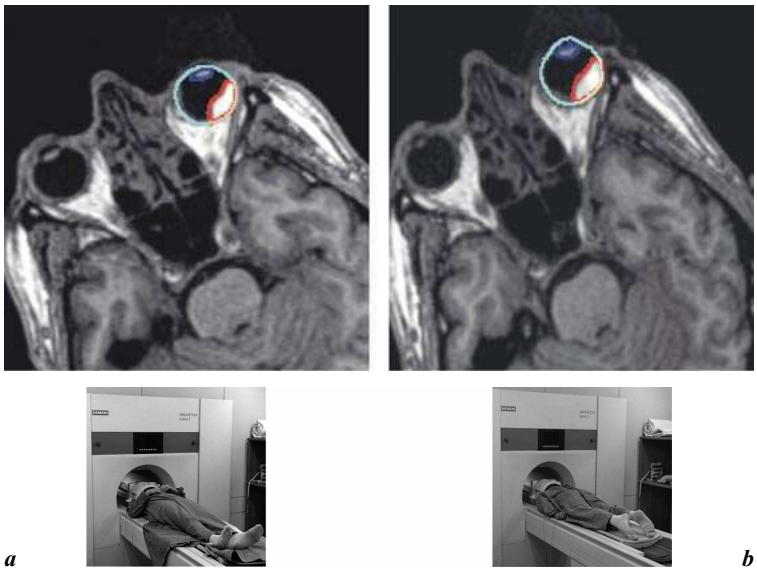

a ***b***

Fig. 3. Evaluation of potential discrepancies between prone and supine MRI. Three volumes including eye, tumor and eye lens were outlined on MRI done in patient supine position (***a***) and then projected to MRI done in patient prone position (***b***). To assess also the stability of eye fixation these two subsequent imaging were done in at least 2 h interval.

Accuracy in Dose Calculations and Treatment Delivery

To assess the accuracy of relative and absolute dose calculations in the treatment planning system and treatment delivery, a special head phantom was constructed. This phantom was filled by water and allowed to fixed in a proper position (eye of the head phantom) dosimeters employed in relative and absolute dosimetry (fig. 4). For absolute dosimetry PinPoint PTW FREIBURG TW 31006 ion chamber (PTW Freiburg, Germany) with chamber volume 0.015 cm^3 and PTW UNIDOS electrometer (PTW Freiburg, Germany) was used. Water filled head phantom with inserted ion chamber was imaged on CT and volume of the ion chamber was defined in the Leksell GammaPlan tretament planning system. Mean dose delivered to the volume of the ion chamber was calculated in the treatment planning system and later compared with ion chamber measured values. For relative dosimetry polymer-gel dosimeter was poured into spherically shaped glass test vessels (inner diameter 46 mm and wall thickness 3 mm) and fixed in the head phantom. A composition, calibration and evaluation of this dosimeter was described elsewhere [15–17]. The phantom with selected dosimeter was fixed in the Leksell stereotactic frame and underwent imaging, treatment planning and treatment according to normal patient procedures. Altogether six different treatments taken from clinical practice were simulated and evaluated. These treatments covered different ophthalmic indications including: uveal melanoma, glaucoma and retinoblastoma. Different treatment plans were denoted in this study as: treatment plan 1, treatment plan 2, treatment plan 3, treatment plan 4, treatment plan 5 and treatment plan 6. Detailed information about six simulated treatments is given in table 1.

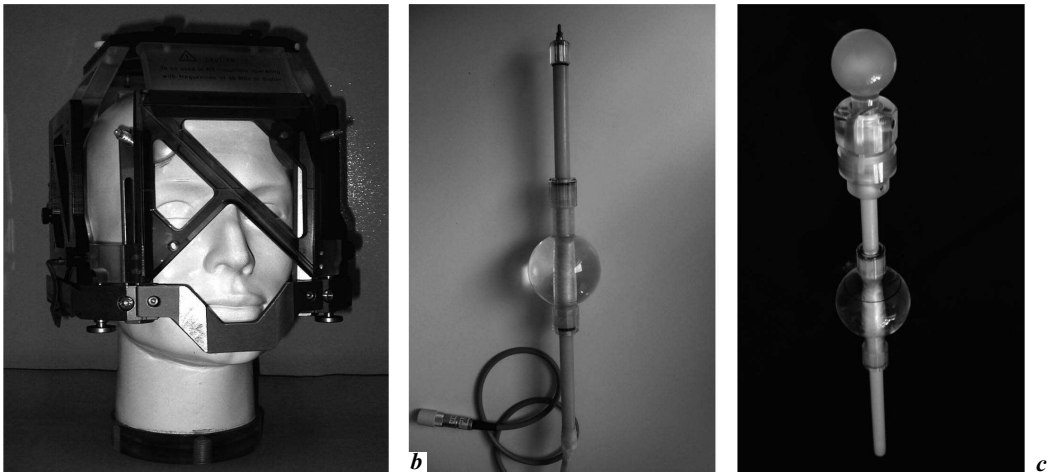

Fig. 4. To assess the accuracy in the treatment planning system relative and absolute dose calculations and treatment delivery, a special head phantom was constructed and used in this study (***a***). PinPoint PTW FREIBURG TW 31006 ion chamber (***b***) and polymer-gel dosimeter (***c***) were used for absolute and relative dosimetry measurements, respectively. Both dosimeters could be fixed for measurements in the eye location of the head phantom.

Table 1. Detailed information about six simulated treatments in this study used for the assessment of the accuracy of absolute and relative treatment planning dose calculations and treatment delivery

Simulated treatment	Collimator size, mm	Total no. of isocenters	Plugging
Treatment plan 1	8	3	None
Treatment plan 2	4	4	None
Treatment plan 3	14	1	72 sources plugged
Treatment plan 4	8	4	58 sources plugged
Treatment plan 5	8	4	None
Treatment plan 6	18	1	None

Results

MRI Geometric Accuracy

Results from phantom measurements for both MRI scanners are presented in table 2. Maximal and average deviations of stereotactic coordinates X, Y, Z of evaluated points caused by image distortion are given for both scanners in these

Table 2. Maximal and average values of image distortion measured for Siemens 1 T EXPERT (*a*) and 1.5 T SYMPHONY (*b*) scanners

	T1 SE deviation mm		T2 SE deviation mm		PD SE deviation mm		3D GE deviation, mm	
(*a*) *Siemens 1 T* EXPERT								
Axial	X	Y	X	Y	X	Y	X	Y
Maximal	1.0	0.2	1.1	0.4	1.0	0.4	0.9	0.4
Average	0.6	0.1	0.6	0.2	0.6	0.2	0.4	0.2
Coronal	X	Z	X	Z	X	Z	X	Z
Maximal	0.5	1.4	0.9	0.6	0.8	1.5	1.3	1.5
Average	0.3	0.9	0.5	0.2	0.3	0.9	0.5	0.2
(*b*) *Siemens 1 .5 T* SYMPHONY								
Axial	X	Y	X	Y	X	Y	X	Y
Maximal	0.6	0.5	0.8	1.3	0.9	1.3	0.7	0.6
Average	0.3	0.3	0.3	1.0	0.3	1.0	0.3	0.3
Coronal	X	Z	X	Z	X	Z	X	Z
Maximal	0.8	1.8	0.7	1.8	0.7	1.9	0.7	2.1
Average	0.4	1.2	0.4	1.3	0.5	1.3	0.3	1.3

Average distortions equal or higher than 1 mm are highlighted.

two tables. Average distortion equal or higher than 1 mm was supposed as unacceptable distortion for imaging accuracy required by clinical use and highlighted in table 2 for better comparison of both scanners and different MRI sequences.

Stability and Rigidity of Eye Fixation

Average deviations in outlined volume structures in X, Y, Z stereotactic coordinates for supine and prone patients' MRI are given in table 3.

Accuracy in Dose Calculations and Treatment Delivery

Results from absolute dosimetry measurements are given as deviations between absolute dose calculated by the treatment planning system and measured one in table 4.

Polymerization that occurs in polymer-gel together with three-dimensional treatment plan can be seen in figure 5. Examples of comparison between profiles calculated by the treatment planning system and measured by polymer-gel are given in figure 6. Deviations between the center (ΔX, ΔY, ΔZ) and deviations between 50% isodose lines of the profile ($\Delta FWHM_X$, $\Delta FWHM_Y$,

Table 3. Average deviations in outlined volume structures in X, Y, Z stereotactic coordinates for supine and prone patient MRI

Average deviations	ΔX, mm	ΔY, mm	ΔZ, mm
Eye volume	0.2	0.4	0.5
Lens volume	0.2	0.5	0.4
Tumor volume	0.2	0.6	0.6

Altogether ten patients were evaluated.

Table 4. Deviations between absolute dose calculated by the treatment planning system and measured one

Treatment	Ion chamber depth, mm	ΔD, %
(*a*) *Measurements with ion chamber located deeper to the surface of the phantom*		
Treatment plan 1	15	−3.6
Treatment plan 2	29	−14.1
Treatment plan 3	29	−0.5
Treatment plan 4	26	0.5
Treatment plan 5	26	−5.5
Treatment plan 6	9	−1.5
(*b*) *Measurements with ion chamber located very close the surface of the phantom*		
Treatment plan 3	5	−15.3
Treatment plan 5	6	−19.2
Treatment plan 6	6	−14.6

$\Delta FWHM_Z$) calculated by the treatment planning system and measured by polymer-gel are given in table 5. Center of the profile was defined as center of 50% isodose line.

Discussion

Purpose of this study was to assess different aspects of ophthalmic radiosurgery accuracy performed on the Leksell Gamma Knife: (1) accuracy of MRI for an eye, (2) stability and rigidity of eye fixation, (3) accuracy of the Leksell GammaPlan treatment planning system calculations and (4) treatment delivery by the Leksell Gamma Knife.

Eye fixation used in this study was achieved by applying local retrobulbar anesthesia and two sutures in the rectus muscles and attaching these sutures to

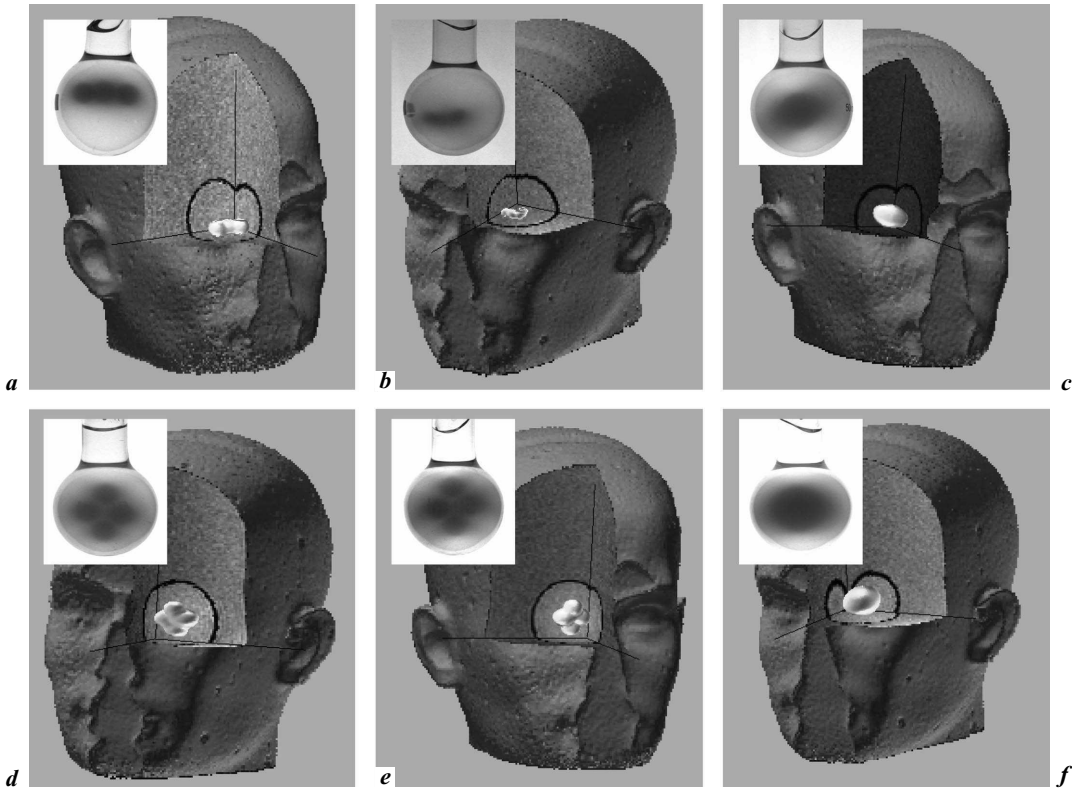

Fig. 5. Polymerization that occurs in polymer-gel together with three-dimensional treatment plan calculated by the treatment planning system. Altogether six different treatments were simulated and evaluated: treatment plan 1 (***a***), treatment plan 2 (***b***), treatment plan 3 (***c***), treatment plan 4 (***d***), treatment plan 5 (***e***) and treatment plan 6 (***f***).

the frontal posts of the Leksell stereotactic frame. This technique has been already presented by Šimonová et al. [6] and by Vladyka et al. [7] when patients with uveal melanoma and glaucoma were treated by the Leksell Gamma Knife, respectively. This technique requires only fast simple surgical procedure (typically not more than 15 min) and is very well tolerated by treated patients. Eye fixation rigidity and stability in time was tested altogether for ten patients when eye was fixed by above described technique. Very good stability of eye fixation was observed for all tested patients in this study. Control MRI performed at least in 2 h time interval have not demonstrated any significant deviations in stereotactic localization of eye structures. Since it is more comfortable for patient to be treated in prone position but imaged on MRI in supine position it

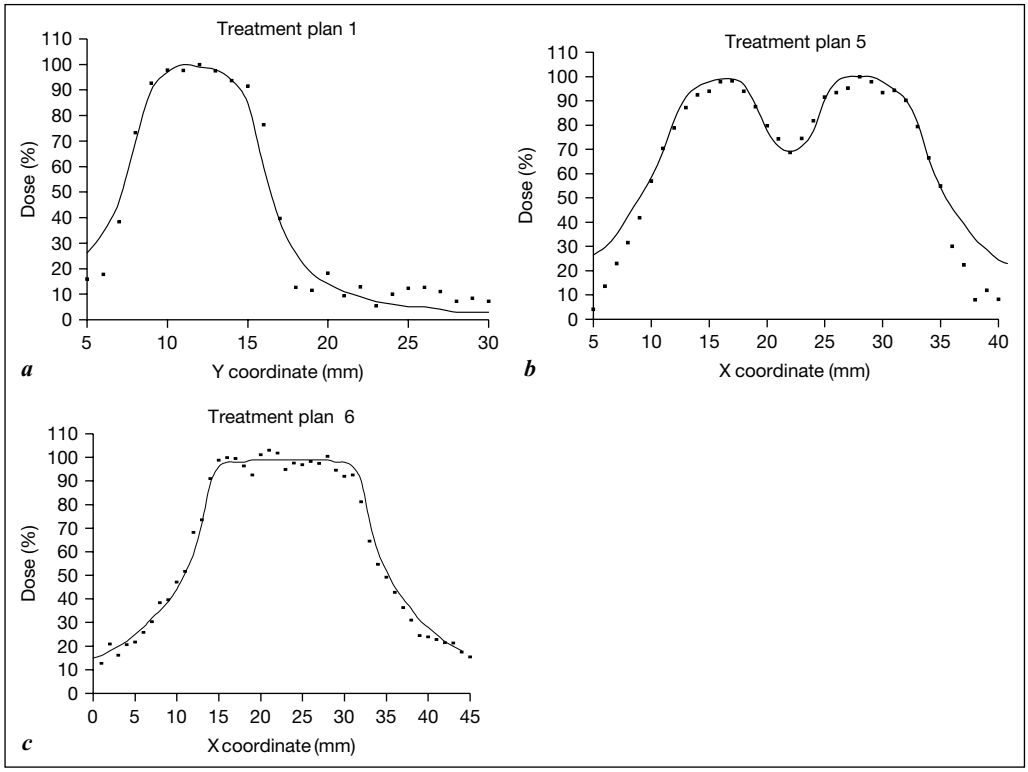

Fig. 6. a–c Examples of comparison between profiles calculated by the treatment planning system (solid line) and measured by polymer-gel (squares).

Table 5. Deviations between the center (ΔX, ΔY, ΔZ) and deviations between 50% isodose line ($\Delta FWHM_X$, $\Delta FWHM_Y$, $\Delta FWHM_Z$) of the profile calculated by the treatment planning system and measured by polymer-gel in each of X, Y, Z stereotactic coordinates

Treatment	ΔX mm	ΔY mm	ΔZ mm	$\Delta FWHM_X$ mm	$\Delta FWHM_Y$ mm	$\Delta FWHM_Z$ mm
Treatment plan 1	0.3	0.4	0.3	0.5	0.9	0.5
Treatment plan 2	0.5	0.4	0.5	0.7	0.2	0.6
Treatment plan 3	0.4	0.2	0.2	0.3	0.3	0.4
Treatment plan 4	0.3	0.5	0.7	0.5	0.7	0.7
Treatment plan 5	0.5	0.1	0.5	0.6	0.4	0.4
Treatment plan 6	0.2	0.3	0.2	0.5	0.5	0.6

was also tested whether there is any deviation in stereotactic localization of eye structures between supine and prone position. As it was demonstrated above there was observed no significant difference in stereotactic localization when MRI was done in supine or prone position. Consequently patient treatment could be done for better patient's comfort in prone position and MRI in supine position without any limitations.

The issue of MRI accuracy has been already addressed in many studies, e.g. [12–14]. The advantages of using MRI in stereotactic procedures include multiplanar imaging, reduced imaging artifacts produced by the stereotactic frame and mainly increased imaging resolution of lesions or various anatomical structures (tissue contrast mostly depends on differences in T_1 and T_2 relaxation times and it can be often enhanced by using contrast agents). However, questions still remain regarding the extent of image geometric distortion and its effect on the accuracy of stereotactic localization using MRI. Since very high accuracy (typically better than 1 mm) is usually required for stereotactic imaging an image geometrical distortion issue is very important. Although imaging of eye lesions includes typically the same MRI sequences as used for intracranial lesions there is main difference in very frontal location of MRI investigated volume compare to stereotactic procedures in intracranial regions. Siemens EXPERT 1 T MRI scanner was found to be better for eye imaging compared to Siemens SYMPHONY 1.5 T in this study in terms of image geometric accuracy. Coronal MRI slices demonstrated higher image distortion and were not accepted for eye imaging. Consequently only MRI axial slices were acquired and reconstruction in the treatment planning system was performed. Three dimensional gradient echo image sequence with 1.3 mm slice thickness was selected for a standard imaging procedure for eye lesions. More information regarding the comparison of both above tested MRI scanners can be found in a separate study [12].

Another specific aspect for the treatment of eye lesions is a difficulty for the treatment planning system to correctly address relative and absolute dose calculations. This is caused mainly by very eccentric location of treated volume or surrounding eye structures. This issue is even more important for eye surface structures e.g. eye lens, eye lid, cornea and etc. than for target volumes itself since these structures are located in depths smaller than built-up of employed photon energy of ^{60}Co. Absolute doses measured by pinpoint ion chamber at depths of 10 mm and deeply showed relatively good agreement with the treatment planning system calculated data. Absolute doses delivered during head phantom irradiation were systematically lower than calculated ones usually within 5% or even within 3%. Absolute doses measured by pinpoint ion chamber in depths less than 10 mm showed relatively large deviation compare to the treatment planning system calculated data. In this situation, absolute doses delivered

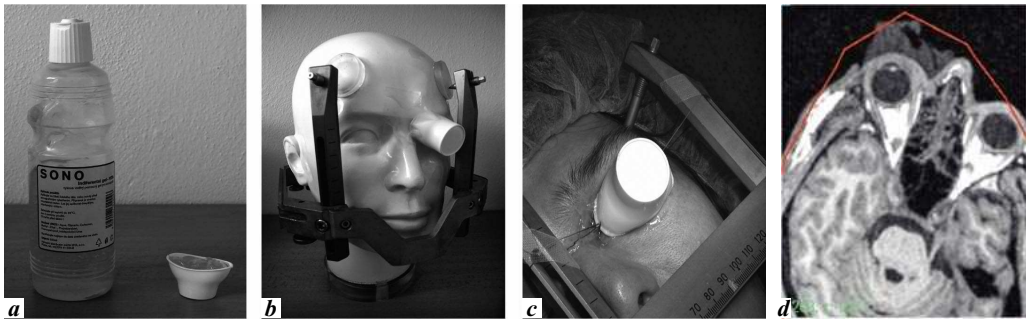

Fig. 7. Application of tissue equivalent built-up material on a treated eye was tested in this study to reduce inaccuracy in dose calculations. A gel used for ultrasound was poured in a special vessel (***a***), then fixed on a phantom (***b***) and patient's eye (***c***) and used as a built-up material. Built-up material is also included in skull geometry measurements (***d***).

during phantom irradiation were systematically lower usually within 15–20%. Relatively large deviation was observed for treatment plan 2 consisting exclusively from 4 mm isocenters. Although ion chamber was located almost 30 mm bellow the phantom surface the observed deviation was almost 15%. This can be explained as a dependence of calculation error of the Leksell GammaPlan treatment planning system on collimator size. This kind of experimental measurements have not been part of this study and should be done in the future separate research (one can create hypothesis that the calculation error will increase with decreasing collimator size but this idea has to be experimentally proved).

Application of tissue equivalent built-up material on a treated eye was tested in this study to reduce inaccuracy in absolute dose calculations (fig. 7). A gel used for ultrasound was poured in a special vessel and then fixed on a patient eye and used as a built-up material. Such a built-up material was well-tolerated by all patients and help also to protect eye during the whole treatment procedure. Preliminary measurements with above mentioned head phantom demonstrated that calculation errors should not probably exceed more than 10% even at surface structures when built-up material is used. However more measurements and analysis is needed to prove this hypothesis. Measurements with different detectors and in vivo measurements directly on patients are further needed. Different built-up geometry and materials should be also tested.

Relative dose distributions measured by polymer-gel dosimeter in the region of target volumes were in a good agreement with the Leksell GammaPlan calculated data. Deviations between the center (ΔX, ΔY, ΔZ) and deviations between 50% isodose line ($\Delta FWHM_X$, $\Delta FWHM_Y$, $\Delta FWHM_Z$) of the profile

calculated by the treatment planning system and measured by polymer-gel in each of X, Y, Z stereotactic coordinates were all within 1 mm.

Conclusions

It was demonstrated in this study that Leksell Gamma Knife can be used for ophthalmic radiosurgery with sufficient accuracy. Stability of eye fixation and geometric accuracy of MRI can be achieved with careful quality control. Siemens EXPERT 1 T MRI scanner was found to be better for eye imaging compared to Siemens SYMPHONY 1.5 T in terms of geometric accuracy. Coronal MRI slices demonstrated higher image distortion and were not accepted for eye imaging. Three dimensional gradient echo image sequence with 1.3 mm slice thickness was selected for a standard imaging procedure for eye lesions. Eye fixation technique used in this study was achieved by applying local retrobulbar anesthesia and two sutures in the rectus muscles and attaching these sutures to the front posts of the Leksell stereotactic frame. This eye fixation technique showed very good stability and rigidity in time, patient prone versus supine position had no effect on stereotactic target and eye structures localization. Treatment planning system calculations for relative doses demonstrated good agreement with measured data. Absolute doses measured by pinpoint ion chamber at depths of 10 mm and deeper showed relatively good agreement with the treatment planning system calculated data (delivered doses were systematically lower than calculated ones usually within 3–5%). Absolute doses measured by pinpoint ion chamber in depths less than 10 mm showed relatively large deviation compare to the treatment planning system calculated data (delivered doses were systematically lower than calculated ones of about 15–20%). One should be aware of this, especially when reporting doses for structures as eye lid, eye lens and etc. Calculation errors can be probably reduced by a sufficient volume of a proper built-up material fixed on a patient eye.

References

1 Lunsford LD, Kondziolka D, Flickinger JC (eds): Gamma Knife Brain Surgery. Prog Neurol Surg. Basel, Karger, 1998, vol 14.
2 Gildenberg PL, Tasker RR: Textbook of Stereotactic and Functional Neurosurgery. The McGraw-Hill Companies Inc., 1998, pp 1585–1599.
3 Tokuuye K, Akine Y, Sumi M, Kagami Y, Ikeda H, Kaneko A: Fractionated stereotactic radiotherapy for choroidal melanoma. Radiother Oncol 1997;43:87–91.
4 Zehetmayer M, Menapace R, Kitz K, Ertl A: Suction fixation system for stereotactic radiosurgery of intraocular malignancies. Ophthalmologica 1994;208:119–121.
5 Langmann G, Pendl G, Schröttner O: Gamma knife of uveal melanoma radiosurgery for intraocular melanomas. Preliminary report. Spectrum Augenheilkd 1995;9(suppl 1):16–21.

6 Šimonová G, Novotný J Jr, Liščák R, Pilbauer J: Leksell gamma knife treatment of uveal melanoma. J Neurosurg 2002;97(suppl 5):635–639.
7 Vladyka V, Liščák R, Šimonová G, Pilbauer J, Hejduková I, Nováček L: Progress in glaucoma tretament research: a nonrandomized prospective study of 102 patients with advanced refractory glaucoma treated by Leksell gamma knife radiation. J Neurosurg 2005;102(suppl):214–219.
8 Bellmann C, Fuss M, Holz FG: Stereotactic radiation therapy for malignant choroidal tumors, preliminary, short-term results. Ophthalmology 2000;107:358–365.
9 Debus J, Fuss M, Engenhart-Cabillic R: Stereotaktische konformierende Bestrahlung von Aderhautmetastasen. Ophthalmologe 1998;95:163–167.
10 Courdi A, Caujolle JP, Grange JD: Results of proton therapy of uveal melanomas treated in Nice. Int J Radiat Oncol Biol Phys 1999;45:5–11.
11 Petersch B, Bogner J, Dieckmann K, Pötter R, Georg D: Automatic real-time surveillance of eye position and gateing for stereotactic radiotherapy of uveal melanoma. Med Phys 2004;31: 3521–3527.
12 Novotny J Jr, Vymazal J, Novotny J, Tlachacova D, Schmitt M, Chuda P, Urgosik D, Liscak R: Does new magnetic resonance imaging technology provide better geometrical accuracy during stereotactic imaging? J Neurosurg 2005;102(suppl):8–13.
13 Fransson A, Andreo P, Pötter R: Aspects of MRI image distortions in radiotherapy treatment palnning. Strahlenther Onkol 2001;177:59–73.
14 Walton L, Hampshire A, Forster D: Accuracy of stereotactic localization using magnetic resonance imaging. A comparison between two- and three-dimensional studies. Stereotact Funct Neurosurg 1996;66(suppl):49–56.
15 Novotný J Jr, Dvořák P, Spěváček V, Tintěra J, Novotný J, Čechák T, Liščák R: Quality control of the stereotactic radiosurgery procedure with the polymer-gel dosimetry. Radiother Oncol 2002;63: 223–230.
16 Novotný J Jr, Spěváček V, Hrbáček J, Judas L, Novotný J, Dvořák P, Tlacháčová D, Schmitt M, Tintěra J, Vymazal J, Čechák T, Michálek J, Přádný M, Liščák R: Measurement of relative dose distributions in stereotactic radiosurgery by the polymer-gel dosimeter; in Kondziolka D (ed): Radiosurgery. Basel, Karger, 2004, vol 5, pp 225–235.
17 Novotný J Jr, Novotný J, Spěváček V, Dvořák P, Čechák T, Liščák R, Brožek G, Tintera J, Vymazal J: Application of polymer gel dosimetry in gamma knife radiosurgery. J Neurosurg 2002;97(suppl 5): 556–562.

Josef Novotný, Jr., MSc, PhD
Na Homolce Hospital, Department of Medical Physics
Roentgenova 2
CZ–150 30 Prague 5 (Czech Republic)
Tel. +420 604 203 197, Fax +420 257 272 972
E-Mail josef.novotnyml@homolka.cz

Kondziolka D (ed): Radiosurgery. Basel, Karger, 2006, vol 6, pp 86–97

How Can Tumor Effect and Normal Tissue Effect Be Balanced in Stereotactic Body Radiotherapy

Wolfgang A. Tomé[a,b], *John D. Fenwick*[c], *Minesh P. Mehta*[a]

Departments of [a]Human Oncology and [b]Medical Physics, University of Wisconsin, Madison, Wisc., USA; [c]Department of Physics, Clatterbridge Centre for Oncology, Bebington, Wirral, UK

Abstract

Methods for selection of appropriate dose fractionation schedules for stereotactic body radiotherapy that have both an equivalent tumor effect for lesions of varying size and ensure an acceptable risk of clinically manifest radiation pneumonitis have not been adequately developed or tested. We have developed a model-based methodology for selection of an appropriate dose fractionation schedule for radioablation of peripheral T1/T2 N0 M0 lung tumors that putatively achieves a progression free survival at 30 months of ≥80% while keeping the incidence of significant radiation pneumonitis below 20%. Because of the short schedules used in stereotactic body radiation therapy, accelerated repopulation is not a concern; a schedule that has a minimal peripheral tumor $NTD_{10} \geq 84\,Gy_{10}$ is projected to achieve ≥80% progression free survival at 30 months. Our modeling shows that in order to achieve this, the mean normalized total dose to the residual healthy lung (both lungs – PTV) has to be kept below $19\,Gy_3$, the dose at which the risk of pneumonitis would be acceptable. Choice of a dose fractionation schedule suited to meet these aims is determined by both the ratio of the prescription isodose volume to the residual healthy lung volume and the minimal peripheral local late damage NTD_3^{MP} associated with this fractionation schedule within the prescription isodose volume that one is willing to tolerate for a targeted 30 month progression free survival of 80% or higher.

Stereotactic body radiation therapy (SBRT) has been developed as a means to accurately deliver radiation to extra cranial targets, especially in the liver and lung. By combining techniques of stereotactic localization, conformal treatment delivery, and incorporation of tumor motion into the treatment planning and delivery, SBRT has permitted dose-escalation to lung tumors without

increasing the dose to normal lung beyond its tolerance. Current SBRT fractionation schedules that are associated with a high progression free survival at 30 months deliver a minimal peripheral (MP) tumor normalized total dose (total dose given in 2 Gy equivalents per fraction abbreviated as NTD) of larger than of 84 Gy_{10} to the target [1–6]. Modeling of retrospective clinical data suggests these fractionation schedules will yield a progression free survival rates of $>$80% at 30 months for patients with T1/T2 N0 M0 non-small-cell lung cancer (NSCLC), as compared to 15–25% for a standard treatment regimen of 70 Gy in 2 Gy fractions [7, 8].

Historically, phase I dose-escalation approaches increase dose until acceptable toxicities are reached and these maximum tolerated doses serve as the basis of phase II efficacy studies. In this context, a variety of different doses have been tested, including some with an NTD_{10} in excess of 204 Gy_{10}. All of these, not surprisingly, yield high local control rates, but potentially represent an 'overkill' situation. What is currently required is an appropriate dose fractionation schedule for SBRT that has both an equivalent tumor effect for lesions of varying size and at the same time ensures an acceptable risk of clinically manifest radiation pneumonities. In the following sections, we discuss a model-based methodology for selection of an appropriate dose fractionation schedule for radioablation of peripheral T1/T2 N0 M0 NSC lung tumors that lets one achieve a progression free survival at 30 months of $\geq$80% while keeping the incidence of significant radiation pneumonitis $<$20%.

Materials and Methods

We will first briefly review the evidence for dose-response relationships in NSCLC and discuss the prospects for large increases in long-term progression-free survival.

The dose-response curve for NSCLC with the widest range in dose is that published by Martel et al. [8]. They report on the results of a dose-escalation study in patients with inoperable NSCLC conducted at the University of Michigan. In this study dose was escalated to an NTD of 103 Gy (delivered in five 2 Gy-fractions per week). They have summarized their recurrence free survival at 30 months in a logistic dose-response curve with a D_{50} of 84.5 Gy and a modest γ_{50}-slope of 1.5 (c.f. dashed line in fig. 1). This curve explains why such dismal results are obtained with conventional doses of 60 or 70 Gy in 6–7 weeks. These schedules are predicted to yield 15 or 24% recurrence free survival at 30 months, respectively. For patients in the study of Martel et al. [8] that received 96 Gy in 2 Gy fractions, only one-third recurred locally. Although that level of success is an enormous improvement on the 10–30% local recurrence-free survival which is the current standard at 3 years, it is clear that doses up to NTD = 120 Gy (five 2 Gy fractions a week) would be required to obtain success in the 90% region. However, the overall time of 12 weeks would be unreasonably long. On the other hand in SBRT the entire treatment is delivered in 2 weeks or less. This length of time is shorter than the presumed kick-off time T_k for accelerated repopulation in tumors, reported

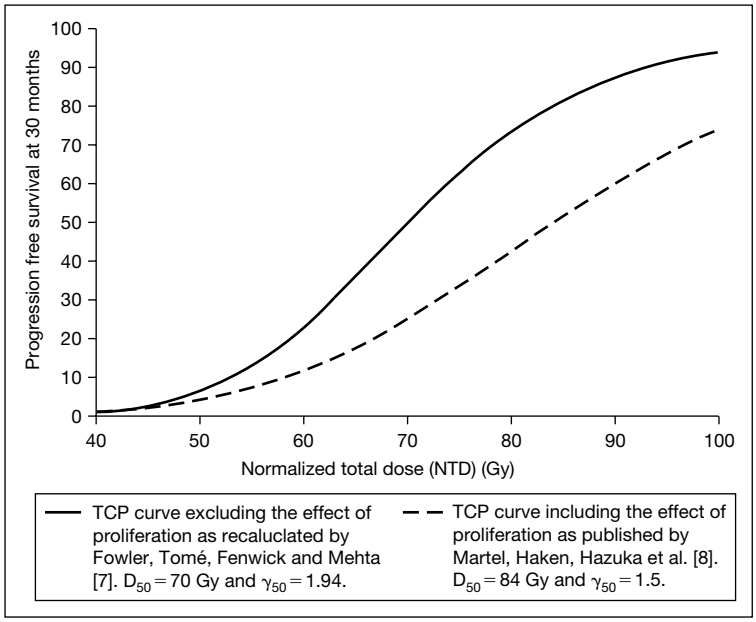

Fig. 1. The solid curve represents the dose-response curve for progression-free survival at 30 months as applicable to SBRT since it excludes proliferation due to tumor cell repopulation as calculated by Fowler et al. [7]. While the dashed curve represents the dose-response curve for progression-free survival at 30 months as applicable to conventional hyperfractionated radiotherapy since it includes proliferation due to tumor cell repopulation as found by Martel et al. [8].

to be 3–5 weeks [9–13]. Therefore, for SBRT one has to correct the dose-response curve obtained by Martel et al. [8] by subtracting the negative effect of proliferation [7]. In their calculation Fowler et al. [7] have assumed a kick-off time for accelerated repopulation of 28 days, a doubling time of 3 days [14], a generic α-value of 0.35 1/Gy, and a α/β-ratio of 10 Gy [15, 16]. Using these parameters, and assuming that no repopulation occurs during SBRT, the solid curve shown in figure 1 represents the dose-response relationship relevant for SBRT. Its γ_{50}-slope of 1.94 is steeper than the γ_{50}-slope of 1.5 of the original curve described by Martel et al. [8], and its $D_{50} = 70$ Gy instead of 84.5 Gy.

In our model for dose selection in SBRT for peripheral lung tumors, we have utilized the above observation (c.f. fig. 1) that if proliferation can be neglected, one can achieve $>80\%$ of progression free survival at 30 months with a fractionation schedule that corresponds to an NTD $\geq 84\,Gy_{10}$. Several other propositions need to be considered.

First we propose that in SBRT for peripheral lung tumors one should consider the high dose volume around the PTV separately from the lower dose contributed by each of the multiple incoming beams to the build up of normalized mean dose in the surrounding lung since one is looking at two different biological end points. Inside the high dose volume one aims to

ablate the tissue, while outside the high dose volume one aims to reduce the risk of inducing a normal tissue complication.

Second we propose to define the residual healthy lung volume as the total lung volume minus the PTV (not the total lung volume minus the GTV). This proposal is based on the observation that the PTV is the volume of lung one intends to ablate in SBRT, since it is this volume that has to account for the breathing motion of the CTV and systematic and random errors in treatment setup. So even though the PTV contains normal tissue this normal tissue must be considered as tumor, and therefore has to be ablated.

Thirdly, we propose that the prescription isodose volume (PIV) should be used in place of the PTV when talking about the volume of normal tissue irradiated to the prescription dose. The PIV is the volume one actually irradiates to at least the prescription dose. The PIV is at best equal to the PTV if it perfectly conforms to the PTV, but is most commonly larger. The size of the PIV is determined by several factors such as the number of beams used, the beam orientation employed (coplanar or non-coplanar), the margins that have been selected between the GTV, CTV, and PTV, respectively, and last but not least by the treatment planning technique one employs (3D CRT or IMRT). Since the PIV is always larger than or equal to the PTV, it contains normal tissue that is not part of the PTV and therefore does not need to be ablated. On the other hand, as pointed out above, the PTV contains normal tissue, that *must* be considered as tumor, and therefore has to be ablated even if it is normal tissue. The normal tissue that is part of the PIV but not of the PTV is ablated not because it contains tumor, but because of ones inability to conform the prescription dose exactly to the PTV.

There is of course no way that the incoming beams, which all intersect on the PTV, can avoid contributing to the dose-distribution in the surrounding residual healthy lung. Therefore, the dose within the PIV and mean NTD to the residual healthy lung are generally correlated. Figure 2 shows this correlation between the PIV and the residual healthy lung NTD_{mean} for levels of local late complication NTD_3 corresponding to some commonly employed fractionation schedules in SBRT. For example, a 20 Gy times 3 fraction schedule with a PIV to volume of residual healthy lung ratio of 0.02 (or 2%) would be predicted to yield an NTD_{mean} for the residual healthy lung of approximately 14 Gy, a value generally considered 'safe', but if this ratio increases to 0.04 (or 4%), an 'unsafe' NTD_{mean} of approximately 21 Gy is achieved.

Several methods to limit the incidence of grade 2 radiation pneumonitis at no more than a 20% have been discussed in the literature [17–19]. Acceptable correlations between either the percentage of lung receiving $\geq$20 Gy (V_{20}) or mean NTD to the lung (lung-NTD_{mean}) and radiation pneumonities have been reported for conventional schedules. However, it is questionable if volume based cutoffs should be used in SBRT since they have been derived for small doses per fraction of 2 Gy or less. The only way to take the biological effect of the SBRT schedule into account is to convert the SBRT dose volume histogram for the residual healthy lung to a dose volume histogram that uses biologically isoeffective doses for which the volume cutoffs have been determined, i.e. one has to convert from the SBRT schedule to the schedule for which the volume based cutoffs were determined. On the other hand, the mean NTD concept does not suffer form this shortcoming since in this concept one corrects for the biological effect of fraction size in every voxel, whether the dose to the target is 1.2 or 20 Gy per fraction. While Seppenwoolde and Lebesque [18] initially reported that a lung-NTD_{mean} of 22 Gy in 2 Gy fractions predicts a 20% incidence of radiation pneumonitis (grade 2 or higher), this value has recently been adjusted downwards to 19 Gy by De Jaeger et al. [20] taking improved dose estimates of tissue inhomogeneity corrections in the lung into account.

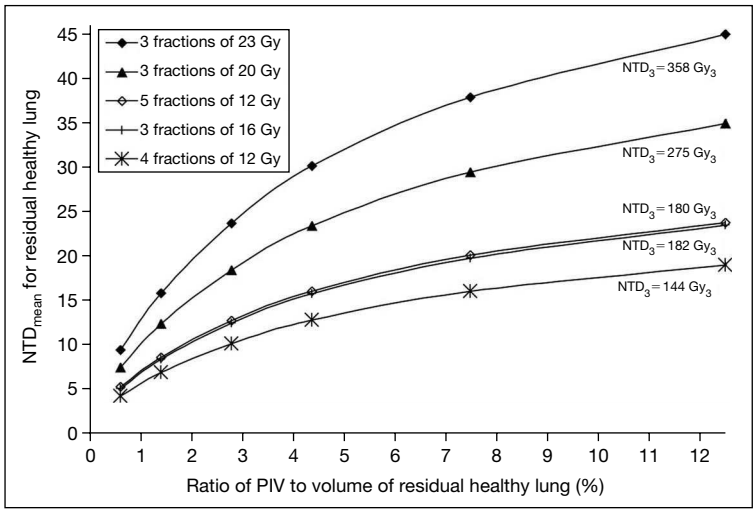

Fig. 2. Mean NTD to the residual healthy lung versus the ratio of the PIV to the volume of the residual healthy lung for peripheral lung lesions. The curves show, on the vertical axis, the variation of residual healthy lung mean NTD for five commonly employed SBRT fractionation schedules, graphed as a function of the ratio of the PIV to the residual healthy lung volume. Each curve corresponds to a different fractionation schedule. Treatment plans were generated and optimized such that 100% of the PTV was covered by 80% of the maximum dose to ensure the steepest fall-off of dose outside the PIV and such that the dose 2 cm away from the PIV in any direction was less or equal than 50% of the MP dose around the PTV for small lesions and to less or equal 58.5% for large lesions. The curves for the fractionation schedules 3 times 16 Gy and 5 times 12 Gy nearly coincide, which indicates that the late damage within the PIV, for which the late local damage MP NTD_3^{MP} has been taken as a surrogate, and the incidence of clinically significant radiation pneumonitis of grade 2 or higher are correlated.

To summarize, in the present model we consider at least three conceptually different, although interconnected, dose constraints all of which require future work to determine their predictive value as precisely as possible. One dose constraint is the dependence of the MP dose around the PTV on the volume of the PTV and the biological effects within the PIV in terms of Gy_{10}. The second constraint concerns the mean NTD to the residual healthy lung. A residual healthy lung-NTD_{mean} of 19 Gy or less should limit the incidence of clinically significant radiation pneumonitis of grade 2 or higher to less or equal to 20%. So far in SBRT the mean NTD for the residual healthy lung seem to be well below 19 Gy since the reported incidence of clinically significant radiation pneumonitis of grade 2 or higher has been low. The third constraint relates to the gradient of the dose falloff outside the PTV. In order to mimic the properties of dose distribution obtained in intracranial stereotactic radiosurgery one has to ask for a rapid fall-off of dose past the MP dose surface, i.e. on has to ask for a rapid isotropic dose fall-off from the PIV in all directions. In accord with the ROTG 0236 protocol, we have employed in this work a dose fall-off constraints that limits the dose 2 cm

away from the PIV in any direction to less or equal than 50% of the MP dose around the PTV for small lesions and to less or equal 58.5% for large lesions. In addition to that, there are organs risk such as the spinal cord, heart, esophagus, and major airways whose dose tolerance limits to these large fractions are poorly understood and have to be respected. The current RTOG 0236 SBRT protocol suggests limiting doses for these organs at risk that are based on the clinical experience accumulated so far for the dose fraction schedule of three fractions of 20 Gy. These tolerance doses can be converted to tolerance doses appropriate to any dose fraction schedule one wishes to employ in SBRT using the fraction size equivalent dose concept introduced by Tomé and Fenwick [21]. In the next section, we take the local late complication NTD_3^{MP} corresponding to the MP dose surrounding the PTV as a surrogate for the biological effect of the dose inside the PIV.

Results

As pointed out above there is of course no way that the incoming beams that all intersect on the PTV can avoid contributing to the buildup of dose in the surrounding tissues. The question now becomes the following: How can one use the ratio of the PIV to the residual healthy lung volume, the NTD_3^{MP}, and the NTD_{mean} to the residual healthy lung to select an appropriate fractionation schedule that will give a chance for a progression free survival at 30 months of $\geq$80% while respecting the normal tissue constraints?

The first step in this process is to calculate the ratio of the PIV to the residual healthy lung volume and use it to select a MP local late damage NTD_3^{MP} curve in figure 3 that lies below the Kwa-Seppenwoolde-De Jaeger (K-S-DJ) line, so that the incidence of clinically significant radiation pneumonitis of grade 2 or higher is limited to 20% or less. Any curve that lies below the K-S-DJ line is acceptable; late complications will likely increase with higher NTD_3^{MP}. For example, if we have a residual healthy lung volume of 4860.57 cm^3 (as determined form a free breathing CT) and a PIV of 72.9 cm^3 then the ratio of the PIV to the residual healthy lung is 1.5%. Depending on what MP local late complication NTD_3^{MP}, one is willing to accept all curves would be acceptable in terms of $<$20% risk of grade 2 radiation pneumonities.

However, for a PIV of 170.12 cm^3, the ratio of the PIV to the residual healthy lung is 3.5% and only the lowest four curves corresponding to the four lowest MP local late damage NTD_3^{MP} levels would be acceptable.

In step 2 one then selects the number of fractions and dose per fraction such that the expected MP tumor NTD_{10} of this schedule is larger than 84 Gy_{10} and its expected MP local late damage NTD_3^{MP} is less or equal to the MP local late damage NTD_3^{MP} determined in step 1 using the nomogram shown in figure 4. The nomogram shown in figure 4 consists of a sequence of quasi-parallel curves that relate the corresponding MP local late damage NTD_3^{MP} in Gy_3 to a

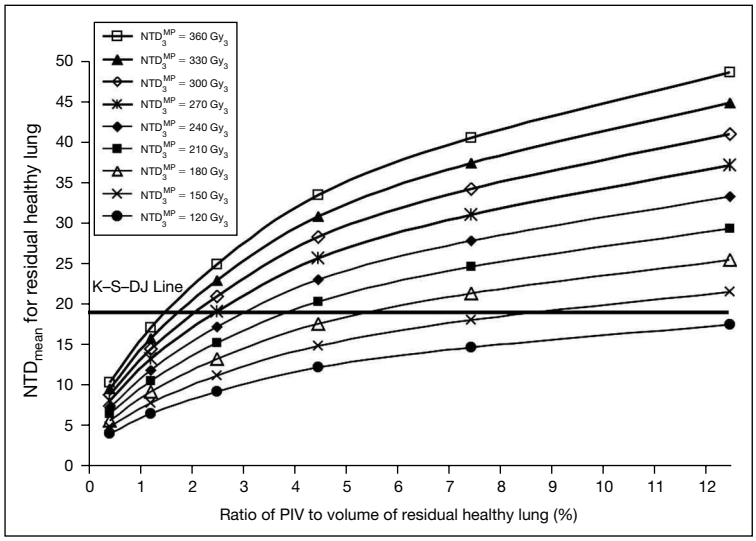

Fig. 3. Mean NTD for residual healthy lung versus the ratio of the PIV to the volume of residual healthy lung for peripheral lung lesions. The curves relate the late local damage MP NTD_3^{MP} corresponding to the biological effect of the physical dose within the PIV to the mean NTD received by the residual healthy lung, which is plotted against the percentage of the ratio of the PIV to residual healthy lung volume. The K-S-DJ line represents the level of late local damage NTD_3^{MP} limiting dose, below which the incidence of clinically significant radiation pneumonitis of grade 2 or higher is less or equal to 20%. The same treatment planning constraints as in figure 2 were used. The curves were generated using schedules with a fixed number of fractions (12) for which the dose per fraction was adjusted to yield the appropriate NTD_3^{MP} level. This nomogram can be used in the following way. For a given plan one calculates the ratio of the PIV to residual healthy lung as a percentage. Using this percentage one can then pick a NTD_3^{MP} curve that lies below or at the K-S-DJ line. Any curve that lies below or at the K-S-DJ line is allowed, and curves with larger NTD_3^{MP} values correspond to more aggressive fraction schedules both in terms of expected local control and late complications. The chosen NTD_3^{MP} then becomes the *upper limit* in the nomogram shown in figure 4. In the application of this nomogram it is important to bear in mind that these curves are only applicable to lung tumors that lie in the peripheral part of the lung and may well not be applicable for lesions that are located in the central part of the lung due to physiological differences in function between peripheral and central lung regions.

wide range of number of fractions and dose per fraction. Figure 4 shows these curves as thin lines, ranging from 4 to 24 Gy in dose per fraction and from 1 to 14 fractions. Each curve represents a certain MP local late damage NTD_3^{MP} level in Gy_3, as indicated in the key. We assume that intervals between successive fractions are long enough to allow full repair of sublethal radiation injury,

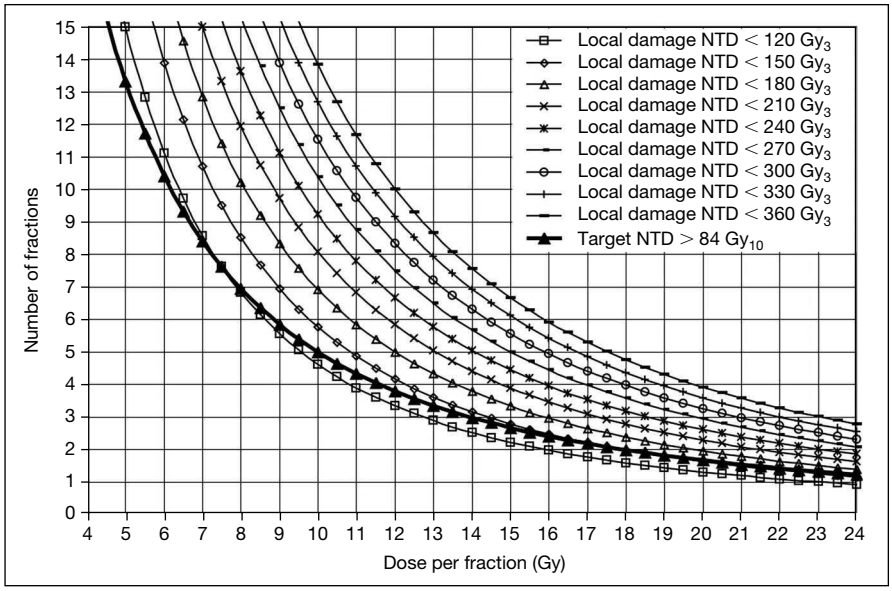

Fig. 4. Nomogram for the selection of the number of fractions and dose per fraction based on the constraint models MP $NTD_{10} > 84\,Gy_{10}$ and the MP late local damage NTD_3^{MP} selected form the nomogram shown in figure 3. The thick curve with the solid triangles corresponds to all schedules that deliver a MP tumor $NTD_{10} = 84\,Gy_{10}$, while the thin curves correspond to schedules that will deliver a chosen MP late local damage NTD_3^{MP}. Allowed fractionation schedules have to lie inside the wedge formed by a chosen late local damage NTD_3^{MP} curve from the nomogram shown in figure 3 and the thick NTD_{10} curve. Figures 3 and 4 are specific to the treatment planning constraints we have used (c.f. legend of figure 2) and should not be generalized to other treatment planning methods that do not meet these constraints. Moreover, it is emphasized that for any resulting treatment plan and chosen fractionation schedule employing these nomograms, the resulting mean NTD of the residual healthy lung has to be calculated to ensure that it is below $19\,Gy_3$.

at least 1 or 2 days. The lowest curve represents all schedules that provide a MP late local damage NTD_3^{MP} of $120\,Gy_3$. The second curve up defines schedules that deliver a MP local late damage NTD_3^{MP} of $150\,Gy_3$, and so forth.

The heavy line designated by the full triangles in figure 4 describes the dose schedules that correspond to a MP tumor NTD_{10} of exactly $84\,Gy_{10}$. Given an acceptable MP local late damage NTD_3^{MP} level determined from figure 3, the object of figure 4 is to find the points that lie above the heavy line for the MP tumor NTD_{10} and below the relevant chosen thin curve for the MP local late damage NTD_3^{MP} determined in step 1. The intersections of the heavy curve corresponding to a MP tumor $NTD_{10} = 84\,Gy_{10}$ and the thin curves corresponding to the allowed MP local late damage NTD_3^{MP} level represent the points where the

number of fractions and the doses per fraction are just sufficient to give both a MP tumor $NTD_{10} = 84\,Gy_{10}$ and the MP local late damage NTD_3^{MP} level denoted on that thin curve. Therefore, all theoretically acceptable fraction schedules in terms of MP tumor NTD_{10} and allowed MP local late damage NTD_3^{MP} levels lie inside the wedge above the heavy MP tumor NTD_{10} curve and below a chosen thin MP local late damage NTD_3^{MP} curve. For example, if the tumor size is such that only a MP local late damage NTD_3^{MP} level of $120\,Gy_3$ is acceptable, then we can look inside the wedge formed by the heavy $84\,Gy_{10}$ MP tumor NTD_{10} curve and the thin $120\,Gy_3$ MP local late damage NTD_3^{MP} curve, to see which combinations of dose per fraction and numbers of fraction are acceptable. Allowable combinations include 14 fractions of 5 Gy, 13 fractions of 5.25 Gy, 11 fractions of 6 Gy and 10 fractions of 6.25 Gy. It is emphasized that both the levels of Gy_{10} and Gy_3 should be chosen with appropriately updated relevant information.

If however, a MP NTD_3^{MP} level of $180\,Gy_3$ would be acceptable – say we are dealing with a smaller PTV or PIV or we are able to achieve a lower mean NTD for the residual healthy lung, then 12 fractions of 7 Gy, 10 fractions of 8 Gy, eight fractions of 9 Gy, six fractions of 10 Gy, four fractions of 12 Gy, four fractions of 13 Gy, three fractions of 15 Gy, and two fractions of 19 Gy would represent theoretically acceptable fractionation schedules (c.f. fig. 4). Timmerman et al. [4] have used three fractions of 23 Gy in the treatment of T1/T2 N0 M0 NSC lung cancer. As one can see from figure 3 this would require a PIV volume small enough that a MP local late damage NTD_3^{MP} level of $360\,Gy_3$ would be acceptable.

Discussion

Any fractionation schedule selected in this way should be used with extreme care and only in situations where it is acceptable that the entire target volume (PIV) and organizational tissue matrix in it may be destroyed; i.e. where no critical structures such as major bronchi or major blood vessels are part of the target volume. If no such critical structures are part of the PIV, then figure 4 could represent a provisional upper-limit guide in balancing the benefit of a high MP tumor NTD_{10} with an acceptable MP local late damage NTD_3^{MP}.

It is emphasized that this proposal is provisional and requires further data to confirm, or alter, particular dose levels. The use of any particular schedule should be limited to ratios of PIV to the residual healthy lung volume that are less than the intercept of the MP local late damage NTD_3^{MP} curve with the horizontal K-S-DJ line, which represents the NTD_{mean} value for the residual healthy lung corresponding to a 20% incidence of radiation pneumonitis of grade 2 or higher.

When the MP local late damage NTD_3^{MP} level is largest, the curve rises most steeply and intersects the horizontal K-S-DJ line at the smallest PIV to residual-healthy-lung-volume ratio. This indicates that the dose within the PIV cannot rise to extremely high values for any practical size of the GTV, since margins have to be added to the GTV that account for breathing motion of the GTV and the extent of microscopic disease. Thus the largest MP local late damage NTD_3^{MP} level used is actually similar to the upper curve of $NTD_3^{MP} = 360\,Gy_3$, which is the biological equivalent in 2 Gy fractions of three 23 Gy fractions. This curve intersects the K-S-DJ line at a ratio of PIV to the residual healthy lung volume of 1.5%.

However, for schedules having a lower predicted MP NTD_3^{MP} level such as for instance $180\,Gy_3$ clinically manifest radiation pneumonitis of grade 2 or higher would not become theoretically dose limiting until a PIV to the residual lung volume ratio of 5.5 % is reached. Using the above value of 4860.57 cm^3 for the residual healthy lung volume, this yields a prescription isodose volume of 267.31 cm^3. To test the sensitivity of the model to variations of the α/β ratio we have repeated the calculations in figure 3 assuming a α/β ratio of 2 and 4 Gy, respectively instead of 3 Gy. The critical PIV volumes represented were then 21% smaller and 24% larger respectively.

It is emphasized that the nomograms shown in figures 3 and 4 should only be used as a guide for the selection of a fractionation schedule. The size of the PIV must be known. For example a schedule corresponding to a predicted MP local late damage NTD_3^{MP} level of $270\,Gy_3$ would only be suitable if the PIV is smaller than about 2.5% of the residual healthy lung volume. It is additionally emphasized that for any *resulting treatment plan and chosen fractionation schedule employing these nomograms*, the resulting mean NTD of the residual healthy lung *has to be calculated* to check that it is well below $19\,Gy_3$. Furthermore, other clinical factors such as prior or concomitant chemotherapy and overall lung function should be taken into account when choosing a value for the mean NTD to the residual healthy lung one deems save. This means that the K-S-DJ line may have to be adjusted downwards for certain patient populations (c.f. Fowler et al. [7] in this respect).

Conclusions

Our modeling shows that the selection of a dose fractionation schedule for a targeted 30 month progression free survival of 80% or higher depends on the following factors: The PIV, the MP late local damage NTD_3^{MP} around the high dose volume, and the mean NTD of the residual healthy lung. Therefore, in order to be able to choose the fractionation schedule that gives the highest 30 month progression free survival one needs to minimize the PIV as far as

possible without compromising adequate PTV coverage, i.e. one needs to minimize the PIV to PTV ratio while maintaining good dose volume coverage as evidenced by the PTV-DVH. This clearly indicates the need to incorporate advanced treatment planning techniques, 4D imaging techniques, and volumetric image guided treatment delivery techniques into the SBRT treatment process.

Inverse planning can be used to reduce the PIV by conforming the prescription isodose more closely to the PTV. While 4D imaging techniques, such as 4D-CT and/or 4D-PET, can be used to better define the PTV. Last but not least volumetric image guided treatment delivery such as cone beam CT or MVCT can be used to reduce the systematic and random setup errors down to the imaging uncertainty, and therefore allow one to reduce margins to only take account of breathing motion of the GTV, the extent of microscopic disease, and residual measurement errors [22], yielding a reduced PTV.

References

1 Uematsu M, Shioda A, Suda A, et al: Computed tomography-guided frameless stereotactic radiotherapy for stage I non-small cell lung cancer: a 5-year experience. Int J Radiat Oncol Biol Phys 2001;51:666–670.

2 Nagata Y, Negoro Y, Tetsuya A, et al: Clinical outcomes of 3D conformal hypofractionated single high-dose radiotherapy for one or two lung tumors using a stereotactic body frame. Int J Radiat Oncol Biol Phys 2002;52:1041–1046.

3 Nagata Y, Takayama K, Aoki T, et al: Clinical outcome of 3-D conformal hypofractionated high-dose radiotherapy for primary and secondary lung cancer using a stereotactic technique. Int J Radiat Oncol Biol Phys 2003;57(suppl 1):S280.

4 Timmerman RD, Papiez L, McGarry RC, et al: Extracranial stereotactic radioablation. Results of a phase I study in medically inoperable stage I non-small cell lung cancer. Chest 2003;124: 1946–1955.

5 Onishi H, Araki T, Shirato H, et al: Stereotactic hypofractionated high-dose irradiation for stage I nonsmall cell lung carcinoma: clinical outcomes in 245 subjects in a Japanese multiinstitutional study. Cancer 2004;101:1623–1631.

6 Wada H, Takai Y, Nemoto K, et al: Univariate analysis of factors correlated with tumor control probability of three-dimensional conformal hypofractionated high-dose radiotherapy for small pulmonary or hepatic tumors. Int J Radiat Oncol Biol Phys 2004;58:1114–1120.

7 Fowler JF, Tomé WA, Fenwick JD, Mehta MP: A challenge to traditional radiation oncology. Int J Radiat Oncol Biol Phys 2004;60:1241–1256.

8 Martel MK, Ten Haken RK, Hazuka MB, et al: Estimation of tumor control probability model parameters from 3-D dose distributions of non-small cell lung cancer patients. Lung Cancer 1999;24:31–37.

9 Withers HR, Taylor JMG, Maciejewski B: The hazard of accelerated tumor clonogen repopulation during radiotherapy. Acta Oncol 1988;27:131–146.

10 Brenner DJ: Accelerated repopulation during radiotherapy: quantitative evidence for delayed onset. Radiat Oncol Invest 1993;1:167–172.

11 Roberts SA, Hendry JH: The delay before onset of accelerated tumor cell repopulation during radiotherapy: a direct-maximum likelihood analysis of a collection of worldwide tumor-control data. Radiother Oncol 1993;29:69–74.

12 Roberts SA, Hendry JH, Brewster AE, Slevin NJ: The influence of radiotherapy treatment time on the control of laryngeal cancer: A direct analysis of data from two British Institute of Radiology trials to calculate the lag period and the time factor. Br J Radiol 1994;67:790–794.
13 Robertson C, Robertson AG, Hendry JH, Roberts SA, Slevin NJ, Duncan WB, Keane TJ: Similar decreases in local control are calculated for treatment protraction and for interruptions in the radiotherapy of carcinoma of the larynx in four centres. Int J Radiat Oncol Biol Phys 1998;40: 319–329.
14 Fowler JF, Chappell R: Nonsmall cell lung tumors repopulate rapidly during radiation therapy. (Letter) Int J Radiat Oncol Biol Phys 2000;46:516–517.
15 Fowler JF: The linear-quadratic formula and progress in fractionated radiotherapy: a review. Br J Radiol 1989;62:679–694.
16 Douglas BG, Fowler JF: The effect of multiple doses of X-rays on skin reactions in the mouse and a basic interpretation. Radiat Res 1976;6:401–426.
17 Kwa LS, Lebesque JV, Theuws JCM, et al: Radiation pneumonitis as a function of mean lung dose: an analysis of pooled data of 540 patients. Int J Radiat Oncol Biol Phys 1998;42:1–9.
18 Seppenwoolde Y, Lebesque J: Partial irradiation of the lung. Sem Radiat Oncol 2001;11:247–258.
19 Seppenwoolde Y, Lebesque J, de Jaeger K, et al: Comparing different NTCP models that predict the incidence of radiation pneumonitis. Int J Radiat Oncol Biol Phys 2003;55:724–735.
20 De Jaeger K, Hoogeman MS, Engelsman M, et al: Incorporating an improved dose-calculation algorithm in conformal radiotherapy of lung cancer: re-evaluation of dose in normal lung tissue. Radiother Oncol 2003;69:1–10.
21 Tomé WA, Fenwick JD: Analysis of radiation-induced liver disease using the Lyman NTCP model: in regards to Dawson et al. IJROBP 2002;53:810–821 (letter). Int J Radiat Oncol Biol Phys 2004;58:1318–1319.
22 Keller H, Tomé WA , Ritter MA, Mackie TR: Design of adaptive treatment margins for non-negligible measurement uncertainty: application to ultrasound-guided prostate radiation therapy. Phys Med Biol 2004;49:69–86.

Dr. Wolfgang A. Tomé, Associate Professor
Department of Human Oncology
600 Highland Ave.
Madison, WI 53792 (USA)
Tel. +1 608 263 8510, Fax +1 608 263 9167
E-Mail tome@humonc.wisc.edu

Kondziolka D (ed): Radiosurgery. Basel, Karger, 2006, vol 6, pp 98–107

Concepts of Conformality and Selectivity in Acoustic Tumor Radiosurgery

L. Dade Lunsford, Douglas Kondziolka, Ajay Niranjan, John C. Flickinger, Ann Maitz

The Departments of Neurological Surgery and Radiation Oncology, University of Pittsburgh School of Medicine, and The University of Pittsburgh Medical Center, Pittsburgh, Pa., USA

Abstract

The goals of acoustic neuroma radiosurgery include cessation of tumor growth, tumor volume regression, elimination of open surgical risks, maintenance of existing cranial nerve function and improvement of patient's symptoms. In order to evaluate current technology usage at the University of Pittsburgh, we reviewed our current stereotactic imaging, and dose planning techniques for acoustic neuroma radiosurgery. We then assessed the impact of highly conformal and selective dose plans on the outcome of acoustic neuroma. Conformality denotes that selected isodose conforms to the three-dimensional target volume and the target dose is high. Selectivity refers to the fact that the integral dose to surrounding tissues outside of the target volume is low. Various conformality indices have been proposed to measure the perfection of a radiosurgical plan where selected isodose volume perfectly matches the 3-D geometry of the image defined target volume. A variety of technologies have been developed to enhance conformality and selectivity over the years. High resolution MRI is necessary to define the 3-D tumor volume and to delineate adjacent critical structures including the cochlea, semi-circular canals, and cranial nerves. Multiple isocenter plans using the Gamma Knife achieves a very high conformality and permits very high selectivity using small beams. The incorporation of robotic dose delivery facilitates highly accurate delivery of radiation, maximizing both conformality and selectivity.

The goal of acoustic neuroma management is to provide the best outcome possible for patients with a tumor which is increasingly being recognized when smaller, and when hearing preservation is both possible and desirable. Minimally invasive treatment strategies for acoustic neuroma have replaced the

prior open surgical paradigm, since abundant data now establishes the hearing and facial nerve preservation rates as superior to either observation or microsurgical removal [1–5]. In addition, radiosurgery does not have the associated potential medical risk factors that still produce poor outcomes in some patients who select microsurgical management. Between 1969 and 2004, over 26,000 patients worldwide out of a total benign tumor population of almost 100,000 had acoustic neuroma Gamma Knife® radiosurgery. In the same interval, 7,136 acoustic tumor patients underwent Gamma Knife radiosurgery in the United States alone.

At the University of Pittsburgh, the goals of acoustic neuroma radiosurgery include cessation of tumor growth, tumor volume regression, elimination of open surgical risks, maintenance of existing cranial nerve function and improvement of patient's symptoms.

In order to evaluate current technology usage, we have reviewed our current planning techniques, imaging techniques and outcome variables derived from an 18 year experience in the management of acoustic neuromas at the University of Pittsburgh Center For Image Guided Neurosurgery. We then assessed the impact of highly conformal and selective management of acoustic neuromas using the Gamma Knife.

Review of Total Experience

During the 18 year interval from 1987 to 2005, 1,105 patients (551 female, 554 male) underwent Gamma Knife radiosurgery for management of their newly diagnosed or recurrent or residual acoustic neuroma. Past management strategies included gross total resection in 38 (3.4%) and sub-total resection in 155 (14%). Presenting symptomatology included imbalance symptoms in 516 (46.7%), hearing loss in 979 (88.6%), tinnitus in 517 (46.8%), and facial sensory dysfunction in 149 (13.5%) patients. Clinical outcomes were evaluated by serial imaging studies, preferentially using MRI scans. Volume measurements were made using the methodology of Linskey et al. [6] multiplying the distances perpendicular to the petrous bone, parallel to the petrous bone, and in the superior–inferior dimension. In long-term follow-up, 98% of patients had long-term tumor control, and by year nine or ten, 70% of patients had volumetric regression of their tumors, and 30% had no further change. Less than 2% of patients required delayed additional tumor management, either microsurgical resection or CSF diversion for hydrocephalus.

Current clinical outcomes indicated that 70–75% of patients maintained useful hearing in our analysis of patients with useful hearing present at the time of the procedure. In addition, 75% of patients maintained their pre-radiosurgical

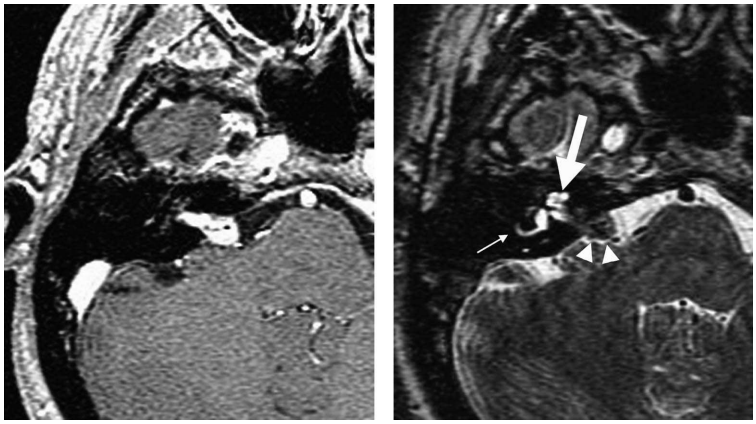

Fig. 1. Contrast enhanced spoiled gradient recalled acquisition in steady state intraoperative MR Axial images (left) showing enhancing acoustic tumor. The T2 weighted 3D image helps delineate cochlea (large white arrow), and semicircular canals (small white arrow) in addition to showing the acoustic tumor (arrow heads).

Gardner-Robertson hearing Class. No patient had additional hearing loss with more than two years of observation.

Current prescription doses for the three-dimensional margins of acoustic tumors using conformal MRI dose planning is 12.5–13 Gy, usually treated at the 50% isodose. The usual tumor maximum dose is 25–26 Gy. In the last ten years, facial nerve preservation has been maintained in 100% of patients at these doses.

Imaging Technique

The optimal current imaging technique requires high resolution MR imaging using spoiled gradient recalled acquisition in steady state sequence with 1 mm to 1.5 mm axial slices. In addition, a 3-D T2 weighted acquisition is performed using 1 mm slices (thereby rendering CSF white and the tumor volume dark). This provides the best definition not only of cranial nerve structures, but also the relationship of the tumor to the brainstem, as well as optimal definition of the cochlea and the semi-circular canals. Using the high resolution 3-D T2 weighted volume sequence, the cochlea, the semi-circular canals, vascular structures, and cranial nerve structures are readily identified (fig. 1). In addition, the fast imaging employing steady state acquisition sequence can also be used.

Planning

Dose planning is performed using both imaging sequences to define the tumor margin and to achieve highly 3D conformal dose delivery to the edge of the tumor. The importance of selectivity and conformality has been defined by a number of investigators including del Valle et al. [7]. Invariably, small isocenters (e.g. 4 and 8 mm beams) are used. Increasingly over the last 10 years, we rely more on small volume isocenters using 4 and 8 mm beam diameters to maximize conformality and improve selectivity. Conformality refers to the fact that the selected isodose conforms to the three dimensional target volume (TV) and the target dose is high. Selectivity is an equally important aspect of effective radiosurgery, and refers to the fact that the integral dose to surrounding tissues outside of the TV is low.

Single procedure marginal doses of between 12 and 13 Gy to the tumor edge are associated with high tumor control rates at long-term follow-up. Radiation delivery is accomplished under the guidance of a multi-disciplinary team including a neurosurgeon, radiation oncologist and medical physicist. The dose is delivered using robotic positioning of the automatic positioning system on either the C or the 4-C Gamma Knife.

Discussion

Various conformality indices have been proposed to measure the perfection of a radiosurgical plan where selected isodose volume perfectly matches the 3-D geometry of the image defined TV. One conformality index proposes that the planned isodose volume (PIV), divided by the TV should equal one [8]. An imperfect plan wherein the dose delivered is entirely outside of the tumor volume would result in a conformality index of zero. More elaborate conformality indices [9–13] have been proposed including that of Paddick [14] who suggested that a conformality index could be determined by $(\text{TV in PIV})^2/\text{TV} \times \text{PIV}$. This concept is useful, but somewhat complex.

In a perfect plan, the conformality index of one requires that the technique provides high 3-D conformality and high selectivity (reduced dose to surrounding critical structures). When the conformality index is less than one, the procedure would be associated with low conformality and low selectivity. Under treatment, wherein the conformality index is also less than one, might also include low conformality with high selectivity. If there were imaging shifts (and the TV resulted in partial tumor treatment) the conformality index would also be less than one. If coordinates were inappropriately set, then a conformality index of zero relating to incorrect dose delivery to normal structures could be identified. These concepts are outlined in figure 2. The imaging outcome of

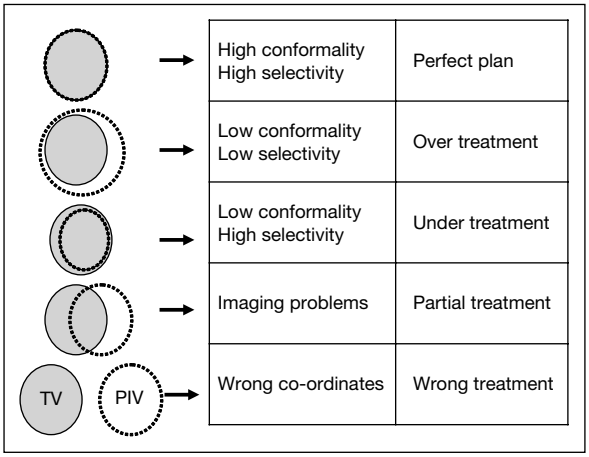

Fig. 2. The diagrammatic representation (left) of concepts of the conformality index. PIV = Planned isodose volume; TV = tumor.

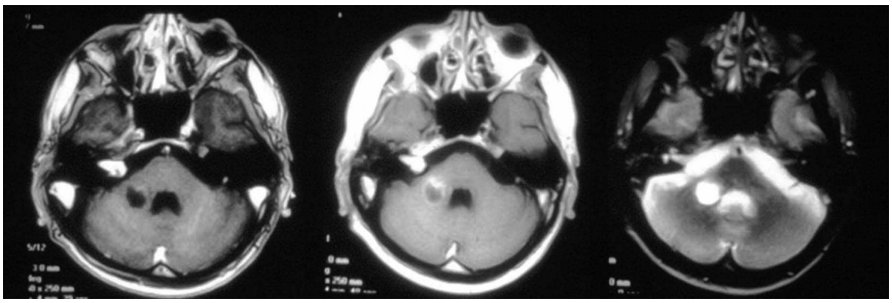

Fig. 3. Follow-up MR images of a patient who was treated for a right sided acoustic tumor using LINAC radiosurgery at an outside facility. The axial images show a radiation effect in the middle cerebellar peduncle which is completely outside the TV (tumor). This patient developed profound ipsilateral limb ataxia 6 months after undergoing LINAC radiosurgery.

conformality index of zero could be seen in figure 3, in this case a LINAC radiosurgery procedure delivered to inappropriate TVs, resulting in radionecrosis in the middle cerebellar peduncle rather than in the tumor volume. This patient developed profound ipsilateral limb ataxia 6 months after undergoing LINAC radiosurgery.

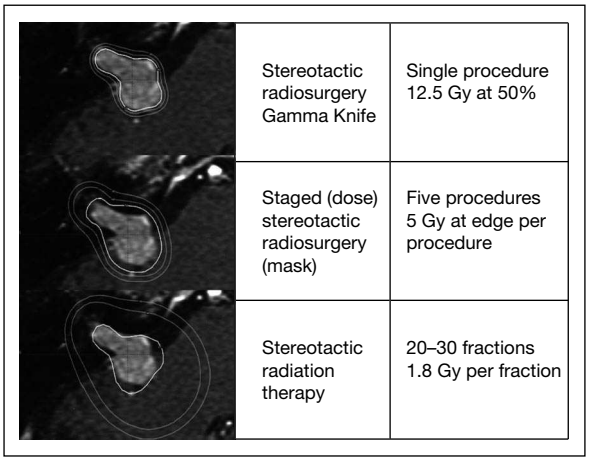

Fig. 4. A hypothetical representation of dose plans showing difference in conformality and selectivity. The Gamma Knife plan (top) is actual. The other plans are theoretical. Isodose shells depicted are 50, 30, and 20%.

Implications for Patient Selection and Management

When a technology such as Gamma Knife radiosurgery using robotic positioning and multiple small isocenters is available, both high conformality and high selectivity are possible. This facilitates delivery of the entire radiation in a single surgical session (stereotactic radiosurgery) as initially practiced beginning in 1967. Other technologies may result in high conformality, perhaps using intensely modulated radiation therapy, or image-guided radiation therapy, wherein the fractionally delivered dose seeks to achieve high 3-D conformality. Typically, slow dose fall-off leads to high dose to the surrounding brain (low selectivity). Multiple session radiation therapy perhaps done in a hypofractionated scheme or staged stereotactic radiosurgery (e.g. CyberKnife®) may maintain similar levels of patient safety (fig. 4). Of course such patients are treated with non-frame mask techniques, and require multiple sessions of radiation. Long-term results assessing equivalency of outcomes are not available.

When the radiation delivery technique results in both low conformality and low selectivity, it is important to use conventional fractionated radiation therapy techniques for delivery of the radiation at low doses over multiple fractions (e.g. 20–30 fractions). Our experience with Gamma Knife radiosurgery in a single surgical session shows excellent long term tumor growth control with tumor volume reduction noted in the majority of patients at between 1 and 7 years.

Table 1. Comparison of relative professional roles in Gamma Knife, CyberKnife, and other LINAC based radiosurgery systems

	Stereotactic radiosurgery	Staged (dose) stereotactic radiosurgery	Stereotactic radiation therapy
Immobilization	NS	NS, RO	RO
Imaging	NS, MP	MP	MP
Dose planning	NS, RO, MP	NS, RO, MP	RO, MP
Dose delivery	NS, RO, MP	RT	RT

NS = Neurosurgeon; MP = medical physicist; RO = radiation oncologist; RT = radiation therapist.

Implications for Roles

Conformality and selectivity issues pose questions related to physician responsibility and education. Stereotactic radiosurgery is a single surgical session paradigm which requires accurate immobilization using a stereotactic guiding device, high-resolution stereotactic imaging and conformal dose planning performed under the direction of a neurological surgeon. Final dose selection and dose delivery are performed (at least in the United States) under the combined direction of a neurosurgeon, a radiation oncologist and an authorized medical physicists (table 1).

Staged stereotactic radiosurgery (e.g. CyberKnife) using hypo fractionated stereotactic radiation with a re-locatable mask, shifts responsibilities for immobilization, imaging, dose planning, and dose delivery towards the radiation oncology and medical physics team. In this treatment technique, dose delivery is performed by a radiation therapist and the physical presence of a physician may not be necessary. Similarly, when stereotactic radiation therapy is performed, mask immobilization is performed under the surveillance of a radiation oncologist or medical physicist; imaging and dose planning are often completed after outlining or estimating the treatment volume. Many systems use CT based imaging which is not sufficient for acoustic tumor management. Dose delivery is under the direction of a radiation therapy technician and a medical physicist. The physical presence of a neurosurgeon or radiation oncologist may not be required. Neurosurgeons appear to have little role in hypofractionated radiation therapy of skull base tumors, who instead may be relegated to the role of dealing with failures. Surgeons may not even provide informed consent about therapeutic options to individual patients. Conformality and selectivity issues also influence decisions related to integral dose to tumor, integral dose to surrounding brain and

Table 2. Comparison of technologies used in Gamma Knife, CyberKnife, and other LINAC based radiosurgery systems

	Gamma Knife	CyberKnife	LINAC
Robotics	+	+	−
MRI dose planning	+	−	±
Image fusion	±	±	±
Multileaf collimator	−	−	±

cranial nerve structures, tumor control, cranial preservation rates, and long term outcome data. Determination of conformality and selectivity promote efficiency, reliability, and reproducibility at the same center and between centers, and facilitate uniformity of therapeutic approaches.

At the present time, Gamma Knife radiosurgery in centers across the world has been associated with a 98% tumor control rate at 10–15 year intervals. Hearing preservation is possible in 50–100% of patients depending on tumor volume. Facial nerve preservation is possible in virtually all patients. Trigeminal sensory dysfunction occurs (even in patients with larger tumors) in less than 10% of patients. Currently, comparable results of staged stereotactic radiosurgery or hypofractionated radiation therapy are not available beyond three to four years. It is unlikely that any comparative technology and outcome studies will be possible for such relatively rare tumors as acoustic neuroma, thought to affect only about 2,000 U.S. citizens each year. In order to establish the superiority of one management strategy versus another, e.g. by determining cranial nerve preservation rates and long-term tumor control, a prospective scientific trial require thousands of patients in each treatment arm.

A variety of technological improvements have been developed to enhance conformality and selectivity over the years. Robotics are used in both Gamma Knife and CyberKnife technologies, but generally not in other Linear accelerator based radiation therapy techniques (table 2). MRI dose planning is felt to be crucial for target definition using the Gamma Knife, but is generally available only as a fusion algorithm for Linear accelerator based technologies. Increasingly, Gamma Knife centers use a variety of small beams with an average of 6–12 isocenters per patient in order to develop an appropriate conformal geometry plan. Current outcome data shows that the potential advantage of fractionation in limiting brain and cranial nerve toxicity only makes sense if the radiation is affecting excessive volumes of normal brain or adjacent cranial nerve.

Table 3 shows the concept of conformality and selectivity issues. Stereotactic radiosurgery can be done in a single procedure because of high

Table 3. Physicians and patients can select radiation delivery technology (Gamma Knife, CyberKnife, or IMRT) based on the conformality and selectivity issues

Low conformality Low selectivity	Fractionated radiation therapy
High conformality Low selectivity	Hypofractionated radiation therapy versus staged stereotactic radiosurgery
High conformality High selectivity	Stereotactic radiosurgery

conformality and high selectivity. When there is high conformality but low selectivity, the radiation should be divided into multiple sessions using either staged radiosurgery or hypofractionated radiation therapy techniques. When both low conformality and low selectivity are inherent to the technology, the radiation delivery should be divided into 20–30 fractions at standard fractionation schedules such as 1.8 Gy per fraction.

Conclusions

At the present time, stereotactic radiosurgery, a single surgical procedure, wheels in to wheels out, has excellent long-term outcomes in terms of tumor growth control and cranial nerve preservation. High resolution MRI is necessary to define the 3-D tumor volume and to delineate adjacent critical structures including the cochlea, semi-circular canals, and cranial nerves. Multiple isocenter plans using the gamma knife achieves a very high conformality and permits very high selectivity using small beams (4 or 8 mm in diameter). Doses of 12–13 Gy at the margin result in tumor growth control rates at ten years in the 98% range. The incorporation of robotic dose delivery facilitates highly accurate delivery of radiation, maximizing both conformality and selectivity.

References

1 Chung WY, Liu KD, Shiau CY, et al: Gamma knife surgery for vestibular schwannoma: 10-year experience of 195 cases. J Neurosurg 2005;102(suppl):87–96.

2 Flickinger JC, Kondziolka D, Niranjan A, et al: Acoustic neuroma radiosurgery with marginal tumor doses of 12 to 13 Gy. Int J Radiat Oncol Biol Phy 2004;60:225–230.

3 Hasegawa T, Kida Y, Kobayashi T, et al: Long-term outcomes in patients with vestibular schwannomas treated using gamma knife surgery: 10-year follow up. J Neurosurg 2005;102:10–16.

4 Kondziolka D, Lunsford LD, McLaughlin MR, et al: Long-term outcomes after radiosurgery for acoustic neuromas [see comment]. N Engl J Med 1998;339:1426–1433.
5 Lunsford LD, Niranjan A, Flickinger JC, et al: Radiosurgery of vestibular schwannomas: summary of experience in 829 cases. J Neurosurg 2005;102(suppl):195–199.
6 Linskey ME, Lunsford LD, Flickinger JC: Neuroimaging of acoustic nerve sheath tumors after stereotaxic radiosurgery. Am J Neuroradiol 1991;12:1165–1175.
7 del Valle R, Perez M, Ortiz J, et al: Stereotactic noninvasive volume measurement compared with geometric measurement for indications and evaluation of gamma knife treatment. J Neurosurg 2005;102(suppl):140–142.
8 Nakamura JL, Verhey LJ, Smith V, et al: Dose conformity of gamma knife radiosurgery and risk factors for complications. Int J Radiat Oncol Biol Phy 2001;51:1313–1319.
9 Leung LH, Chua DT, Wu PM: A new tool for dose conformity evaluation of radiosurgery treatment plans. Int J Radiat Oncol Biol Phys 1999;45:233–241.
10 Lomax NJ, Scheib SG: Quantifying the degree of conformity in radiosurgery treatment planning. Int J Radiat Oncol Biol Phys 2003;55:1409–1419.
11 Surber G, Hamm K, Kleinert G: Significance of different conformity indices for evaluation of radiosurgery treatment plans for vestibular schwannomas. J Neurosurg 2004;101(suppl 3):334–340.
12 Wagner TH, Bova FJ, Friedman WA, et al: A simple and reliable index for scoring rival stereotactic radiosurgery plans. Int J Radiat Oncol Biol Phys 2003;57:1141–1149.
13 Wu QR, Wessels BW, Einstein DB, et al: Quality of coverage: conformity measures for stereotactic radiosurgery. J Appl Clin Med Phy 2003;4:374–381.
14 Paddick I: A simple scoring ratio to index the conformity of radiosurgical treatment plans. Technical note. J Neurosurg 2000;93(suppl 3):219–222.

L. Dade Lunsford
Department of Neurological Surgery, Suite B-400
University of Pittsburgh Medical Center
200 Lothrop Street
Pittsburgh, PA 15213 (USA)
Tel. +1 412 647 6781, Fax +1 412 647 6483
E-Mail lunsfordld@upmc.edu

Kondziolka D (ed): Radiosurgery. Basel, Karger, 2006, vol 6, pp 108–117

Stereotactic Radiosurgery in the Management of Glomus Jugulare Tumors

Francisco Mascarenhas[a], *António Gonçalves Ferreira*[b], *Herculano Carvalho*[b], *Alvaro Almeida*[c], *Miguel Santos*[a], *Maria B. Cattoni*[b], *Sara Germano*[a]

Departments of [a]Radiotherapy, [b]Neurosurgery and [c]Radiology, Hospital de Santa Maria, Lisboa, Portugal

Abstract

Purpose: This retrospective study evaluate the efficacy and toxicity of stereotactic radiosurgery (SRS) in the management of the glomus jugulare tumors. **Methods:** Fifteen patients were submitted to SRS with a 6 MV LINAC at the Hospital Santa Maria in Lisbon between July 1997 and February 2005. Median age was 55.4 years (range 30–77) of twelve females and three males. Six patients have failed to previous treatment modalities. The reasons to manage these patients with SRS included residual or recurrent tumors after surgery and embolization (6), geriartric/medically unsuitable for surgery or unresectable tumors (5) and patient preference (4). The tumor volume ranged from 2.3 to 10.4 ml (mean, 6.3 ml). The median marginal dose was 13.8 Gy (range, 12–15 Gy) and the median maximum dose was 17.6 Gy (range, 16.3–18.7 Gy). **Results:** The median time from date of SRS to the last follow-up was 47.3 months (range, 2–92 months) including six and nine patients with more than 60 and 36 months respectively. Improvement of the symptoms and cranial nerve disfunctions were presented in fourteen patients with no melioration in symptoms in one patient who remained with stable tumor. After last surveillance magnetic imaging eleven tumors were shrinkaged and four remained stable being considered as local control achieved in all patients. No acute or late toxicity was detected. **Conclusions:** Our experience in this series presenting excellent tumor control rate and a favorable toxicity profile support the effectiveness of SRS for patients with glomus jugulare tumors.

Glomus jugulare tumors (GJT) otherwise known as chemodectomas and paragangliomas are rare neoplasms but one of the most frequent skull base tumors and may occur in intracranial and extracranial locations. Their incidence

is estimated to be 1 in 1 million persons but they represent the most common benign lesions of the middle ear [1]. They arise from the paraganglionic tissue surrounding the adventitia of the jugular bulb with potential invasion of the temporal bone or along the Jacobson's nerve or more rarely along the Arnold–Cruveiller's nerve and vagus nerve. These neoplasms are normally benign although 2–5% have been reported as exhibiting malignant degeneration with metastatic dissemination to bone, lung and liver [2–4]. They are slow-growing lesions with an indolent progression before diagnosis but causing clinical pictures with several grades of severity by compression or local invasion of neurovascular structures within the jugular foramen, hypoglossal canal and temporal bone. The symptoms are related with the compromise of the brain stem and the cranial nerves and can present neuropathies of the seventh–twelfth cranial nerves.

The traditional management of the GJT includes microsurgical resection associated or not to endovascular embolization. External radiotherapy is another treatment option that is recommended in advanced lesions with potential risk of surgical morbidity [5–8]. The choice of treatment modality remains controversial and depends on some factors mainly the volume and location of the tumor, the age and medical conditions of the patients, the presence of unresectable or recurrent tumors and the preference of the patients [5, 6]. The preferred treatment of the GJT is the microsurgical resection associated or not to endovascular embolization with conservation of the cranial nerves and preservation of major vessels and brainstem. This modality supported by modern imaging techniques and associated to interventional radiological procedures has presented a rate of complications of cranial nerves ranged between 49 and 83% and a mortality rate from 0 to 5% [3, 6]. In a considerable number of patients surgery can be potentially associated with a high risk of morbidity and this risk should not be higher than the risk of the therapeutic alternatives. Conventional external radiotherapy is one possible treatment modality that can prevent the progression of the tumor and meliorate the symptoms with improvement of quality of life [7, 8]. A high long-term control rate after this therapy is referred in the literature [7–12].

Post-irradiation complications as osteoradionecrosis of the temporal bone, chronic otitis, auditory canal stenosis, pharyngitis, cataracts and radiation-induced second malignancy are also described. Stereotactic techniques of radiotherapy using a highly focused beam associated to a stereotactic guidance can provide a high long-term tumor control, symptom relief and improvement of quality of life with minimal adverse effects [13–16].

The purpose of this study was to evaluate the long-term results of radiosurgery in patients with GJT in our institution in terms of local control and complications.

Table 1. Patient data, prior treatments, tumor characteristics and pre-radiosurgical cranial nerve deficits

Patient	Sex/age	Prior treatment	Fisch classification [17]	Volume tumor, cm^3	Cranial nerve dysfunction
1	M/56	none	D1	2.3	VIII, IX, X, XI, XII
2	F/62	E	D1	2.4	VIII
3	F/71	none	D1	3.0	IX, X, XI, XII
4	M/30	E + S	D2	2.7	VII, VIII, IX, X, XI, XII
5	F/39	S	D1	5.6	VIII, IX, X
6	F/60	none	D1	8.0	IX, X, XI, XII
7	F/66	none	D1	4.4	VIII
8	F/60	none	D2	10.0	VIII, IX, X, XI, XII
9	F/44	S + E + S	D2	9.9	VII, VIII, IX, X, XI, XII
10	F/36	S	D2	10.4	VII, VIII, IX, X, XI, XII
11	M/43	none	D2	9.7	VIII
12	F/50	S + S + S	D1	7.1	VII, VIII, IX, X, XII
13	F/72	none	D1	5.4	IX, X, XII
14	F/77	none	D1	5.4	VIII, IX, X, XII
15	F/65	none	D2	8.8	VIII, IX, X, XII

E = Endovascular embolization; S = surgical resection.

Methods and Materials

From July 1997 to February 2005 fifteen patients with GJT were treated with LINAC-based stereotactic radiosurgery (SRS). The criteria defined to include these patients for RS were age less than 80 years, marked symptoms caused by the lesions, good performance status with Karnofsky of 70 or above and greater tumor diameter below 40 mm. Patients with larger lesions are treated with stereotactic fractionated radiotherapy in our institute since 2001. Five of these patients had been treated and followed up for more than 7 years and eight for more than 4 years after their radiosurgery. The medium imaging MR follow-up was 49.3 months (4.1 years).

Patients and Tumor Characteristics

The reasons for the choice of SRS were the potential morbidity for unresectable tumors in five patients, the recurrence after surgical resection and embolization in six patients and the preference of patients in four. Twelve females and three males with a median age of 55.4 years (ranged from 30 to 77 years) presented a median tumor volume of 6.3 cm^3 (ranged from 2.3 to 10.4 cm^3). The most frequent signs and symptoms before SRS were tinnitus and hearing loss (80%), swallowing disturbances (80%), hoarseness (73.3%), muscles atrophy (46.7%), facial paralysis (20%) and are described in table 1. A 36-years aged woman with an advanced recurrent tumor after embolization and surgical resection lived during 8 months with a permanent percutaneous gastrostomy by severe disturbances of swallowing. All patients were submitted to audiograms, CT and MRI and nine realized angiography before SRS. Written informed consent was always performed in every patient.

The patients were followed up every 3–6 months since their treatment and CT or MRI was performed at varying intervals depending on the patients' symptoms and departments' facilities. All the imaging studies of follow-up were compared with the MRI previous to SRS and neuroradiologist measured any changes of tumor volume. Local control was defined as tumor shrinkage or stabilization of the dimensions of the last imaging study compared with the previously made before SRS. Adverse effects or complications of SRS were clinically evaluated by MRI.

SRS Techniques

Ten patients were submitted to SRS with a Leksell frame supported by a floor stand device (3-D Line) and with 6-MV photons from a Siemens LINAC (Mevatron MD2) and in five patients treatments were performed with a BRW frame, a Radionics couch stand device and with 6-MV photons from a Varian LINAC (Clinac 2100 C/D). The Nucletron Plato planning system (SRS version v. 2.0-B001) was used. Both techniques have been previously described [18, 19]. The treatment planning were done based on a double contrast-enhanced CT scan, 2 mm-slice thickness with or without image fusion gadolinium-enhanced MRI. A median marginal dose of radiation was 13.8 Gy (range, 12–15 Gy) and the median maximum dose was 17.6 Gy (range, 16.3–18.7 Gy). The dose was prescribed to the 80% isodose line in 13 patients and to the 70% isodose line in two patients. A dose of 15 Gy was administered in seven patients with smallest tumors (volumes $\leq 5\,cm^3$), 12.5–14.5 Gy in six patients with intermediate-sized tumors (volumes of 5–10 cm^3) and 12 Gy in two patients with largest tumors (volumes $>10\,cm^3$).

Results

All patients are alive and have been submitted to periodical follow-up. No acute or late toxicity related to SRS was identified in this series.

MRIs were used in all patients to determine the largest diameter in axial, coronal and sagittal axis of each lesion in the last follow-up and were compared with previous studies performed before SRS. Any increase in any dimension would be considered as tumor growth. These studies revealed a reduction >20% of tumor volume (major reduction) in 2 patients (13.3%), a reduction ≤20% (minor reduction) in 11 patients (73.3%) and stabilization of the tumor size in 3 patients (20%). The patient 10 had a significant improvement of swallowing difficulty 1 month after SRS and removed definitively the percutaneous gastrostomy after this time. The MRI realized in 37 months after SRS revealed a major reduction in tumor volume (fig. 1). In the most recent follow-up fourteen patients (93.3%) reported subjective improvement in one or more of their presenting symptoms more likely decrease of the intensity of tinnitus, improvement of speech and voice quality and improvement of swallowing. In one patient (6.7%) there was no melioration in symptoms and tumor remained stable with no dimensional reduction or enlargement. There was no identification of tumor growth in any patient (table 2). No acute or late complications were detected.

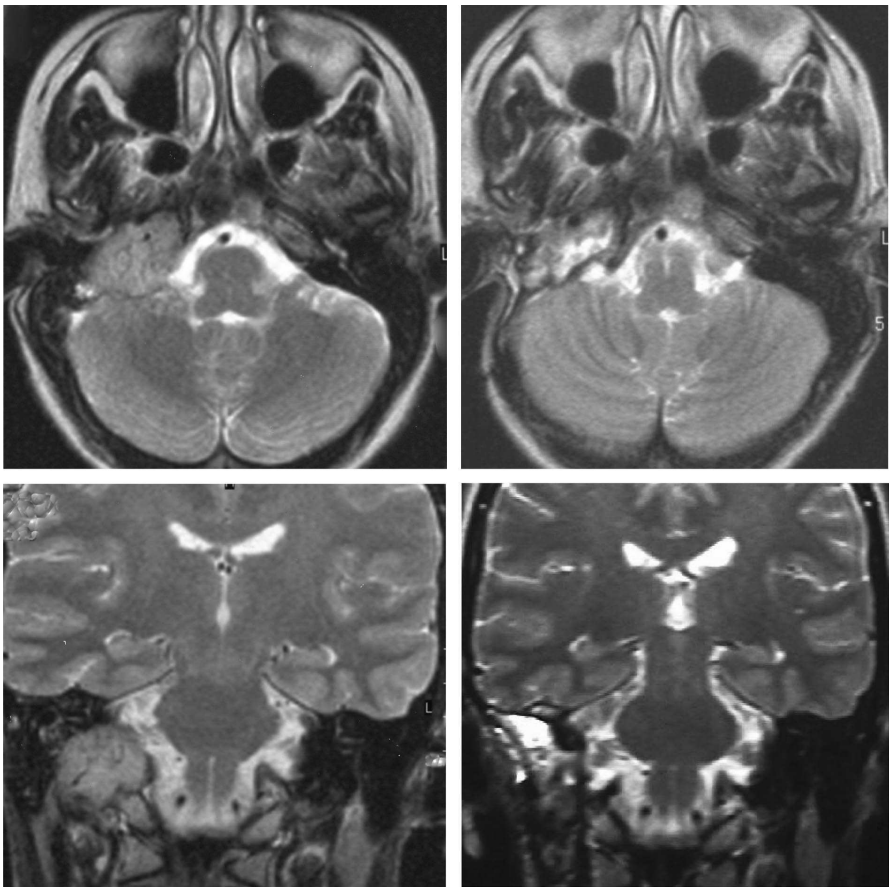

a ***b***

Fig. 1. ***a*** Pre-radiosurgical MRI (axial and coronal views) in sequence T2 flair with gadolinium in patient 10 presenting a right-sided glomus jugulare tumor after embolization and surgical resection. Patient, 36-year-old female, had a permanent percutaneous gastrostomy three months before embolization. Radiosurgery was realized on September 2002 and 12 Gy were applied to the tumor margins at the 80% isodose volume curve. In follow-up 1 month after SRS patient presented a clinically significant rehabilitation from cranial nerve X and removed definitively the gastrostomy. ***b*** Latest MR scan (axial and coronal views with the same sequence) performed 37 months after SRS revealing the maintenance of considerable reduction tumor volume.

Discussion

Surgery has been considered since long time as the mainstay of management for GJT. Microsurgical resection associated or not to endovascular embolization is generally recommended as standard treatment for young patients with small

Table 2. Radiosurgical doses, clinical and radiological results and imaging MR follow-up

Patient	Dose (Gy) marginal/ maximum	Symptoms improvement	Imaging evaluation post-SRS	Imaging MR follow-up, months
1	14.4/18	partial	major reduction	99
2	14.4/18	partial	minor reduction	95
3	15/18.75	partial	minor reduction	86
4	15/18.75	partial	minor reduction	86
5	15/18.75	partial	minor reduction	66
6	12/15.0	partial	inor reduction	73
7	15/18.75	partial	minor reduction	58
8	12/15.0	partial	stable	44
9	14/17.5	partial	minor reduction	47
10	12/17.14	partial	major reduction	37
11	15/18.75	partial	minor reduction	16
12	14/17.5	no change	stable	8
13	13/16.25	partial	minor reduction	7
14	12.7/18.3	partial	minor reduction	9
15	13/17.33	partial	stable	8

tumors. Nevertheless, the optimal management of GJT seems to remain controversial [16, 20]. The advances nowadays obtained in all therapeutic modalities including base skull surgical techniques the treatment option must be decided according to the risks of acute and chronic toxicities, morbidity, mortality and the impact of treatment modality on the patients' quality of life must be conscientiously weighted. The resection of GJT remains a complex surgical challenge by the site of the lesions and their relationships with the vascular and neural structures. Surgical resection in selected lesions has been associated with severe morbidity including the development of new permanent neurological deficits in about 50% of patients [14, 20, 21] and mortality as high as 4% [6, 22, 23]. Other surgical complications like CSF leakage, stroke, meningitis, pneumonia, pulmonary embolism, wound infection, etc. have been also reported [3, 6, 12, 21].

Conventional external radiation therapy was considered in the last three decades the alternative treatment for GJT in large lesions, inoperable, recurrent or residual tumors or in elderly or medically unsuitable patients for surgery. The improvement of clinical picture with a reduction or amelioration of symptoms and neurological function preservation in as many as 71% of patients and a shrinkage of tumor size in up to 61% of the cases achieved with this therapy have been reported [24]. The long-term local control rate ranges between 69 and 100% [12, 22, 25]. The local recurrence rate only of 2% is described in a review of literature in more than 200 patients [26]. The use in the past of orthovoltage energy

radiations and excessively high radiation total doses are frequently considered as the main reason for major complications or acute and late sequelae [7, 16, 26]. However, the size of radiation fields and the normal tissues and structures necessarily included within the high dose irradiation volumes used with conventional radiation in the last 2 decades could be probably related with the morbidity described in literature. Post-irradiation complications like pharyngitis, cranial nerve palsy, osteoradionecrosis, radiation encephalopathy or secondary malignancy are uncommon but have been reported by several series [2, 7, 21, 25].

The new techniques of MRI fusion integrated with three dimensional treatment planning and conformal radiotherapy supported by high precision in the delineation and determination of the target through stereotactic procedures are emerging as alternative treatment options for selected patients in the management of GJT [27]. SRS allow deliver more precisely a high single dose of radiation improving the dose coverage of the tumor and the rapid radiation fall off outside the target volume resulting in a significant sparing of the surrounding normal tissues to lower levels than the conventional radiotherapy. Excellent results in local control and an extremely low risk of major long-term late complications are expected with this modality. The long-term follow-up after SRS in our series showing a clinical improvement in 93.3% of patients, no evidence of tumor growth and absence of toxicity or morbidity are similar to other reported series presented in table 3 [13, 14, 20, 28–31]. No late complications are reported in our population and in other previous series [13, 31]. However, these results need to be confirmed with larger numbers of patients and much longer follow-up times. The risk of radiation-associated carcinogenesis related to SRS is documented as extremely low but is real, although, not yet well understood. It must be considered in the treatment decision and weighted with the potential risk of major morbidity and mortality of alternative therapies. There are only six radiation-associated second tumors reported in English literature in more than 200,000 submitted to SRS over the past 3 decades for several malignant and benign pathologies [32, 33]. Four cases were treated with Gamma Knife (GK) and two were treated with protons. Loeffler et al. argued about the likelihood that a second tumor can occur within a region of brain that has received a very low of radiation and that the risk of development of a second tumor is relative to the volume of irradiated brain [33]. The wide spatial separation of GK sources leading to an increase in the volume of normal brain receiving low doses and the overlapping radiation spheres of multiple isocenters produce high-dose regions (hot spots) are related with the irradiated volume [34]. The low maximum dose of radiosurgery in our series, the technique based in the LINAC radiosurgery and smaller volume of brain receiving low dose of radiation are theoretical factors expected to reduce at maximum the risk of radiation-associated malignancies.

Table 3. Radiosurgical results for glomus jugulare tumors

Author	No. of patient	Modality	Dose (Gy) marginal: maximum	Follow-up (months) median/mean: range	Tumor response regression/ stable/ progression/ unknown	Complications
Foote et al. [27]	25	GK	15:31.2 (median)	37 median:11–118	8/17/0/0	1
Liscák et al. [28]	66	GK	16.5:32 (median)	24 median:4–70	19/28/0/19	3
Eustacchio et al. [13]	13	GK	13.5:nr	37.6 median:5–68	4/6/0/3	0
Jordan et al. [14]	8	GK	16:33 (mean)	27 mean:7–102	4/3/0/1	1
Saringer et al. [29]	13	GK	12:24 (median)	50.4 mean:8–80	3/10/0/0	2
Lim et al. [19]	9	LINAC or CyberKnife	21.5:26.9 (median)	21.5 median:3–126	1/8/0/0	1
Maarouf et al. [30]	12	LINAC	15:39 (median)	48 median:9–108	8/4/0/0	0
Present report	15	LINAC	13.8:17.6 (median)	49.3 median:7–99	12/3/0/0	0

GK = Gamma Knife; LINAC = linear accelerator; nr = not referred.

Conclusions

The effectiveness of radiosurgery in management of the GJT is generally defined in terms of stabilization of tumor size with evidence of absence of progression or growth of the lesions. Our experience with SRS confirms the good outcome with no morbidity and mortality in patients with selected GJT and supports the place of this non-invasive modality as a safe and promising treatment option in the management of these tumors.

References

1 Thedinger BA, Glasscock III ME, Cueva RA, Jackson CG: Postoperative radiographic evaluation after acoustic neuroma and glomus jugulare tumour removal. Laryngoscope 1992;102:261–266.

2 Gabriel EM, Sampson JH, Dodd LG, Turner DA: Glomus jugulare tumor metastatic to the sacrum after high-dose radiation therapy: case-report. Neurosurgery 1995;37:1001–1005.

3 George B: Jugulare foramen paragangliomas. Acta Neurochir (Wien) 1992;118:120–126.
4 Konefal JB, Pilepich MV, Spector GJH, et al: Radiation therapy in the treatment of chemodectomas. Laryngoscope 1987;97:1331–1335.
5 Briner HR, Linder TE, Pauw B, et al: Long-term results of surgery for temporal boné paragangliomas. Laryngoscope 1999;97:152–157.
6 Green JD Jr, BracKmann DE, Nguyen CD, Arriaga MA, Telischi FF, De la Cruz: Surgical management of previously untreated glomus jugulare tumors. Laryngoscope 1994;104:917–921.
7 Cole JM, Beiler D: Long-term results of treatment for glomus jugulare and glomus vagale tumors with radiotherapy. Laryngoscope 1994;104:1461–1463.
8 Guedea F, Mendenhall WM, Parsons JT, et al: Radiotherapy for chemodectomas of the carotid body and ganglion nodosum. Head Neck 1991;13:509–513.
9 Larner JM, Hahm SS, Spaulding CA, Constable WC: Glomus jugulare tumors. Long-term control by radiotherapy. Cancer 1992;69:1813–1817.
10 Konefal JB, Pilepich MV, Spector GJH, et al: Radiation therapy in the treatment of chemodectomas. Laryngoscope 1987;97:1331–1335.
11 Mumber MP, Greven KM: Control of advanced chemodectomas of the head and neck with irradiation. Am J Clin Oncol 1995;18:389–391.
12 Powell S, Peters N, Harmer C: Chemodectoma of the head and neck: results of treatment in 84 patients. Int J Radiat Oncol Biol Phys 1992;22:919–924.
13 Eustacchio S, Leber K, Trummer M, Unger F, Pendl G: Gamma knife radiosurgery for glomus jugulare tumors. Acta Neurochir (Wien) 1999;141:811–818.
14 Jordan JA, Roland PS, McManus C, Weiner RL, Giller CA: Stereotactic radiosurgery for glomus Jugulare tumors. Laryngoscope 2000;110:35–38.
15 Mendenhall WM, Amdur RJ, Hinerman RW, Antonelli PJ, Villaret DB, et al: Radiotherapy and radiosurgery for skull base tumors. Otolaryngol Clin North Am 2001;34:1065–1077.
16 Zabel A, Milker-Zabel S, Huber P, Schulz-Ertner D, Schlegel W, et al: Fractionated stereotactic conformal radiotherapy in the management of large chemodectomas of the skull base. Int J Radiat Oncol Biol Phys 2004;58:1445–1450.
17 Fish U: Infratemporal fossa approach for glomus jugulare tumors of temporal bone. Ann Otol Rhinol Laryngol 1982;91:474–479.
18 Mascarenhas F, Sá da Costa M, Ortiz M, Almeida A, Carvalho H, Gonçalves Ferreira AJ, et al: Stereotactic radiosurgery in the intracranial benign neoplasms and malignant tumors of the brain. Acta Med Port 2005;18:45–60.
19 Sá da Costa M, Vieira S, Mascarenhas F, Gomes da Silva MH: Quality assurance in radiosurgery using linear accelerator. Radiother Oncol 1999;51(suppl 1):S67.
20 Lim M, Gibbs I, Adler J, Martin D, Chang S: The efficacy of linear accelerator stereotactic radiosurgery in treating glomus jugulare tumors. Techn Cancer Res Treat 2003;2:261–265.
21 Woods CI, Strasnick B, Jackson CG: Surgery for glomus jugulare tumors: the otology group experience. Laryngoscopy 1993;103(suppl)60;65–70.
22 Wang ML, Hussey DH, Doornbos JF, Vigliotti AP; Wen BC: Chemodectoma of the temporal bone: a comparison of surgical and radiotherapeutic results. Int J Radiat Onc Biol Phys 1988;14:643–648.
23 Netterville JL, Reilly KM, Robertson D, Reiber ME, Armstrong WB, et al: Carotid body tumors: A review of 30 patients with 46 tumors. Laryngoscope 1995;105:115–126.
24 Schild SE, Foote RL, Buskirk SJ, Robinow JS, Bock FF, et al: Results of radiotherapy for chemodectomas. Mayo Clin Proc 1992;67:537–540.
25 Sharma PD, Johnson AP, Whitton AC: Radiotherapy for jugulo-tympanic paragangliomas (glomus jugulare tumors). J Laryngol Otol 1984;98:621–629.
26 Kim JA, Elkon D, Lim ML: Optimum dose of radiotherapy for chemodectomas of the middle ear. Int J Radiat Onc Biol Phys 1980;6:815–819.
27 Foote BL, Coffey RJ, Gorman DA, Earle JD, Schomberg PJ, et al: Stereotactic radiosurgery for glomus jugulare tumors: a preliminary report. Int J Radiat Oncol Biol Phys 1997;38:491–495.
28 Foote RL, Pollock BE, Gorman DA, Schomberg PJ, Stafford SL, et al: Glomus jugular tumor: Tumor control and complications after stereotactic radiosurgery. Head Neck 2002;24:332–339.
29 Liscák R, Vladyka V, Wowra B, Kemeny A, Forster D, et al: Gamma knife radiosurgery of the glomus jugulare tumor – early multicentre experience. Acta Neurochir (Wien) 1999;141:1141–1146.

30 Saringer W, Khayal H, Ertl A, Schoeggl A, Kitz K: Efficiency of gamma knife radiosurgery in the treatment of glomus jugulare tumors. Minim Invasive Neurosurg 2001;44:141–145.
31 Maarouf M, Voges J, Landwehr P, Bramer R, Treuer H, et al: Strereotactic linear accelerator-based radiosurgery for the treatment of patients with glomus jugulare tumors. Cancer 2003;97:1093–1098.
32 McIver JI, Pollock BE: Radiation-induced tumors after stereotactic radiosurgery and whole-brain irradiation: case-report and review of literature. J Neurooncol 2004;66:301–305.
33 Loeffler JS, Niemierko A, Chapman PH: Second tumors after radiosurgery: tip of the iceberg or a bump in the road? Neurosurgery 2003;52:1436–1442.
34 Brada M, Ajithkumar TV, Minniti G: Radiosurgery for pituitary adenomas. Clin Endocrinol (Oxf) 2004;3:211–216.

Francisco Mascarenhas, MD
Department of Radiotherapy, Hospital de Santa Maria
Av. Prof Egas Moniz
PT–1699 Lisboa (Portugal)
Tel. +351 21 7805616, Fax + 351 21 3541179
E-Mail fmascarenha@hsm.min-saude.pt

Kondziolka D (ed): Radiosurgery. Basel, Karger, 2006, vol 6, pp 118–130

Gamma Knife Radiosurgery for Cavernous Sinus Meningiomas

John Y.K. Lee[a], *Martina Stippler*[b], *Ajay Niranjan*[b], *Douglas Kondziolka*[b,c], *John C. Flickinger*[b,c], *L. Dade Lunsford*[b,c]

[a]Department of Neurological Surgery, University of Pennsylvania, Philadelphia, Pa., Departments of [b]Neurological Surgery and [c]Radiation Oncology, University of Pittsburgh Medical Center, Pittsburgh, Pa., USA

Abstract

Objective: To evaluate the long-term outcomes after stereotactic radiosurgery for cavernous sinus meningiomas, we retrospectively reviewed all patients who had at least ten years of possible follow-up. **Methods:** Eighty-two patients had meningiomas centered within the cavernous sinus. Three patients were lost to follow-up leaving 79 evaluable patients. Thirty-nine patients (49%) underwent adjuvant radiosurgery after one or more attempts at surgical resection. Conformal multiple isocenter Gamma Knife radiosurgery was performed. The median marginal tumor dose in this historical cohort was 15 Gy. **Results:** The actuarial tumor control rate for patients with typical meningiomas was 95 ± 2.8% at 5 years and 88.2 ± 7.0% at 12 years. Two of the four failures can be excluded, because one was an out-of-field failure and the other was based on imaging and targeting in the era before magnetic resonance imaging. Adverse radiation effects occurred after 10 procedures (12.7%). **Conclusion:** Stereotactic radiosurgery provided effective management of cavernous sinus meningiomas. With reduced doses to the margin, we believe it is the preferred management strategy for tumors of suitable volume (average tumor diameter ≤ 3 cm or volume ≤15 cm^3). Long-term follow-up is mandatory in these patients.

Cushing and Eisenhardt published their seminal treatise in 1922 [1], and since that time surgeons have pursued the complete and total resection of meningiomas. As microsurgical techniques advanced, access to the skull base including the cavernous sinus region became increasingly feasible [2]. Despite the achievements and published success in the surgical resection of these formidable lesions [3–7], however, surgery within the cavernous sinus often resulted in serious morbidity or mortality [5, 8, 9]. Meningiomas of the cavernous sinus

are intimately associated with critical neurovascular structures and have been shown to invade cranial nerve fascicles, making complete or even aggressive subtotal resection impossible [10, 11].

Advocates of stereotactic radiosurgery for cavernous sinus meningiomas have published their initial results in the management of these tumors [12–15]. The present report expands the follow-up interval and analyzes the outcomes for cavernous sinus meningioma radiosurgery performed from 1987 to 1995, and thus follow-up data of at least 10 years is available for this cohort. Long-term follow-up of the radiosurgical treatment of these tumors continues with increasing vigilance.

Methods and Materials

Patient Population

Between October 1987 and December 1995, 82 consecutive patients with symptomatic cavernous sinus meningiomas underwent Gamma Knife stereotactic radiosurgery. Cavernous sinus meningiomas were defined as those tumors with a predominant cavernous sinus component. Included in this definition were both primary cavernous sinus meningiomas, as well as petroclival and sphenoid wing meningiomas that had been previously resected, leaving behind the cavernous sinus component. Clinical and imaging follow-up was available for 79 patients (median age 56 years, range 12–87 years). Fifty-nine patients (73%) were female. Included in this analysis were all patients initially reported by Lee et al. (2002).

Thirty-nine patients (49%) had undergone at least one attempted tumor resection prior to adjuvant radiosurgery. The remainder, forty patients (51%) underwent primary radiosurgery for cavernous sinus tumors presumed to be meningiomas by neurodiagnostic criteria alone (location, contrast pattern, presence of a dural tail along the tentorium).

Radiosurgical Technique

All patients underwent application of a Leksell Model G stereotactic frame (Elekta Instruments, Atlanta, Ga., USA) after local anesthetic injection. Supplemental intravenous sedation (50 mg Fentanyl, 1 mg midazolam) was provided to some patients. After 1991, high-resolution, contrast-enhanced, multiplanar magnetic resonance imaging (MRI) replaced computed tomography (CT) based planning. Since 1993, a specific MR volume-acquisition protocol with 1 or 1.5 mm slices provided detailed graphic, three-dimensional visualization of the tumor and adjacent critical structures. The images were transferred to a dose-planning computer in the radiosurgery center via a fiberoptic ethernet system. Computerized dose-planning was performed initially on a Micro-VAX II work station (Digital Equipment Corporation, Westminster, Mass., USA) and later on a Hewlett-Packard work station, using GammaPlan® software (Elekta Instruments, Atlanta, Ga., USA). The maximum radiation dose, isodose, and margin dose delivered were determined by consultation between the neurosurgeon, radiation oncologist, and medical physicist. Radiosurgery was performed using a 201-source cobalt-60 Leksell Gamma Knife Model U or Model B unit (Elekta Instruments). At the time of completion of radiosurgery, each patient received a single intravenous 40-mg dose of methylprednisolone.

Radiation Dosimetry

The median tumor volume was 6.5 cm^3, and the median marginal dose was 15 Gy. Multiple isocenters were used in all but one patient. Three-dimensional conformal radiosurgery was performed by placing the 50% or greater isodose at the irregular tumor margin. Overall dose selection was adjusted based on our evolving experience with meningiomas, specific tumor volumes and location, the risk of radiation-induced complications predicted by the integrated logistic formula, and any history of previous fractionated radiation therapy. The prescription dose range has remained consistent since 1991; however, as documented in a prior publication, the median marginal dose of the group of patients treated earlier in the experience was statistically higher as compared to more recent doses (15 versus 13 Gy more recently).

Follow-Up and Statistical Analysis

After radiosurgery, patients were instructed to have clinical evaluations and serial imaging at 6-months, and at years1, 2, 4, 8, and 12 years. For patients residing a significant distance from Pittsburgh, evaluation and imaging studies were performed locally by their referring physicians and were submitted to our institution for review. Actuarial Kaplan-Meier analysis was performed with SPSS®.

Results

Perioperative Period

Each patient underwent stereotactic radiosurgery and was discharged home to resume normal activities within 24 h after the procedure. Brief discomfort located at the pin sites were observed by some patients.

The median volume was 6.5 cm^3 for this group of patients. The median marginal dose was 15 Gy, and the median number of isocenters was six. Neurological evaluations of the 79 evaluable patients were obtained by the referring physicians, by the treating neurosurgeons, or by direct telephone contact (median follow-up period 79 months). The median radiographic follow-up time was 79 months (range, 2–145 months).

Four patients with MRI evidence of increased tumor size were defined as having failed radiosurgery. Three patients failed adjuvant radiosurgery after having previously undergone craniotomies for their tumors, and one patient failed primary radiosurgery. One patient who failed adjuvant radiosurgery developed a sixth nerve palsy 5 years after radiosurgery, at which time the referring surgeon interpreted the MRI as showing growth of the previously resected meningioma outside of the original radiosurgery volume. The referring neurosurgeon performed a craniotomy and debulking of the tumor which extended into the contralateral hypothalamus. The patient developed a post-operative hematoma and died. A second patient had a craniotomy for debulking two years prior to radiosurgery. Four years after Gamma Knife radiosurgery with 13 Gy to

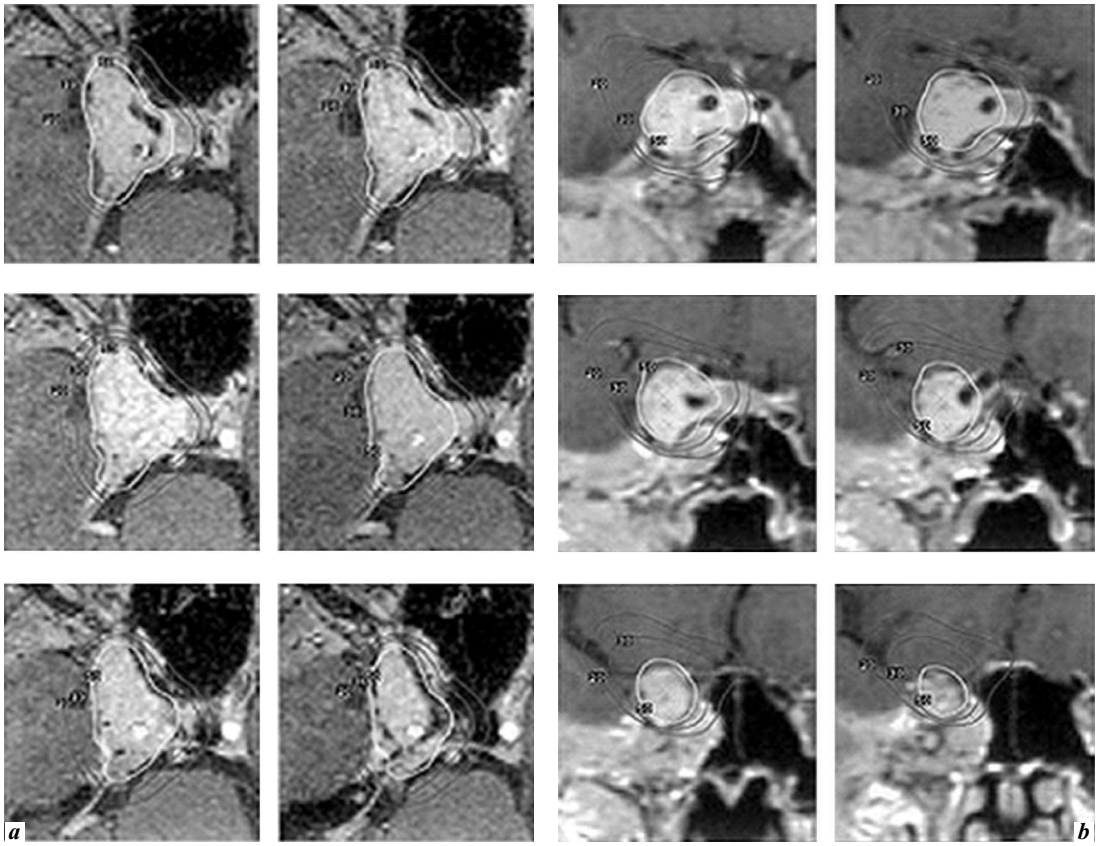

Fig. 1. ***a***, ***b*** Axial (left, ***a***) and coronal (right, ***b***) gadolinium-enhanced MR scans of a 44-year-old man showing a right-sided cavernous sinus meningioma. This lesion was treated with Gamma Knife radiosurgery using 15 Gy to the tumor margin. Note the presence of contrast enhancement outside of the colored radiodose lines.

the 50% isodose margin, he developed increase in tumor size outside of the field of radiosurgery (figs. 1 and 2). A third patient had two prior craniotomies and was then treated with Gamma Knife radiosurgery in 1992. Eleven years later, a follow-up MRI scan demonstrated a small interval increase in the size of the tumor. Since the patient remained asymptomatic, a decision was made to follow with another MRI scan. The only failure of primary radiosurgery was among the first few patients ever treated in the United States with Gamma Knife radiosurgery. This patient was diagnosed and treated in 1987, prior to the advent of the routine clinical use of the MRI scan. The patient underwent CT-based Gamma

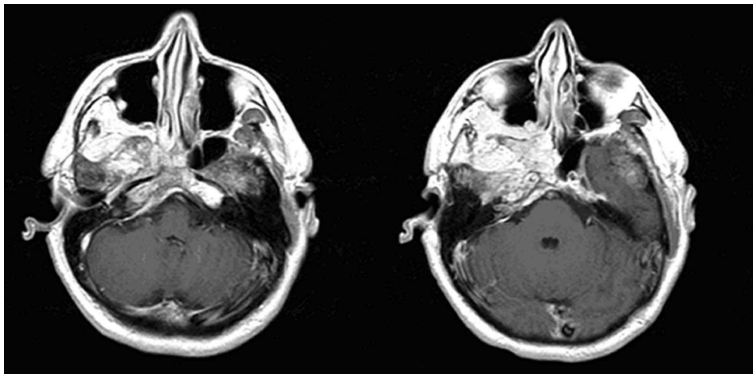

Fig. 2. Follow-up axial MR scans of the same patient 4 years after radiosurgery showing tumor progression outside of the field of radiosurgery.

Knife radiosurgery, with 20 Gy to the margin in three shots. Five years later the tumor recurred, and since that time she has underwent two resections, one of them 5 years after radiosurgery, and the second one 10 years after radiosurgery.

Tumor control rates were analyzed by Kaplan-Meier survival analysis. The actuarial tumor control rate for all patients without malignant or atypical meningiomas was 95 ± 2.8% at 5 years and 88.2 ± 7.0% at 12 years (fig. 3). If you compare patients who had prior craniotomies versus those patients who were treated based on imaging findings alone, the actuarial tumor control rate is 83.7% with surgery versus 96.2% for those patient without surgery at twelve years (fig. 4; $p = 0.511$).

Adverse Radiation Effects

Ten patients (12.7%) had adverse radiation effects. All ten of these have been described in a prior publication. These patients were defined by the presence of clinical or neurologic deterioration in the absence of tumor growth on several studies MRI (table 1) The mean time to clinical deterioration was 24.8 months (range, 5–98 months).

Two patients had visual deterioration. The first patient developed progressive optic neuropathy 5 months after CT-based radiosurgery. The estimated

Fig. 3. The Kaplan-Meier survival curve showing the actuarial tumor control rate of 88.2 ± 7.0% at 12 years for patients with typical meningiomas in the cavernous sinus.

Fig. 4. Kaplan-Meier plots of actuarial tumor control for patients with typical meningiomas in the cavernous sinus with and without surgical resection prior to radiosurgery. The difference was not significant ($p = 0.511$).

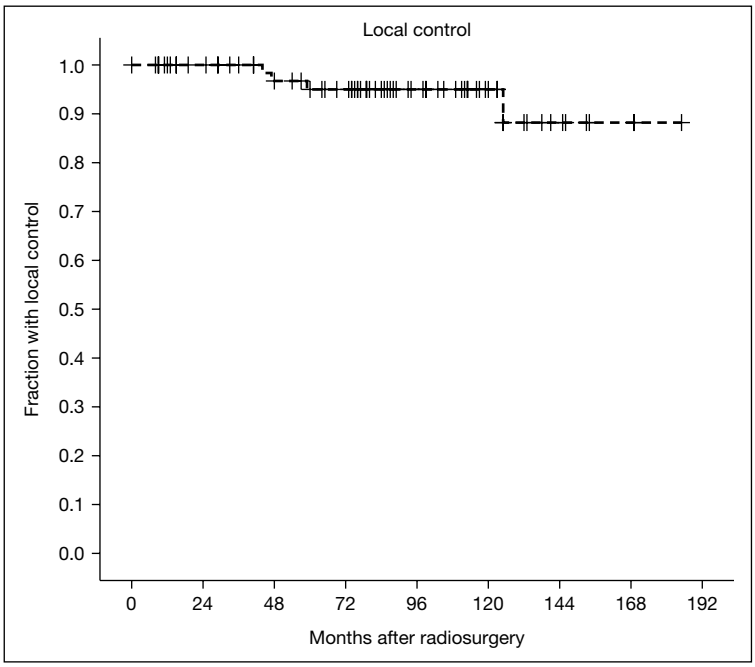
Local control
Fraction with local control
1.0
0.9
0.8
0.7
0.6
0.5
0.4
0.3
0.2
0.1
0.0
0
24
48
72
96
120
144
168
192
Months after radiosurgery

3

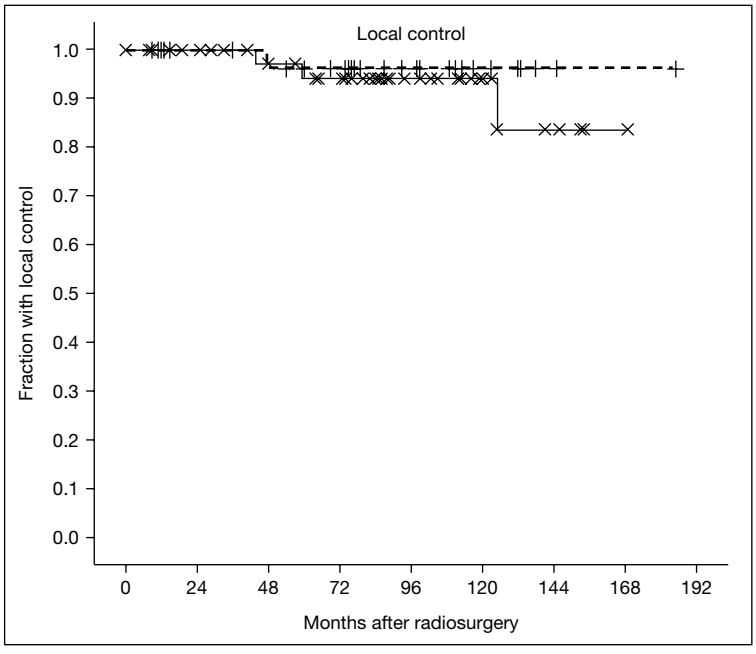
Local control
Fraction with local control
1.0
0.9
0.8
0.7
0.6
0.5
0.4
0.3
0.2
0.1
0.0
0
24
48
72
96
120
144
168
192
Months after radiosurgery

4

Table 1. Stereotactic radiosurgery for cavernous sinus meningiomas: adverse radiation effects (n = 79 patients)

	Transient, n	Permanent, n
Visual		
Loss of visual acuity		1
Field cut		1
Trigeminal		
Neuralgia		2
Paresthesias	1	0
Keratitis		2
Cognitive		1
Temporal lobe seizures	2	
Total	3	7

7 Gy dose to the optic nerve was recalculated to be 12 Gy. This patient was treated with steroids and the symptoms stabilized over the next two years of follow-up. The second patient developed a delayed visual field deficit 98 months after radiosurgery. The consulting neurosurgeon performed a craniotomy for 'optic nerve decompression'. Post-operatively, the patient suffered a third and fourth cranial nerve palsy but her visual deficit remained stable.

Five patients developed new trigeminal nerve dysfunction. One patient developed transient V2 and V3 paresthesias. Two patients developed typical trigeminal neuralgia. The first patient's pain was controlled with medications, while the second patient ultimately achieved benefit from acupuncture. Two patients developed corneal ulcerations (neurotrophic keratitis). In both of these patients, their complication was managed by local corneal care or tarsorrhaphy.

Two patients developed partial complex seizures 16 months after radiosurgery and recovered with medical treatment. Both of these patients were treated prior to 1992. Although it is possible that the mesial temporal lobe had developed untoward adverse radiation effects, there was no such correlation on MR imaging. In addition, these two patients had both had prior craniotomies, and one of the patients had abruptly discontinued antiepileptic drugs.

One patient developed 'cognitive deterioration' 7 months after radiosurgery. The symptoms suggested normal pressure hydrocephalus and responded to a lumboperitoneal shunt. Overall, the incidence rate of presumed adverse radiation effects was 12.7% (10 of 79 procedures), which is based on the historical use of CT-based planning and higher median doses than currently used.

Discussion

Although surgical resection of a meningioma and its dural base (Simpson Grade I) is the preferred treatment for many patients [16–19], complete resection of meningiomas of the cavernous sinus is not feasible without serious neurological morbidity or mortality. Overall, the estimated likelihood of obtaining a complete resection of a cavernous sinus tumor ranges from 22.9 to 100% [2, 4, 9, 14, 20–24]. The mortality rate in modern microsurgical series ranges from 0 to 7% [9, 21, 25]. Permanent cranial nerve deficits were noted in a significant percentage of patients (8–26%) [9, 21, 26]. In order to reduce morbidity and mortality rates, some surgeons have opted for a less aggressive resection, but such strategies fail to affect tumor progression rates [27]. Kallio et al. [28] studied 225 patients with meningiomas and determined recurrence rates after complete resection of 7, 20, and 32% at 5, 10, and 15 years. In contrast, the rates of tumor progression after subtotal resection were 37, 55, and 91%, respectively at the same time intervals. Such data provides a compelling reason to use radiosurgery as primary management for cavernous sinus meningiomas.

The role of external beam fractionated radiation in the management of meningiomas has generally been limited to post-operative adjunctive treatment. Recent studies have demonstrated improved outcome and increased survival rates in patients who underwent subtotal resection plus radiation therapy. Several studies indicate 5-year progression free survival rates between 89 and 100%, and 10-year progression free survival rates between 81 and 92.8% [29–33]. Thus, tumor control rates can be improved with adjunctive external beam fractionated radiation therapy. However, this therapy has been associated with a significant potential morbidity. Al-Mefty et al. [34] retrospectively analyzed 58 patients who underwent radiation therapy between 1958 and 1987. Thirty-eight percent of these patients developed major complications including visual loss, pituitary dysfunction, and brain radiation necrosis. In contrast, Dufour et al. [29] reported a series of 31 patients with cavernous sinus meningiomas treated with recent generation radiation therapy techniques. In this study, no patient developed adverse radiation effects. Understandably, fractionated external beam radiation therapy has become safer as the techniques of conformal fractionated delivery have evolved. Of interest, though, in this same study by Dufour et al. [29], four times as many patients with cavernous sinus tumors were treated with radiosurgery as opposed to radiation therapy, suggesting that a selection bias existed even within this study.

Stereotactic radiosurgery provides conformal, highly focused, single fraction radiation of irregular tumor volumes with a steep dose gradient. Multiple isocenter dose planning, configured with small beam diameters facilitates precise delivery of the radiation dose to the irregular margins of the tumor. The

Table 2. Stereotactic radiosurgery for cavernous sinus meningiomas: summary of cavernous sinus meningiomas treated with Gamma Knife radiosurgery

References	No. of cases	Tumor size decreased, %	Tumor size unchanged %	Actuarial 5-year progression free survival	Actuarial 10-year progression free survival	Median follow-up months
Duma et al. [12][a]	34	56	44			24
Pendl et al. [14]	41	34	63			39
Liscak et al. [13]	67	52	48			19
Roche et al. [15]	99	31	64	93		30
Lee et al. [39]	159	34	60	93		24
Subset[b]	79	37	59	98		59
Lee et al. (current study)	79	37	56	96	85	79

[a]This series by Duma et al. is included in the study by Lee et al. [39].
[b]Subset of 79 patients with long-term follow-up is the same cohort as the current study.

steep radiation fall-off of radiosurgery significantly protects adjacent critical structures from delayed radiation-induced injury. This benefit is reduced as the tumor volume increases. In order to understand the outcomes after radiosurgery, long-term follow-up is mandatory.

Outcomes

In a prior publication, in order to emphasize the long-term rates of the success of radiosurgery, we focused on our initial 8 years of radiosurgery experience [39]. The median follow-up time in that publication was 59 months. Our analysis of the first 79 evaluable patients revealed an actuarial tumor control rate of 97.5 ± 2.5% at 5 and 10 years. In this study, we have followed this cohort for a longer period of time and now have a median follow-up of 79 months. Since that time, there have been three additional failures of radiosurgery, leading to a 5 year actuarial tumor control rate of 95 ± 2.8% and 88.2 ± 7.0% at 12 years. This actuarial freedom from progression is comparable to other radiosurgical series [12–15, 35, 36] (table 2). Morita et al. [36] and Roche et al. [15] documented progression free survival rates of 95 and 93% respectively. In a recent study of 40 patients, Shin et al. [37] reported a tumor control rate of 86.4% at 3-years and 82.3% at 10-years.

Kallio et al. [28] studied the long-term survival of more than 900 patients with meningiomas during a 20-year period and found that the median postoperative time until recurrence was 7.5 years. Cavernous sinus meningiomas,

however, tend to recur earlier than calvarial meningiomas after surgery because gross total removal is impossible [18, 27]. Based on the 10 year median follow-up of these 79 patients, we again suggest that Gamma Knife radiosurgery for cavernous sinus meningiomas provides tumor control rates that exceed the control rates after surgery alone.

As experience accumulates and the number of patients treated with Gamma Knife radiosurgery increases, there is an increasing burden on the practitioners to carefully document the long-term follow-up of this treatment modality. Since our prior publication, we have identified three additional treatment failures, although one of these was outside of the treatment field and the other was a patient treated in 1987 based on CT scans alone. Nevertheless, with continued vigilance we will document the results of radiosurgery in this patient population. As of this time, there has been no precipitous or dramatic increase in the number of radiosurgery failures, and therefore radiosurgery continues to be the best treatment strategy for these patients.

Our results suggest that outcomes may be better for patients who undergo primary radiosurgery rather than adjuvant radiosurgery after attempted surgical resection. There should be no biologic difference between tumors that have had prior surgical resection versus 'virgin' tumors. However, tumors that have been previously resected may be more difficult to define on radiosurgical imaging studies. For example, fat signal may be confused for tumor or post-operative meningeal enhancement may be confused for tumor. This limitation may be avoided with the use of additional imaging sequences and also by waiting several weeks before adjuvant radiosurgery. In this way, out-of-field failures may be avoided.

Adverse Radiation Effects

Adverse radiation effects after radiosurgery of the cavernous sinus manifested primarily as delayed cranial neuropathies. With greater follow-up, no new adverse radiation effects were identified in this patient cohort, and hence, all of the adverse radiation effects have been previously reported in a prior publication by Lee et al.

In summary, the motor nerves of the cavernous sinus, (cranial nerves three, four and six) appear to be relatively resistant to radiosurgery. In our series, there was no evidence of deterioration of the oculomotor nerves after radiosurgery in the absence of tumor progression. Many nerves remained functionally preserved, and in 25 patients oculomotor function actually improved. In contrast to the motor nerves of the cavernous sinus, the trigeminal nerve appears to be more susceptible to adverse radiation effects. In our series, four patients developed permanent trigeminal nerve dysfunction. Four of these deficits were permanent. Three of these patients had pre-existing trigeminal dysfunction before

radiosurgery. The relatively higher incidence of trigeminal deterioration after radiosurgery (compared to other cranial nerves) has been observed in other studies.

The special sensitivity of the visual pathways to radiation injury is well known [38]. In this series, two patients developed radiation-induced optic neuropathy. Our cumulative experience supports the concept that the single fraction optic nerve tolerance is 8–10 Gy depending on the volume of nerve involved. Leber et al. [35] found that when the maximum radiation dose to the visual pathways was less than 10 Gy, no signs of radiation-induced optic neuropathy were observed. However, when the dose ranged from 10 to less than 15 Gy, the incidence of radiation-induced optic neuropathy was 26.7%. When the dose was 15 Gy or more, the incidence was 77.8%. Morita, et al. [36] adopted a policy of allowing for short segments of visual pathways to tolerate 12–16 Gy.

The occurrence of cognitive deficits after radiosurgery is rare, and in a previous report [12], we described two patients who developed partial complex seizures at an average of 16 months after radiosurgery for cavernous sinus meningiomas. Both patients had undergone prior craniotomies and partial tumor removal. Neither of these patients had imaging evidence of temporal lobe necrosis or temporal lobe edema.

Conclusion

The present study supports the long-term benefit of radiosurgery in the management of cavernous sinus meningiomas. Using marginal tumor doses of 15 Gy, we obtained long-term growth control and preserved neurologic function in most patients with actuarial tumor control rates of 95 $\pm$ 2.8% at 5 years and 88.2 $\pm$ 7.0% at 12 years. Two of these four failures, however, can be excluded on the basis of either being an out-of-field recurrence, or because of technical limitations in the planning strategies used almost 20 years ago. Hence, using median marginal tumor doses of 15 Gy, we truly observed only two failures in this patient cohort.

Stereotactic radiosurgery should be the primary management for patients with small or medium sized cavernous sinus meningiomas (e.g. volume $\leq$15 cm^3 or diameter $\leq$3 cm). Patients with larger tumors should undergo subtotal extracavernous resection followed by stereotactic radiosurgery for the residual cavernous sinus component. Long-term follow-up of this patient cohort will continue to reveal the advantages of gamma knife radiosurgery as a minimally-invasive alternative to the treatment of patients with this tumor.

References

1 Cushing HW EL: Meningiomas: Their Classification, Regional Behavior, Life History, and Surgical End Results. Springfield, Charles C Thomas, 1938.
2 Dolenc VV: Anatomy and Surgery of the Cavernous Sinus. New York, Springer-Verlag, 1989.
3 Al-Mefty O: Management of the cavernous sinus and carotid siphon. Otolaryngol Clin North Am 1991;24:1523–1533.
4 Al-Mefty O, Smith RR: Surgery of tumors invading the cavernous sinus. Surg Neurol 1988;30: 370–381.
5 De Jesus O, Sekhar LN, Parikh HK, et al: Long-term follow-up of patients with meningiomas involving the cavernous sinus: recurrence, progression, and quality of life. Neurosurgery 1996;39: 915–919.
6 Sekhar LN, Lanzino G, Sen CN, et al: Reconstruction of the third through sixth cranial nerves during cavernous sinus surgery. J Neurosurg 1992;76:935–943.
7 Sekhar LN, Patel S, Cusimano M, et al: Surgical treatment of meningiomas involving the cavernous sinus: evolving ideas based on a ten year experience. Acta Neurochir Suppl 1996;65: 58–62.
8 Cusimano MD, Sekhar LN, Sen CN, et al: The results of surgery for benign tumors of the cavernous sinus. Neurosurgery 1995;37:1–9.
9 O'Sullivan MG, van Loveren HR, Tew JM Jr: The surgical resectability of meningiomas of the cavernous sinus [Review] [45 refs]. Neurosurgery 1997;40:238–244.
10 Larson JJ, van Loveren HR, Balko MG, et al: Evidence of meningioma infiltration into cranial nerves: clinical implications for cavernous sinus meningiomas [see comments]. J Neurosurg 1995;83:596–599.
11 Sen C, Hague K: Meningiomas involving the cavernous sinus: histological factors affecting the degree of resection [see comments]. J Neurosurg 1997;87:535–543.
12 Duma CM, Lunsford LD, Kondziolka D, et al: Stereotactic radiosurgery of cavernous sinus meningiomas as an addition or alternative to microsurgery. Neurosurgery 1993;32:699–704.
13 Liscak R, Simonova G, Vymazal J, et al: Gamma knife radiosurgery of meningiomas in the cavernous sinus region. Acta Neurochir 1999;141:473–480.
14 Pendl G, Schrottner O, Eustacchio S, et al: Cavernous sinus meningiomas – what is the strategy: upfront or adjuvant gamma knife surgery? Stereotact Funct Neurosurg 1998;70(suppl 1):33–40.
15 Roche PH, Regis J, Dufour H, et al: Gamma knife radiosurgery in the management of cavernous sinus meningiomas. J Neurosurg 2000;93(suppl 3):68–73.
16 Borovich B, Doron Y: Recurrence of intracranial meningiomas: the role played by regional multicentricity. J Neurosurg 1986;64:58–63.
17 Mahmood A, Ramasastry S, Malik GM: Intracranial meningiomas: analysis of recurrence after surgical treatment. Acta Neurochir 1994;126:53–58.
18 Mathiesen T, Lindquist C, Kihlstrom L: Recurrence of cranial base meningiomas. Neurosurgery 1996;39:2–9.
19 Naumann M, Meixensberger J: Factors influencing meningioma recurrence rate. J Neurosurg 1998;88:831–839.
20 Cioffi F, Bernini FP, Punzo A, et al: Cavernous sinus meningiomas. Neurochirurgia (stuttg) 1987;30:40–47.
21 DeMonte F, Smith HK, Al-Mefty O: Outcome of aggressive removal of cavernous sinus meningiomas [see comments]. J Neurosurg 1994;81:245–251.
22 Lanzino G, Hirsch WL, Pomonis S, et al: Cavernous sinus tumors: neuroradiologic and neurosurgical considerations on 150 operated cases. J Neurosurg Sci 1992;36:183–196.
23 Sekhar LN, Pomeranz S, Sen CN: Management of tumours involving the cavernous sinus. Acta Neurochir Suppl 1991;53:101–112.
24 Sephernia A, Samii M, Tatagiba M: Management of intracavernous tumors: an 11-year experience. Acta Neurochir Suppl 1991;53:122–126.
25 Sekhar LN, Ross DA, Sen C: Cavernous sinus and sphenocavernous neoplasms: Anatomy and surgery; in Sekhar LN, Janecka IP (eds): Surgery of Cranial Base Tumors. New York, Raven Press, 1992, pp 605–659.

26 Hirsch WL, Sekhar LN, Lanzino G, et al: Meningiomas involving the cavernous sinus: value of imaging for predicting surgical complications. AJR Am J Roentgenol 1993;160:1083–1088.
27 Mirimanoff RO, Dosoretz DE, Linggood RM, et al: Meningioma: analysis of recurrence and progression following neurosurgical resection. J Neurosurg 1985;62:18–24.
28 Kallio M, Sankila R, Hakulinen T, et al: Factors affecting the operative and excess long-term mortality in 935 patients with intracranial meningioma. Neurosurgery 1992;31:2–12.
29 Dufour H, Muracciole X, Metellus P, et al: Long-term tumor control and functional outcome in patients with cavernous sinus meningiomas treated by radiotherapy with or without previous surgery: is there an alternative to aggressive tumor removal? Neurosurgery 2001;48:285–294.
30 Goldsmith BJ, Wara WM, Wilson CB, et al: Postoperative irradiation for subtotally resected meningiomas: a retrospective analysis of 140 patients treated from 1967 to 1990. J Neurosurg 1994;80:195–201.
31 Maguire PD, Clough R, Friedman AH, et al: Fractionated external-beam radiation therapy for meningiomas of the cavernous sinus. Int J Radiat Oncol Biol Phys 1999;44:75–79.
32 Nutting C, Brada M, Brazil L, et al: Radiotherapy in the treatment of benign meningioma of the skull base. J Neurosurg 1999;90:823–827.
33 Taylor BW Jr, Marcus RB Jr, Friedman WA, et al: The meningioma controversy: Postoperative radiation therapy. Int J Radiat Oncol Biol Phys 1988;15:299–304.
34 Al-Mefty O, Kersh JE, Routh A, et al: The long-term side effects of radiation therapy for benign brain tumors in adults. J Neurosurg 1990;73:502–512.
35 Leber KA, Bergloff J, Pendl G: Dose-response tolerance of the visual pathways and cranial nerves of the cavernous sinus to stereotactic radiosurgery. J Neurosurg 1998;88:43–50.
36 Morita A, Coffey RJ, Foote RL, et al: Risk of injury to cranial nerves after gamma knife radiosurgery for skull base meningiomas: experience in 88 patients. J Neurosurg 1999;90:42–49.
37 Shin M, Kurita H, Sasaki T, et al: Analysis of treatment outcome after stereotactic radiosurgery for cavernous sinus meningiomas. J Neurosurg 2001;95:435–439.
38 Girkin CA, Comey CH, Lunsford LD, et al: Radiation optic neuropathy after stereotactic radiosurgery. Ophthalmology 1997;104:1634–1643.
39 Lee JY, Niranjan A, McInerney J, Kondziolka D, Flickinger JC, Lunsford LD: Stereotactic radiosurgery providing long-term tumor control of cavernous sinus meningiomas. J Neurosurg 2002;97:65–72.

L. Dade Lunsford, MD
Department of Neurological Surgery, Suite B-400
University of Pittsburgh Medical Center
200 Lothrop Street
Pittsburgh, PA 15213 (USA)
Tel. +1 412 647 6250, Fax +1 412 647 6483
E-Mail lunsfordld@upmc.edu

Kondziolka D (ed): Radiosurgery. Basel, Karger, 2006, vol 6, pp 131–139

Fractionated Stereotactic Radiotherapy of Base of Skull Meningiomas: A Preliminary Comparison in the Delineation of the Gross Tumor Volume between Four Medical Specialities

C. Mitine[a], *L. Gilbeau*[a], *F. Dessy*[a], *H. Rooijackkers*[b], *C. Pirson*[a], *J. Rosier*[a], *M. Hoornaert*[a], *L. Harzee*[a], *A. Doneux*[a], *M. Beauduin*[a]

Departments of [a]Radiotherapy and [b]Neurosurgery, Jolimont Hospital, Haine St Paul, Belgium

Abstract

Purpose: To study the interobserver variability of base of skull meningiomas delineation on computed tomography. **Methods and Materials:** A group of eight physicians working in the same institution (two neurosurgeons, two neuroradiologists, two radiation oncologists and two medical oncologists) were asked to delineate the gross tumor volume of two patients on sequential CT slices. The same clinical information is provided to each observer. The results of the delineation by the four specialties are compared to each other. The mean of the volumes delineated by all observers are calculated. To determine the variation in the anatomical position of the target volume, a 3D comparison between an arbitrary point determined in the tumor and the most distant point of the tumor in the three directions is realized. For the interobserver variability, the coefficient of variance is used. **Results:** Large differences are observed between the eight physicians both for the estimation of the tumor volume and its anatomical position. The value of the ratio of the largest to the smallest volumes is 8.8 for the first patient and 3.3 for the second. Those ratios become 1.19 and 1.66 for the medical oncologists, 1.07–1.57 for the neuroradiologists, 1.07–1.08 for the neurosurgeons and 1.14–6.5 for the radiation oncologists. The intersecting volume (on which all physicians agree) represents only 32% for the first patient and 34% for the second. Compared to radiation oncologists and medical oncologists, neurosurgeons and neuroradiologists delineate slightly smaller volumes. The results for the radiation group need to be taken cautiously because of the large delineation of one of the two observers. The lowest coefficient of variations, indicator of a smallest interobserver variation, are found for the group of neurosurgeons and neuroradiologists. **Conclusions:** The first step of 3D treatment planning, the delineation of base of skull meningiomas tumor is crucial. A good co-operation within a

multidisciplinary team is mandatory. Different imaging modalities such as NMR and methionine PET are used. Difference between radiation oncologists and other specialties could be unconscious integration of geometrical uncertainties relevant in radiotherapy as the set-up variation, organ motion.

Accurate anatomical delineation of the gross tumor volume (GTV) is crucial for effective stereotactic radiotherapy treatment of brain tumors. In absence of a clear definition of the GTV for a given pathology and of detailed contouring procedures, the GTV is likely to be estimated rather arbitrarily with the risk of tumor underdosage or detriment to the surrounding healthy tissues. Error in tumor delineation leads to a systematic miss during the treatment which could impair the probability of controlling the tumor. For a variety of malignancies such prostate, lung, breast, esophagus, gynecologic and brain tumors, several authors [1–10] have drawn the attention to the interobserver variability in the shape, volume and location of delineated GTVs. The use of computerized tomography (CT) images fused with magnetic resonance images (MRI) has greatly improved the accuracy of tumor localization [3, 6, 11, 12].

The aim of this study is to analyze the interobserver variability of base of skull meningiomas delineation on computed tomography.

Methods and Materials

Observers

Eight physicians working in the same center were asked to delineate the GTV of two patients on sequential CT slices. Contouring was done by two neurosurgeons, two radiologists, two medical oncologists and two radiation oncologists.

Patients – Treatment Preparation

Images of two patients with skull base meningiomas were used to compare the interobserver delineation. The patients were referred by the neurosurgeon after a subtotal resection.

The same clinical information is provided to each observer. Patients are immobilized by an individual fixation mask and CT scans images are acquired each 1 mm.

Contouring

Physicians enter their contours directly on a radiotherapy treatment planning console (Eclipse, Varian). The target outline was delineated on sequential CT slices directly on the computer screen by four medical specialties. Only the GTV is asked to be delineating: neurosurgeons and radiologists cannot be expected to have exact knowledge on microscopic spread.

Analysis

Results of the delineation by the four specialties are compared to each other. For each observer, the volume of the contoured GTV is calculated as the sum of the areas within the contours in each slice multiplied by the interslice distance. To identify the physician's level of agreement, encompassing and common volumes are calculated for every patient. The intersecting volume is the largest volume that is part of all GTVs of one patient. The encompassing volume is the outer contour of all the drawings by the eight observers.

If the location and volume of the delineated GTV are the same for the eight observers, there is no difference between the intersection volume and the encompassing volume, and neither between the mean volume and the intersecting volume.

To determine the variation in the anatomical position of the target volume, we also evaluated the variation in the position of the GTV borders two-dimensionally by comparing the maximum extensions of each observer's volume relative to a fixed point on each CT series. For the interobserver variability, the coefficient of variance is used. The coefficient of covariance (COV) is the standard deviation expressed as the mean of those volumes delineated by different observers using CT (COV % = mean/s × 100). If all physicians identified the same target volume in the same case, the mean ratio becomes 1. On the opposite, the greater the differences among the target volumes identified by the eight physicians, the greater the mean ratio becomes.

Results

Quantitative Analysis: Interobserver Variability for On-Screen GTV Delineation using CT

Figure 1 illustrates the delineation of the GTV by the eight physicians for both patients. Large differences are observed between the eight physicians both for the estimation of the tumor volume and its anatomical position. The value of the ratio of the largest to the smallest defined volumes is 8.8 for the first patient and 3.3 for the second. Those ratios become 1.19 and 1.66 for the medical oncologists, 1.07–1.57 for the neuroradiologists, 1.07–1.08 for the neurosurgeons and 1.14–6.5 for the radiation oncologists.

Delineated volumes as large as 402% of the mean volume and as small as 35% of the mean volume were recorded. The intersecting volumes (on which all physicians agree) represented only 32% of the mean volume for the first patient and 34% for the second. The results are summarized in table 1.The highest discrepancy is found for patient 1 for the delineation of one of the radiotherapist (RT2).

The results obtained in the four specialties are compared to each other and are presented in figure 2. Compared to radiation and medical oncologists, neurosurgeons and neuroradiologists tend to delineate slightly smaller volumes; the results for the radiation group need to be taken cautiously because of the large delineation of one of the two observers (RT2).

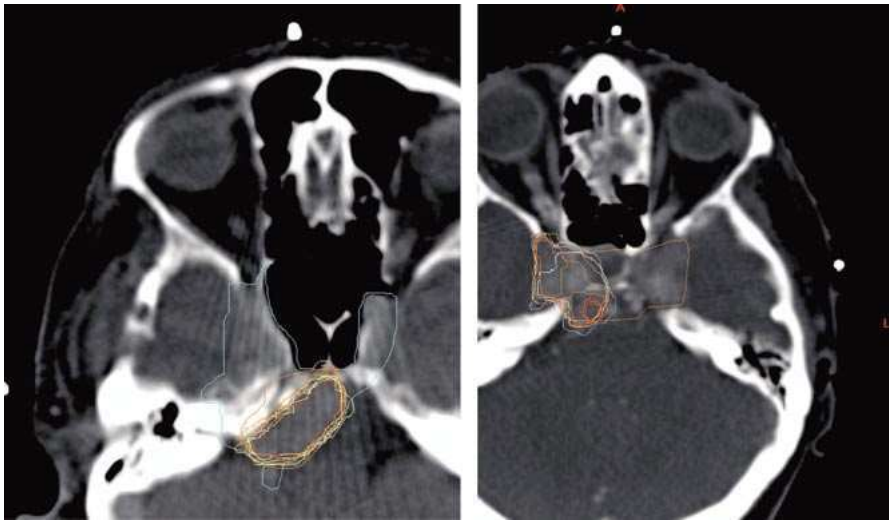

a ***b***

Fig. 1. GTV delineations of the eight observers on a transverse CT slice for the first (***a***) and second (***b***) patient.

Table 1. Interobserver variability for on-screen GTV delineation on CT scans: the volume in cm^3 for each observer, the mean volume and standard deviation, the volumes of intersection and the encompassing volumes (as a % of the mean volume) are given

V in cm^3	CT	Patient 1	Patient 2
Neurosurgeons	N1	4.93	7.62
	N2	5.28	7.04
Radiologists	R1	4.47	7.25
	R2	4.79	4.61
Medical oncologists	M1	7.37	15.4
	M2	6.16	9.26
Radiation oncologists	RT1	6.01	10.29
	RT2	39.38	11.83
	Mean V	9.8	9.2
	SD	11.9	3.4
	V intersection (% of mean volume)	32.2	34.3
	V encompass (% of mean volume)	386	164.5

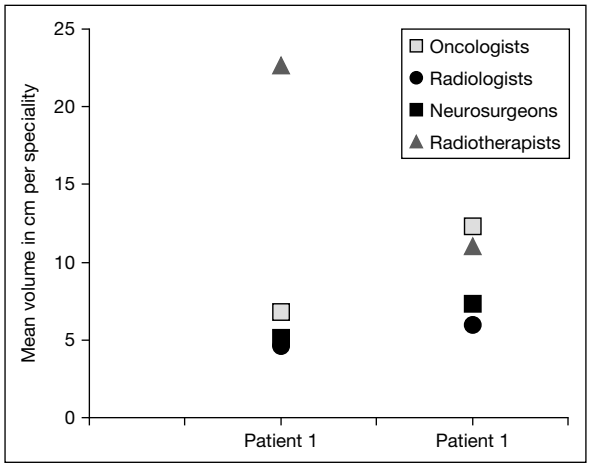

Fig. 2. GTV delineations on CT scan alone: Mean volumes in cm^3 per speciality.

Table 2. GTV delineations on CT: coefficients of covariance (COV) given as the mean per specialty

COV	Patient 1, %	Patient 2, %	All, %
Neurosurgeons	4.84	5.59	5.2
Radiologists	4.88	31.4	18.14
Medical oncologists	12.60	35.2	23.9
Radiation oncologists	103.6	9.80	56.7

Table 2 summarizes the interobserver variability as expressed using COV. Lowest COVs, indicator of a smallest interobserver variation, are found for the group of neurosurgeons and radiologists.

To assess the differences in anatomical location of the GTV, the variations between the different observers concerning the maximum extensions of the GTV relative to a fixed point in the GTV are measured. The maximum variation is 37 mm in the right–left direction; 45 mm in the anterior–posterior and 14 mm in the cranio-caudal for the first patient and 15, 13, 9 mm for the second patient. The best agreement was observed in the cranio-caudal direction. Variations in the position of gravity centers are shown in figure 3.

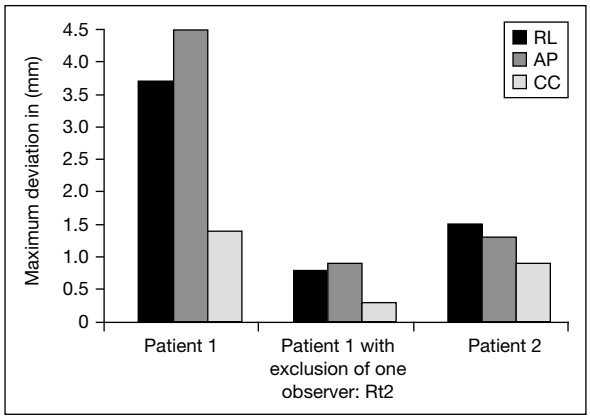

Fig. 3. Variation in the location of the gravity center-maximum differences between observers in the right-left (RL), antero-posterior (AP) and cranio-caudal (CC) direction.

Discussion

Delineation of the target volume is the fundamental first step of 3D treatment planning, unfortunately there is no standard method for making this determination. Major discordances are observed between delineated volumes indicating that this step needs to be improved. Except for brain tumors delineation, the problem of the accuracy on GTV delineation has been the subject of many publications. Studies on prostate delineation have demonstrated a good agreement on target volumes with a ratio of 1.2 [1–6, 11] but studies on head and neck tumors, lung, oesophageal, bladder delineation have a wide range between 3 and 5 [2–5, 7, 8, 11].

The superiority of MRI over CT in tumor definition is reported in some articles [3, 6, 11, 12]. For head and neck malignancies, Rash has pointed out that the GTV delineation was larger on CT than MRI and the MRI reduced the interobserver's variability [6].

For prostate delineation, a better visualization of the seminal vesicles and the prostatic apex is obtained on MRI slices and the amount of irradiated rectal wall can be reduced.

For brain tumors, only scarce information is available in the literature. In 1993, Leunens [4] was the first author to publish the interobserver differences in the delineation of brain tumors. The reported variations are linked to both differences in medical decision making and errors in the transfer of the data from the diagnostic CT to orthogonal radiographs. Weltens [9] has conducted later a study in the same hospital and demonstrated that the delineations directly

on the computer screen did not reduce the interobserver variability with respect to the volume.

In our study, the size of volumes varies enormously among the eight participating physicians: the value of the ratio of the largest to the smallest defined volumes is 8.8 for the first patient and 3.3 for the second: 1.19–1.66 for the medical oncologists, 1.07–1.57 for the neuroradiologists, 1.07–1.08 for the neurosurgeons and 1.14–6.5 for the radiation oncologists.

The intersecting volumes (32–34% of the mean volume) are even smaller than those reported by Leunens (25–73%) [4] and Weltens (38–59%) [9] reported. The present article studies only the GTV delineations on CT slices; MRI slices are not used. Using CT alone, the soft tissue enhancement of meningiomas may not be as well visualized, resulting in poorer definition of the tumor extension and possibly larger interobserver variation. For base skull meningiomas, Khoo [3] has demonstrated that there was less difference between the volumes determined by the observers on MRI than between those defined on CT. The tumor volumes defined on MRI were larger than those defined on CT but the two imaging modalities were complementary including parts of target volumes excluded by the other. Ten haken [12] indicated that the best imaging modality remains uncertain until histopathological studies are performed; MRI defines larger volumes in comparison with CT scan volumes. The use of MRI enhances the ability to visualize soft tissues lesions near bony prominences such the base of the skull or encloses such as the spinal cord. MRI is the gold standard in detecting CNS soft tissue changes; it provides better delineation of tumor tracking along the nerves, along tissue planes or along bony plates. The presence of intrinsic image distortion for the tumor delineation, the lack of attenuation coefficient information needed for the correction of tissues inhomogeneities (treatment planning) and the absence of bone information for portal verification necessitates also the use of the CT images.

Similar to the literature it could be shown that the radiotherapist tend to outline larger contours than other specialists. Compared to radiotherapist, radiologists and neurosurgeons showed a better consistency in the location and volume of their GTV. Differences between the radiation oncologists and other specialties could be an unconscious integration of geometrical uncertainties relevant in radiotherapy.

For the group of radiotherapist and particularly for one of them, lack of radiological expertize result in incorrect GTV contouring. For brain tumors, the physician has for each individual case the task to define what he considers to be the visible tumor and what he considers to be normal surrounding tissue and oedema. A better training of radiotherapists and an increased collaboration with radiologists and neurosurgeons should decrease this variability. The collaboration with the radiologists can help to choice the good image quality and an optimal

window level: inadequate window setting can lead in over and underestimation of tumor boundaries and thereby increase inconstancies of target volume definition among observers. Collaboration with neurosurgeons can help in the knowledge of normal and pathological anatomy. Neurosurgeons can also describe the surgical manipulation leading to a macroscopic description of the lesion.

Conclusions

Following the ICRU 50 recommendations, the uncertainties linked to patient position and organ motion are taken into account in the treatment planning but no margins are foreseen to compensate the GTV errors delineation leading to systematically geographical miss. Until now no gold standard has been defined on how to deal with the observed variability. The success of stereotactic radiotherapy technique relies on an accurate determination of the GTV and necessitates a good cooperation with a multidisciplinary team, the radiologist and neurosurgeons team, by using different imaging modalities as MRI and methionine PET.

References

1 Fiorino C, Reni M, Bolognesi A, et al: Intra and inter-observer variability in contouring prostate and seminal vesicles: implications for conformal treatment planning. Radiother Oncol 1998;47:285–292.
2 Giraud P, Elles S, Helfre S, et al: Conformal radiotherapy for lung cancer: different delineation of the gross tumor volume by radiologists and radiation oncologists. Radiother Oncol 2002;62:27–36.
3 Khoo VS, Adams EJ, Saran F, et al: A comparison of clinical target volumes determined by CT and MRI for the radiotherapy planning of base of skull meningiomas. Int J Radiat Oncol Biol Phys 2000;46:1309–1317.
4 Leunens G, Menten J, Weltens C: Quality assessment of medical decision making in radiation oncology: variability in target volume delineation for brain tumors. Radiat Oncol 1993;29: 169–175.
5 Logue JP, Sharrocck CL, Cowan RA, Read G, et al: Clinical variability of target volume description in conformal radiotherapy planning. Int J Radiat Oncol Bio Phys 1998;41:929–931.
6 Rash C, Barillot I, Remeijer P, et al: Definition of the prostate in CT and MRI: a multi-observer study. Int J Radiat Oncol Biol Phys 1997;43:57–66.
7 Tai P, van Dyk J, Yu E, Battista, et al: Variability of target volume delineation in cervical oesophageal cancer. Int J Radiat Oncol Biol Phys 1998;42:277–288.
8 Van de steene J, Linthout N, de Mey J, et al: Definition of gross tumor volume in lung cancer: interobserver variability. Radiother Oncol 2002;62:37–49.
9 Weltens C, Menten J, Feron M, et al: Interobservers variations in gross tumor volume of brain tumors on computed tomography and impact of magnetic resonance imaging. Radiother Oncol 2001;60:49–59.
10 Yamamoto M, Nagata Y, Okajima K, et al: Differences in target outline delineation from CT scans of brain tumours using different methods and different observers. Radiother Oncol 1999;50: 151–156.

11 Rash C, Keus R, Pameijer FA, et al: The potential impact of CT-MRI matching on tumor volume delineation in advanced head and neck cancer. Int J Radiat Oncol Biol Phys 1997;39:841–848.
12 Ten haken R, Thornton A, Sandler H, et al: A quantitative assessment of the addition of MRI to CT-based 3D treatment planning of brain tumors. Radiother Oncol 1992;25:121–133.

Dr. C. Mitine
Service de Radiothérapie-Oncologie
Jolimont Hospital Rue Ferrer 159
BE–7100 Haine St. Paul (Belgium)
Tel. +32 64 234181, Fax +32 64 233844
E-Mail c.mitine@tiscali.be

Kondziolka D (ed): Radiosurgery. Basel, Karger, 2006, vol 6, pp 140–151

Optic Nerve Sheath Meningiomas: The Role of Stereotactic Radiotherapy

R. Smee, M. Schneider, J. Williams

Department of Radiation Oncology, Prince of Wales Hospital, Randwick, Australia

Abstract

Purpose: Primary orbital meningiomas are rare, the usual site of origin being the optic nerve sheath. These represent 1–2% of all meningiomas. This is a review of a single centre's experience. **Materials and Methods:** Between 1990 and February 2004 26 patients were referred and 16 patients were treated by radiotherapy (mean age 51 years). This retrospective study evaluated 16 patients – 18 tumours (1 patient with NF2 had bilateral optic nerve tumours and 1 optic nerve was treated twice). Nine patients were treated with newly diagnosed lesions, and 7 recurrent after prior treatment including radiotherapy for 1 patient. The median duration of symptoms to onset was 2 months. Treatment consisted of stereotactic radiosurgery (median dose 20 Gy) where vision was not a consideration, and fractionated SRT (median dose 5,040 Gy in 28 fx) for vision preservation. **Results:** Median follow up is 46.8 months. Recurrence after SRT occurred in 1 patient (a geographical miss) leading to progressive disease and blindness, this new lesion was treated with stereotactic radiosurgery, the tumour controlled with subsequently some vision improvement. Only one other patient had progressive disease, thus for an ultimate local of 94%. For fractionated patients only the above patient had worse vision after treatment. **Conclusion:** Radiotherapy provides high local control, utilising fractionated treatment provided it covers the full length of the nerve, is necessary to have the option of preserving vision.

Optic nerve sheath meningiomas (ONSM) are uncommon benign tumours arising from the dural tissue encircling the optic nerve, typically arising in the orbital component of the nerve capable of spreading along the nerve to become intracranial and involving the optic chiasm. The latter situation is more common in the context of neurofibromatosis type 2 (NF2) the only know causative association for this disease. ONSM represents only 1–2% of all meningiomas and have as their means of presentation slow deterioration of visual function [1, 2]. In 95%

of cases it is unilateral, and may also be associated with mild retro-orbital headaches and proptosis [3]. The 5% that are bilateral is that group more commonly associated with NF2. Various reports include so called secondary ONSM in which extension along the optic nerve may occur secondarily to origin of the meningioma on the sphenoidal ridge with direct extension via the optic canal into the orbit. In this article the description will only apply to primary ONSM.

As with all meningiomas a typical patient is a female aged between 35 and 60 years of age, with a many month history of visual deterioration [2, 4], although it has been described as occurring in children, in this context behaving in a more aggressive fashion. Diagnosis relies upon formal ophthalmological evaluation with documentation of visual acuity, fundoscopy and perimetry for visual field deficit. In circumstances where the presenting feature is merely visual blurring with retention of acuity, more subtle abnormalities such as colour vision testing and mild dyschromatopsia, and a Marcus Gunn pupil may be the only abnormalities [3]. Limitation of ocular movement is an unlikely occurrence although the presence of proptosis should be considered and assessed. Ocular swelling can occur, and if prolonged can lead to the development of opticociliary shunt vessels on the surface of the disc. Diagnosis is now based on the MR imaging characteristics displaying a thickened optic nerve, with fat suppression views necessary to define the true dimensions of the tumour. Other conditions need to be considered as part of the differential diagnosis [3]. Specific imaging characteristics usually enable separation of the other entities, occasionally a trial of steroids is necessary to exclude the inflammatory conditions that can involve the optic nerve. Schick [1] has described a three tier staging system the differentiating features being the amount of intracranial extension. Type I defines the tumour as being entirely intraorbital, Type II with extension through the optic canal or superior orbital fissure, and Type III has widespread intracranial tumour.

Management has historically been dominated by a form of surgery ranging from biopsy and decompression of the optic nerve to microsurgical resection [1, 2, 4, 5]. The former approach invariably results in progression of the meningioma whilst both methods ultimately have a high rate of visual deterioration. Increasingly radiotherapy is regarded as the preferred treatment approach, Carrasco reporting that this ‘represents an enormous improvement in a disease entity with typically poor visual prognosis’ [5]. Fractionated approaches provide a high opportunity of local control of the tumour plus good prospect of at least visual stabilisation [6–10]. Current stereotactic approaches can dramatically reduce the risk of complications associated with conventional radiotherapy approaches. Thus, the main role for surgery in the future will be for decompression where significant mass effect is evident thus relying upon radiotherapy to control the tumour a feature now applicable to meningiomas at all sites [11, 12].

The aim of this review is to evaluate a single centre's experience with this uncommon tumour across a timeframe where MRI was available for all patients at the time of treatment, and stereotactic irradiation became increasingly the preferred method of treatment.

Materials and Methods

This Ethics approved retrospective study sourced all patients with a diagnosis of meningioma from the clinical database of all patients registered in the Department of Radiation Oncology at Prince of Wales Hospital (POW). 1990 was chosen as a starting point for this review as it was the year that stereotactic radiosurgery (SRS) became available at this facility. Subsequently a specific meningioma database has been established and all tumours coded for sites of involvement. It was thus possible to define origin from the optic nerve, and exclude all those as secondarily involving the optic nerve. February 2004 was the closure point for this study thus allowing for a minimum 18 months of follow up from presentation. Information relating to these patients was obtained from the meningioma database, POW radiotherapy records, referral letters, imaging reports, follow up correspondence from specialists and local medical officers, and if necessary directly with the patient.

Referral was from ophthalmologists or neurosurgeons, with decreased visual acuity in all patients with MRIs to document the extent of disease. Unfortunately the available reports and documentation do not allow categorisation according to the Schick classification.

Treatment techniques evolved over the timeframe of this study as well as being influenced by the treatment aim. In the early years of the study patients were referred with little to no retained vision, and thus the aim was tumour control. Where vision preservation was integral to care, fractionation was used ranging from conventional treatment with 2–3 fields, to stereotactic methods with cones and 'jaws' for pseudo rectangular field shaping, and a MMLC (with 4 mm leaf width collimation) using multiple fixed fields or in intensity modulated radiotherapy (IMRT) mode.

All patients were treated with 6 MeV photons with head fixation appropriate to the treatment method. For the SRS this was with the BRW headframe (Radionics, Burlington, USA), and for fractionated stereotactic it was with the GTC relocatable headframe (Radionics, Burlington, USA). All stereotactic treatments were planned with the same software (Radionics, XKnife, and Xplan) with multiple programme upgrades over the years of the study. This treatment is all given as an outpatient. A consistent rigid quality assurance programme has existed over the timeframe to assure the accuracy and reproducibility of treatment.

Outcomes were measured according to two criteria: radiological assessment of tumour growth, and ophthalmological evaluation of visual acuity and fields. For tumour control this was scored as lack of progression within the volume treated, since many of these patients were treated from other states the follow up reports did not allow sufficient quantification of the amount of reduction to enable tumour decrease to be scored accurately. The report, however, of tumour growth as 'yes or no' was consistent.

In terms of visual evaluation this was rated according to the ophthalmologists reports and the patients more subjective comments. The latter obviously was of more relevance to the patients as it described their day-to-day reaction to treatment. To this extent, visual evaluation was defined as 'no change, better, or worse' noting the timeframe over which this occurred.

Table 1. Patient population – Prince of Wales Hospital

Patient numbers	Initial treatment	Recurrent/progression
Gender		
Male	1	4
Female	8	3
Total	9	7
Age, range (years)	22–74	7–68
Symptom duration		
<3 months	2	2
3–12 months	3	3
>12 months	4	2
Total	9	7

Results

From September 1990 (when the SRS programme began) to February 2004, allowing a minimum follow up of 18 months with a maximum follow up to 13 years for the first patient treated, 26 patients were seen of whom 10 were seen as consultation only. This resulted in 16 patients being seen and treated, 1 patient (with NF2) had bilateral optic nerve involvement, 1 patient had the same optic nerve treated twice, thus resulting in 18 optic nerves being evaluated for a treatment outcome.

There were 11 females and 5 males with a range of 7–74 years. The youngest patient a male, with NF2, had bilateral disease. This population could be conveniently divided into two groups determined by whether the treatment delivered at POW Hospital was provided following previous treatment, or as part of their management at diagnosis (table 1). Of note, it is only for the initially diagnosed group that the typical predominance of females was evident. Proptosis was apparent in 4 patients with 'headaches' documented in 3.

As for treatment, table 2 indicates the three different treatment approaches used over this timeframe. Two of the treatment approaches reflect the historical aspect of this series. The median dose of 20 Gy for SRS was a reflection of the high dose felt necessary to treat meningiomas prior to 1995. The more recently treated patient (vide infra) received 14 Gy, with the SRS patients typically dosed to the 80–100% isodose. The conventionally treated patients were managed prior to the availability of the relocatable GTC headring for fractionated stereotactic radiotherapy in 1995. However, the total dose and number of fractions has remained constant with a median of 50.4 Gy in 28 fx over the duration of the study.

Table 2. Treatment characteristics

	Initial treatment (Pts)	Recurrence (Pts)
SRS	1	1
SRT	6	4
Conventional	2	1
Dose	SRS – median	20 Gy
	SRT – median	50.40 Gy in 28 fx

Fractionated SRT used where vision maintained and to be preserved.

Table 3. Outcome – radiological and visual – optic nerves

	Initial	Recurrent
Acuity		
Worse	2*	–
No change	5	3
Better	3	5*
Radiological		
Stable	8*	8
Increased	–	2*

*Includes patient with geographical miss, subsequently treated with controlled disease. This patient is included in more than 1 category.

In terms of outcome, no patient has had radiological progression within the volume treated (table 3), 1 patient had progression outside of this for a geographic miss. For vision only 2 patients were worse after initial treatment, with 1 patient subsequently improving. Six patients had improved vision although 1 patient (the 7-year-old boy with NF2) blind in one eye had subject and objective improvement in his 'good eye' 6 months post-treatment, however subsequent objective evaluation showed a 1 level Snellen chart change back to his pre-treatment vision. This patient feels his vision remains the same as that at initial post-radiotherapy evaluation (he thus has a difference between subjective and objective evaluation).

The importance of the volume to be treated can be gained from the following case event.

Case History: A 51-year-old woman presented with a 9 month history of visual deterioration in the left eye. MRI imaging indicated findings consistent

with an ONSM confined to the intraorbital component of the nerve (Schick Type 1) [1]. As there was retained vision in the left eye fractionated SRT was given. Radiologically and visually the patient was stable for 15 months after treatment. At 2 years after initial treatment she returned with a 4 month history of blindness in the left eye. Follow up MRI indicated a globular mass involving the intracranial component of the optic nerve with no change in the size and shape of the intraorbital component. SRS was then used abutting up to the previously treated component distally and to the lateral aspect of chiasm proximally. Subsequent follow up 18 months later indicates stable disease in both treated areas (with a small area of gliosis in adjacent frontal lobe at the junction of the 2 fields) with the patient now able to detect shapes and colours. Where the chiasm needs to be included in the treatment field, thus requiring a long segment of nerve to be addressed dose critical structures such as the pituitary, hypothalamus and temporal lobes become important, Stereotactic IMRT is then used in this situation. By this means with inverse planning the dose limit to these structures is respected (fig. 1) and highly conformal coverage of the tumour is achieved. For the 7-year-old boy (at presentation) 3 years later there is (to date) no pituitary deficit, and his school marks remain stable.

Discussion

In discussing the management of meningiomas it is important to differentiate between those that primarily arise from the optic nerve sheath versus those that secondarily involve the nerve. The latter situation includes those tumours arising along the sphenoidal ridge, and the parasellar area. As far back as Craig and Gogela [13] described three groups of primary intraorbital meningiomas:

(1) Optic canal meningiomas
(2) ONSM
(3) Extra dural meningiomas

All three can present with the same clinical features of progressive visual loss plus or minus proptosis. The timing of the proptosis in terms of visual change may give some clue as to the site of origin. Other conditions that may involve the optic nerve (including optic nerve glioma in patients with NF2) need to be considered, however current MRI protocols usually allow distinction [3]. A feature that clinically may allow differentiation is the strong predominance of females with meningioma. The near equivalence of males and females in our 'Recurrence' group is more likely artefactual given the dominance of females to males in all other series [1, 4, 6, 14].

Clinical features of relevance include the incidence of bilateral disease as well as the extent of intracranial disease. Schick et al. [1] reported 8 of their

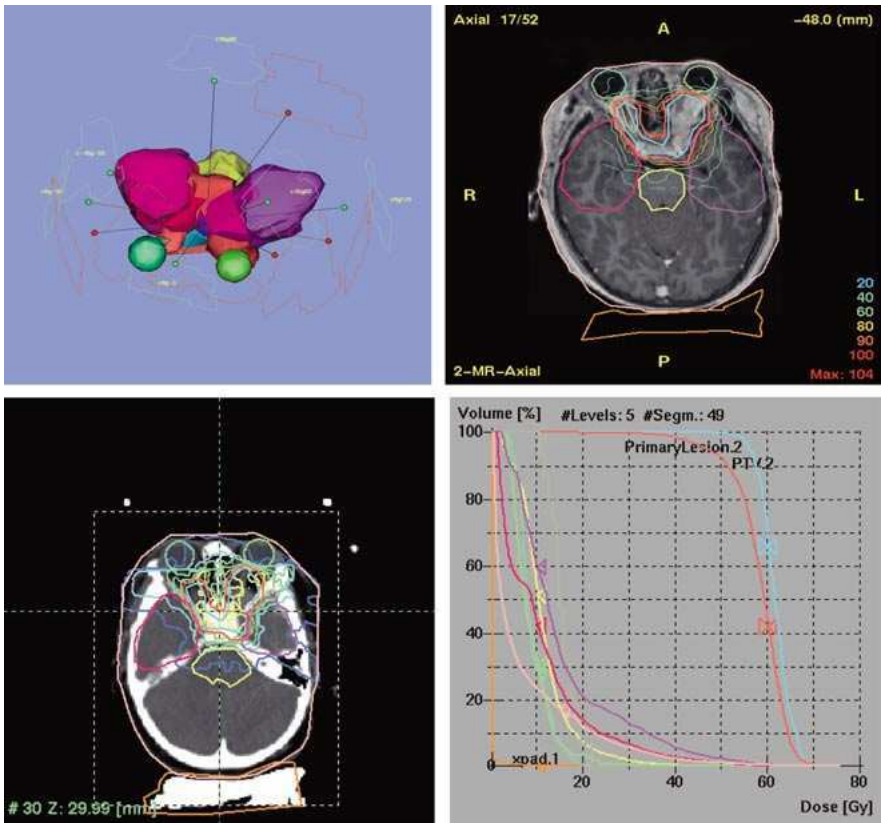

Fig. 1. Stereotactic IMRT of 7-year-old boy with bilateral optic nerve meningioma. Dose-critical structures include bilateral globe, hypothalamus, pituitary, temporal lobes and brain stem. DVHs demonstrate separation of dose to these structures, from that to the U-shaped tumour.

73 patients had spread to the contralateral side, whilst 28 had involvement of the chiasm. Dutton [2] reported 38% involvement of the contralateral nerve if the intracanalicular portion of the nerve on the ipsilateral side was effected. Turbin and Pokorny [14] described 9.4% (6 of 64 patients) with bilateral spread. In this series of 16 patients treated there is only one patient with bilateral disease although one of the patients seen as a consultation also had bilateral involvement (not surprisingly also with NF2). None of the above series report on the prevalence of NF2 in their population. Intracranial spread defines a more aggressive pattern, or longer evolution of disease. As stated separation of the sites of origin is appropriate given the different patterns of spread that can occur. A meningioma arising along the sphenoidal ridge and extending medially to involve the

optic nerves has a very different pattern of lateral extension than that of an ONSM. Similarly Schick et al. [1] Type IIb with a predominant cavernous sinus component has a greater likelihood of posterior extension. Basso et al. [3] highlights the difficulties of separating primary from secondary types where there is significant intracranial extension. Whilst this distinction could be important in determining the preparedness for and type of surgical procedure, radiotherapy can be considered as definitive treatment in both circumstances with the opportunity for visual improvement.

Surgical management has long been the mainstay of treatment for this tumour [2]. The extent of surgery ranges from mere biopsy and decompression to attempted resection. Basso et al. [3] raises concern about the former approach indicating it has 'usually not been successful in preserving vision' but more importantly 'may lead to orbital spread of tumour'. Kennerdell et al. [15] reported only 10% of their surgically treated patients had visual improvement post-op. Continuing this theme Schick et al. [1] noted that very few cases of visual improvement occurred after microsurgical resection. In that series of 73 patients who had surgery performed only 6 had visual improvement. A cautionary note however is recorded as visual acuity may become worse 'with longer follow up period'. Given the slow growth of many of these tumours decompressing the optic canal may provide for stable vision for a limited period where this structure is the main compressive element.

Surgery is not without its risks. Turbin and Pokorny [14] in reporting on a population of 64 patients treated by mixed means (observation, surgery, surgery + radiotherapy, and radiotherapy alone) noted that 66% of patients treated by surgery alone developed a complication related to the surgery. Similarly those treated by surgery and radiotherapy had a 62.5% incidence of complications. Others have reported visual complications rates up to 40% [2, 15]. Schick et al. [1] noted a lower incidence with a transient morbidity rate of 12.3%, and a permanent morbidity rate of 2.7%. Even these surgical authors now recognise the specific benefits of radiotherapy, although Schick advises it to be only used where visual deterioration occurs, this however is the very circumstance that results in these patients coming to medical attention.

Radiotherapy has been used in many modes for the treatment of meningiomas for many years, the outcome of success being lack of progression [11, 16, 17]. With variable follow up periods there is a consistent success rate using this criteria of benefit, of greater than 85%. In our experience in a larger population of all patients [12] with a diagnosis of meningioma treated by radiotherapy the local control rate is 96% with up to 14 years of follow up. Becker et al. [18], Richards et al. [9], Pitz et al. [19] and Liu et al. [20] all reported 100% tumour control although the median follow up for all patients was less than 5 years. For this specific series all patients were locally controlled, although

there was an out of field failure, subsequently salvaged with further radiotherapy. However, not all series report the same success. Turbin and Pokorny [14] noted that 8 of 16 patients having surgery and radiotherapy, and 2 of 18 patients with radiotherapy only, had radiographic progression. Basso et al. [3] reports progression in 3 of 14 patients treated with no details of dose or technique used. Turbin and Pokorny [14] reports a range of doses used. The largest published series is by Andrews et al. [6] who reported on 30 patients and 33 optic nerves treated by fractionated SRT. All patients and optic nerves had tumour control (i.e. 100%) with median follow up of 89 weeks. Functional activity of the meningiomas was evaluated in 6 patients with 'In Octreotide' uptake pre- and post-radiotherapy, all 6 had a decrease in isotope uptake within 6 months of treatment.

In terms of visual outcome there is almost universal agreement that radiotherapy is the best option in terms of obtaining the best result [7–10, 21]. Turbin and Pokorny [14] reports that patients with ONSM receiving radiation alone demonstrated the best visual outcome with the appropriate caveat 'during the follow up period'. Baumert et al. [22] noted (with a median follow up of 20 months) 95% visual control (21 of 22) with visual improvement in 16 patients, this being apparent in 1–3 months after concluding treatment. One patient had visual deterioration. Becker et al. [18] reported stable to improved visual acuity and fields in all 15 patients with primary ONSM. Liu et al. [20] similarly reported no worsening of vision in 5 treated patients, 4 having improved vision. Narayan et al. [8] reported only 1 patient (of 15) with worse vision as a consequence of radiation retinopathy. Schick et al. [1] noted 4 patients with visual deterioration after radiotherapy, Andrews et al. [6] noted vision worse permanently in only 2 patients. In this series of 16 patients treated 13 patients were treated with the intent of visual stabilisation. There was 1 infield deterioration, and 1 out of field blindness with subsequent visual improvement. Thus 12 patients have stable to improved vision.

There are two radiotherapy aspects that need to be considered: the volume to be treated, and the dose and fractionation used. There is little description in the radiotherapy literature of how much of the optic nerve needs to be treated irrespective of the extent of radiological abnormality. Schick's et al. [1] series indicates that the majority of patients have disease extending beyond the intraorbital aspect with 23 patients having involvement of the chiasm. Hence the field coverage at least needs to be up to the chiasm. This was highlighted in this series in which despite applying a 1 cm margin proximal to the radiologically evident abnormality an out of field failure still occurred, fortunately this has to date been successfully salvaged. Whilst extending the field coverage more proximally introduces more dose critical normal structures into the proximity of the treatment volume, modern 3D conformal approaches can address this.

Interestingly one of the consultation cases in this series was a young boy with NF2 who had bilateral optic nerve involvement but with a MRI normal optic chiasm, whose parents raised considerable concern with the concept of treating bilateral optic nerves and chiasm to address the risk as well as the evidence of disease. They have subsequently found a centre that will treat the radiologically abnormal area, however the concept of treating abutting fields in the future is of concern. In terms of dose and fractionation Parsons et al. [23] noted a 0% incidence of optic nerve injury (in 106 optic nerves) where total doses of less than 59 Gy were used with fraction size of less than 1.9 Gy. In the quoted series there has been a range of dose and fractions used from 40 Gy in 23 fx to 54 Gy in 30 fx all reporting comparable control. It is difficult to know however whether the few failures occurred in the patients receiving the lower dose. For this series (as well as the larger population) [12] a consistent median dose of 50.4 Gy in 28 fx has been used with good outcome in terms of tumour control, and visual improvement/stabilization thus there is little necessity to change. When using SRS an accepted tolerance dose of 8 Gy has been given to the chiasm and nerve, although some reports are now indicating that 10 Gy may be tolerated. The patient in the case history received 14 Gy and has had subsequent improvement. None of the patients treated in the earlier years of this study who received 20 Gy had visual improvement post treatment. In this context a SRS dose of less than 20 Gy should be regarded as reasonable.

Radiotherapy is not without its toxicity as well. Most series report some degree of short-term toxicity that should resolve (such as hair loss, and fatigue). However, Turbin [4] noted that 33% (6/18) receiving radiotherapy only had complications related to that treatment. This was retinopathy/vascular occlusion in 4, iritis in 1, and 1 case of temporal lobe atrophy. Richards et al. [9] also reported radiologically detected cerebral change in 1 of 4 patients. Andrews et al. [6] had 1 patient with reversible optic neuritis. Retinopathy is certainly a recognised complication of treatment of the retina and has been described after fractionated doses as low as 45 Gy. Large volumes of the retina certainly do not need to be treated in this disease entity, and with modern approaches the iris would not be regarded as needing to be included within the structures to be treated. With modern highly conformal methods [17] (incorporating stereotactic approaches, IMRT, and dose volume constraints) the likelihood of long-term complications should be low as evidenced in this treated population where there are no reported long-term complications. However, long-term follow up needs to continue for all the published series to provide adequate documentation that the appropriate outcomes (both tumour control and visual effect) are maintained, as well as reporting on any long-term complications.

The diagnosis of an optic nerve sheath meningioma had in previous years defined the effected patient as ultimately going blind. However, there is now

very clear recognition, even amongst the surgical centres, that radiotherapy is the preferred outcome both in terms of achieving tumour control, and in the great majority, of visual stabilisation. Given this consensus there are now two obligations on the part of the radiotherapy community: to report short and long-term outcomes, and to deliver the treatment safely. In terms of the latter stereotactic fractionated radiotherapy (including IMRT) is the ideal vehicle. This is the standard by which all subsequent series should be judged.

References

1 Schick U, Dott U, Hassler W: Surgical management of meningiomas involving the optic nerve sheath. J Neurosurg 2004;101:951–959.
2 Dutton JJ: Optic nerve sheath meningiomas. Surg Ophthalmol 1992;37:167–183.
3 Basso A, Carrizo A, Kreutel A, Tomecek F: Primary Intraorbital Meningiomas. Meningiomas and their Surgical Management. Philadelphia, Schmidek, WB Saunders Co, 1991, 28, pp 311–323.
4 Turbin RE, Thompson CR, Kennerdell JS, Cockerham KP, Kupersmith MJ: A long-term visual outcome comparison in patients with optic nerve sheath meningioma managed with observation, surgery, radiotherapy, or surgery and Radiotherapy. Ophthalmology 2000;109:890–900.
5 Carrasco JR, Penne RB: Optic nerve sheath meningiomas and advanced treatment options. Curr Opin Ophthalmol 2004;15:406–410.
6 Andrews DW, Faroozan R, Yang BP, et al: Fractionated stereotactic radiotherapy for the treatment of optic nerve sheath meningiomas: preliminary observations of 33 optic nerves in 30 patients with historical comparison to observation with or without prior surgery. Neurosugery 2002;51: 890–904.
7 Lui JK, Forman S, Hershewe GL, et al: Optic nerve sheath meningiomas: visual improvement after stereotactic radiotherapy. Neurosugery 2002;50:950–957.
8 Narayan S, Cornblath WT, Sandler HM, et al: Preliminary visual outcomes after three-dimensional conformal radiation therapy for optic nerve sheath meningioma. Int J Radiat Oncol Biol Phys 2003;56:537–543.
9 Richards JC, Roden D, Harper CS: Management of sight-threatening optic nerve sheath meningioma with fractionated stereotactic radiotherapy. Graefes Arch Clin Exp Ophthalmol 2005;33: 137–141.
10 Melian E, Jay WM: Primary radiotherapy for optic nerve sheath meningioma. Semin Ophthalmol 2004;19:130–140.
11 Debus J, Wuendrich M, Pirzkall A, Hoess A, Schlegel W, Zuna I, Engenhart-Cabillic R, Wannenmacher M: High efficacy of fractionated stereotactic radiotherapy of large base-of-skull meningiomas: long-term results. J Clin Oncol 2001;19:3547–3553.
12 Smee R, Schneider M, Williams J: Current radiotherapy management of meningiomas (In preparation).
13 Craig W, Gogela L: Intraorbital meningiomas: a clinicopathologic study. Am J Ophthalmol 1949;32:1663.
14 Turbin RE, Pokorny K: Diagnosis and treatment of orbital optic nerve sheath meningioma. Cancer Control 2004;11:334–341.
15 Kennerdell JS, Maroon JC, Malton M, et al: The management of optic nerve sheath meningiomas. AM J Ophthalmol 1988;106:450–457.
16 Selch M, Ahn E, Laskari A, Lee S, Agazaryan N, Solberg T, Cabatan-Awang C, Frighetto L, Desalles A: Stereotactic radiotherapy for treatment of cavernous sinus meningiomas. Int J Radiat Oncol Biol Phys 2004;59:101–111.
17 Pirzkall A, Debus J, Haering P, Rhein B, Grosser K, Hoss A, Wannenmacher M: Intensity modulated radiotherapy (IMRT) for recurrent, residual, or untreated skull-base meningiomas: preliminary clinical experience. Int J Radiat Oncol Biol Phys 2003;55:362–372.

18 Becker G, Jeremic B, Pitz S, Buchgeister M, Wilhelm H, Schiefer U, Paulsen F, Zrenner E, Bamberg M: Stereotactic fractionated radiotherapy in patients with optic nerve sheath meningioma. Int J Radiat Oncol Biol Phys 2002;54:1422–1429.
19 Pitz S, Becker G, Schiefer U, Wilhelm H, Jeremic B, Bamberg M, Zrenner E: Stereotactic fractionated irradiation of optic nerve sheath meningioma: a new treatment alternative. Br J Ophthalmol 2002;86:1265–1268.
20 Liu J, Forman S, Hershewe G, Mororthy CR, Benzil D: Optic nerve sheath meningiomas: visual improvement after stereotactic radiotherapy. Neurosurgery 2002;50:950–957.
21 Moyer PD, Golnik KC, Breneman J: Treatment of optic nerve sheath meningioma with three-dimensional conformal radiation. Am J Ophthalmol 2000;129:694–696.
22 Baumert BG, Villa S, Studer G, Mirimanoff RO, David JB, Landau K, Ducrey N, Arruga J, Lambin P, Pica A: Early improvements in vision after fractionated stereotactic radiotherapy for primary optic nerve sheath meningioma. Radiother Oncol 2004;72:169–174.
23 Parsons JT, Bova FJ, Fitzgerald CR, et al: Radiation optic neuropathy after megavoltage external-beam irradiation: analysis of time-dose factors. Int J Radiat Oncol Biol Phys 1994;30:755–763.

Dr. R. Smee
Stereotactic Radiosurgery Unit, Prince of Wales Hospital
Randwick, NSW 2031 (Australia)
Tel. +61 2 93 82 2539, Fax +61 2 9382 2550
E-Mail robert.smee@sesiahs.health.nsw.gov.au

Kondziolka D (ed): Radiosurgery. Basel, Karger, 2006, vol 6, pp 152–163

New Treatment Strategy for Craniopharyngioma using Gamma Knife Radiosurgery

From Long-Term Results of 100 Consecutive Cases

Tatsuya Kobayashi[a], *Yoshimasa Mori*[a], *Yukio Uchiyama*[a], *Naoki Hayashi*[a], *Yoshihisa Kida*[b], *Toshinori Hasegawa*[b]

[a]Nagoya Radiosurgery Center, Nagoya Kyoritsu Hospital, Nagoya,
[b]Gamma Knife Center, Komaki City Hospital, Komaki, Japan

Abstract

One hundred craniopharyngioma cases were treated by Gamma Knife and followed-up for a mean of 65.5 (6–148) months. Mean tumor diameter and volume were 18.8 mm and 3.8 ml. The tumors were treated with a maximum dose of 21.8 Gy, a marginal dose of 11.5 Gy, and a mean of 4.5 isocenters. Overall, the complete response rate was 19.4%, response rate 67.4%, control rate 79.6% and progression rate 20.4%. Analysis of complete response cases revealed age (adult), solid tumors less than 15.9 mm in diameter and fewer previous treatments to be good prognostic factors, along with a mean marginal dose of 12.1 Gy. Eighteen of 20 progression cases had cystic-mixed tumors and the cause of progression was cyst enlargement in 9, tumor regrowth in 8 and a new lesion in 3 cases. Among these factors, being an adult was a significantly favorable factor, while cystic and mixed tumor types were significant poor prognostic factors. Regarding the changes in neurological and pituitary-hypothalamic symptoms after Gamma Knife radiosurgery, overall improvement was seen in 17 (18.7%), no change in 59 (64.8 %) and deterioration in 15 (16.5%). Three cases each had visual and endocrine deteriorations thought to represent side effects of Gamma Knife radiosurgery. Outcomes were excellent in 45, good in 23, fair in 4, poor in 3 and death in 16. A new treatment strategy has been proposed, in which small residual or recurrent tumors at the so-called 'R-site' (tumor origin) are targets for Gamma Knife radiosurgery, as an alternative to total removal. With this strategy, permanent cure can be expected without neuro-endocrine deficit. In conclusion, stereotactic Gamma Knife radiosurgery is safe and effective, with minimal side effects, as adjuvant or boost therapy for residual and/or recurrent craniopharyngiomas after surgical removal.

Craniopharyngioma treatment remains controversial. Total removal is ideal but complete removal without deterioration of neurological functions has been difficult to achieve because of the proximity of these tumors to the hypothalamus, pituitary gland and optic pathway. The recurrence rate is reportedly not low even after 'total' removal [1, 2]. Another strategy involves combined treatment with partial removal of the tumor and fractionated focal irradiation. Cure or complete control of the tumor has also been difficult and late radiation injury to surrounding organs can produce major side effects [3–5]. Recently, stereotactic radiosurgery has been found to be an effective and safe treatment for craniopharyngiomas [6–9]. This retrospective analysis of the long-term results of 100 patients treated by Gamma Knife radiosurgery, over a 12 year period, has prompted the matter to propose a new strategy for treating craniopharyngiomas using the Gamma Knife.

Materials and Methods

One hundred and seven craniopharyngioma cases were treated with the Gamma Knife at Komaki City Hospital during the period from 1991 to 2003. One hundred were followed up for more than 6 months after treatment. Characteristics of the cases include a mean age of 33.6 (3–80) years, 38 children (age at diagnosis less than 15) and 62 adults, a male to female ratio of 55:45, 40 tumors classified as solid, 24 as cystic and 36 as mixed, and a mean tumor diameter of 18.8 mm. Surgical treatments prior to Gamma Knife radiosurgery included subtotal removal of tumor in 24, partial removal in 107, biopsy in 10, placement of an Ommaya reservoir in 26 and of a V-P shunt in 5 times. Fractionated focal irradiation in 13 cases, and chemotherapy using Bleomycine in 3 cases, were combined with surgical treatments (table 1).

The dose planning for Gamma Knife radiosurgery was based on T1 weighted enhanced 3D MR images obtained with the Gamma Plan. Accurate and safe dose planning was attempted using small multiple isocenters as well as a lower marginal dose, if in case in whom the tumor was located close to the optic pathways. The mean tumor diameter was 18.8 mm, the mean volume 3.5 ml. The tumors were treated with a mean maximum dose of 21.8 Gy and a marginal dose of 11.5 Gy, using a mean of 4.5 isocenters. Every effort was made to keep the prescribed dose low enough to be tolerable for the optic nerve [10], i.e. to reduce the risk of radiation injury. The mean dose to the tumor margin gradually decreased, being only 10.7 Gy in the most recent 31 cases, while having been 12.7 Gy in the earliest 30 cases. The tumor volume was also smaller in the most recent cases than in the earliest cases (table 2).

After treatment, patients were followed up every 3–6 months with repeated MRIs and by assessing changes in neuro-endocrine status and side effects. The MRI findings were classified into four groups: complete response (CR = disappearance of tumor), partial response (PR = more than 25% decrease in tumor size), no change (NC = no change or less than 25% decrease) and progression (PG = increase in tumor size). Changes in neurological and endocrine symptoms were assessed using clinical records and/or questionnaire responses. The final outcome was determined by asking the patients directly. Univariate statistical analyses (Chi-square test) were conducted for factors related to the effects of Gamma Knife radiosurgery. Survival rates were analyzed by the Kaplan-Meier method.

Table 1. Characteristics of cases (N = 100)

Age of patients	Mean 33.6 (3–80); child:adult = 38:62	
Nature of lesions	Solid 40, cystic + mixed 60	
Size of tumor	I small (<1 cm) 13	63
	II medium (1–2 cm) 50	
	III large (2–3 cm) 26	37
	IV huge (>3 cm) 11	
Previous treatment	Surgery 172 times	
	Radiation 13 cases	
	Chemotherapy 3 cases	

Table 2. Change of tumor size and dose planning (123 lesions/107 cases)

Period	Lesion no	Mean diameter mm	Mean volume ml	Isocenters	Maximum dose, Gy	Marginal dose, Gy
1991.8–1995.5	30	19.1	3.7	4.5	24.7	12.7
1995.7–1997.2	31	21.4	5.2	5.6	22.8	11.4
1997.3–1999.2	31	18.6	3.4	4.2	20.6	11.1
1999.2–2002.12	31	16.3	2.3	3.8	19.2	10.7
Mean	123	18.8	3.5	4.54	21.8	11.5

Results

The mean follow-up period of the 100 cases was 65.5 (6–148) months, median 63 months. Final overall responses were assessable in 98 cases, of which 19 showed CR (19.4%), 47 PR (48%), 12 NC (12.2%) and 20 PG (20.4%). Therefore, CR, response, tumor control and progression rates were 19.4, 67.4, 79.6 and 20.4%, respectively.

The CR group had a child to adult ratio of 4:15, mean age of 37.4 years, solid type tumors in 12 and cyst mixed type in 7 cases, and a mean tumor diameter 15.9 mm. The tumors were treated with a maximum dose of 22 Gy and a marginal dose of 12.1 Gy. There had been 1.31 previous surgical treatments per person and none had received fractionated irradiation prior to Gamma Knife radiosurgery. The CR had been stable for a mean duration of 75.1 months. There was only one accidental death, due to a head injury, 9 years after the treatment (table 3).

In the 20 PG group cases, mean age was 27 and the child to adult ratio was 12:8. The tumor was solid in 3 and cyst-mixed in 17 cases. As to previous

Table 3. Analysis of CR cases (N = 19)

Age	Mean 37.4 (child 4, adult 15)
Tumor nature	Solid 12, cystic 6, mixed 1
Mean size	15.9 mm (<20 mm 16, ≥20 mm 3)
Previous treatments	Surgery 1.2 times/pt
	No RT, nor chemotherapy
Dose planning	Mean maximum D = 22 Gy, marginal D = 12.1 Gy
Mean duration of CR	75.1 months

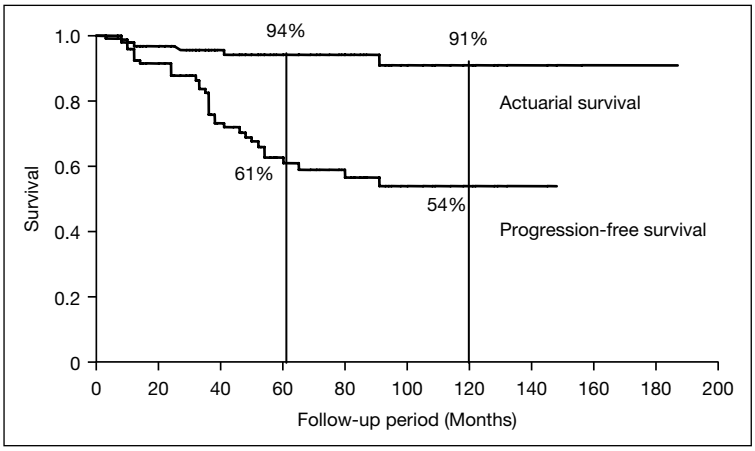

Fig. 1. Actuarial survival and progression-free survival rates.

treatments, there had been 2.47 surgeries per person and radiation therapy had been given to five patients. The mean tumor diameter exceeded 2 cm in 12 cases. The cause of tumor progression was cyst enlargement in 9 (45%), tumor regrowth in 8 (40%) and new lesions in 3 cases (15%). Mean time to progression was 24.5 months. These tumors were treated by reoperation in 14 and a second Gamma Knife radiosurgery in 1 case. No further treatment was administered in the other 5 cases. The outcome was excellent in 1, good in 4, fair in 3, poor in 2 and death in 8 cases. The causes of death were tumor progression in 6, and hypopituitarism and hypothalamic deficiency in one each.

The actuarial 5- and 10-year survival rates were 94.1 and 91%, while 5- and 10-year progression free survival rates were 60.8 and 53.8%, respectively (fig. 1).

Changes in neurological and endocrine symptoms were examined employing patient clinical records and/or questionnaires in 91 cases. Overall results

Table 4. Changes of neuro-endocrine symptoms (N = 91)

	Improved (%)	Unchanged (%)	Deteriorated (%)	Total
CR	7 (36.8)	12 (63.2)	–	19
PR	7 (19.4)	24 (66.6)	5 (13.9)*	36
NC	2 (15.3)	10 (76.9)	1 (7.7)*	13
PG	1 (4.3)	13 (56.5)	9 (39.1)	23
Total	17 (18.7)	59 (64.8)	15 (16.5)	91

*3 visual (3%) and 3 endocrine (3%) complications were found as side effects.

were improvement in 17 (18.7%), no change in 59 (64.8%) and deterioration in 15 cases (16.5%). Among those showing improvement, 10 had better vision and 7 had improved hypothalamic-pituitary functions. Deterioration of visual and endocrine functions were noted as side effects of irradiation in 3 and 3 cases, respectively, from the PR and NC groups. Nine PG group cases showed deterioration and all died of tumor progression (table 4).

The outcomes of 91 patients were assessed by direct inquiry or by questionnaire. The patients' conditions were classified into five grades; 'Excellent' indicates an ability to do one's job well or attend school independently, without severe neurological deficits, 'Good' means that the subject is unable to work but can perform daily activities at home independently with minor neurological or endocrine deficits, 'Fair' means that the patient is dependent and must stay at home all the time, and 'Poor' indicates a bedridden condition or the necessity for medicaid. Death was due to tumor progression or other causes. Overall, outcomes were excellent in 45, good in 23, fair in 4, poor in 3, and death in 16 cases. The mean time from Gamma Knife radiosurgery until death was 44.8 months. The cause of death was tumor progression in 6, others in 9 and unknown in one case. The other causes included hypothalamic-pituitary dysfunction in 4, stroke in 2 and infection, heart attack and head injury in one case each.

Case Presentation

Case 1

A 9-year-old boy with short stature developed visual acuity deterioration in his left eye (1.0, 0.2) and bitemporal hemianopsia in October, 1991. A suprasellar tumor was subtotally removed by the right frontotemporal approach. His visual symptoms normalized but a small cystic tumor was identified in the retrochiasmal area in contact with the pituitary stalk 3 months after surgery. Mean tumor

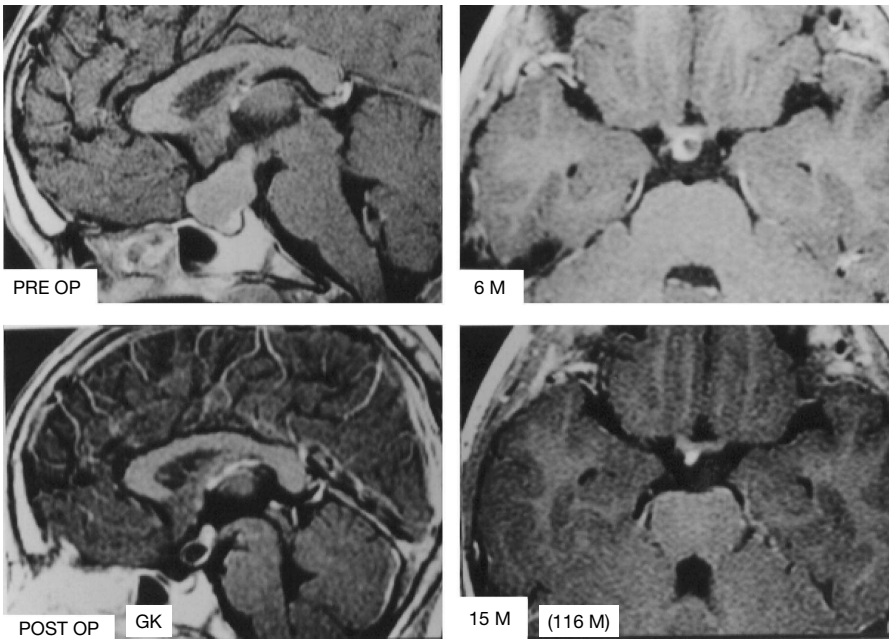

Fig. 2. Small residual tumor at 'R-site' and follow-up MRI after GK. A 9-year-old boy had a suprasellar mass compressing the optic nerve (left). The tumor was subtotally resected and a small cystic tumor (13.6 mm) in the retrochiasmal region was treated by Gamma Knife radiosurgery using a marginal dose of 15 Gy and 5 isocenters (RS). The tumor was decreased in size at 12 months (12), CR was obtained at 15 months, and the tumor has been stable for more than 116 months to date (116). Mental and physical development normalized after treatment and the patient graduated from university.

diameter was 13.6 mm and the mass was treated with Gamma Knife radiosurgery using a marginal dose of 15 Gy and 5 isocenters. The tumor was decreased in size and showed CR at 12 months after treatment, and has been stable for more than 116 months to date (fig. 2). The patient graduated from university and has neither neuro-endocrine deficits nor any sign of physical maldevelopment.

Case 2

A 52-year-old male presented with memory loss and loss of visual acuity (0.2, 0.2). MRI revealed a suprasellar solid tumor and hydrocephalus in January, 1999. After open biopsy through the lamina terminalis, a small solid tumor (2.1 ml) in the third ventricle was initially treated by Gamma Knife radiosurgery with a maximum dose of 15 Gy and a marginal dose of 9.85 Gy on

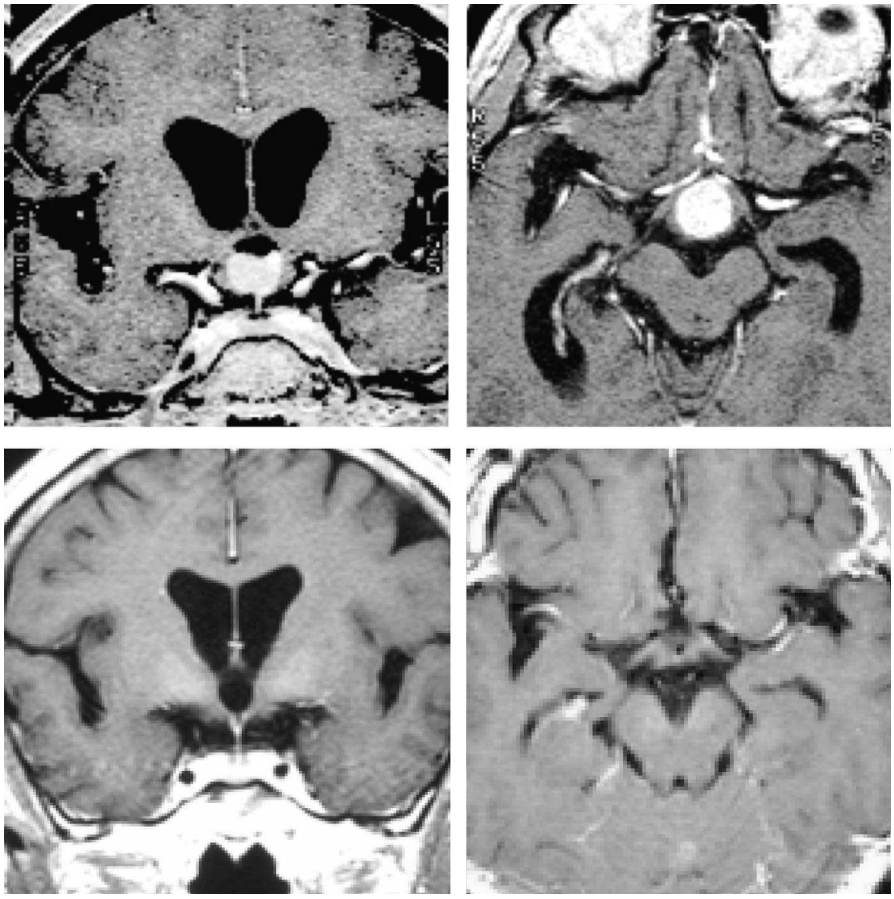

Fig. 3. Small tumor at 'R-site' and follow-up MRI after GK. A 52-year-old man had a suprasellar, solid mass and hydrocephalus with memory loss and visual acuity disturbance. After biopsy via the lamina terminalis approach, a small tumor in the third ventricle (15.9 mm) was treated by GK radiosurgery with a marginal dose of 9.85 Gy. The tumor showed CR at 24 months and has been stable for more than 5 years, to date, with improvement of symptoms.

January 28th. The patient's memory loss improved and his visual acuity normalized. The tumor showed CR at 24 months after treatment and has been stable for 60 months to date. The optic nerve and stalk showed normalization. The patient has since been enjoying a productive life without neuro-endocrine deficits (fig. 3).

Discussion

Regarding the long-term results of combined surgery and fractionated radiotherapy, Fischer et al. [11], Hetelekidis et al. [12] and Varlotto et al. [13] reported 10- and 20-year control rates of nearly 90 and 50%, respectively. Habrand et al. [14] found actuarial survival rates at 5- and 10-years with childhood craniopharyngiomas to be as high as 91 and 78%, but relapse free survivals were low at 65 and 56.5%, respectively. In the present study, we found higher actuarial survival rates to be obtained by Gamma Knife radiosurgery but progression free survival was essentially the same as that with conventional radiotherapy. This was attributed to delayed recurrence at a mean of 24.5 months after treatment. The development or worsening of neuro-endocrine symptoms after conventional radiotherapy is another important issue. Functional outcomes indicated severe impairment in 30 out of 35 cases (86%): impaired endocrine functions in 97%, neurological deficits in 40% and visual disturbances in 34% [14]. In contrast, the present study revealed side effects involving visual and pituitary functions, in only 3 cases each, among patients receiving Gamma Knife radiosurgery.

The Gamma Knife delivers high dose irradiation to a relatively small intracranial volume in a single session without significant irradiation of the surrounding brain [15]. Gamma Knife radiosurgery for craniopharyngioma was initially reported by Leksell et al. [15] and Backlund et al. [16], who obtained good results in some cases. However, numerous studies have been conducted [6–9] since MRI became available for dose planning and follow-up study. Our group reported that a higher response rate, including disappearance of the tumor (CR), was obtained for solid tumors with Gamma Knife treatment using relatively low marginal doses [7]. Our previous report of 33 cases with a mean follow-up of 42.1 months [8] revealed a higher CR rate of 30%, control rate of 85.8% and lower progression rate of 15.2%, with a relatively low complication rate. Chung et al. [6] reported almost the same results that we obtained, while Ulfarsson et al. [9], based on their experience in Sweden with extremely low dose treatment, found a low tumor contol rate of 36%, progression rate of 64% and a high complication rate of 57%.

In comparison with previous reports, the current results indicate lower response and higher progression rates to have been obtained but with fewer side effects. This is attributable to an intentional reduction in the marginal dose and longer follow-up time, with the irradiation dose being decreased from 12.7 Gy in the earliest 30 cases to 10.7 Gy in the most recent 31 cases (table 5).

Factors related to better responses (CR and PR) to radiosurgery include age (adult), solid tumors, fewer previous treatments and smaller tumors. Among these factors, only being an adult was significantly favorable ($p = 0.046$).

Table 5. Comparative effects of dose reduction

Year reported Case no Follow-up	Tumor size, mm Vol, ml	Dose, Gy Maximum/ Marginal (OPN dose)	Response* CR, RR, Con, PG	Complications due to GK
1999				
33	20.3	23.3/12.8 (<12.0)	CR = 30.3 RR = 81.8	Hypopituitarism: 2 (6%) VF cut: 1
41.2 M	4.4		Con = 84.8 PG = 15.2	Loss of VA: 1 (6%)
2004				
100	18.8	21.8/11.5 (<10.7)	CR = 19.4 PR = 67.3	Hypopituitarism: 3 (3%)
65.5 M	3.5		Con = 79.5 PG = 20.4	Visual disturbances: 3 (3%)

*CR = Complete response rate; RR = response rate; Con = control rate; PG = progression rate.

Table 6. Tumor effects and prognostic factors

	Age child:adult	Nature solid:C+M	Tumor size I + II:III + IV	Previous surgeries (mean times)
CR +PR (66)	20:46*	34:32	46:20	89 (1.41)
NC (12)	4:8	3:9	9:3	26 (1.86)
PG (20)	8:12	3:17**	8:12	57 (2.48)

*Adults: favorable prognostic factor ($p = 0.046$).
**Cyst/mixed: unfavorable factor ($p = 0.035$).

Factors predicting tumor progression after radiosurgery include age (child), cystic or mixed tumor type, several previous treatments and larger tumors. Among these factors, the nature of the tumor (cyst) was the only significant predictor of tumor progression ($p = 0.035$) (table 6).

It is also important to understand that the site of origin of craniopharyngiomas is along the pituitary stalk (squamous cell nest) from the floor of the third ventricle to the pituitary gland. Small residual or recurrent tumors can persist or arise, even

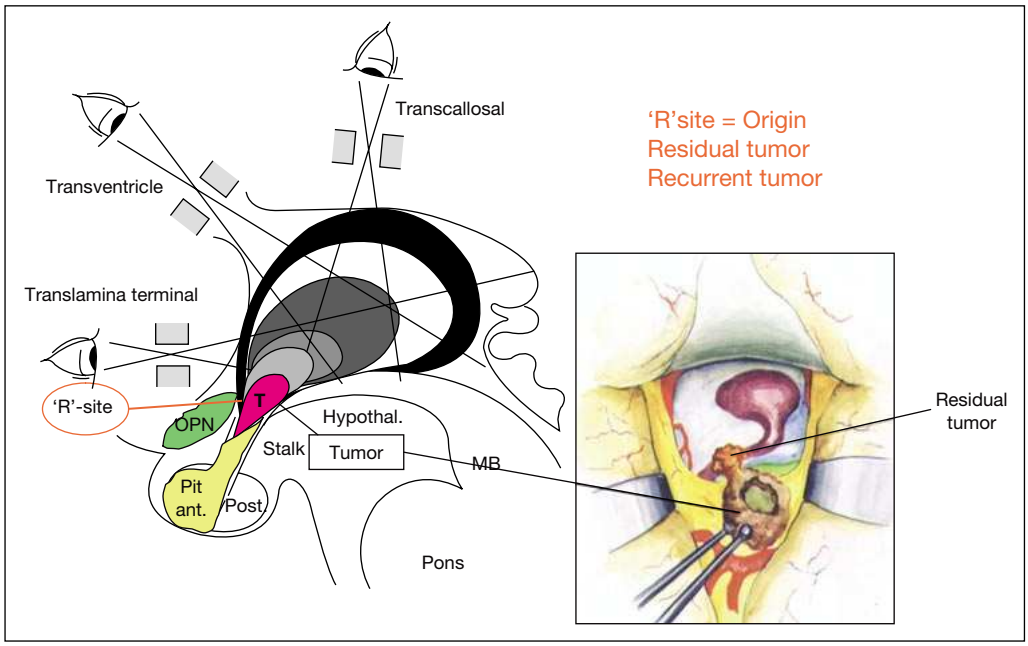

Fig. 4. Schema of small tumor at 'R site' and surgical view [21, fig 11]. The tumor origin is between the optic nerve and the stalk (squamous cell nest). Small tumors which can persist or arise at this location ('R-site') are appropriate target of Gamma Knife radiosurgery and cure can be achieved.

after extensive removal, at this location (so called 'R-site'), as in our cases 1 and 2. From the autopsy findings of untreated tumors at this site [17], tumor cells invade close to hypothalamic neurons without intervention of the arachnoid membrane or glial cleavage, where tumor tissue adheres tightly to the optic nerve and pituitary stalk, making it difficult to remove without seriously damaging visual functions or causing diabetes insipidus (fig. 4). A new strategy is to manage such small tumors with Gamma Knife radiosurgery instead of total removal, allowing permanent cure to be achieved without neuro-endocrine deficits.

Regarding the optimal dose for tumor control, 12.1 Gy was found to be the marginal dose necessary for diminishing tumor (cure) for an extended period of time. This may be contradictory to the dose reduction policy. However, Larson et al. [18] reported that the tolerance of the surrounding normal brain is higher when multiple small isocenters are used than with a single large isocenter. Marks et al. [19] also stated that a tolerable dose for the normal brain is related to the volume of the adjacent tumor. The excellent results obtained in our case 1, in whom a small cystic tumor (1.3 ml) adhering to the optic nerve was treated with a

marginal dose of 15 Gy using 5 isocenters, illustrates how well the optic nerve can tolerate a relatively high dose of radiation. However, caution must be exercised in using a higher dose, even for small tumors, in cases undergoing re-irradiation. Another possible approach to saving optic function is stereotactic radiotherapy for craniopharyngiomas, which might reduce side effects involving the surrounding brain while enhancing the anti-tumor effects [20]. However, long-term results for a significant number of cases are necessary to evaluate these effects.

Conclusion

Gamma Knife radiosurgery was effective and safe as adjuvant or additional treatment for residual and/or recurrent craniopharyngioma. Pathological type, nature of tumor, age of the patient and previous treatments are the prognostic factors for Gamma Knife radiosurgery of craniopharyngioma. Dose reduction resulted in decrease of tumor responses and an increase of progression but decrease of complications due to irradiation.

The site of tumor origin ('R-site') is difficult for complete removal without damage of neuro-endocrine functions. Cure can be obtained by Gamma Knife radiosurgery of small residual or recurrent tumor at 'R-site' with the marginal dose around 12 Gy.

References

1 Hoffman HJ, De Silva M, Humphreys RP, Drake JM, Smith ML, Blaser SI: Aggressive surgical management of craniopharyngioma in children. J Neurosurg 1992;76:47–52.
2 Yasagil MG, Curic M, Kis M, Siegenthaler G, Teddy PJ, Roth P: The total removal of craniopharyngiomas: approaches and long-term results in 144 patients. J Neurosurg 1992;73:3–11.
3 Ellenberg L, McComb JG, Siegel SE: Factors affecting intellectual outcome in pediatric brain tumor patients. Neurosurgery 1987;21:638–644.
4 Glauser TT, Packer RJ: Cognitive deficits in long-term survivors of childhood brain tumors. Childs Nerv Syst 1991;7:12.
5 Thomsett HJ, Conte FA, Kaplan SC, Grumbach MM: Endocrine and neurologic outcome in childhood craniopharyngioma; review of effect of treatment in 42 patients. J Pediatr 1980;97:728–735.
6 Chung WY, Pan DHC, Shiau CY, Guo WY, Wang LW: Gamma knife radiosurgery for craniopharyngiomas. J Neurosurg 2000;93(suppl 3):47–56.
7 Kobayashi T, Tanaka T, Kida Y: Stereotactic gamma knife radiosurgery for craniopharyngiomas. Pediatr Neurosurg 1994;21(suppl 1):69–74.
8 Kobayashi T, Kida Y, Mori Y: Effects and prognostic factors in the treatment of craniopharyngioma by gamma knife; in Kondziolka D (ed): Radiosurgery 1999, Radiosurgery. Basel, Karger, 2000, vol 3, pp 192–204.
9 Ulfarsson E, Lindquist C, Roberts M, Rahn T, Lindquist M, Thoren M, Lippitz B: Gamma knife radiosurgery for craniopharyngiomas: long-term results in the first Swedish patients. J Neurosurg 2002;97(suppl 5):613–622.

10 Leber KA, Bergloeff J, Pendle G: Dose responce tolerance of the visual pathways and cranial nerves of the cavernous sinus to stereotactic radiosurgery. J Neurosurg 1998;88:43–50.
11 Fischer EG, Welch K, Shillito J Jr, Winston KR, Tarbell NJ: Craniopharyngiomas in children; long-term effects of conservative surgical procedures combined with radiation therapy. J Neurosurg 1990;73:534–540.
12 Hetelekidis S, Barnes PD, Tao ML, Fischer EG, Schneider L, Scott RM, Tarbell NJ: 20-year experience in childhood craniopharyngioma. Int J Radiat Oncol Biol Phys 1993;27:189–195.
13 Varlotto JM, Flickinger JC, Kondziolka D, Lunsford LD, Deutsch M: External beam irradiation of craniopharyngiomas; long-term analysis of tumor control and morbidity. Int J Radiat Oncol Biol Phys 2002;54:492–499.
14 Habrand JL, Ganry O, Couanet D, Rouxel V, Levy-Piedbois C, Pierre-Kahn A, Kalifa C: The role of radiotherapy in the management of craniopharyngioma: a 25-year experience and review of the literature. Int J Radiat Oncol Biol Phys 1999;44:255–263.
15 Leksell L, Backlund EO, Johanson L: Treatment of craniopharyngioma. Acta Chir Scand 1967;133:345–350.
16 Backlund EO, Johanson L, Sarby B: Study on craniopharyngiomas. II. Treatment by stereotaxis and radiosurgery. Acta Chir Scand 1972;138:749–759.
17 Kobayashi T, Kageyama N, Yoshida J, Shibuya N, Yonezawa T: Pathological and clinical basis of the indication for treatment of craniopharyngiomas. Neurol Med Chir 1981;21:39–47.
18 Larson DA, Flickinger JC, Loeffler JS: The radiobiology of radiosurgery. Int J Radiat Oncol Biol Phys 1993;25:557–561.
19 Marks LB, Spencer DP: The influence of volume on the tolerance of the brain to radiosurgery. J Neurosurg 1991;75:177–180.
20 Tarbell NJ, Scott M, Gouminerva LC, Pomeroy SL, Black PM, Barnes P, Billett A, LaVally B, Schrieve D, Helmus A, Kooy HM, Loeffler JS: Craniopharyngioma; preliminary results of stereotactic radiation therapy; in Kondziolka D (ed). Radiosurgery 1995, Radiosurgery. Basel, Karger, 1996, vol 1, pp 75–82.
21 Kanno T (ed): Brain Tumor Surgery. Tokyo, Neuron Pub. Co., 2002, p 47.

Tatsuya Kobayashi, MD, PhD
Nagoya Radiosurgery Center, Nagoya Kyoritsu Hospital
1–172 Hokke, Nakagawa-ku
Nagoya 454–0933 (Japan)
Tel. +81 52 362 5151, Fax +81 52 353 9126
E-Mail ttkobayashi@kaikou.or.jp

Kondziolka D (ed): Radiosurgery. Basel, Karger, 2006, vol 6, pp 164–172

Radiosurgery of Epidermoid Tumors with Gamma Knife: Possibility of Radiosurgical Nerve Decompression

Yoshihisa Kida, Masayuki Yoshimoto, Toshinori Hasegawa, Shigeru Fujitani

Department of Neurosurgery, Komaki City Hospital, Komaki City, Japan

Abstract

Long-term results of radiosurgery for epidermoid tumors are reported. There are 7 cases including 2 males and 5 females, ages ranging from 6 to 46 (mean: 33.3 years). At radiosurgery whole tumor was covered in 4 and partially covered in 3 for the attempt of relieving cranial nerve dysfunctions like trigeminal neuralgia and facial spasm. The mean maximum and marginal dose were 25.6 Gy and 14.6 Gy respectively. In the mean follow-up of 52.7 months, all the tumors showed a good tumor control without any progression and tumor shrinkage is confirmed in 2 out of 7 cases. Symptomatic trigeminal neuralgia improved or disappeared in all 4 cases and facial spasm disappeared in one. No neurological deterioration was found in any case after the treatment. In conclusion it is apparent that epidermoid tumors do respond well to radiosurgery and the accompanying hyperactive dysfunction of cranial nerves are significantly improved by Gamma Knife treatment either with entire or partial tumor coverage. Therefore the radiosurgical nerve decompression for epidermoid tumor is seemingly achieved by gamma-radiosurgery.

Intracranial epidermoid tumors are rarely found, chiefly in cerebello-pontine angle, parasellar region or in pineal region [1, 2]. The main presenting symptoms are hyperactive dysfunction of cranial nerves, like trigeminal neuralgia or facial spasm. It is well known that these tumor may cause chemical meningitis due to irritative deposits of keratin material inside the tumors. Although surgical resection of the tumor has been recommended, total removal including tumor capsule attached to the brain and cranial nerves are very difficult and so often harmful

Table 1. Characteristics of the cases with epidermoid tumor

Case	Age/sex	Location	Symptom	Prior operation
1	6/F	CPA	Deafness	None
2	41/M	CPA	Facial pain Facial spasm	Twice
3	35/F	CPA	Facial pain	Twice
4	23/F	Pineal	None	None
5	39/F	CPA	IIIrd N palsy	Once
6	43/F	CPA	Facial pain	None
7	46/M	CPA	Facial pain	None
Total and mean	33.3 years	CPA (6/7)	Neuralgia (4/7)	Operation (3/7)

CPA = Cerebello-pontine angle.

[3–7]. If the tumors are not totally removed, tumor recurrence may occur. Radiosurgery for epidermoid tumors was not reported in the past, partly because the tumors are too large and the major parts of the tumor are cyst containing keratin materials. In this report, our experiences of radiosurgery of epidermoid tumors are described and the treatment strategy for this tumor is discussed.

Materials and Methods

Since the installation of Gamma Knife in our institution on 1991, we have encountered 7 cases of epidermoid tumor. There are 2 males and 5 females, whose ages ranged from 6 to 46 with a mean of 33.3 years. The locations of the tumor are cerebello-pontine angle in 6 and in pineal region in 1. Presenting symptoms at radiosurgery are trigeminal neuralgia in 4, facial spasm in 1 and oculomotor palsy in 1. Among 7 cases, three cases underwent surgical resection (5 times in total), the other four cases were diagnosed radiologically with CT and MRI (table 1).

At radiosurgery, Leksell G-Frame is firmly fixed to the head of patients and enhanced T1, heavy T2 images are taken. FIESTA (GE MRI: Fast Imaging Employing Steady-State Acquisition) clearly visualize the tumor in the cistern and very helpful (fig. 1). But it is not used for dose planning directly because these images are not obtained under frame fixation. The images were transferred to the GammaPlan after being processed in the Digital Imaging and Communication in Medicine (DICOM) and dose planning was made. Irradiation inside the Gamma Knife (B or C type) was performed, For small tumors whole tumors were covered with radiosurgery, but partial coverage was chosen for large and scattered tumors for the purpose of relieving cranial nerve symptoms.

After the radiosurgery, follow-up studies with neurological signs and MRI was taken every 3 months in the first year and every 6 months thereafter. Serial changes of tumor size were evaluated in terms of complete remission, partial remission, minor response, no change and progression.

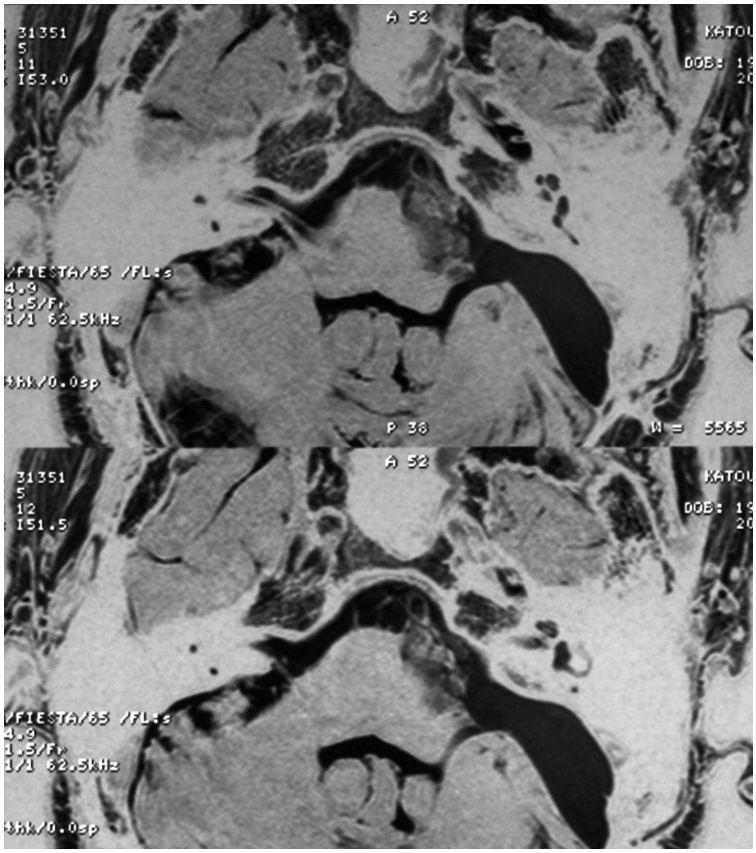

Fig. 1. Remnants of epidermoid tumor are clearly visualized with special MRI. Sequence named FIESTA.

Results

Tumor Size and Radiosurgical Dose

Tumor size at radiosurgery ranged from 12.9 to 26.3 mm (mean 18.7 mm). In 3 cases attempting partial tumor coverage, only the sizes of treatment area are demonstrated. The mean maximum and marginal doses are 25.6 and 14.6 Gy (range 12.6–17 Gy) respectively (table 2). The partial tumor coverage was carefully done including the tumor mass attached to the cranial nerve.

Table 2. Tumor size, treatment volume and radiosurgical dose

Case	Location	Size, mm	Maximum dose, Gy	Marginal dose, Gy
1	CPA	12.9	23	16.1
2	CPA	17.3*	27 (1st)*	14.9
			24 (2nd)*	14.4
3	CPA	16.4*	30*	15.0
4	Pineal	21.8	34	17
5	CPA	26.3	26	13
6	CPA	22.3	21	12.6
7	CPA	14.2*	20*	14
Total and mean	CPA (6)	18.7	25.6	14.6

*Partial treatment.
CPA = Cerebello-pontine angle.

Neurological Changes

Follow-up period ranged from 8 to 129 months with a mean of 53.7 months. Trigeminal neuralgia was either disappeared or decreased in all (4/4). Administration of carbamazepin was discontinued in all. Facial spasm in one case far decreased within 9 months and completely disappeared by 24 months. Oculomotor palsy and hearing loss in each 1 case were not improved and totally unchanged.

Radiological Changes

There have been no recognizable shrinkage of tumor, but two tumors showed a minor shrinkage which is confirmed with FIESTA study.

Illustrative Cases

Case 1: 43-Year-Old Female

An epidermoid tumor in left cerebello-pontine angle (fig. 2a), presenting with left trigeminal neuralgia, was treated with Gamma Knife (maximum dose: 21 Gy, marginal dose: 12.6 Gy). Entire tumor was covered with radiosurgery. Trigeminal neuralgia disappeared just 1 day after radiosurgery and showed no recurrence of neuralgia thereafter. The tumor disclosed a minor response at 17 months follow-up (fig. 2b).

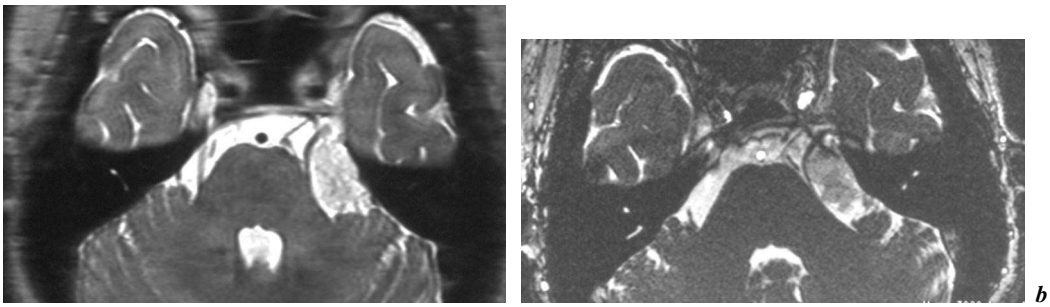

Fig. 2. An epidermoid tumor in left cerebello-pontine angle (***a***), presenting with left trigeminal neuralgia, was treated with Gamma Knife (maximum dose: 21 Gy, marginal dose: 12.6 Gy). Entire tumor was covered with radiosurgery. Trigeminal neuralgia disappeared just one day after radiosurgery and showed no recurrence of neuralgia thereafter. The tumor disclosed a minor response at 17 months follow-up (***b***).

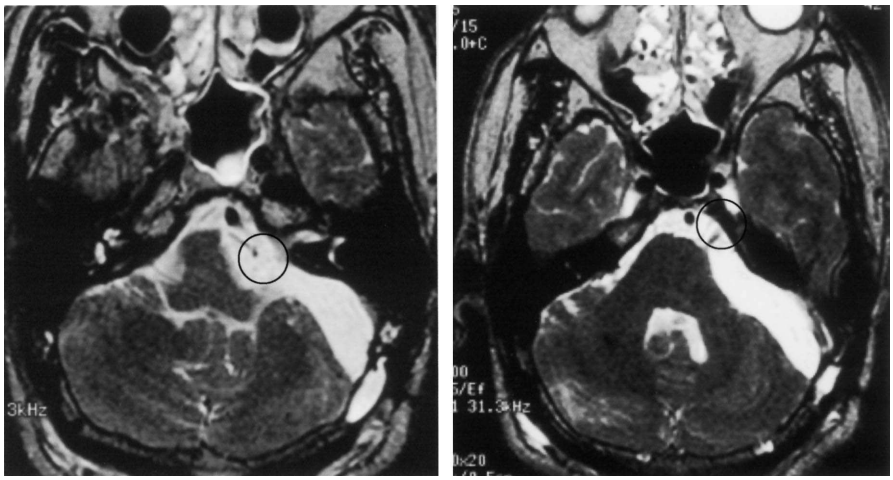

Fig. 3. A large epidermoid tumor operated twice showed facial spasm and trigeminal neuralgia. Both hyperactive nerve dysfunctions totally disappeared by two partial treatments (partial coverage) of radiosurgery involving the facial nerve (***a***) and trigeminal nerve (***b***).

Case 2: 41-Year-Old Male

The patient has been suffering from left hearing disturbance and ataxia. His MRI showed a large tumor in left cerebello-pontine angle, extending superiorly into tentorial edge and inferiorly to foramen magnum. After two surgical resections of the tumor, he complained of trigeminal neuralgia and facial spasm (fig. 3).

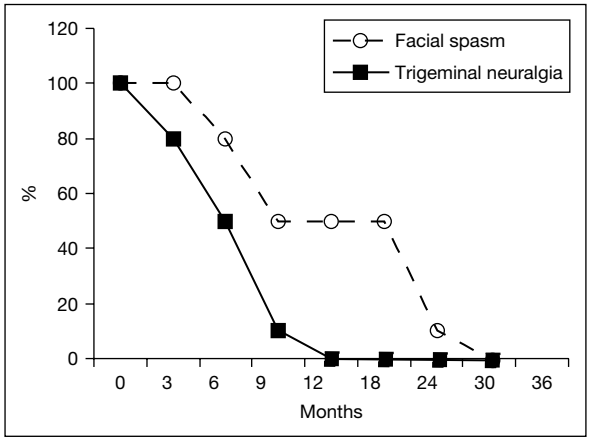

Fig. 4. Serial changes of facial spasm and trigeminal neuralgia after radiosurgery. Both trigeminal neuralgia and facial spasm have completely disappeared within 12 and 24 months after radiosurgery, respectively.

First radiosurgery for the attempt of relieving facial spasm (maximum dose: 27 Gy, marginal dose: 14.9 Gy) was carried out with the partial coverage of tumor. Facial spasm decreased gradually and completely disappeared within 2 years. Thereafter second radiosurgery for the attempt for relieving trigeminal neuralgia was performed (maximum dose: 24 Gy, marginal dose: 14.4 Gy). Trigeminal neuralgia disappeared within a year. No neurological signs except for left hearing loss were seen 8 years later (fig. 4).

Discussion

Intracranial epidermoid tumor may originate in cerebello-pontine angle, parasellar and pineal region [1, 2]. In general this tumor grows very slowly, and therefore develop a large tumor when it becomes symptomatic [8]. Presenting symptoms are so often mild, and the carnial nerve dysfunctions like trigeminal neuralgia or facial spasm are most frequently found [9–12]. Surgical resection is the main treatment for symptomatic tumors and many active trials have been reported [3–7]. Since the tumor cells do exist in the tumor capsule, it is necessary to remove the thin membrane consisting of tumor capsule to prevent the recurrence. However, this operative procedures are not easy and harmful because the membrane attached to the cranial nerves and brainstem. In fact cranial nerve signs, especially bulbar palsy and resultant aspiratin pneumonia are

Table 3. Results of radiosurgery for epidermoid tumors

Case	Age/sex	Follow-up, months	MRI	Signs
1	6/F	120	NC	NC (deaf)
2	41/M	96	MR*	No neuralgia No facial spasm
3	35/F	58	NC*	No neuralgia
4	23/F	18	NC	None
5	39/F	52	NC	Diplopia
6	43/F	17	MR	No neuralgia
7	46/M	8	NC*	No neuralgia
Mean	33.3 years	52.7 months	NC (5/7) MR (2/7)	No neuralgia (4/4) No facial spasm (1/1)

*Partial treatment.
CPA = Cerebello-pontine angle.

so often dangerous for the patients. Therefore, the percentage of the total tumor removal in those reports is not high. Samii et al. [3] reported that he has completed total tumor resection including tumor capsule in 30 out of 40 cases. He has emphasized that the attempt for total removal should be despaired when the lower cranial nerves are involved (table 3).

The main effects of radiosurgery are lethal or sublethal damage to the tumor cell, controlling the tumor growth, adjusting the nerve and brai function and causing intimal hypertrophy. Radiosurgery may cause perifocal edema or radiation necrosis as adverse effects. Since the epidermoid tumor contains massive amount of keratin deposits, inside direct effects of radiosurgery to these materials are not expected and irradiation to the tumor capsule is apparently required. There found no report on radiosurgery of epidermoid tumor, but found a few reports for epidermoid cancer [13, 14]. Some investigators reported the results of radiotherapy for recurrent epidermoid tumors [15]. Epidermoid tumors so often present with hyperactive dysfunction of cranial nerves like trigeminal neuralgia or facial spasm. Moreover, these nerve dysfunctions are long lasting and sole signs in many cases. In our series, tumor control after radiosurgery seems to be excellent, and some showed a regression. More importantly trigeminal neuralgia has been improved in almost all the cases with or without total tumor coverage and the fastest pain relief was obtained at the next day of radiosurgery. Similarly facial spasm has improved and disappeared for more than 7 years. These results apparently indicate that epidermoid tumos are moderately sensitive to radiosurgery, with the marginal dose less than

15 Gy. The main causes of these effects may be related to the regional tumor shrinkage or to decreased stimulation to the cranial nerves. Therefore, radiosurgical nerve decompression can be achieved by Gamma Knife with less than 30 Gy at the center and 15 Gy at the margin, which are much lower in dose for trigeminal neuralgia. Radiosurgery is definitely useful for small intracranial epidermoids and for recurrent tumors as well as residual tumor after microsurgery. For scattered tumors widely in the cerebello-pontine cistern, cranial nerve dysfunctions can be relieved by radiosurgery. Whether or not similar effects to relieve cranial nerve dysfunction can be expected in other tumors like neurinomas, meningiomas should be discussed.

Conclusion

We have reported the long-term results of radiosurgery for epidermoid tumors. They respond well to radiosurgery with or without total coverage of the tumors. Main presenting symptoms like trigeminal neuralgia and facial spasm are either improved or totally disappeared. Thus hyperactive dysfunctions of cranial nerves can be improved and radiosurgical nerve decompression can be achieved. Primary epidermoid tumor, residual or recurrent tumors are indicated for radiosurgery if they are small. In larger tumors, hyperactive dysfunction of cranial nerves can be relieved by radiosurgery.

References

1 Caldarelli M, Colosimo C, Di Rocco C: Intra-axial dermoid/epidermoid tumors of the braistem in children. Surg Neurol 2001;56:97–105.
2 Ulrich J: Intracranial epidermoids: a study on their distribution and spread. J Neurosurg 1964;21:1051–1057.
3 Samii M, Tatagiba M, Piouer J, Carvalho GA: Surgical treatment of epidermoid cysts of the cerebellopontine angle. J Neurosurg 1996;84:14–19.
4 Talacchi A, Sala F, Alessandrini F, Turazzi S, Bricolo A: Assessment and surgical management of posterior fossa epidermoid tumors: report of 28 cases. Neurosurgery 1998;42:242–252.
5 Vinchon M, Pertuzon B, Lejeune JP, Assaker R, Pruvo JP, Christiaens JL: Intradural epidermoid cysts of cerebellopontine angle: diagnosis and surgery. Neurosurgery 1995;36:52–57.
6 Yamakawa K, Shitara N, Genka S, et al: Clinical course and surgical prognosis of 33 cases of intracranial epidermoid tumors. Neurosurgery 1989;24:568–573.
7 Yasargil MG, Abernathey CD, Sarioglu AC: Microsurgical treatment of intracranial dermoid and epidermoid tumors. Neurosurgery 1989;24:561–567.
8 Alvord EC Jr: Growth rates of epidermoid tumors. Ann Neurol 1977;2:367–370.
9 Iwasaki K, Kondo A, Otsuka S, Hasegawa K, Ohbayashi T: Painful tic convulsive caused by a brain tumor: case report and review of the literature. Neurosurgery 1992;30:916–919.
10 Barker FG, Jannetta PJ, Babu RP, Pomonis S, Bissonite Jho HDJ: Long-term outcome for trigeminal neuralgia in patients with posterior fossa tumors. J Neurosurg 1996;86:818–826.

11 Kobata H, Kondoh A, Iwasaki K: Cerebellopontine angle epidermoids presenting with cranial nerve hyperactive dysfunction: pathogenesis and long-term surgical results in 30 patients. Neurosurgery 2002;50:276–286.
12 Kobata H, Kondoh A, Iwasaki K, Nishioka T: Combined hyperactive dysfunction syndrome of the cranial nerves: trigeminal neuralgia, hemifacial spasm, and glossopharyngeal neuralgia: 11-year experience and review. Neurosurgery 1998;43:1351–1362.
13 Link MJ, Cohen PL, Breneman JC, Tew JM: Malignant squamous degeneration of a cerebellopontine angle epidermoid tumor. J Neurosurg 2002;97:1237–1243.
14 Mori Y, Suzuki Y, Tanasawa T, Yoshida J, Wakabayashi T, Kobayashi T: A case report of epidermoid carcinoma in the cerebello-pontine angle. No Shinkei Geka 1995;23:905–909.
15 Parikh S, Milosevic M, Wong CS: Recurrent intracranial epidermoid cyst treated with radiotherapy. J Neurooncol 1995;24:293–297.

Dr. Yoshihisa Kida
Department of Neurosurgery
Komaki City Hospital, 1-20, Jhobusi
Aichi Prefecture, Komaki City, 485–8520 (Japan)
Tel. +81 0568 76 4131, Fax +81 0568 76 4145
E-Mail yoshi9@go2.enjoy.ne.jp

Kondziolka D (ed): Radiosurgery. Basel, Karger, 2006, vol 6, pp 173–185

Radiosurgical Pathology Observations on Cerebral Metastases after Gamma Knife Radiosurgery

Dave S. Atteberry[a], *György T. Szeifert*[b], *Douglas Kondziolka*[a], *Marc Levivier*[c], *L. Dade Lunsford*[a]

[a]Center for Image-Guided Neurosurgery, University of Pittsburgh Medical Center, Presbyterian Hospital, Pittsburgh, Pa., USA; [b]National Institute of Neurosurgery and Department of Neurological Surgery, Semmelweis University, Budapest, Hungary; [c]Centre Gamma Knife, Hôpital Erasme, Université Libre de Bruxelles, Brussels, Belgium

Abstract

Background: Comprehensive human pathological investigations, exploring fundamental radiosurgical effects on metastatic brain tumors are sparse in the medical literature. The aim of this study was to analyze histopathological and immunohistochemical findings in a set of cerebral metastases following radiosurgery. **Methods:** Out of a series of 7,000 (900 in Brussels + 6,100 in Pittsburgh) patients that had radiosurgery, 2,020 (200 Brussels + 1,820 Pittsburgh) patients harbored cerebral metastases. Eighteen patients underwent 24 craniotomies for tumor removal in a 1–59 months interval after high-dose irradiation. Histological and immunohistochemical investigations were performed on the surgically resected tissue specimens. Besides routine hematoxylin-eosin and Mallory's trichrome staining, immunohistochemical reactions were carried out to characterize the phenotypic nature of tumor tissues and the accompanying reactive inflammatory cell population following radiosurgery. **Results:** Light microscopy revealed three basic categories of histological responses namely acute-type, subacute-type, and chronic-type tissue reactions in a variety of different metastatic tumors. A moderate to intense inflammatory cell component was seen in the tissue reactions of well controlled neoplasms (lasting >5 months before craniotomy), while this inflammatory response was missing or faint in the poorly controlled cases (requiring <5 months before craniotomy required) after radiosurgery. Immunohistochemical characterization demonstrated prominent $CD68^+$ macrophage and $CD3^+$ T-lymphocyte populations in the inflammatory reaction. **Conclusions:** Though causality was not established, histopathological and immunohistochemical findings suggest that an inflammatory role is important in the local tumor control following radiosurgery of metastatic brain tumors.

Stereotactic radiosurgery has become a treatment modality in the armamentarium of physicians who manage cerebral metastases during the past four decades [1–12]. Although over a hundred thousand cases harboring brain metastases have already been treated around the world with radiosurgery, relatively little is known about the biological and pathophysiological mechanisms of radiosurgery resulting in tumor destruction, local tumor control or treatment failure. Surgical pathology or autopsy specimen investigations are uncommon following radiosurgery. Apart from some fundamental animal experiments and scarce human reports, comprehensive pathological reviews of the effects of single high-dose irradiation on brain metastases have not been available [13–20]. The aim of the present study was to explore the histopathological changes and immunohistochemical findings in a set of cerebral metastasis radiosurgery, and to see what information can be learned about the biology of the tumor response.

Clinical Materials and Methods

Out of a series of 7,000 [900 Brussels + 6,100 Pittsburgh] cases treated with radiosurgery, 2,020 [200 Brussels + 1,820 Pittsburgh] patients harbored cerebral metastases. Eighteen patients underwent twenty-four craniotomies for tumor removal after radiosurgery because of radiological and clinical progression. Among them eleven patients underwent single procedures, six patients underwent two procedures and one patient underwent three procedures. The primary tumor was lung carcinoma in 9 patients, breast carcinoma in 4 patients, malignant melanoma in 3 patients and renal cell carcinoma in 2 patients. Clinical and pathological characteristics of the cases are summarized in table 1. Procedures were performed in the Center for Image-Guided Neurosurgery, University of Pittsburgh Medical Center, Presbyterian Hospital, Pittsburgh, Pennsylvania (11 patients), and in the Center Gamma Knife, Hôpital Erasme, Université Libre de Bruxelles, Brussels, Belgium (7 patients). Radiosurgery was carried out using the Leksell Gamma Knife® Model U, B or C (Elekta Instruments AB, Stockholm, Sweden). Dose planning was based on MR and CT imaging, and/or metabolic data of positron emission tomographic studies were also integrated when available [21, 22]. Tumor volumes varied between 35 and 23,600 mm^3 (median 3,800 mm^3). Tumors received 14–24 Gy as marginal dose (median 18 Gy) at the 30–60% isodose line (median 50%); with 28–48 Gy maximal dose (median 36 Gy). Tumors were removed by craniotomy in a subsequent procedure due to neurological and/or radiological progression after 1–59 months interval following radiosurgery (median 12 months).

Histopathological investigations were carried out on the surgical pathology specimens. The resected specimens were fixed in 10% neutral buffered formaldehyde, processed routinely, and embedded in paraffin. Hematoxylin-eosin, PAS, Luxol fast blue and Masson's trichrome staining were used for general histopathology. Immunohistochemical reactions were carried out for synaptophysin, EMA, pankeratin, CK7, CK20, CAM5.2, LCA, CD3, CD4, CD8, CD20, CD31, CD34, CD68 (PGM1), CD79, UCHT1, L26 and GFAP antigens to characterize phenotypic nature of tumor tissues and the reactive cell populations around neoplastic islands. Biotin-streptavidin-peroxidase complex methods were performed according

Table 1. Case demographics and radiosurgical parameters

Case no.	Sex/age	Preliminary diagnosis	RS-CR months	Volume mm^3	Peripheral dose Gy/isodose (%)	Pathological diagnosis
1.	F/47	n.s.c. lung ca.	4	2,683	16/50	met., n.s.c., lung ca.
2a.	F/44	breast ca.	29	2,800	19/50	met., breast ca.
2b.			17	4,600	16/50	met., breast ca.
3.	M/41	melanoma	4	2,800	20/50	radionecrosis
4a.	M/53	n.s.c. lung ca.	22	3,200	20/50	met., n.s.c., lung ca.
4b.			12	5,900	16/50	met., n.s.c., lung ca.
5a.	M/60	n.s.c. lung ca.	59	11,540	15/50	met., n.s.c., lung ca.
5b.			25	454	16/60	met., n.s.c., lung ca.
6.	F/44	renal cell ca.	10	10,600	18/50	met., renal cell ca.
7.	F/64	n.s.c. lung ca.	20	8,500	16/50	radionecrosis
8.	M/57	renal cell ca.	7	5,700	17/50	radionecrosis
9a.	M/72	n.s.c. lung ca.	16	15,700	14/30	radionecrosis
9b.			6	23,600	14/50	radionecrosis
10.	F/50	n.s.c. lung ca.	6	3,800	16/50	met., n.s.c., lung ca.
11.	F/50		3	3,200	18/55	met., small cell lung ca.
12a.	M/75	n.s.c. lung ca.	5	8,090	16/50	met., n.s.c., lung ca.
12b.			5	6,530	16/50	met., n.s.c., lung ca.
13.	M/32	melanoma	1	1,320	18/50	melanoma
14a.	F/47	breast ca.	10	76	24/50	radionecrosis
14b.			10	110	24/50	radionecrosis
14c.			29	5,000	24/50	radionecrosis
15a.	F/51	breast ca.	33	3,300	18/50	met., breast ca.
15b.			26	35	18/50	met., breast ca.
16.	F/33	melanoma	9	5,100	20/48	melanoma
17.	F/54	breast ca.	15	433	20/48	met., breast ca.
18.	F/70	n.s.c. lung ca.	17	3,600	20/50	met., n.s.c., lung ca.

ca. = Carcinoma; met. = metastatic; n.s.c. = non small cell; RS-CR = radiosurgery-craniotomy interval.

to standard protocols on 5 μm sections. Five cases of resected specimens from different histological types of cerebral metastases but without previous radiation therapy or radiosurgery served as non-irradiated controls.

Results

The morphological features of pathological lesions that appeared following radiosurgery are summarized in table 2. Three basic histological responses were encountered in the surgical pathology specimens of irradiated metastatic tumors.

Table 2. Histopathological features of specimens after SRS

Case no.	Type of tissue response seen after SRS	Necrosis	Inflammatory reaction	Gliosis/ scar	Vasculopathy	Residual tumor	Hyaline degeneration
1.	Acute	XXX	X	Absent	Absent	Present	Absent
2a.	Chronic	X	XX	XXX	XX	Present	Present
2b.	Acute/subacute	XXX	XX	X	X	Present	Absent
3.	Acute	XXX	X	Absent	X	Present	Absent
4a.	Subacute	XX	XX	Absent	X	Present	Absent
4b.	Subacute	XX	XX	Absent	X	Present	Absent
5a.	Subacute	XX	XXX	Absent	Absent	Present	Absent
5b.	Subacute	XX	XXX	Absent	Absent	Present	Absent
6.	Subacute	X	XXX	Absent	X	Present	Absent
7.	Subacute	XX	XX	Absent	X	Absent	Absent
8.	Subacute	XX	XX	XX	XX	Absent	Absent
9a.	Subacute	XXX	XX	XX	XX	Absent	Absent
9b.	Subacute	XXX	XX	XX	XX	Absent	Absent
10.	Subacute	XXX	XX	Absent	XX	Present	Absent
11.	Acute	XXX	Absent	Absent	XXX	Present	Absent
12a.	Acute	XXX	X	Absent	Absent	Present	Absent
12b.	Subacute	X	XXX	X	X	Present	Absent
13.	Acute	XXX	Absent	Absent	Absent	Present	Absent
14a.	Acute	XXX	XX	Absent	Absent	Absent	Absent
14b.	Acute	XXX	XX	Absent	Absent	Absent	Absent
14c.	Subacute	XX	XX	XX	X	Absent	Absent
15a.	Subacute/chronic	X	XXX	XXX	XX	Present	Present
15b.	Subacute	XX	XX	XX	XX	Present	Present
16.	Subacute/chronic	X	XXX	XXX	X	Present	Present
17.	Subacute/chronic	XX	XXX	XXX	XXX	Present	Present
18.	Subacute/chronic	X	XXX	XXX	XXX	Present	Present

X = Mild presence; XX = moderate presence; XXX = extensive presence.

The acute-type response was characterized by a sharply demarcated coagulation necrosis in the parenchyma and stroma of metastases. The center of the lesion consisted of homogeneous eosinophilic fibrin strands intermingled with some tissue debris (fig. 1a). There was usually a faint to moderate cellular accumulation at the periphery of the necrosis containing pycnotic apoptotic elements accompanied with an inflammatory reaction, mostly polymorphonuclear leukocytes. This type of histological response was recognized in 8 cases out of the 26 tissue samples. The acute-type response occurred at 1–17 months time interval (median 4 months) following radiosurgery. Among these eight cases, two cases

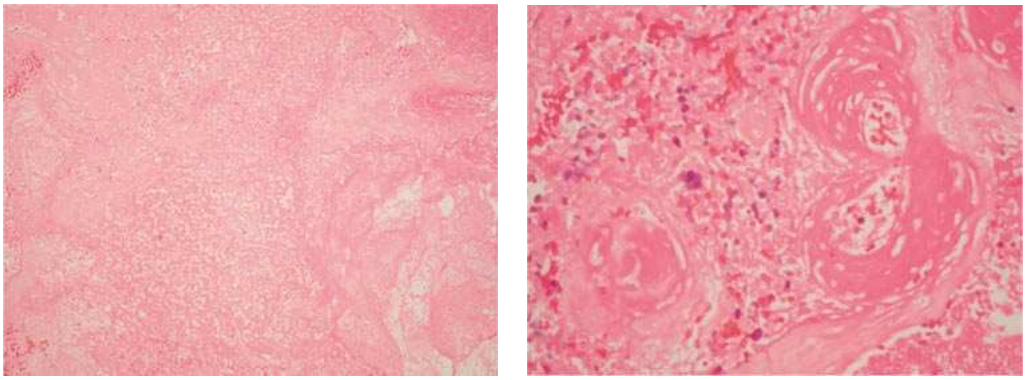

Fig. 1. Histological characteristics of acute-type tissue reaction in metastatic brain tumors following radiosurgery. ***a*** Homogeneous coagulation necrosis without cellular elements in a small cell lung carcinoma metastasis 3 months after RS (HE, ×100); (***b***) scattered pycnotic apoptotic cells and fibrinoid necrosis of vessel walls at the periphery of the lesion (HE, ×200).

with the shortest local tumor control (1 month and 3 months) did not have any cellular reaction for the high-dose irradiation. Three other cases with a local tumor control <5 months revealed only minimal inflammatory reaction following radiosurgery. There were residual neoplastic tissue islands recognized outside of the radiosurgery lesions in six samples out of the eight acute cases, but in two instances no remaining tumor tissue was verified at all. In all cases, the amount of cells making up these tumor islands was no more than 5% of the cells observed. Gliosis around the radiolesions was not remarkable. In three cases, acute vasculopathy with endothelial destruction and different degrees of fibrinoid necrosis in the vessel walls of the tumor were expressed (fig. 1b).

The largest group, with 18 cases, demonstrated subacute-type radiolesions. These radiolesions had the necrotic center surrounded by granulation tissue infiltrated with inflammatory cells, consisting of mainly macrophages with loaded cytoplasm expressing phagocytotic activity (fig. 2a, b). Immunohistochemical reactions demonstrated CD68 (PGM1) positive cells in a great majority of these macrophages (fig. 2c), but CD31 positive macrophages were also present in a moderate number. Macrophages seemed to originate from perivascular spaces of the granulation tissue (fig. 2d). Gliosis appeared in mild to moderate extent demarcating the radiolesion from the surrounding tissues (fig. 2e). Vasculopathy was present in the majority of the cases characterized by different degrees of endothelial destruction accompanied with subendothelial spindle shaped cell proliferation narrowing the lumen (fig. 2f). Eighteen out of the twenty-six subacute-type cases presented similar histological features in a 5–59 months interval (median 16 months) after high-dose irradiation. Complete tumor destruction was

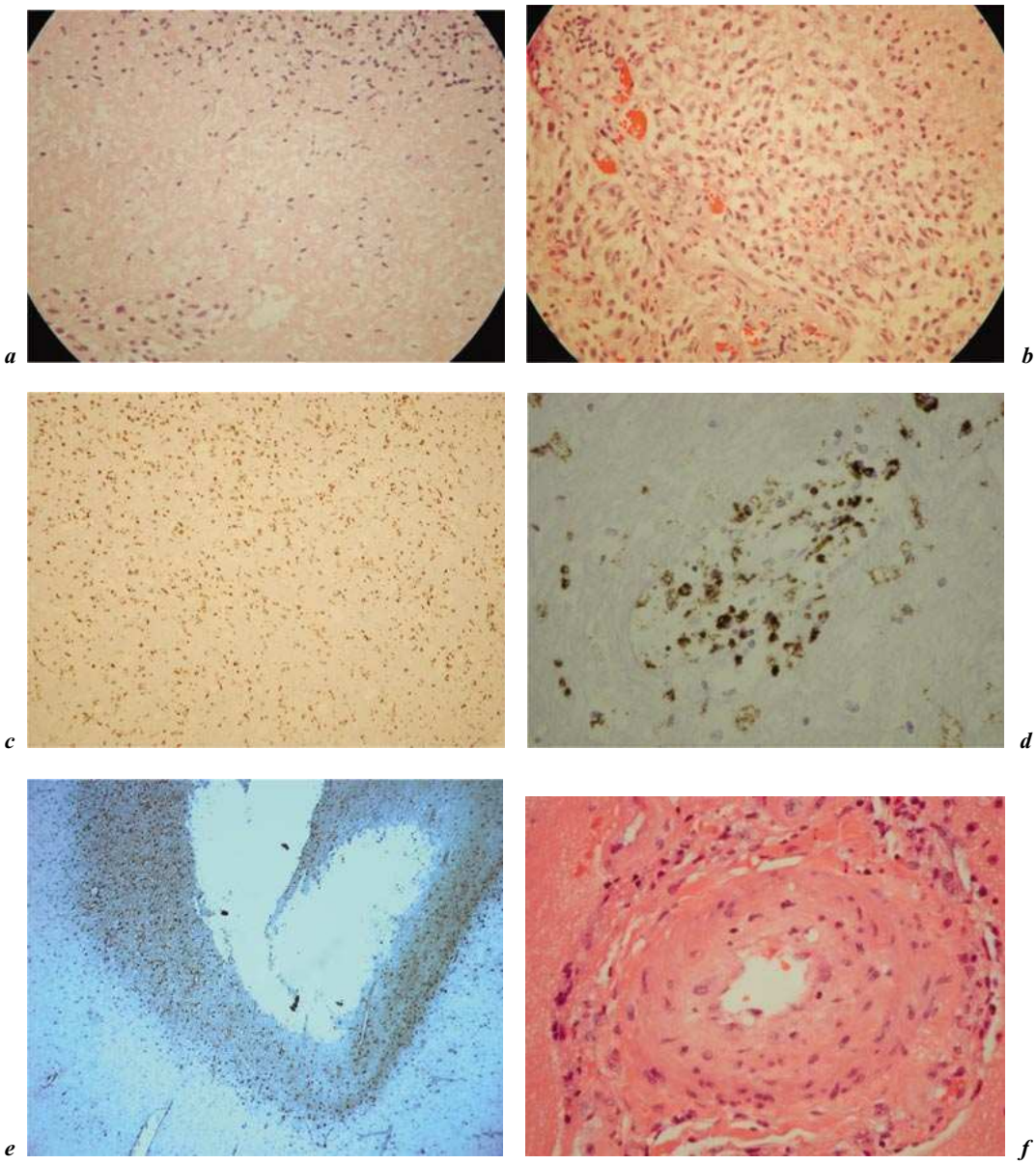

Fig. 2. Morphological pictures of subacute-type pathological lesions evolved in secondary cerebral neoplasms after radiosurgery. ***a*** Central necrosis surrounded by an inflammatory cell reaction from a renal cell carcinoma metastasis 7 months following radiosurgery (HE, ×100); ***b*** highly cellular granulation tissue around the necrotic core (HE, ×200);

seen in 5 tissue samples, but in the remaining 13 cases, various amounts of residual tumor cell nests were seen.

Five cases evolved partial or complete chronic-type radiolesions at an interval of 9–33 months (median 17 months) following radiosurgery. In these cases the majority of coagulation necrosis was replaced by hypocellular, gliotic or collagen rich scar tissue undergoing various degree of hyaline degeneration, calcification or even ossification (fig 3a). Moderate to intense inflammatory cellular reactions consisting of mainly lymphocytes infiltrated these lesions (fig. 3b). Immunohistochemistry disclosed the presence of $CD3^+$ T-lymphocytes in a prominent number of these specimens (fig. 3c). Postradiosurgery vasculopathy with various degrees of endothelial damage and subendothelial spindle cell proliferation narrowing the lumen accompanied by perivascular fibrosis or scar tissue formation was a frequent finding (fig. 3d). There was no significant correlation revealed between the type of radiolesion seen and either the volume of the metastasis or the histological type of metastatic tumor undergoing radiosurgery.

Discussion

Considering that brain metastases are the most frequent of all intracranial tumors they constitute the major part of radiosurgery indications [8, 23]. Brain metastasis develop in up to 30% of patients suffering from cancer, and almost one half of them originate from lung carcinoma [9, 24]. The natural history of untreated patients harboring brain metastases is around 1 month median survival time [25, 26]. Fractionated whole-brain radiation therapy prolonged survival for 3–6 months in several large series [27, 28]. Surgical excision combined with radiotherapy improved the outcome over whole-brain radiation therapy alone [29–31]. However, surgery is limited to patients with a good preoperative medical condition and is generally recommended for solitary, accessible tumors. Recent publications have demonstrated that radiosurgery is an effective method for the management of brain metastasis of different histological subtypes; including tumor types thought of traditionally as being radioresistant [2–8, 10, 11]. Complications following radiosurgery are uncommon, and the risk for permanent neurological deficit related to radiosurgery is low [32].

The goal of radiosurgery in the management of single or multiple intracranial metastases is total tumor destruction, or at least to stop further neoplastic

c immunohistochemistry demonstrated the conspicuous presence of CD68 positive macrophages in the inflammatory cell reaction (×100); ***d*** macrophages seems to originate from a perivascular space (CD68; ×400); ***e*** gliotic rim demarcating the radiolesion (GFAP; ×40); ***f*** subendothelial proliferation narrowing vessels lumina (HE, ×100).

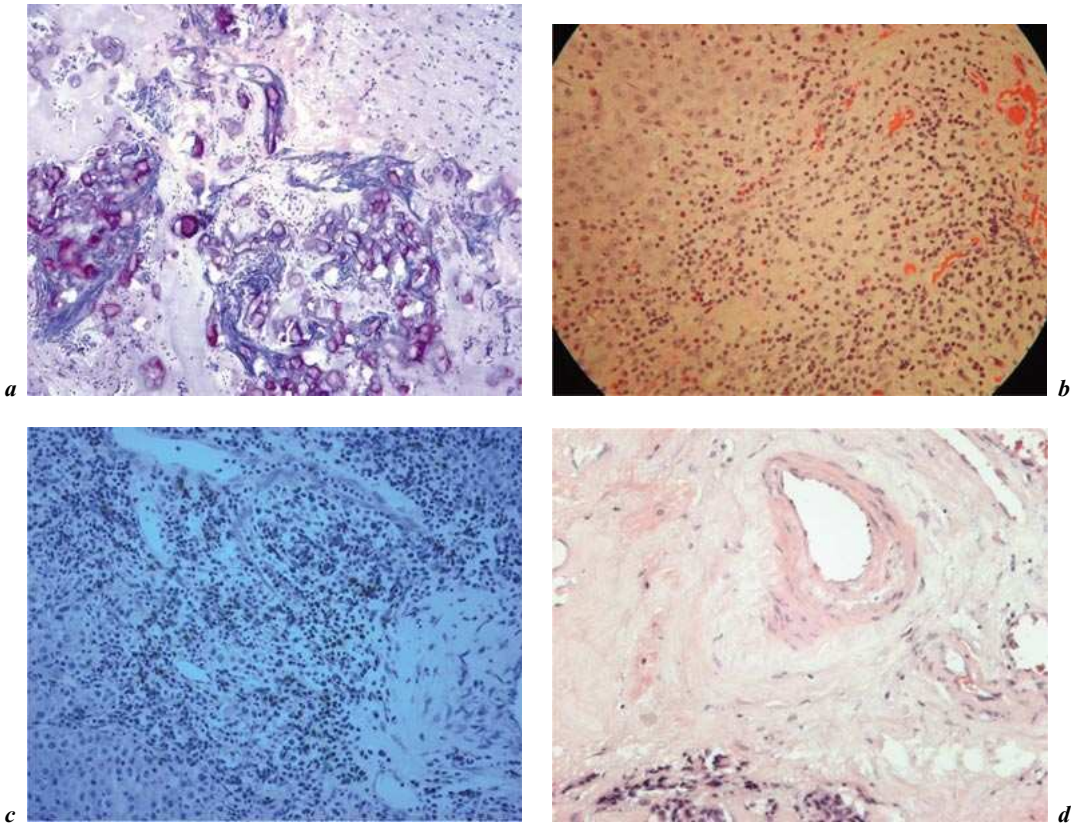

Fig. 3. Histological features of chronic-type tissue responses in brain metastases that underwent radiosurgery. ***a*** Hypocellular scar tissue with extensive degenerative calcification and ossification sharply demarcated from the surrounding brain in a metastatic breast cc 15 months following radiosurgery (HE, ×100); (***b***) chronic inflammatory cell infiltration at the boundary of the gamma radiolesion and tumor islands (HE, ×200); (***c***) immunohistochemistry revealed a prominent $CD3^+$ T-lymphocytic component in the inflammatory reaction (×200); (***d***) proliferative vasculopathy and marked perivascular scar tissue formation with hyaline degeneration (HE, ×100).

progression. This task may be achieved theoretically in different ways. One such way is to produce coagulation necrosis and vascular damage in the tumor tissue. Another is to enhance apoptosis of the neoplastic cell populations. Contrary to the fact that more than 100,000 stereotactic radiosurgery procedures have already been performed worldwide to manage metastatic brain tumors, the pathological mechanisms and the underlying radiobiological processes leading to destruction of cerebral metastases is poorly understood. One of the criticisms of radiosurgery is the lack of sufficient information to understand pathological, pathophysiological,

and radiobiological mechanisms [33]. Apart from early basic investigations, most available pathological data of radiation initiated alterations on human brain tissue were derived from poorly documented autopsy cases, or were connected with conventional whole-brain radiotherapy [34–36]. The rapid development of neuroimaging techniques during the past two decades, and the precise, isodose related radiation delivery in radiosurgery call for sophisticated pathological analysis to explain postirradiation modifications. These studies will facilitate a better understanding of the biological mechanisms leading to radiation induced changes and would enable us to treat new disorders, promote more effective disease control and reduce undesired side effects.

One theory on how radiosurgery destroys, or controls the targeted neoplastic cell proliferation is by either direct early cytotoxic effects (coagulation necrosis, apoptosis), or by late vascular changes. It has been suggested that the radiobiological mechanism of radiosurgery on benign tumors is a combination of both cytotoxic and vascular effects [37]. The direct cellular influence might be the consequence of DNA damage by the ionizing energy of the gamma-ray, leading to cell death entering the next cell cycle (apoptosis, i.e. programmed cell death). Rapidly proliferating tumors with high turnover, like metastases or malignant gliomas, therefore react earlier to irradiation compared to slowly growing benign tumors with low turnover. Lesions without any proliferating capacity, like AVMs, react with an even more prolonged latency period. Late vascular effects of radiosurgery appear through the modification of the vessel wall. Therapeutic radiosurgical doses usually do not affect normal brain vessels [38–40]. However, the pathological vessels of tumors or vascular malformations have a relative sensitivity to radiosurgery in comparison to normal surrounding or feeding arteries [41–44].

Reviewing the literature we have found only three papers providing pathological data on brain metastasis after radiosurgery but a comprehensive systematic study does not exist [18–20]. These publications described decreased tumor cell populations, increased fibrous stroma, central necrosis, macrophage rim development, lymphocytic infiltration, vascular changes and reactive astrocytosis after radiosurgery. Results of the present histopathological study suggest that radiosurgery evokes necrotic changes in brain metastases involving both tumor parenchyma and vascular stroma accompanied by a sterile inflammatory reaction. These findings are summarized in table 3. Three histological types: acute-type, subacute-type, and chronic-type of the tissue responses were observed in different metastases following radiosurgery. There was a tendency suggesting a temporal development in these lesions from one type to the next but the study design did not allow us to prove this. There was no significant correlation between the oncogenetic nature of tumors and the type of lesion seen following radiosurgery. The inflammatory reaction seen after radiosurgery seemed to have an important role in the local tumor control process. Out of the 26 cases analyzed there were 5 with

Table 3. Summary features of the 3 types of responses observed

Type	Parenchymal changes	Stromal alterations	Vasculopathy	Time range over which observations were seen, months
Acute	Sharply demarcated coagulation necrosis	No cellular reaction/or scattered apoptotic cells and polymorphonuclear leukocytes around the necrosis	Dilated small venules; endothelial destruction, undulation of internal elastic membrane, fibrinoid changes in vessels' wall, vacuolar degeneration	1–17
Subacute	Well circumscribed coagulation necrosis	Macrophage reaction around the necrosis; granulation tissue; mild reactive gliosis	Proliferative vasculopathy with narrowing the lumen	5–59
Chronic	Replaced by scar tissue	Focal lymphocytic infiltration; hyaline degenerated scar tissue, calcification	Subendothelial cell proliferation; subtotal or complete lumen obliteration; hyaline degeneration in the wall, focal calcification	9–33

<5 months of local tumor control which had minimal or no inflammatory reaction around the acute-type necrotic gamma radiolesion following radiosurgery. The other 21 neoplasms with >5 months of local tumor control demonstrated moderate to intense inflammatory response after the focussed irradiation. Immunohistochemistry demonstrated a predominance of $CD68^+$ macrophages in the subacute-type lesions and $CD3^+$ T-lymphocytes in the chronic-type tissue reactions. The role of this macrophage and T-cell rim around the necrotic center of the lesion is unknown but might be to remove tissue debris and localize the inflammatory reaction evoked by the focused irradiation. The sparse inflammatory reactivity in the less controlled neoplasms (<5 months) raises the question of the important role this inflammatory cell population is playing in the control process.

The pathophysiological mechanism by which radiosurgery evokes an inflammatory response in brain metastases may act by double targeting. One possibility could be the impairment of the blood-tumor barrier by the ionizing energy of high-dose irradiation, which might enable cellular elements of the blood, especially leukocytes, to escape from the vessels to extravascular territories. This theory would be supported by the histopathological observation that much of these inflammatory cell infiltration seemed to originate and propagate in perivascular spaces of the tumor and surrounding brain tissue. An alternative potential target

might be the direct stimulatory effect of focused irradiation on the immune system of the brain, as it was observed in other pathological conditions like AVMs after radiosurgery [37, 42, 45, 46]. The original concept of immune privilege of the central nervous system has already been modified, and a variety of studies demonstrated that both afferent and efferent immune pathways are present in the normal CNS [47]. Ionizing radiation can reduce tumor growth outside the field of radiation, a concept known as the abscopal effect. The activation of the immune system is supposedly behind this phenomenon as well. Recent investigations have demonstrated that this mechanism is also immune mediated, and that T-cells are required to mediate distant tumor inhibition induced by radiation [48].

Conclusion

The present histopathological study suggests that radiosurgery evokes acute-type, subacute-type, and chronic-type tissue responses accompanied by an inflammatory cell reaction in a variety of cerebral metastases with different histological subtypes. Immunohistochemistry revealed a preponderance of $CD68^+$ macrophages and $CD3^+$ T-lymphocytes in the inflammatory infiltrates developed in well controlled, and missing in poorly controlled neoplasms following stereotactic irradiation. Though causality was not established in this small series, histopathological and immunohistochemical findings suggest that an inflammatory role is important in the local tumor control following radiosurgery of metastatic brain tumors.

Acknowledgments

The authors wish to thank Marta Couce, M.D., Ph.D., Department of Neuropathology, U.P.M.C., Presbyterian Hospital, Pittsburgh, Pa., and Isabelle Salmon, M.D., Ph.D., Department of Anatomo-pathology, Hôpital Erasme, U.L.B., Brussels, Belgium, for processing and providing the pathological material.

Dr. Szeifert was supported by a Congress of Neurological Surgeons/Elekta Clinical Fellowship in Radiosurgery, and the Hungarian Ministry of Health & Welfare (ETT 395/KO/03).

References

1 Leksell L: The stereotaxic method and radiosurgery of the brain. Acta Chir Scand 1951;102:316–319.
2 Loeffler JS, Kooy HM, Wen PY, Fine HA, Cheng CW, Mannarino EG, et al: The treatment of recurrent brain metastases with stereotactic radiosurgery. J Clin Oncol 1990;8:576–582.
3 Adler JR, Cox RS, Kaplan I, Martin DP: Stereotactic radiosurgical treatment of brain metastases. J Neurosurg 1992;76:444–449.
4 Alexander E 3rd, Moriarty TM, Davis RB, Wen PY, Fine HA, Black PM, et al: Stereotactic radiosurgery for the definitive, noninvasive treatment of brain metastases. J Natl Cancer Inst 1995;87:34–40.

5 Alexander E 3rd, Moriarty TM, Loeffler JS: Radiosurgery for metastases. J Neurooncol 1996;27: 279–285.
6 Auchter RM, Lamond JP, Alexander E, Buatti JM, Chappell R, Friedman WA, et al: A multiinstitutional outcome and prognostic factor analysis of radiosurgery for resectable single brain metastasis. Int J Radiat Oncol Biol Phys 1996;35:27–35.
7 Breneman JC, Warnick RE, Albright RE Jr, Kukiatinant N, Shaw J, Armin D, et al: Stereotactic radiosurgery for the treatment of brain metastases. Results of a single institution series. Cancer 1997;79:551–557.
8 Kim YS, Kondziolka D, Flickinger JC, Lunsford LD: Stereotactic radiosurgery for patients with nonsmall cell lung carcinoma metastatic to the brain. Cancer 1997;80:2075–2083.
9 Boyd TS, Mehta MP: Radiosurgery for brain metastases. Neurosurg Clin N Am 1999;10:337–350.
10 Gerosa M, Nicolato A, Foroni R, Zanotti B, Tomazzoli L, Miscusi M, et al: Gamma knife radiosurgery for brain metastases: a primary therapeutic option. J Neurosurg 2002;97(suppl):515–524.
11 Payne BR, Prasad D, Szeifert G, Steiner M, Steiner L: Gamma surgery for intracranial metastases from renal cell carcinoma. J Neurosurg 2000;92:760–765.
12 Kondziolka D, Patel A, Lunsford LD, Kassam A, Flickinger JC: Stereotactic radiosurgery plus whole brain radiotherapy versus radiotherapy alone for patients with multiple brain metastases. Int J Radiat Oncol Biol Phys 1999;45:427–434.
13 Larsson B, Leksell L, Rexed B, Sourander P, Mair W, Andersson B: The high-energy proton beam as a neurosurgical tool. Nature 1958;182:1222–1223.
14 Leksell L, Larsson B, Andersson B, Rexed B, Sourander P, Mair W: Lesions in the depth of the brain produced by a beam of high energy protons. Acad Radiol 1960;54:251–264.
15 Andersson B, Larsson B, Leksell L, Mair W, Rexed B, Sourander P, et al: Histopathology of late local radiolesions in the goat brain. Acta Radiol Ther Physs Biol 1970;9:385–394.
16 Lunsford LD, Altschuler EM, Flickinger JC, Wu A, Martinez AJ: In vivo biological effects of stereotactic radiosurgery: a primate model. Neurosurgery 1990;27:373–382.
17 Kondziolka D, Lunsford LD, Claassen D, Maitz AH, Flickinger JC: Radiobiology of radiosurgery: Part I. The normal rat brain model. Neurosurgery 1992;31:271–279.
18 Hirato M, Hirato J, Zama A, Inoue H, Ohye C, Shibazaki T, et al: Radiobiological effects of gamma knife radiosurgery on brain tumors studied in autopsy and surgical specimens. Stereotact Funct Neurosurg 1996;66(suppl 1):4–16.
19 Szeifert GT, Salmon I, David P, Devriendt D, De Smedt F, Rorive S, Brotchi J, Levivier M: Tumor control and growth in a patient with two cerebral metastases treated with the Leksell Gamma Knife; in: Kondziolka D (ed): Radiosurgery. Basel, Karger, 2002, vol 4, pp 152–161.
20 Thompson BG, Coffey RJ, Flickinger JC, Lunsford LD: Stereotactic radiosurgery of small intracranial tumors: neuropathological correlation in three patients. Surg Neurol 1990;33:96–104.
21 Levivier M, Wikier D, Goldman S, David P, Metens T, Massager N, et al: Integration of the metabolic data of positron emission tomography in the dosimetry planning of radiosurgery with the gamma knife: early experience with brain tumors. Technical note. J Neurosurg 2000;93(suppl 3):233–238.
22 Levivier M, Wikler D Jr, Massager N, David P, Devriendt D, Lorenzoni J, et al: The integration of metabolic imaging in stereotactic procedures including radiosurgery: a review. J Neurosurg 2002;97(suppl):542–550.
23 Lorenzoni J, Devriendt D, Massager N, David P, Ruiz S, Vanderlinden B, et al: Radiosurgery for treatment of brain metastases: estimation of patient eligibility using three stratification systems. Int J Radiat Oncol Biol Phys 2004;60:218–224.
24 Pickren J, Lopez G, Tzukada J: Brain metastases. Cancer Treat Symp 1983;2:295–313.
25 Harzra T, Mullins GN, Lott S: Management of cerebral metastases from bronchogenic carcinoma. Johns Hopkins Mad J 1972;130:377–383.
26 Posner JB: Diagnosis and treatment of metastases to the brain. Clin Bull 1974;4:47–57.
27 Cairncross JG, Kim JH, Posner JB: Radiation therapy for brain metastases. Ann Neurol 1980;7:529–541.
28 Hendrickson FR: The optimum schedule for palliative radiotherapy for metastatic brain cancer. Int J Radiat Biol 1977;2:165–168.
29 Noordijk EM, Vecht CJ, Haaxma-Reiche H: The choice of treatment of single brain metastasis should be based on extracranial tumor activity and age. Int J Radiat Biol 1994;29:711–717.

30 Patchell RA, Tibbs PA, Walsh JW, et al: A randomized trial of surgery in the treatment of single metastases to the brain. N Engl J Med 1990;322:494–500.
31 Sundaresan N, Galicich JH: Surgical treatment of brain metastases. Clinical and computerized tomography evaluation of the results of treatment. Cancer 1985;55:1382–1388.
32 Chin LS, Lazio BE, Biggins T, Amin P: Acute complications following gamma knife radiosurgery are rare. Surg Neurol 2000;53:498–502; discussion 02.
33 Yamamoto M: Gamma Knife radiosurgery: technology, applications, and future directions. Neurosurg Clin N Am 1999;10:181–202.
34 Steiner L, Forster D, Leksell L, Meyerson BA, Boëthius J: Gammathalamotomy in intractable pain. Acta Neurochir (Wien) 1980;52:173–184.
35 Julow J, Slowik F, Kelemen J: Late post-irradiation necrosis of the brain. Acta Neurochir (Wien) 1979;46:135–150.
36 Wolf D, Germano IM: Radionecrosis: clinical and histological aspects; in: Germano I (ed): LINAC and Gamma Knife Radiosurgery, ed 1, Park Ridge, AANS, 2000, vol 1, pp 75–82.
37 Kondziolka D, Lunsford LD, Flickinger JC: The radiobiology of radiosurgery. Neurosurg Clin N Am 1999;10:157–167.
38 Szeifert G: Radiosurgery and AVM histopathology. J Neurosurg 1998;88:356–357.
39 Szeifert G, Major O, Fazekas I, Nagy Z: Effects of radiation on cerebral vasculature: a review. Neurosurgery 2001;48:452–453.
40 Major O, Szeifert GT, Radatz MW, Walton L, Kemeny AA: Experimental stereotactic gamma knife radiosurgery. Vascular contractility studies of the rat middle cerebral artery after chronic survival. Neurol Res 2002;24:191–198.
41 Szeifert GT, Kemeny AA, Timperley WR, Forster DM: The potential role of myofibroblasts in the obliteration of arteriovenous malformations after radiosurgery. Neurosurgery 1997;40:61–65; discussions 65–66.
42 Schneider BF, Eberhard DA, Steiner LE: Histopathology of arteriovenous malformations after gamma knife radiosurgery. J Neurosurg 1997;87:352–357.
43 Yamamoto M, Hara M, Ide M, Ono Y, Jimbo M, Saito I: Radiation-related adverse effects observed on neuro-imaging several years after radiosurgery for cerebral arteriovenous malformations. Surg Neurol 1998;49:385–397; discussions 97–98.
44 Major O, Kemeny AA, Forster DM, Jakubowski J, Morice AH: In vitro contractility studies of the rat middle cerebral artery after stereotactic Gamma Knife radiosurgery. Stereotact Funct Neurosurg 1996;66(suppl 1):17–28.
45 Szeifert G, Kemeny AA, Major O, Timperley WR, Forster DMC: Histopathological changes in cerebral arteriovenous malformations following stereotactic irradiation with the Gamma Knife; in: Kondziolka D (ed): Radiosurgery. Basel, Karger 1997, vol 2, pp 129–136
46 Szeifert GT, Salmon I, Baleriaux D, Brotchi J, Levivier M: Immunohistochemical analysis of a cerebral arteriovenous malformation obliterated by radiosurgery and presenting with re-bleeding. Case report. Neurol Res 2003;25:718–721.
47 Wikstrand C, Ashley DM, Bigner DD, Hale LP: Cellular immunology. Lymphocyte populations, cytokines and target-effector systems; in: Bigner D, McLendon R, Bruner JM (ed): Russell and Rubinstein's Pathology of Tumors of the Nervous System, ed 6. London, Arnold, 1998, vol 1, pp 231–249.
48 Demaria S, Ng B, Devitt ML, Babb JS, Kawashima N, Liebes L, Formenti SC: Ionizing radiation inhibition of distant untreated tumors (abscopal effect) is immune mediated. Int J Radiat Oncol Biol Phys 2004;58:862–870.

Douglas Kondziolka, MD, FRCS (C), FACS
Center for Image-Guided Neurosurgery
Department of Neurological Surgery, Suite B-400
Presbyterian University Hospital, 200 Lothrop Street
Pittsburgh, PA 15213 (USA)
Tel. +1 412 647 6782, Fax +1 412 647 0989,
E-Mail kondziolkads@upmc.edu

Kondziolka D (ed): Radiosurgery. Basel, Karger, 2006, vol 6, pp 186–198

Gamma Knife Surgery for Metastatic Brain Tumors from Lung Cancer without Prophylactic Whole Brain Radiation Therapy

Toru Serizawa[a], *Yoshinori Higuchi*[a], *Junichi Ono*[a], *Shinji Matsuda*[b], *Toshihiko Iuchi*[c], *Osamu Nagano*[d], *Naokatsu Saeki*[d]

Departments of [a]Neurosurgery and [b]Neurology, Chiba Cardiovascular Center, [c]Division of Neurosurgery, Chiba Cancer Center, [d]Department of Neurological Surgery, Graduate School of Medicine, Chiba University, Chiba, Japan

Abstract

Objective: We retrospectively analyzed the effectiveness of Gamma Knife surgery (GKS) for metastatic brain tumors from lung cancer without prophylactic whole brain radiation therapy. **Methods:** Six hundred eight consecutive patients who satisfied the following 5 criteria were analyzed: (1) lung cancer primary; (2) no surgically inaccessible lesions; (3) tumor number and size limited to 10 J of total skull internal dose; (4) no symptomatic carcinomatous meningitis; (5) Karnofsky performance status score no lower than 70 due to systemic disease. Large tumors were totally removed, while smaller lesions were all irradiated with GKS. New lesions detected with follow-up magnetic resonance imaging were appropriately re-treated with GKS. Overall survival (OS), neurological survival (NS), qualitative survival (QS) and new lesion-free survival curves were calculated and the prognostic values of covariates were obtained. **Results:** In total, 1,101 separate sessions were required to treat 6,427 lesions. This series includes 68 small cell cancers and 80 craniotomies. The median OS period was 10.4 months. In multi-variate analysis, significant prognostic factors for OS were extracranial disease (risk factor: active), Karnofsky performance status score (<70) and gender (male). NS and QS at 1 year were 88.0 and 81.3%, respectively. The only significant poor prognostic factor for NS was carcinomatous meningitis. Male gender, active extracranial disease, low Karnofsky performance status score, magnetic resonance imaging evidence of carcinomatous meningitis and a large total tumor volume were significant factors influencing QS. New lesion-free survival at 6 months was 71.5%. The treatment cost of this protocol was estimated USD 9,000 per patient, which is nearly the same as that of GKS with upfront whole brain radiation therapy. **Conclusion:** In terms of NS and QS, GKS alone for metastatic brain tumors from lung cancer provides excellent palliation without prophylactic whole brain radiation therapy. Close observation

and appropriate salvage treatment are essential for prevention of neurological death and maintaining of activities of daily living.

The efficacy of radiosurgery for cases with a few small metastatic brain tumors is now well established, but the necessity of upfront whole-brain radiation therapy (WBRT) with radiosurgery remains controversial [1–6]. This is a retrospective review of Gamma Knife surgery (GKS), without upfront WBRT, for brain metastases from lung cancer. All patients were treated according to the same local protocol, by one of the authors (TS), at one institution.

Patients and Methods

Among 1,066 cases with brain metastases treated with GKS at Chiba Cardiovascular Center from January 1998 to August 2005, 608 consecutive patients who satisfied the following 5 criteria were analyzed: (1) lung cancer primary; (2) no surgically inaccessible lesions; (3) tumor number and size limited to 10 J of total skull internal dose (TSID); (4) no symptomatic carcinomatous meningitis; (5) and in those with systemic disease, a Karnofsky performance status (KPS) score of at least 70. At diagnosis of brain metastases, the primary physician evaluated systemic disease status using X-ray films, computerized tomography (CT) and radionuclide scanning. For diagnosis and dose planning, all metastatic lesions were visualized on gadolinium-enhanced magnetic resonance imaging (MRI) (1.5 T, Magnetom Vision, Siemens). Large tumors (≥35 mm) were totally removed, and smaller lesions (<35 mm) were all irradiated with GKS. New distant lesions detected by MRI every 2–3 months were appropriately re-treated with GKS, if the patient's condition allowed. The TSID calculated with the Leksell GammaPlan™ (Elekta Instruments, Atlanta, Ga., USA) for each radiosurgical procedure was less than 10 J, thus preventing acute brain swelling, as previously reported [2–4, 7]. This 10 J TSID is equivalent to 3 Gy of whole brain irradiation. If the lesions were scattered and similar in size, the upper numerical limits were approximately 25 for tiny (8 mm in diameter), 10 for small (14–18 mm) and 4 for medium-sized lesions (25 mm), with 20 Gy at the periphery, as illustrated in figures 1 and 2. Primary physicians determined chemotherapy protocols. Neurological evaluations and enhanced MRI were performed every 2–3 months until the KPS score was below 70. Thereafter, enhanced MRI or CT was obtained at the primary hospital, for as long as possible, and sent to us for evaluation. The dates and causes of death and impaired activities of daily living (ADL) were documented by the primary physicians. Control of the GKS-treated lesion was defined as the absence of any significant increase in tumor diameter (<10%), as confirmed by axial or coronal MRI. Thallium-201 Chloride (Tl) SPECT, as previously reported [4], was employed to differentiate tumor recurrence from radiation injury. The definitions of tiny, small, medium and large lesions are ≤1.0 cm, >1.0 but ≤2.0 cm, >2.0 but ≤3.0 cm, and >3.0 cm, respectively. Neurological death was defined as death due to all forms of intracranial disease, including tumor recurrence, carcinomatous meningitis, cerebral dissemination, and other unrelated intracranial diseases, as described by Patchell et al. [2]. Impaired ADL was defined as an impaired neurological status as reflected by a KPS score <70 (functionally dependent).

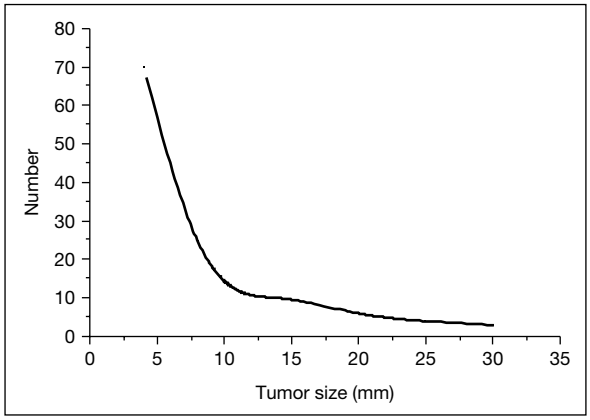

Fig. 1. Lesion number and size limits for safe GKS. The limits of brain lesion number and size for GKS, in a single session at Chiba Cardiovascular Center, are presented. The curve indicates a TSID of 10 J calculated using the GammaPlan, with 20 Gy (50%) peripheral doses.

A distant new lesion was defined as the appearance of a new brain metastasis at a site different from the original one.

The intervals from the date of diagnosis of brain metastases at our center until the date of death (overall survival, OS), neurological death (neurological survival, NS), impaired ADL (qualitative survival, QS), and the appearance of new distant lesions (new lesion-free survival, NLFS) were calculated by the Kaplan-Meier method. Tumor-progression-free survival for all lesions treated with GKS during the observation period was also analyzed. Prognostic values of the individual covariates for OS, NS, QS and NLFS were obtained with the Cox proportional hazards model. The following 12 dichotomized covariates were entered: age ($<$65 years versus $\geq$65 years); gender (male versus female); pre-treatment KPS score ($<$70 versus $\geq$70); extracranial lesion status (controlled versus active); simultaneous (synchronous) versus later (metachronous) detection of metastasis, lung cancer histology (non-small cell versus small cell cancer); number of brain lesions ($\leq$10 versus $>$10); maximum lesion diameter ($<$25 versus $\geq$25 mm); initial tumor volume ($\leq$10 versus $>$10 cm^3); MRI evidence of carcinomatous meningitis (yes versus no); chemotherapy (yes versus no) and craniotomy (yes versus no). A probability value $<$0.05 was considered statistically significant.

Results

The distributions of patient and treatment factors are summarized in table 1. The lung cancer histologies were adenocarcinoma in 404 patients (66.5%), squamous cell carcinoma in 68 (11.2%), small cell carcinoma in 68 (11.2%), large cell carcinoma in 15 (2.5%), and others/undetermined in 53 (8.7%). The median number of lesions treated with the initial GKS was 3, range 1–25. During follow-up,

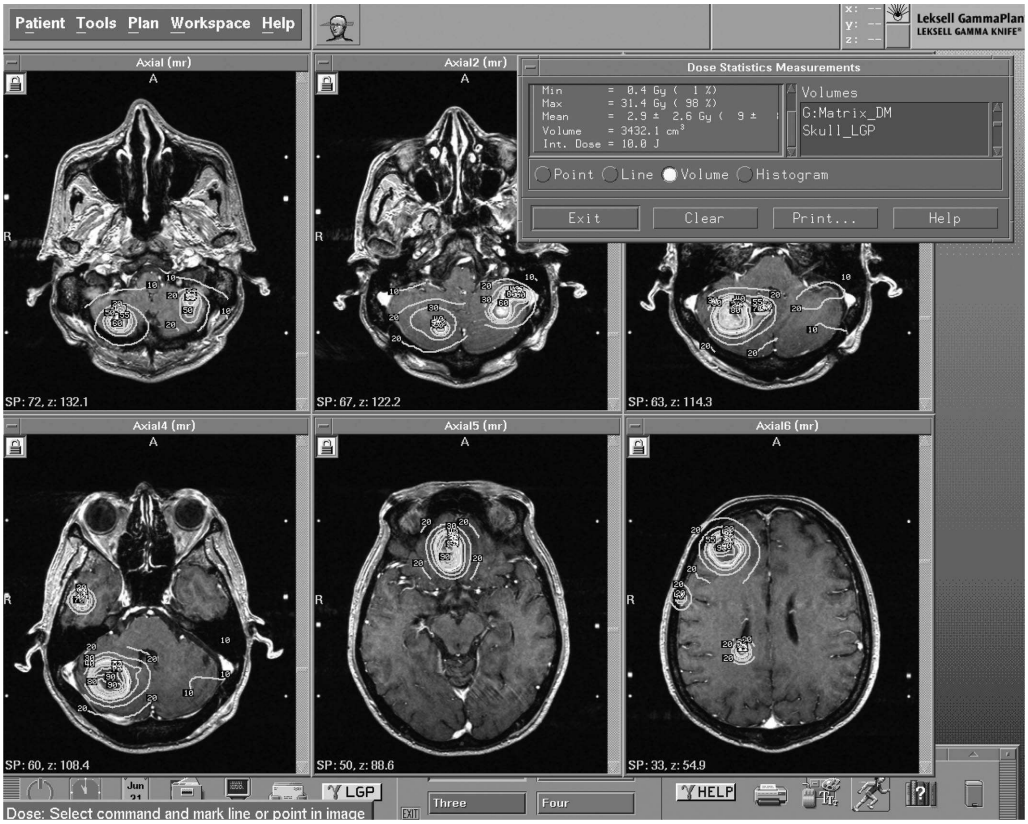

Fig. 2. Calculation of TSID with GammaPlan. This case had 14 small to medium-sized lesions irradiated by GKS with 50% 20 Gy at the periphery. The TSID is easily calculated with the GammaPlan. The dose statistics include 10 J (10,000 mJ) of TSID and a 2.9 Gy mean irradiated dose to the skull.

the number of GKS procedures for new distant and recurrent GKS-treated lesions averaged 1.8 ± 1.5, varying between 1 and 17, and the mean number of lesions treated with GKS per patient was 10.5 ± 14.4, range 1–83. In total, 1,101 separate GKS procedures were required to treat 6,427 lesions. The mean calculated tumor volume was 0.67 ± 2.00 cm^3 (median 0.10 cm^3). The minimum dose applied to the tumor margin was 15–30 Gy (mean ± SD: 20.7 ± 1.7 Gy, median: 20 Gy) with a 72.7% isodose contour (range 30–98%). The mean prescribed doses were 20.8 Gy in 5,557 tiny, 20.4 Gy in 574 small, 19.5 Gy in 235 medium-sized, and 18.2 Gy in 61 large lesions. Figure 3 shows cumulative tumor-progression-free survival curves according to tumor volume. Differences were

Table 1. Dichotomized patient characteristics

Characteristics	
Age, years	
<65	277
≥65	331
Sex	
Male	424
Female	184
Extracranial disease	
Controlled	75
Active	533
Pre-treatment KPS score	
<70	82
≥70	526
Histology	
Non-SCLC	540
SCLC	68
Number of brain lesions	
≤10	449 (single 99)
>10	159
Maximum lesion size, mm	
<25	557
≥25	151
Total tumor volume, cm^3	
≤10	484
>10	124
Carcinomatous meningitis	
Yes	62
No	546
Chemotherapy	
Yes	230
No	378
Craniotomy	
Yes	80
No	528
Metastasis	
Synchronous	261
Metachronous	347

KPS = Karnofsky performance status; SCLC = small cell lung cancer.

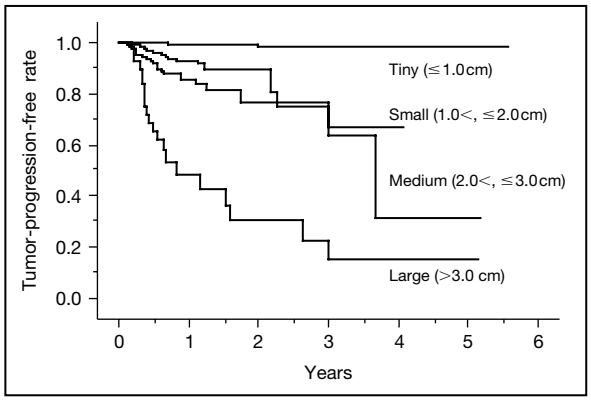

Fig. 3. Tumor-progression-free survival. Cumulative tumor-progression-free survival curves, according to tumor volume, are shown. The maximum diameters of tiny, small, medium and large lesions are ≤1.0 cm, >1.0 but ≤2.0 cm, >2.0 but ≤3.0 cm, and >3.0 cm, respectively. The mean prescribed doses were 20.8 Gy in 5,557 tiny, 20.4 Gy in 574 small, and 19.5 Gy in 235 medium-sized, and 18.2 Gy in 61 large lesions. There were statistically significant differences among survival curves ($p < 0.0001$).

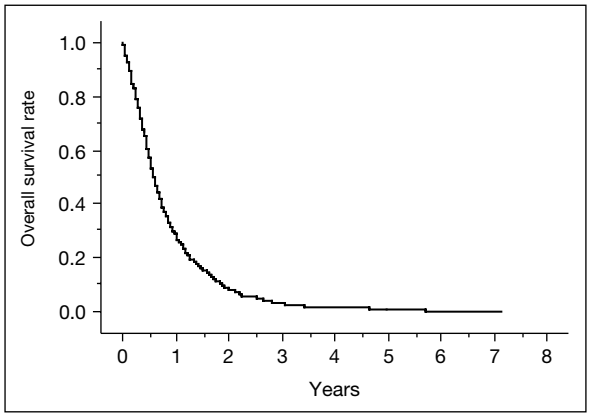

Fig. 4. Overall survival. The OS curve is presented. The median OS period was 10.4 months.

statistically significant ($p < 0.0001$). Among 90 lesions showing progression, we diagnosed tumor recurrence in 39 and radiation injury in 51. The median OS period was 10.4 months (fig. 4). In multivariate analysis, significant prognostic factors for OS were active extracranial disease, low pre-treatment KPS score and

Table 2. Prognostic variables for overall survival

Variables	High risk group	p Value*	HR*	p Value**	HR**
Age	<65	0.7680	1.029		
Sex	Male	<0.0001	1.927	<0.0001	2.005
Extracranial disease	Active	<0.0001	4.065	<0.0001	4.444
Initial KPS score	<70	<0.0001	2.058	<0.0001	2.561
Histology	Non-SCLC	0.7119	1.058		
Number of lesions	>10	0.2578	1.152		
Maximum lesion size	≥25 mm	0.4042	1.096		
Total tumor volume	>10 cm^3	0.0749	1.152		
Presence of CM	Yes	0.5704	1.097		
Chemotherapy	No	0.3401	1.100		
Craniotomy	No	0.8136	1.032		
Metastasis	Metachronous	0.3582	1.094		

*Monovariate analysis; **multivariate analysis (Cox's proportional hazard model).

HR = Hazard ratio; KPS = Karnofsky performance status; CM = carcinomatous meningitis; SCLC = small cell lung cancer.

Table 3. Prognostic variables for neurological survival

Variable	High risk group	p Value*	HR*	p Value**	HR**
Age	<65	0.1909	1.369		
Sex	Male	0.0696	1.640		
Extracranial disease	Active	0.0033	2.809		
Initial KPS score	<70	0.2430	1.556		
Histology	SCLC	0.2568	1.433		
Number of lesions	>10	0.0052	2.132		
Maximum lesion size	≥25 mm	0.0052	2.312		
Total tumor volume	>10 cm^3	0.0071	2.220		
Presence of CM	Yes	<0.0001	3.971	<0.0001	3.971
Chemotherapy	Yes	1.019	1.063		
Craniotomy	Yes	0.1471	1.516		
Metastasis	Metachronous	0.6771	1.110		

*Univariate analysis; **multivariate analysis (Cox's proportional hazard model).

HR = Hazard ratio; KPS = Karnofsky performance status; CM = carcinomatous meningitis; SCLC = small cell lung cancer.

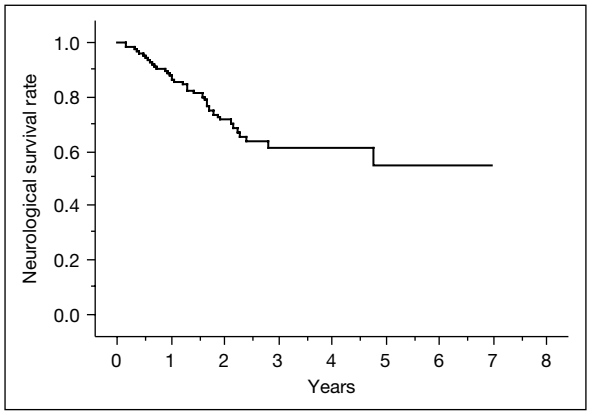

Fig. 5. Neurological survival. The NS curve is shown. The neurological death free rate following GKS was 88.0% at 1 year, 71.5% at 2 years.

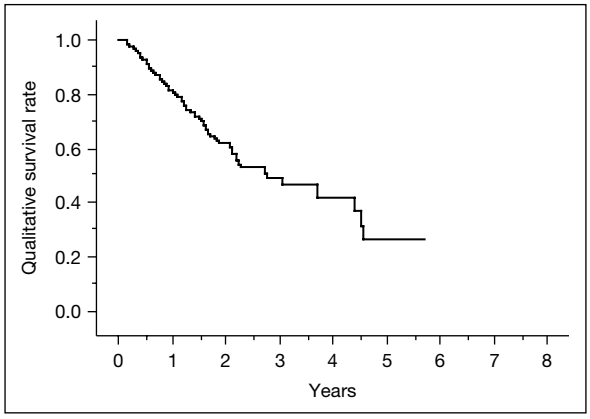

Fig. 6. Qualitative survival. The QS curve is presented. The functionally-dependent-free rate was 81.3% at 1 year, 61.7% at 2 years.

male gender, as shown in table 2. NS and QS were presented in figures 5 and 6. Of the 436 mortalities, 74 (17.0%) were attributed to neurological death. Causes of neurological death were carcinomatous meningitis in 37, cerebral dissemination in 15, recurrence of the treated lesion in 11, progression of an untreated lesion in 8 and other in 3. Among 112 cases with functional dependence due to brain lesions, the cause was radiation injury in 30. The only significant poor prognostic factor for NS was carcinomatous meningitis, as shown in table 3. Male gender, active extracranial disease, low KPS score, MRI evidence of carcinomatous

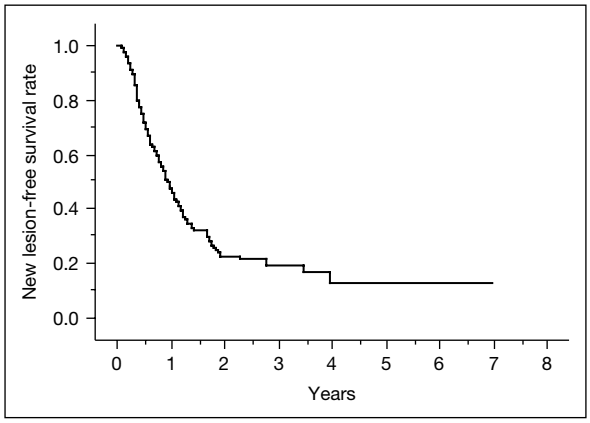

Fig. 7. New lesion-free survival. The NLFS curve is shown. The NLFS rate was 72.5% at 6 months, 47.4% at 1 year.

meningitis and a large total tumor volume were confirmed to be significant factors influencing QS in multivariate analysis (table 4). The NLFS curve is shown in figure 7. According to multivariate analysis, the only significant poor prognostic factor for NLFS was active extracranial disease (table 5).

Discussion

A few retrospective and randomized controlled studies concerning radiosurgery versus radiosurgery plus upfront WBRT have been reported [1, 6]. However, controversy persists as to which treatment should be chosen, and for what categories of patients with various degrees of intra and extracranial disease. In this retrospective study, a very large series of results for GKS without upfront WBRT for brain metastases from lung cancer was carefully reviewed with special attention to NLFS and salvage treatment, as well as to NS and QS.

New Distant Lesions and Salvage Treatment

Since the advent of CT scanning, it has come to be widely believed that even patients with only a single metastatic lesion have microscopic metastases [1, 8]. Modern high-resolution MRI can detect tumors only a few millimeters in diameter and even these tiny metastatic lesions can be safely and accurately irradiated with GKS. The survival period may be too short for invisible metastases or true new lesions to be identified on follow-up MRI or to cause neurological symptoms. Chemotherapy may, of course, play an additional role in

Table 4. Prognostic variables for qualitative survival

Variable	High risk group	p Value*	HR*	p Value**	HR**
Age	≥65	0.5748	1.112		
Sex	Male	0.0008	1.726	0.0028	1.726
Extracranial disease	Active	0.0002	2.639	0.0028	1.879
Initial KPS score	<70	0.0017	2.274	0.0001	2.849
Histology	SCLC	0.2169	1,365		
Number of lesions	>10	0.0003	2.315		
Maximum lesion size	≥25 mm	0.0654	1.453		
Total tumor volume	>10 cm^3	0.0003	2.110	0.0121	1.684
Presence of CM	Yes	<0.0001	2.818	<0.0001	2.706
Chemotherapy	Yes	0.6270	1.098		
Craniotomy	Yes	0.6287	1.098		
Metastasis	Metachronous	0.9254	1.019		

*Univariate analysis; **multivariate analysis (Cox's proportional hazard model).

HR = Hazard ratio; KPS = Karnofsky performance status; CM = carcinomatous meningitis; SCLC = small cell lung cancer.

Table 5. Prognostic variables for new lesion-free survival

Variable	High risk group	p Value*	HR*	p Value**	HR**
Age	< 65	0.0785	1.252		
Sex	Male	0.0493	1.306		
Extracranial disease	Active	0.0005	1.876	0.0005	1.876
Initial KPS score	≥70	0.3671	1.235		
Histology	SCLC	0.0578	1.399		
Number of lesions	>10	0.0574	1.362		
Maximum lesion size	<25 mm	0.8622	1.027		
Total tumor volume	>10 cm^3	0.0826	1.316		
Presence of CM	No	0.1161	1.501		
Chemotherapy	Yes	0.5380	1.084		
Craniotomy	No	0.4321	1.157		
Metastasis	Synchronous	0.2680	1.153		

*Univariate analysis; **multivariate analysis (Cox's proportional hazard model).

HR = Hazard ratio; KPS = Karnofsky performance status; CM = carcinomatous meningitis; SCLC = small cell lung cancer.

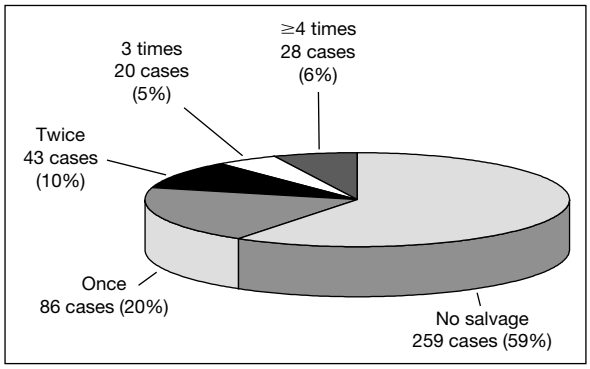

Fig. 8. Number of salvage treatments. Among 436 deceased cases, the number of salvage GKS treatments for new distant new lesions was zero in 259 cases (59.4%), one in 86 (19.7%), two in 43 (9.9%), three in 20 (4.6%), ≥4 in 28 (6.4%).

controlling microscopic lesions, especially in SCLC. The author's experience suggests that local control is the most important clinical goal for patients with brain metastases and that it is not necessary to treat invisible metastases. Indeed, about 60% of patients in this series did not require salvage treatment (fig. 8). Salvage WBRT was employed in only 8 cerebral dissemination cases. If new lesions are detected, appropriate salvage treatment, taking patient condition into consideration, may be warranted. WBRT should be used only with great caution because of its invasive nature. The current study demonstrates that a local GKS treatment protocol without upfront WBRT can provide highly satisfactory results in selected patients receiving close observation and appropriate salvage treatment.

Cost

The cost of any local treatment protocol, without prophylactic WBRT, must always be considered. In Japan, GKS is relatively inexpensive, 5,000 US dollars, while WBRT is 3,000 US dollars. In this series, the mean number of salvage GKS per patient was 0.8. The incidence of new distant lesions which can be controlled GKS is expected to be 50%, if all invisible microscopic lesions are controlled by upfront WBRT. Thus, the total treatment costs come to approximately 9,000 US dollars for GKS without prophylactic WBRT (5,000 + 5,000*0.8) and 10,000 US dollars for GKS with prophylactic WBRT (5,000 + 3,000 + 5,000*0.4). This local treatment is thus estimated to be less expensive than GKS with upfront WBRT, though some patients require frequent salvage GKS. Furthermore, the Japanese public insurance system covers all initial and salvage GKS procedures as well as follow-up MRI. Economic

factors impacting radiosurgery and radiotherapy apparently differ markedly among countries. If the portions of fees for radiosurgery and radiotherapy covered by health insurance are similar to those in Japan, the cost of our local treatment protocol without prophylactic WBRT would appear to be quite reasonable.

Indications for and Limitations of Our Local Treatment Protocol

Factors limiting GKS in a single session include not only the number, but also the size of lesions. However, earlier reviews focused solely on number. To resolve this problem, we have proposed the TSID concept, which provides information on the limitations of safe GKS in a single session [9, 3–5]. A TSID of 10 J is equivalent to 3 Gy of whole brain irradiation. This is the WBRT one-fraction dose used for metastatic brain tumors (30 Gy/10 fractions). With these limits, 25 tiny (8 mm single isocenter), 10 small (14 or 18 mm single isocenter) or 4 medium-sized (25 mm, multiple isocenters) lesions would be the numerical limits of a single GKS session, if the peripheral dose is 50% 20 Gy, as calculated by the GammaPlan. Adverse early radiation effects such as acute brain swelling were not observed in the present series with TSID below 10 J. Yamamoto and Yang, using higher radiation doses than allowed by the criteria employed herein, reported the safety of GKS for numerous brain metastases [10, 11]. Furthermore, the present study found patients with carcinomatous meningitis to have significantly poorer NS and QS results. The present criteria exclude symptomatic carcinomatous meningitis, but MRI for dose planning with double contrast and thin slice (2 mm) revealed asymptomatic carcinomatous meningitis, to be a highly significant poor prognostic factor for NS and QS. In univariate analysis, tumor numbers exceeding 10 also affected NS and QS, although tumor number was not found to be significant in multivariate analysis. Thus, the indication criteria for this treatment are (1) no surgically inaccessible large ($>$35 mm) tumors, (2) tumor number and size limited to TSID within 10 J, (3) no MRI evidence of carcinomatous meningitis, and (4) no cerebral dissemination more than 10 lesions.

Conclusions

In terms of NS and QS, GKS without upfront WBRT for brain metastases from lung cancer provides excellent palliation considering the patients' short life expectancies. However, careful follow-up MRI and appropriate salvage treatment are essential to preventing neurological death and maintaining favorable ADL.

References

1 Kondziolka D, Patel A, Lunsford LD, et al: Stereotactic radiosurgery plus whole brain radiotherapy versus radiotherapy alone for patients with multiple brain metastases. Int J Radiat Oncol Biol Phys 1999;45:427–737.

2 Patchell RA, Tibbs PA, Walsh JW, et al: A randomized trial of surgery in the treatment of single metastases to the brain. N Engl J Med 1990;322:494–500.

3 Serizawa T, Ono J, Iuchi T, et al: Gamma knife radiosurgery for metastatic brain tumors from lung cancer. Comparison between small cell cancer and non-small cell cancer. J Neurosurg 2002;97(suppl 5):484–488.

4 Serizawa T, Saeki N, Higuchi Y, et al: Gamma knife surgery for brain metastases: indications for and limitations of a local treatment protocol. Acta Neurochir (Wien) 2005;147:721–726.

5 Sneed PK, Lamborn KR, Forstner JM, et al: Radiosurgery for brain metastases: is whole brain radiotherapy necessary? Int J Radiat Oncol Biol Phys 1999;43:549–558.

6 Sneed PK, Suh JH, Goetsch SJ, et al: A multi-institutional review of radiosurgery alone vs. radiosurgery with whole brain radiotherapy as the initial management of brain metastases. Int J Radiat Oncol Biol Phys 2002;53:519–526.

7 Serizawa T, Saeki N, Higuchi Y, et al: Diagnostic value of thallium-201 chloride single-photon emission computed tomography in differentiating tumor recurrence from radiation injury after gamma knife surgery for metastatic brain tumors. J Neurosurg 2005;102(suppl 2):266–271.

8 Arriagada R, Le Chevalier T, Borie F, et al: Prophylactic cranial irradiation for patients with small-cell lung cancer in complete remission. J Nat Cancer Inst 1995;87:183–190.

9 Serizawa T, Iuchi T, Ono J, et al: Gamma knife treatment for multiple metastatic brain tumors compared with whole-brain radiation therapy. J Neurosurg 2000;93(suppl 3):32–36.

10 Yang CC, Ting J, Wu X, et al: Dose volume histogram analysis of the gamma knife radiosurgery treating twenty-five metastatic intracranial tumors. Stereotact Funct Neurosurg 2002;70:41–49.

11 Yamamoto M, Ide M, Nishio S, et al: Gamma knife radiosurgery for numerous brain metastases: Is this a safe treatment? Int J Radiat Oncol Biol Phys 2002;3:1279–1283.

Toru Serizawa, MD, PhD
Department of Neurosurgery, Chiba Cardiovascular Center
575 Tsurumai
Ichihara, Chiba 2900512 (Japan)
Tel. +81 436 88 3111, Fax +81 436 88 3032
E-Mail QWT03231@nifty.ne.jp

Kondziolka D (ed): Radiosurgery. Basel, Karger, 2006, vol 6, pp 199–210

Radiosurgery for the Management of Spinal Metastases

Peter C. Gerszten, Steven A. Burton, Cihat Ozhasoglu, William J. Vogel, Annette E. Quinn, William C. Welch

Departments of Neurological Surgery and Radiation Oncology, University of Pittsburgh Medical Center, Pittsburgh, Pa., USA

Abstract

Background/Aims: Large clinical experience with spinal radiosurgery to properly assess clinical experience has previously been limited. This study evaluated the clinical outcomes of single fraction radiosurgery as part of the management of metastatic spine tumors. **Methods:** Five hundred patients with spinal metastases underwent radiosurgery (ages ranged from 18 to 85 years, mean 56 years). Lesion location included 73 cervical, 212 thoracic, 112 lumbar, and 103 sacral. The most common metastatic tumors were renal cell (93 cases), breast (83 cases), and lung (80 cases). **Results:** The primary indication for radiosurgery was pain in 336 cases, as a primary treatment modality in 65 cases, for radiographic tumor progression in 51 cases, for post-surgical treatment in 9 cases, for progressive neurological deficit in 32 cases, and as a radiation boost in 7 cases. The maximum intratumoral dose ranged from 12.5 to 25 Gy (mean 20 Gy). Tumor volume ranged from 0.20 to 264 ml (mean 46 ml). Axial and/or radicular pain improved in 290 of 336 patients (86%). Long-term tumor control was demonstrated in 90% of lesions treated with radiosurgery as a primary treatment modality and in 88% of lesions treated for radiographic tumor progression. Twenty-seven of 32 patients (84%) with a progressive neurological deficit prior to treatment experienced at least some clinical improvement. **Conclusions:** Spinal stereotactic radiosurgery is demonstrated to be a feasible, safe, and clinically effective technique for the treatment of spine metastases.

Studies have previously determined the clinical efficacy of single fraction therapy for painful bone metastases [1, 2]. A primary factor that limits radiation dose for local vertebral tumor control with conventional radiotherapy is the relatively low tolerance of the spinal cord to radiation. Conventional external beam radiotherapy lacks the precision to deliver large single-fraction doses of radiation to the spine near radiosensitive structures such as the spinal cord. It is

the low tolerance of the spinal cord to radiation that often limits the treatment dose to a level that is far below the optimal therapeutic dose [3–5]. Radiotherapy may provide less than optimal clinical response since the total dose is limited by the tolerance of the spinal cord. Precise confinement of the radiation dose to the treatment volume, as is the case for intracranial radiosurgery, should increase the likelihood of successful tumor control at the same time that the risk of spinal cord injury is minimized [5–13]. The emerging technique of spinal radiosurgery represents a logical extension of the current state-of-the-art radiation therapy.

Since Hamilton et al. [14] first described the possibility of linear-accelerator based spinal stereotactic radiosurgery in 1995, multiple centers have attempted to pursue large fraction conformal radiation delivery to spinal lesions using a variety of technologies [5, 7–12, 14–22]. Researchers have shown the feasibility and clinical efficacy of hypofractionated stereotactic body radiotherapy for metastases to the spine [5–13, 23–26]. Stereotactic radiosurgery for tumors of the spine has more recently been demonstrated to be accurate, safe, and efficacious [5, 7, 8, 10–15, 17–19, 27–29]. The purpose of this study was to evaluate the safety and clinical efficacy of radiosurgery for the treatment of metastases to the spine.

Materials and Methods

This study involved the prospective evaluation of 500 lesions in 393 consecutive patients with histologically proven metastases to the spine who were treated using the CyberKnife Image-Guided Radiosurgery System® with the Dynamic Tracking System (DTS) 3.0 software. All patients were treated at the University of Pittsburgh Medical Center, Pittsburgh, Pa., USA, and the protocol was approved by the University of Pittsburgh's institutional review board. Spinal metastases were diagnosed by computed tomography (CT) and/or MR imaging. There were 251 women; ages ranged from 18 to 85 years (mean 56 years). Follow-up ranged from 3 to 53 months (median 21 months). Table 1 summarizes the characteristics of the treatment group, including the primary indications for spinal stereotactic radiosurgery that were used for patient selection for this study. Table 2 summarizes the primary sites. The most common indication for treatment was pain in 336 patients, as a primary treatment modality in 65 patients, for asymptomatic radiographic tumor progression on serial imaging in 51 patients, for progressive neurologic deficit in 32 patients, for postsurgical treatment in 9 patients, and as a radiation boost in 7 patients. The levels of involvement included 73 cervical, 212 thoracic, 112 lumbar, and 103 sacral.

Three hundred and forty-four lesions had previously undergone external beam irradiation that precluded further conventional irradiation to the involved level. In these 344 patients, prior irradiation was delivered using fractionation schedules ranging from 3 Gy × 10 to 2.5 Gy × 14. Radiosurgery was felt to be indicated in order to limit further radiation dose to the neural structures. Tumor dose was not decreased in a uniform manner in these previously irradiated patients. Instead, the maximum dose to the spinal cord or cauda equina was more

Table 1. Characteristics of the treatment group (n = 500)

Characteristic	Number of cases
Patients with multiple lesions treated	98
Previous external beam irradiation	344
Primary indications for radiosurgery treatment	
Pain	336
Primary treatment modality	65
Tumor progression	51
Progressive neurologic deficit	32
Post-surgical treatment	9
Radiation boost	7
Levels treated	
Cervical	73
Thoracic	212
Lumbar	112
Sacral	103
Skull tracking	68
Fiducial tracking	432
Mean tumor volume, cm^3 (range, 0.20–264)	46
Mean maximum dose, Gy (range, 12.5–25)	20
Mean volume of spinal canal dose >8 Gy, cm^3	0.6

Table 2. Lesion histopathologies (n = 500)

Renal cell	93
Breast	83
Lung	80
Melanoma	38
Colon	32
Sarcoma	26
Prostate	24
Multiple myeloma	18
Unknown primary	14
Squamous cell (laryngeal)	12
Thyroid	11
Other	69

strictly limited, constrained by the CyberKnife's® inverse treatment planning system. The combination of a steep dose gradient and high conformality of the CyberKnife treatment allows for such high doses to be delivered so close to the adjacent critical structures (e.g. the spinal cord). Except in a single case, patients with myelopathy or cauda equina syndrome from direct tumor progression were not felt to be candidates for radiosurgery treatment.

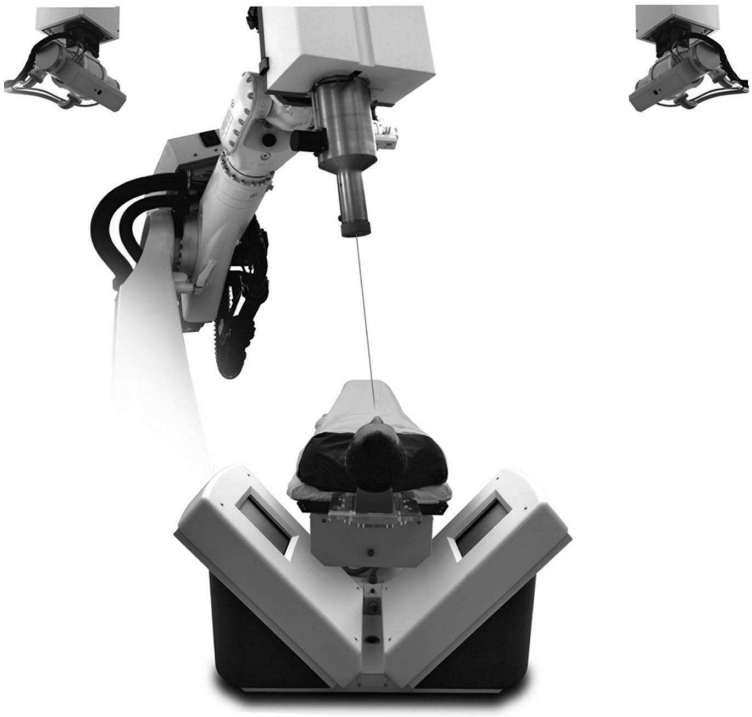

Fig. 1. The CyberKnife radiosurgical system. Note the two amorphous silicon X-ray screens positioned orthogonally to the treatment couch. The couch can move to position the fiducials in front of the cameras. The CyberKnife consists of a linear accelerator mounted on a 6-axis robotic manipulator that permits a wide range of beam orientations.

Exclusion criteria for CyberKnife treatment were: (1) evidence of overt spinal instability or (2) neurologic deficit resulting from bony compression of neural structures. For evaluation of pain relief, a 10-point visual analog scale with intensity description was administered to all patients prior to radiosurgery and 1 month after radiosurgery. The last pain score was used to determine long-term pain control. Pain scores range from (0 = no pain) to 10 (10 the worst imaginable pain). Analgesic usage was also documented.

The CyberKnife system has been described elsewhere (fig. 1) [5, 15, 28, 30–34]. The CyberKnife treatment consists of three distinct components: (1) CT image acquisition based upon skull bony landmarks or implanted bone fiducials (2) treatment planning, and (3) the treatment itself [35, 36]. For cervical spine lesions, CT images were acquired using 1.25 mm thick slices from the top of the skull to the bottom of the cervical spine. All other lesions underwent fluoroscopically-guided percutaneous placement of four to six gold fiducial markers (Alpha-Omega Services, Inc., Bellflower, Calif., USA) into the pedicles immediately adjacent to the lesion to be treated (fig. 2) [36]. CT images were acquired using 1.25 mm thick slices to include the lesion of interest as well as all fiducials and critical

Fig. 2. Gold seed fiducials, stainless steel screws, or tacks may be used for image tracking.

structures. In each case, the radiosurgical treatment plan was designed based on tumor geometry, proximity to spinal cord and location. The prescription dose was independent of the tumor volume. All treatments were performed using a single fraction technique. During the treatment, real time digital X-ray images of the implanted fiducial markers were obtained (fig. 3). The location of the vertebral body being treated was established from these images and is used to determine tumor location as previously described.

Results

Table 1 provides a summary of the clinical characteristics and treatment of the patient cohort. The tumor dose was maintained at 12.5–25 Gy contoured to the edge of the target volume (mean 20 Gy). The prescription dose was chosen based upon currently used intracranial radiosurgery doses as well as the limitation of the maximum dose to the spinal cord as the primary critical structure for each treatment plan. The planning treatment volume was defined as the gross tumor volume with no margin. The dose was prescribed to the 80% isodose line, which covered the planning treatment volume in all cases. Seventy-three cases (i.e. all lesions limited to the cervical spine) were treated using bony landmarks for image guidance. The remaining 427 cases (thoracic, lumbar, and sacral cases) were treated using fiducial tracking. Tumor volume ranged from 0.2 to 264 cm^3 (mean 46 cm^3). During a follow-up ranging from 3 to 53 months (median 21 months), there were no clinically detectable neurological signs that

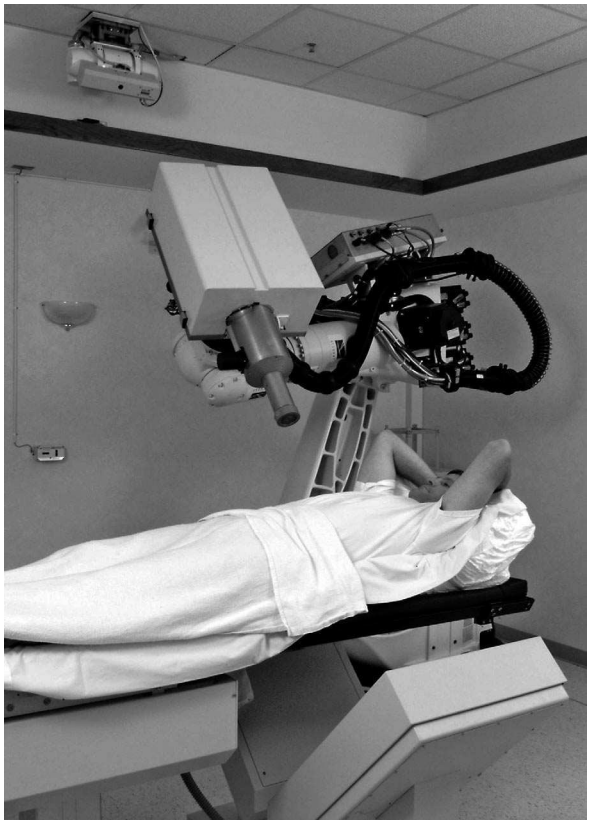

Fig. 3. Patient setup on the CyberKnife treatment couch. The patient is positioned supine with legs in an alpha cradle for comfort and to limit motion. The couch will move rostrally to place the fiducials between the amorphous silicon detectors.

could be attributable to the acute or subacute radiation-induced spine cord injury. Post-treatment magnetic resonance imaging failed to reveal any changes suggestive of radiation induced spinal cord toxicity.

The most frequent indication for the treatment of spinal tumors is pain, and pain was the primary indication for spinal radiosurgery in 336 patients (67%). Radiation is well known to be effective as a treatment for pain associated with spinal malignancies. Spinal radiosurgery was found to be highly effective at decreasing pain in this difficult patient population, with an overall long-term improvement of pain in 290 of the 336 patients (86%), depending upon primary histopathology (table 3). Long-term pain improvement was demonstrated in 96% of women with breast cancer, 96% of patients with melanoma, 94% of patients with renal cell carcinoma, and 93% of lung cancer patients [37, 38].

Table 3. Summary of pain and radiographic outcome for the four most common histopathologies (n = 294)

Long-term pain improvement	
All patients	86%
Renal cell	94%
Breast	96%
Lung	93%
Melanoma	96%
Long-term radiographic control	
All patients	88%
Renal cell	87%
Breast	100%
Lung	100%
Melanoma	75%

Sixty-five patients (13%) underwent spinal radiosurgery as their primary treatment modality (meaning no prior irradiation to the lesion). The ideal lesion should be well circumscribed such that the lesion can be easily outlined (contoured) for treatment planning. The benefits for this treatment option include a single treatment with minimal radiation dose to adjacent normal tissue. In addition, a much larger radiobiologic dose can be delivered compared to external beam irradiation. When used as a primary treatment modality, long-term tumor control was demonstrated on follow-up imaging overall in 90% of cases (in all breast, lung, and renal cell carcinoma metastases, and 75% of melanoma metastases) [37, 38].

Spinal radiosurgery was used to treat radiographic tumor progression in 51 patients (10%). These lesions had already received irradiation with significant spinal cord doses. Currently, spinal radiosurgery is often employed as a 'salvage' technique for those cases in which further conventional irradiation or surgery are not appropriate. Overall long-term radiographic tumor control was 88% for all cases (table 3). Radiographic tumor control differed based upon primary pathology: breast (100%), lung (100%), renal cell (87%), and melanoma (75%). Seven patients with radioresistant tumors (e.g. renal cell carcinoma, melanoma, sarcoma) were treated with spinal radiosurgery after conventional irradiation with or without intensity modulated radiotherapy for a 'boost' treatment with equal long-term radiographic control.

Nine patients (2%) were treated as a post-surgical treatment. Given the steep falloff gradient of the CyberKnife target dose, such treatments can be given early in the post-operative period as opposed to the usual significant delay before standard external beam irradiation is permitted by the surgeon. With the ability to effectively perform spinal radiosurgery, the current surgical approach to these lesions might change. Open surgery for spinal metastases will

likely evolve in a similar manner in which malignant intracranial lesions are debulked in such a way as to avoid neurological deficits and minimize surgical morbidity. The spinal tumors can be removed away from neural structures allowing for immediate decompression, the spine can be instrumented if necessary, and the residual tumor can be safely treated at a later date with radiosurgery, thus further decreasing surgical morbidity. We have found that anterior corpectomy procedures in certain cases can be successfully avoided by posterior decompression and instrumentation alone followed by radiosurgery to the remaining anterior lesion.

Thirty of 35 patients (85%) with progressive neurological deficits prior to treatment experienced at least some improvement. The five patients (renal cell carcinoma 3, lung 2) who failed to improve after radiosurgery had all received prior conventional irradiation. In all five of these cases, open surgical decompression was precluded because of medical co-morbidities. In three patients, the neurological status stabilized; the remaining two progressed to paraplegia.

Discussion

Metastatic spine tumors affect a large number of patients each year resulting in significant pain, destruction of the spinal column causing mechanical instability, and neurological deficits. Standard therapeutic options include surgery and fractionated external beam radiotherapy [3, 39–45]. The first option can be associated with significant morbidity and limited local tumor control. On the other hand, radiotherapy may provide less than optimal pain relief and tumor control since the total dose is limited by the tolerance of adjacent tissues such as the spinal cord. The emerging technique of spinal radiosurgery represents a logical extension of the current state-of-the-art radiation therapy.

The spinal radiosurgery program at the University of Pittsburgh Medical Center currently represents the largest spinal radiosurgery experience in the world [22–24, 26]. This new modality was initially introduced into the treatment paradigm for spinal tumors to a subset of our institution's oncology patient population who did not meet the criteria for other forms of therapy, including conventional radiotherapy and the latest in open surgical techniques. The indications for spinal radiosurgery at our institution have evolved over time and will continue to evolve as clinical experience increases. This is similar to the evolution of indications for intracranial radiosurgery that occurred in the past.

In our series, maximum tumor dose was maintained at 15–22.5 Gy delivered in a single fraction. The appropriate dose for spinal radiosurgery for metastatic tumors to the spine has not been determined. In this series, a maximum tumor dose of 20 or 16 Gy to the tumor margin appeared to provide a good

tumor control with no radiation induced spinal cord or cauda equina injury. Spinal radiosurgery was found to be safe at doses comparable to those used for intracranial radiosurgery without the occurrence of radiation induced neural injury. In the current series, there were no clinically or radiographically identifiable acute or subacute spinal cord damage attributed to the radiation dose with a follow-up period long enough to have seen such events were they to occur [29, 41, 46–50].

In this series, pain was the primary indication for radiosurgery treatment. Eighty-six percent of patients were found to have long-term improvement in their pain after radiosurgery treatment accounting for level of pain medication use. This is similar to the success reported by others using hypofractionated radiotherapy techniques [6–10, 23–26]. Conventional external beam irradiation may provide less than optimal pain relief since the total dose is limited by the tolerance of adjacent tissues (e.g. spinal cord). In some cases, post-treatment imaging revealed pathologic fractures, likely the cause of pain and the reason for radiosurgical failure. Such fractures require either open or closed internal fixation to alleviate the pain due to spinal instability. Nevertheless, single-fraction spinal radiosurgery achieved rapid and durable pain control as well as radiologically documented tumor control in the majority of this patient cohort.

Overall long-term radiographic tumor control was found to be 88% for all cases. When used as a primary treatment modality, long-term tumor control was demonstrated on follow-up imaging in all breast, lung, and renal cell carcinoma metastases, and 75% of melanoma metastases (overall 90%). Spinal radiosurgery was more frequently employed to treat lesions that had previously been treated with other forms of irradiation. The current status of spinal radiosurgery at the present time as it is utilized at many centers is as a 'salvage' technique for patients in which further conventional irradiation or surgery are not appropriate. As greater experience is gained, the technique will likely evolve into an *initial* upfront treatment for spinal metastases in certain cases (e.g. oligometastases). This is similar to the evolution that occurred for the treatment of intracranial metastases using radiosurgery that occurred over the past decade.

There are several advantages to using a stereotactic radiosurgery technique as a primary treatment modality for spinal tumors. Early treatment of these lesions prior to the patient becoming symptomatic and the stability of the spine threatened has obvious advantages [10]. This approach avoids the need to irradiate large segments of the spinal cord. Early stereotactic radiosurgery treatment of spinal lesions may obviate the need for extensive spinal surgeries for decompression and fixation in these already debilitated patients. It may also avoid the need to irradiate large segments of the spinal column, known to have a deleterious effect on bone marrow reserve in these patients. Avoiding open surgery as well as preserving bone marrow function facilitates continuous

chemotherapy in this patient population. Furthermore, improved local control such as has been the case with intracranial radiosurgery could translate into more effective palliation and potentially longer survival.

Spinal radiosurgery might offer improved pain control and a longer *duration* of pain control by giving larger radiobiologic doses. This technique also allows for the treatment of lesions previously irradiated using external beam radiation. Another advantage to the patient is that irradiation can be completed in a single day rather than several weeks. This technique allows for the treatment of lesions previously irradiated using external beam radiation. A large single fraction of irradiation may be more radiobiologically advantageous to certain tumors such as sarcomas, melanomas, and renal cell metastases compared to prolonged fractionated radiotherapy. Clinical response such as pain or improvement of a neurological deficit might also be more rapid with a radiosurgery technique. Finally, the procedure is minimally invasive compared to open surgical techniques and can be performed in an outpatient setting.

References

1 Bruner D, et al: Prospective health related quality of life valuations (utilities) of 8 Gy in 1 fraction vs 30 Gy in 10 fractions of palliation of painful bone metastases: preliminary results of rtog 97–14, Int J Radiat Oncol Biol Phys 2004;60:5142.

2 Wu JK, et al: Meta-analysis of dose-fractionated radiotherapy trials for the palliation of painful bone metastases. Int J Radiat Oncol Biol Phys 2003;55:594–605.

3 Faul CM, Flickinger JC: The use of radiation in the management of spinal metastases. J Neurooncol 1995;23:149–161.

4 Loblaw DA, Laperriere NJ: Emergency treatment of malignant extradural spinal cord compression: an evidence-based guideline. J Clin Oncol 1998;16:1613–1624.

5 Ryu S, et al: Image-guided hypo-fractionated stereotactic radiosurgery to spinal lesions. Neurosurgery 2001;49:838–846.

6 Amendola B, et al: Gamma knife radiosurgery in the treatment of patients with single and multiple brain metastases from carcinoma of the breast. Cancer J 2000;6:88–92.

7 Benzil DL, et al: Safety and efficacy of stereotactic radiosurgery for tumors of the spine. J Neurosurg 2004;101:413–418.

8 Bilsky MH, et al: Intensity-modulated stereotactic radiotherapy of paraspinal tumors: a preliminary report. Neurosurgery 2004;54:823–830.

9 Chang EL, et al: Phase i clinical evaluation of near-simultaneous computed tomographic image-guided stereotactic body radiotherapy for spinal metastases. Int J Radiat Oncol Biol Phys 2004;59:1288–1294.

10 Desalles AA, et al: Spinal lesions treated with novalis shaped beam intensity modulated radiosurgery and stereotactic radiotherapy. J Neurosurg 2004;101:435–440.

11 Milker-Zabel S, et al: Clinical results of retreatment of vertebral bone metastases by stereotactic conformal radiotherapy and intensity-modulated radiotherapy. Int J Radiat Oncol Biol Phys 2003;55:162–167.

12 Ryu S, et al: Image-guided and intensity-modulated radiosurgery for patients with spinal metastasis. Cancer 2003;97:2013–2018.

13 Shiu AS, et al: Near simultaneous computed tomography image-guided stereotactic spinal radiotherapy: an emerging paradigm for achieving true stereotaxy. Int J Radiat Oncol Biol Phys 2003;57:605–613.

14 Hamilton AJ, et al: Preliminary clinical experience with linear accelerator-based spinal stereotactic radiosurgery. Neurosurgery 1995;36:311–319.
15 Chang SD, Adler JR: Current status and optimal use of radiosurgery. Oncol 2001;209–216; discussion 219–221.
16 Gerszten PC, Welch WC: Cyberknife radiosurgery for metastatic spine tumors. Neurosurg Clin N Am 2004;15:491–501.
17 Medin P, et al: Investigations of a minimally invasive method for treatment of spinal malignancies with linac stereotactic radiation therapy: accuracy and animal studies. Int J Radiat Oncol Biol Phys 2002;52:1111–1122.
18 Ryu S, et al: Patterns of failure after single-dose radiosurgery for spinal metastasis. J Neurosurg 2004;101:402–405.
19 Yin FF, et al: Image-guided procedures for intensity-modulated spinal radiosurgery. J Neurosurg 2004;101:419–424.
20 Colombo F, et al: Linear accelerator radiosurgery of cerebral arteriovenous malformations: an update. Neurosurgery 1994;34:14–21.
21 Hitchcock E, et al: Stereotactic linac radiosurgery. Br J Neurosurg 1989;3:305–312.
22 Pirzkall A, et al: Conformal radiotherapy of challenging paraspinal tumors using a multiple arc segment technique. Int J Radiat Oncol Biol Phys 2000;48:1197–1204.
23 Klish MD, et al: Radiation and intensity-modulated radiotherapy for metastatic spine tumors. Neurosurg Clin N Am 2004;15:481–490.
24 Rock JP, et al: Novalis radiosurgery for metastatic spine tumors. Neurosurg Clin N Am 2004;15: 503–509.
25 Song DY, Kavanagh BD, Benedict SH, Schefter D: Stereotactic body radiation therapy rationale, techniques, applications and optimization. Oncology 2004;18:1419–1436.
26 Yamada Y, et al: Multifractionated image-guided and stereotactic intensity modulated radiotherapy of paraspinal tumors: a preliminary report. Int J Radiat Oncol Biol Phys 2005;62:53–61.
27 Gerszten PC, et al: Cyberknife frameless stereotactic radiosurgery for spinal lesions: clinical experience in 125 cases. Neurosurgery 2004;55:89–99.
28 Guthrie B, Adler J: Computer-assisted preoperative planning, interactive surgery, and frameless stereotaxy. Clin Neurosurg 1991;38:112–131.
29 Hatlevoll R, et al: Myelopathy following radiotherapy of bronchial carcinoma with large single fractions: a retrospective study. Int J Radiat Oncol Biol Phys 1983;9:41–44.
30 Adler J, et al: Image-guided robotic radiosurgery. Neurosurgery 1999;44:1–8.
31 Adler JR, et al: Stereotactic radiosurgical treatment of brain metastases. J Neurosurg 1992;76:444–449.
32 Chang SD, et al: An analysis of the accuracy of the cyberknife: a robotic frameless stereotactic radiosurgical system. Neurosurgery 2003;52:140–147.
33 Murphy M, Cox R: The accuracy of dose localization for an image-guided frameless radiosurgery system. Med Phys 1996;23:2043–2049.
34 Murphy MJ, Cox RS: Frameless radiosurgery using real-time image correlation for beam targeting. Med Phys 1996;23:1052–1053.
35 Gerszten P, et al: Feasibility of frameless single-fraction stereotactic radiosurgery for spinal lesions. Neurosurg Focus 2002;13:1–6.
36 Gerszten PC, Welch WC: Cyberknife radiosurgery for the spine. Techniques in Neurosurgery Radiosurgery 2003;9:232–241.
37 Gerszten PC, Burton SA, Ozhasoglu C, Vogel WJ, Welch WC, Baar J, Friedland DM: Stereotactic radiosurgery for spine metastases from renal cell carcinoma. J Neurosurg Spine 2005;3: 288–295.
38 Gerszten PC, Burton SA, Welch WC, Brufsky AM, Lembersky BC, Ozhasogly C, Vogel WJ: Single fraction radiosurgery for the treatment of breast metastases. Cancer 2005;104:2244–2254.
39 Bilsky MH, et al: Operative management of metastatic and malignant primary subaxial cervical tumors. J Neurosurg Spine 2005;2:256–264.
40 Gerszten PC, Welch WC: Current surgical management of metastatic spinal disease. Oncol (Huntington, N.Y.) 2000;14:1013–1024.
41 Kim YH, Fayos JV: Radiation tolerance of the cervical spinal cord. Radiology 1981;139:473–478.

42 Markoe AM, Schwade JG: The role of radiation therapy in the management of spine and spinal cord tumors; in Rea GL (ed): Spine tumors. American Association of Neurological Surgeons. 1994, pp 23–35.
43 Shapiro W, Posner JB, Medical vs surgical treatment of metastatic spinal cord tumors; in Thompson R JG (ed): Controversies in Neurology. Raven Press, New York, 1983; pp 57–65.
44 Sundaresan N, et al: Treatment of neoplastic spinal cord compression: results of a prospective study. Neurosurgery 1991;29:645–650.
45 Sundaresan N, et al: Metastatic tumors of the spine; in Sundaresan B, Schimidek HH, Schiller AL, Rosenthal DL (eds): Tumors of the Spine. Philadelphia WB, Saunders, 1990, pp 279–304.
46 Abbatucci JS, et al: Radiation myelopathy of the cervical spinal cord: time, dose and volume factors. Int J Radiat Oncol Biol Phys 1978;4:239–248.
47 Boden G: Radiation myelitis of the cervical spinal cord. Br J Radiol 1948;21:464–469.
48 McCuniff AJ, Liang MJ: Radiation tolerance of the cervical spinal cord. Int J Radiat Oncol Biol Phys 1989;16:675–678.
49 Phillips TL, Buschke F: Radiation tolerance of the thoracic spinal cord. AJR Am J Roentgenol 1969;105:659–664.
50 Wara WM, et al: Radiation tolerance of the spinal cord. Cancer 1975;35:1558–1562.

Peter C. Gerszten, MD, MPH
Department of Neurological Surgery, Suite B-400
Presbyterian University Hospital
200 Lothrop St.
Pittsburgh, PA 15213 (USA)
Tel. +1 412 647 0958, Fax +1 412 647 0989
E-Mail gersztenpc@upmc.edu

Kondziolka D (ed): Radiosurgery. Basel, Karger, 2006, vol 6, pp 211–220

Long-Term Follow-Up of Quality of Life after Gamma Knife Radiosurgery Treatment for Arteriovenous Malformations

Michael J. Musacchio, Jr., Brian Kuchay, Nimesh H. Patel, Sepehr B. Sani, Demetrius K. Lopes

Department of Neurosurgery, Rush University Medical Center, Chicago, Ill., USA

Abstract

Introduction: Gamma Knife radiosurgery (GKR) is a standard treatment modality for intracranial arteriovenous malformations (AVMs). The efficacy and safety of this procedure is well accepted; yet, there is a relative lack of long-term studies in the literature to support its low morbidity. The goal of this study is to obtain quality of life and complication rate data at long-term follow-up on patients with AVMs treated by GKR. **Methods:** We independently reviewed 177 GKR procedures performed between 1989 and 2001 at a single institution for the treatment of intracranial AVM. Through chart review and direct patient contact, we attained greater than 4-year follow-up on 40 patients. Clinical outcome was evaluated using a modified Rankin scale. For statistical analysis, we constructed scatter plots and comparison of variables using Student's t-testing to investigate predictors of clinical outcome after GKR. **Results:** Average follow-up was 100 $\pm$ 52 months (range, 48–189). Average pre-operative Rankin score was 1 $\pm$ 0.6 (range, 0–2), compared to average post-operative Rankin score of 0.8 $\pm$ 0.7 ($p = 0.003$). 33 patients (83%) had the same pre and post Rankin score, seven patients (17%) improved, and no patients worsened. Only two patients (5%) experienced major complications defined as requiring surgery for radiation necrosis, occurring at 36 and 64 months. Four others (10%) suffered minor transient neurological events, which were self-limited or resolved with medical therapy. No correlation was found between outcome and AVM grade, location, method of presentation, age of patient, or radiation dosing parameters. **Conclusion:** GKR is a safe and effective modality for the treatment of AVM. The immediate impact of treatment on quality of life is minimal. However, we recommend extended follow-up of these patients for surveillance of potential long-term complications.

Gamma Knife radiosurgery (GKR) has become a widely accepted treatment modality for intracranial arteriovenous malformations (AVM). GKR is particularly appropriate for AVMs located in deep or eloquent brain tissue, which have traditionally been considered suboptimal for surgical resection secondary to the threat of injury to surrounding brain parenchyma. This therapy has been proven to be an effective and safe modality in the treatment of AVMs, but it is not entirely without risks or complications. Post-procedural hemorrhage and cyst formation, as well as various other neurological deficits, are well-described complications of this procedure [1–9].

The literature regarding complication types and rates associated with this therapeutic modality is growing, but there remains a need for more long-term follow-up studies. Of particular importance is the lack of reports on functional outcome after GKR, and on the clinical variables that potentially influence this outcome. The object of this study is to investigate the long-term clinical outcome and complication rate associated with GKR for intracranial AVMs, paying particular attention to clinical variables as predictors of adverse clinical outcomes.

Clinical Materials and Methods

This is an independent review of 177 GKR procedures performed at a single institution over a 12 year period (1989–2001) for the treatment of intracranial AVM. Through chart review and direct patient contact, we obtained clinical outcome and complication rate data on all patients who underwent this therapeutic modality. We then selected only those patients with 4 years or more of clinical follow-up data, compiling the 40 patients in this report.

Patient Population

All 40 patients with received GKR therapy under the care of the Chicago Institute of Neurosurgery and Neuroresearch (CINN) using the Leksell Gamma Knife (Elekta Instruments, Atlanta, Ga., USA).

The average follow-up length of the patients in this study was 100 ± 52 months (range, 48–189 months). There were 21 females and 19 males with an average age of 34 ± 13 years (range, 8–62 years). No patient had more than one AVM treated, and no patient had repeat GKR at this institution.

The methods of AVM presentation in these patients included 16 patients (40%) presenting with seizure, 13 patients (33%) presenting with hemorrhage, and 11 patients (27%) presenting incidentally. There were three (8%) Spetzler-Martin grade I AVMs, seven (18%) grade II, 16 (40%) grade III, nine (22%) grade IV, two (5%) grade V, and three (8%) with indeterminate grade [15]. Thirtyone patients (78%) had there aneurysms located in eloquent brain tissue [10]. Patient demographic and clinical presentation data is summarized in table 1.

Treatment Data

Nine patients underwent treatment of their AVM prior to GKR: seven underwent embolization, one underwent surgical resection, and one had previously undergone both surgery and embolization.

Table 1. Patient demographics and clinical presentation data

Patients	40
Average age	34 years
Ratio of male:female	19:21
Average follow-up	100 months
Method of presentation	
Seizure	16 (40%)
Hemorrhage	13 (33%)
Incidental	11 (27%)
Spetzler-Martin AVM grade	
I	3 (8%)
II	7 (18%)
III	16 (40%)
IV	9 (22%)
V	2 (5%)
AVM location	
Eloquent	31 (78%)
Non-eloquent	9 (22%)

The average maximum dose delivered to the AVMs was 48 ± 9 Gy (range, 18–60 Gy). The average dose delivered to the periphery of the AVM was 22 ± 3 Gy (range, 16–26 Gy). The average number of shots delivered was 9 ± 8 (range, 1–34).

Outcome Measures

The measured outcomes in this study included patient functional outcome and complication rate. Patient functional outcome was qualified using a modified Rankin scale (MRS) which assigns a score ranging from zero (no symptoms) to six (dead) representing patients' level of functionality [11]. By assigning each patient a pre-procedural and post-procedural MRS, we determined functional outcome related to the Gamma Knife procedure. We defined complication by the occurrence of either a worsened post-procedural MRS or need for surgical correction of a post-procedural event.

For statistical analysis, we constructed scatter plots and comparison of variables using Student's t-testing to investigate predictors of clinical outcome after GKR.

Results

There were 40 patients in the series who met the criteria of 4 years or more of clinical follow-up. Two patients (5%) experienced post-procedural complications, both of which were defined as cyst formation requiring surgical resection. No patient experienced a worsened post-procedural MRS. One complication occurred at 36 months post-procedure and the other occurred at 64 months.

Table 2. Summary of main outcome measures

Modified Rankin score	
Mean pre-procedural Rankin score ± SD	1 ± 0.6 (p = 0.003)
Mean post-procedural Rankin score ± SD	0.8 ± 0.7 (p = 0.003)
Post-operative change in Rankin score	
No change	33 (83%)
Improved	7 (17%)
Worsened	0 (0%)
Complications	2 (5%)
Symptomatic radiation necrosis requiring resection	2
Average time to complication	50 months
Transient neurologic deficit	4 (10%)
New onset of seizure	2
Transient hemiparesis	1
Transient visual disturbance	1
Average time to complication	19 months

Both patients recovered to pre-procedural functional baseline after cyst resection (table 2).

Four other patients (10%) experienced post-procedural transient neurological deficit that resolved either spontaneously or with medical therapy. Two of these patients developed new onset of seizure, both of which occurred at six months post-procedure and both were well-controlled with anti-epileptic therapy. One patient experienced transient visual disturbance which was self-limited. The final patient experienced transient hemiparesis which resolved with a short course of corticosteroid therapy. The average time to transient deficit was 19 ± 18 months (range, 6–45 months). The above six patients who experienced either complications or transient neurological deficits are described in greater detail in table 3.

None of the 40 patients in this series displayed a pre- or post-procedural MRS worse than two. The mean pre-procedural MRS was 1 ± 0.6 (range, 0–2), while the mean post-procedural MRS was 0.8 ± 0.7 (range, 0–2) (p = 0.003). 33 patients (83%) experienced no change in their post-procedural MRS compared to their pre-procedural MRS. Seven patients (17%) had an improved post-procedural MRS. No patient (0%) had a worse post-procedural MRS (table 4).

No patients experienced post-procedural hemorrhage. One patient died 5 years after GKR secondary to pneumonia. Three patients (8%) subsequently underwent re-treatment for residual AVM: one patient had a second Gamma Knife procedure at another institution, one patient had embolization, and one patient had surgical resection.

Table 3. Detail of patient demographics and clinical variables associated with the two patients who suffered complications and the four patients with transient neurological deficits

	Time to complication months	Length of follow-up months	Age	Presentation	Grade	Location	Radiation dose, Gy		
							Maximum	Minimum	Shots
Complication									
Radiation necrosis	36	60	32	hemorrhage	4	eloquent	45	18	11
Radiation necrosis	64	174	35	seizure	2	non-eloquent	60	24	10
Transient neurological deficit									
Seizure onset	6	51	33	hemorrhage	5	eloquent	40	20	12
Seizure onset	6	61	62	headache	3	non-eloquent	50	20	12
Transient hemiparesis	45	51	32	seizure	2	non-eloquent	50	20	10
Transient visual deficit	18	185	34	hemorrhage	3	eloquent	50	25	4

Table 4. Comparison of pre-procedural and post-procedural modified Rankin scores divided among those patients who suffered no adverse events, the four patients who experienced transient neurological deficits, and the two patients who suffered post-procedural complications

Rankin score	No events		Transient events		Complications	
	pre-procedural	post-procedural	pre-procedural	post-procedural	pre-procedural	post-procedural
0	9	14	0	0	0	0
1	18	15	4	4	2	2
2	7	5	0	0	0	0

Evaluation of Predictors of Poor Outcome

We evaluated multiple variables for their predictive value of complication or worsened functional outcome after GKR. These variables included radiation dosimetry with regard to level of dose given maximally and to the periphery, as well as number of shots delivered. Furthermore, we evaluated patient age, AVM grade, AVM location, and method of presentation as predictors of clinical outcome. We found no correlation between occurrence of complication and any of the aforementioned variables. No formal statistical analysis was indicated due to the low number of complications.

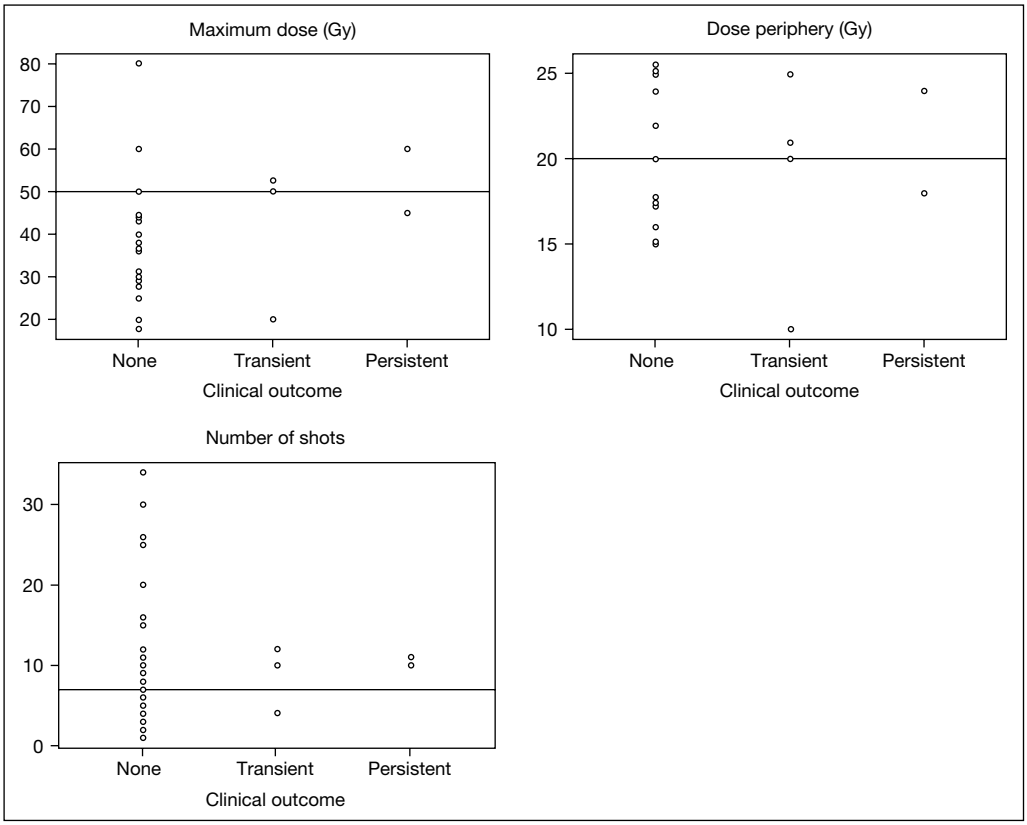

Fig. 1. Scatter plots constructed to illustrate lack of correlation between clinical outcome and maximum radiation dose, dose at periphery, or number of shots delivered. Clinical outcomes are grouped into no deficit, transient deficit, and persistent deficit (correlating to occurrence of complication). The horizontal line in each graph represents the median value.

Level of radiation was quantified as maximum dose delivered, dose delivered to the periphery, and number of shots given. There was no correlation found between these parameters and occurrence of either complication or transient neurological deficit. These results are summarized in figure 1.

The patients in this study encompassed a wide distribution of ages, with average age of 34 and range of 8–62 years. No remarkable aberrancies in age were found among the patients who experienced complication or transient neurological deficits.

The Spetzler-Martin AVM grades of the two patients who experienced complications were grades II and IV. The AVM grades of the four patients who

experienced transient neurological deficits include one grade II, two grade III, and one grade V. Of the two patients who experienced complications, one patient had their AVM in eloquent brain tissue while the other's AVM was located in non-eloquent brain tissue. Two patients who experienced transient neurological deficits had AVMs located in eloquent tissue, while the other two had AVMs in non-eloquent tissue. With both AVM grade and eloquent vs. non-eloquent location, parameters were well-distributed and displayed no correlation to poor clinical outcome after GKR.

Finally, the methods of clinical presentation were evenly distributed among seizure, hemorrhage, and incidental between those patients who experienced complication, transient neurological deficit, or no adverse event. Again, no correlation was found between method of presentation and poor clinical outcome.

Discussion

Occurrence of Adverse Clinical Events after GKR for AVM

Gamma Knife radiosurgery for the treatment of intracranial AVMs has been well-described to be a safe and effective therapeutic modality. Possible adverse events specific to GKR therapy for AVMs include post-procedural cyst formation, hemorrhage, and various neurological deficits typically related to injury to brain structures located in close proximity to the AVM [1–9]. In this series, only two patients (5%) developed complications defined as symptomatic cyst formation requiring surgical resection. Both patients returned to pre-procedural baseline with complete resolution of symptoms after cyst resection.

The sole complication type observed in the 40 patients in this study was formation of a symptomatic post-procedural cyst in two patients. These cysts developed at 36 and 64 months post-procedure. Pan et al. [5], described the incidence of cyst formation to be 1.6% overall, and 3.6% in patients followed for greater than five years. The author found that the incidence of cyst formation increases with increased length of follow-up, with highest incidence in those patients followed for five or more years. Similarly, Yamamoto et al. [8], found a 5% incidence of delayed symptomatic cyst formation after GKR occurring at greater than 5 years after irradiation of AVM, with a 23% incidence of symptomatic or asymptomatic delayed cysts found in patients undergoing neuroimaging follow-up (CT or MR) greater than 5 years after irradiation. Izawa and Hayashi [4], reported a 3% incidence of delayed cyst formation with a mean length of follow-up of almost eight years. In our series, the delayed presentations of symptomatic cysts support the need for extended post-procedural follow-up for identification of potential adverse events.

Transient neurological deficits are likely quite common in patient undergoing GKR, but rarely reported. We observed 10% of our patient population to experience transient neurological deficits as defined by events occurring either in a self-limited fashion or reversible with medical management. While these events had no impact on the long-term clinical outcome of patients who received GKR therapy, they did create short-term disturbances requiring addition of medications, and, potential hospitalization.

Not surprisingly, we found a low rate of adverse clinical events after GKR treatment of AVM in our study. Our complication rate of 5% compares quite favorably to the natural history of intracranial AVMs. With annual rupture rate of AVMs ranging from 2 to 4%, GKR therapy is clearly an acceptable therapeutic modality [3, 12–17]. Of importance in our series, is the high percentage of patients whose AVMs were located in eloquent brain tissue (78%). AVMs in eloquent brain tissue are generally regarded as poor surgical candidates secondary to the risk of injury to surrounding tissue. Our patients were, therefore, appropriately well-selected against surgery as evidenced in the low complication rate and good clinical outcome.

Measuring Patient Functionality

In this study, we qualified patient functional outcome via comparison of pre-procedural and post-procedural modified Rankin scores. We found that treatment of AVM with GKR has no significant negative impact on clinical outcome. No patient is this study had a worsened post-procedural MRS. The vast majority (83%) of the patients in this study exhibited no change in their MRS scores post-procedurally. The few patients that did have improved MRS grades (17%) are more likely to be a reflection of the natural history of the disease rather than a true beneficial effect of gamma knife therapy.

In order to quantify patients with poor clinical outcomes in this study, we determined the definition of a complication to be a patient who suffered either a worsened post-operative MRS or one that required surgical correction of a post-procedural clinically significant event. While we saw no patients with worsened MRS grade, we did see two patients who required surgical resection of symptomatic cysts. These two patients subsequently returned to their pre-procedural functional level after surgical resection of their cysts. We, therefore, can conclude that the functional clinical outcome of patients with AVM is minimally affected by GKR therapy, if at all.

Correlation of Clinical Variables

We reviewed several clinical and radiosurgical variables associated with each patient in order to observe any relationships or patterns that may exist between these variables and clinical outcome after GKR. We found no correlation

between clinical outcome after GKR and patient demographical or radiation dosimetry variables.

Many factors have been described to be associated with higher incidence of complications after GKR for AVM. The most commonly cited variables include patient age, AVM nidus volume, location in eloquent brain tissue, and higher maximum dose of radiation [2, 4, 6]. In this study, we evaluated patient age, AVM grade and location, and method of AVM presentation and found no predictors of poor outcome or occurrence of complication. We also evaluated maximum radiation dose, dose at periphery, and number of shots delivered, again, finding no predictors of adverse events. Due to the low number of complications in this study and the absence of worsened post-procedural MRS grade, no formal statistical analysis was possible.

Limitations

This report is an independent review of patients treated by our affiliated institution (CINN) between 1989 and 2002. We recognize the detriment of only following 40 patients for 4 years or more; however, the impact of this patient follow-up is minimal and does not detract from the overall results of this study.

Conclusion

Intracranial arteriovenous malformations may be safely treated with a low incidence of adverse events by Gamma Knife radiosurgery. The functional outcome of patients treated is minimally impacted upon by GKR. While complications are rare, there occurrence is often delayed indicating the need for long-term clinical follow-up after therapy.

Acknowledgements

We thank the Chicago Institute of Neurosurgery and Neuroresearch (CINN), Leonard J. Cerullo MD, Tomasz Helenowski MD, Harish Thakrar, MD, and Susan Leurgans, PhD.

References

1 Flickinger JC, Kondziloka D, et al: A multiple-institutional analysis of complication and outcomes after arteriovenous malformation radiosurgery. Int J Radiat Oncol Biol Phys 1999;44:67–74.
2 Friedman WA, Blatt DL, Bova FJ, Buatti JM, Mendenhall WM, Kubilis PS: The risk of hemorrhage after radiosurgery for arteriovenous malformations. J Neurosurg 1996;84:912–919.
3 Graf CJ, Perret GE, Torner JC: Bleeding from cerebral arteriovenous malformations as part of their natural history. J Neurosurg 1983;58:331–337.

4 Izawa M, Hayashi M: Long-term complications after gamma knife surgery for arteriovenous malformations. J Neurosurg 2005;102(suppl):34–37.
5 Pan HC, Sheehan J, Stroila M, Steiner M, Steiner L: Late cyst formation following gamma knife surgery of arteriovenous malformations. J Neurosurg 2005;102:124–127.
6 Pollock BE, Flickinger JC: A proposed radiosurgery-based grading system for arteriovenous malformations. J Neurosurg 2002;96:79–85.
7 Pollock BE, Flickinger JC, Lunsford LD, Bissonette DJ, Konziolka D: Hemorrhage risk after stereostactic radiosurgery of cerebral arteriovenous malformations. Neurosurgery 1996;38:652–659.
8 Yamamoto M, Jimbo M, et al: Gamma knife radiosurgery for arteriovenous malformations: Long-term follow-up results focusing on complications occurring more than 5 years after irradiation. Neurosurgery 1996;38:906–914.
9 Yamamoto Y, Coffey RJ: Interim report on the radiosurgical treatment of cerebral arteriovenous malformations: the influence of size, dose, time, and technical factors on obliteration rate. J Neurosurg 1995;83:832–837.
10 Spetzler RF, Martin NA: A proposed grading system for arteriovenous malformations. J Neurosurg 1986;65:476–483.
11 UK-TIA Study Group: The UK-TIA Aspirin Trial: Interim Results. Br Med J 1988;296:L316–L320.
12 Barrow DL, Reisner A: Natural history of intracranial aneurysms and vascular malformations. Clin Neurosurg 1993;40:3–39.
13 Brown RD, Wiebers DO, et al: The natural history of unruptered intracranial arteriovenous malformations. J Neurosurg 1988;68:352–357.
14 Crawford PM, West CR, et al: Arteriovenous malformations of the brain: natural history in unoperated patients. J Neurol Neurosurg Psychiatr 1986;49:1–10.
15 Fults D, Kelly DL: Natural history of arteriovenous malformations of the brain: a clinical study. Neurosurgery 1984;15:658–662.
16 Itoyama Y, Uemura S: Natural course of unoperated intracranial arteriovenous malformations: study of 50 cases. J Neurosurg 1989;71:805–809.
17 Ondra SL, Troupp H, et al: The natural history of symptomatic arteriovenous malformations of the brain: a 24-year follow-up assessment. J Neurosurg 1990;73:387–391.

Michael J. Musacchio, Jr.
1725 West Harrison Street, Suite 1115
Chicago, IL 60612 (USA)
Tel. +1 312 942 6628, Fax +1 312 563 3358
E-Mail Michael_musacchio@rush.edu

Kondziolka D (ed): Radiosurgery. Basel, Karger, 2006, vol 6, pp 221–228

Validation of a Radiosurgery-Based Grading System for Arteriovenous Malformations

John S. Lee[a], *Michael R. Girvigian*[a], *Michael J. Miller*[a], *Javad Rahimian*[a], *Joseph C.T. Chen*[b], *Hugh E. Greathouse*[b], *Michael Tome*[a]

Departments of [a]Radiation Oncology and [b]Neurosurgery, Southern California Permanente Medical Group, Los Angeles, Calif., USA

Abstract

Purpose: The Spetzler-Martin grade (SMG) accurately predicts outcome after surgical resection of arteriovenous malformations (AVM); however, its application to radiosurgery is limited because of insensitivity to AVM volume and location. Recently, a radiosurgical grading system was developed by the University of Pittsburgh/Mayo Clinic to predict outcomes for Gamma Knife® radiosurgery. This retrospective study seeks to independently validate the radiosurgery grade (RSG) and determine its application to linear accelerator-based radiosurgery. **Methods and Materials:** Twenty patients were treated with Radionics XKnife™ LINAC-based radiosurgery for AVMs between 1990 and 2002 (median follow-up, 35 months). Outcomes based on obliteration rates and post-treatment neurological deficits were analyzed according to RSG and SMG. The following equation describes the RSG: AVM score = (0.1) (AVM volume in cm^3) + (0.02) (age in years) + (0.3) (location) with frontal/temporal = 0; parietal/occipital/intraventricular/corpus callosum/cerebellar = 1; and basal ganglia/thalamus/brainstem = 2. **Results:** Overall, 65% had excellent outcomes, 0% good, 5% fair, 25% unchanged, and 5% poor. Excellent outcomes were achieved in 100, 50 and 20% of patients with RSG 0.6–1.3, 1.4–1.7, and 1.9–2.4, respectively. Spearman's correlation coefficient for RSG versus excellent/non-excellent outcomes was 0.70 ($p = 0.0014$). For SMG 1–4, the percentage of patients with excellent outcomes were 100, 56, 80, and 0%, respectively. The SMG Spearman's correlation coefficient was 0.34 ($p = 0.15$). Two patients (10%), with RSGs of 1.9 and 1.6, developed radionecrosis. No post-radiosurgery hemorrhage or AVM-related deaths occurred. **Conclusions:** The RSG accurately predicted excellent patient outcomes, thus validating this grading system and suggesting its applicability to linear accelerator-based radiosurgery for AVMs. Future research for AVMs treated with radiosurgery should now report outcomes using this RSG.

The Spetzler-Martin grade (SMG) for arteriovenous malformations (AVM), which incorporates AVM size, location, and venous drainage pattern, has been proven in multiple surgical series to be predictive of both obliteration and post-operative neurological complications [1–6]. Lesions ≤3 cm with lower SMGs have traditionally been felt to be good surgical candidates. However, the SMG has limited applicability for radiosurgery because of its insensitivity to AVM volume and location. For example, two non-eloquent AVMs measuring 1 and 2.9 cm, would both be categorized as SMG 1; but, the volumes would be approximately 0.5 cm^3 and 13 cm^3, respectively with dramatically different obliteration rates.

Because of these factors, Pollock and Flickinger developed a radiosurgery-based grading system [7–9]. Multivariate analysis and regression analysis modeling of 220 patients, who were treated with Gamma Knife® radiosurgery at the University of Pittsburgh Medical Center, identified AVM volume, patient age, and AVM location as variables predictive of excellent outcomes. A mathematical formula incorporating these variables was then developed to determine patients' RSG [AVM score = (0.1) (AVM volume in cm^3) + (0.02) (age in years) + (0.3) (location)]. This grading system was subsequently tested on 136 patients treated at the Mayo Clinic, which showed excellent outcomes in >95, 80, 70, 60, 50, and <40% for patients with AVM scores ≤1, 1.25, 1.5, 1.75, 2, and >2, respectively.

In this study, we seek to independently validate the RSG for patients treated in the community setting with linear accelerator-based radiosurgery [10–15].

Methods and Materials

Patient Population

Between 1990 and February 2004, 48 patients with AVMs were treated with radiosurgery at the Kaiser Permanente Regional Radiation Oncology Center. Of the initial 34 patients, who received Radionics XKnife™ LINAC-based radiosurgery between 1990 and 2002, 20 had adequate follow-up consisting of angiography or MRI. Fourteen patients were lost to follow-up and excluded from this study. Comparison of these patients showed similar presenting signs, AVM volumes, and SMGs. Another 14 patients were treated with BrainLAB Novalis® Shaped Beam Surgery between October 2002 and February 2004. These patients were also excluded and will be presented in a subsequent study. Patient characteristics are presented in table 1.

Radiosurgical Technique

All patients had Radionics XKnife LINAC-based radiosurgery with BRW head ring immobilization. Treatment planning and AVM demarcation incorporated contrast-enhanced computed tomography and angiography for tumor volume delineation and cone size selection.

Table 1. Patient characteristics

Characteristics	Total: 20 patients
Median age in years (range)	41 (16–68)
Hemorrhage at presentation	55%
Prior embolization	15%
Prior surgery	15%
Prior radiosurgery	5%
Median AVM volume in cm^3 (range)	2.5 (0.22–11)
Spetzler-Martin grade	
1	20%
2	45%
3	25%
4	10%

Table 2. Designation of outcomes

Outcomes	Obliterated AVM versus persistent AVM	New neurological deficit after radiosurgery
Excellent	Obliterated	None
Good	Obliterated	Minor[a]
Fair	Obliterated	Major[b]
Unchanged	Persistent	None
Poor	Persistent	Minor or major

[a]Minor deficit: any new neurological deficit that did not significantly alter the patient's daily function, such as quadrantanopsia, ataxia or cranial nerve abnormality.

[b]Major deficit: any new neurological deficit significantly interfering with the patient's daily function, such as radionecrosis, hemiparesis, aphasia, or homonymous hemianopsia.

In general, 4 or 5 non-coplanar arcs were used to deliver a median dose of 1,600 cGy to the AVM margin (range 1,440–2,000 cGy).

Patient Outcomes

Patients were evaluated with cerebral angiography or magnetic resonance imaging/angiography to document persistent or obliterated AVMs. Outcomes were determined to be excellent, good, fair, unchanged, or poor based on the combination of AVM response to radiosurgery and whether new neurological deficits developed after treatment. Table 2 describes the criteria for each outcome designation.

Table 3. Results after radiosurgery

Results	Number of patients
AVM obliteration	14 (70%)
Post-radiosurgery hemorrhage	0
Radionecrosis	2 (10%)
Patient outcomes	
Excellent	13 (65%)
Good	0
Fair	1 (5%)
Unchanged	5 (25%)
Poor	1 (5%)
Death	0

Grading System

The RSG is as follows: AVM score = (0.1) (AVM volume in cm^3) + (0.02) (age in years) + (0.3) (location) with location given scores of 0 for frontal/temporal, 1 for parietal/occipital/intraventricular/corpus callosum/cerebellar, and 2 for basal ganglia/thalamus/brainstem. AVM volumes were estimated based on measurements from angiography or MRI using $4/3\pi r$ for spherical lesions or $(\pi/6)$ (length) (width) (height) for non-spherical lesions.

Statistical Analysis

Spearman's test was used to correlate excellent and non-excellent outcomes with SMG and RSG. Clinical outcomes for SMG and RSG were also compared using Fisher's exact test. Two-sided p values of ≤ 0.05 were considered statistically significant.

Results

Overall Results

Table 3 shows actuarial results for all evaluated patients not stratified by RSG or SMG. Two cases of radionecrosis were documented at 14 months and 24 months after radiosurgery, which presented as seizure, altered mental status, or slurred speech. Their characteristics are summarized in table 4.

Results by Radiosurgical Grade

Actuarial data for patients grouped by RSG are presented in table 5. For RSG 0.6–1.3, 1.4–1.7, and 1.9–2.4, the percentage of patients with excellent outcomes were 100, 50, and 20%, respectively. An association between RSG and excellent/non-excellent outcomes was shown by Fisher's exact test ($p = 0.0013$) and Spearman's correlation coefficient of 0.70 ($p = 0.0014$).

Table 4. Characteristics of patients having radionecrosis

	Spetzler-Martin grade	Radiosurgery grade	Volume cm^3	Dose at margin, cGy	Time of diagnosis months
Patient 1	2	1.9	7	1,600	14
Patient 2	4	1.6	6.6	1,700	24

Table 5. Results by radiosurgery grade

Radiosurgery score	No. of patients/total	%	Results
0.6–1.3	9/9	100	Excellent
1.4–1.7	3/6	50	Excellent
	1/6	17	Fair
	2/6	33	Unchanged
1.9–2.4	1/5	20	Excellent
	3/5	60	Unchanged
	1/5	20	Poor

Table 6. Results by Spetzler-Martin grade

Spetzler-Martin	No. of patients/ total	%	Results
1	4/4	100	Excellent
2	5/9	56	Excellent
	3/9	33	Unchanged
	1/9	11	Poor
3	4/5	80	Excellent
	1/5	20	Fair
4	1/2	50	Fair
	1/2	50	Unchanged

Results by Spetzler-Martin Grade

Table 6 shows actuarial results for patients stratified by SMG. For SMG 1–4, the percentage of patients with excellent outcomes were 100, 56, 80, and 0%, respectively. Although a correlation was found between SMG and excellent/non-excellent outcomes by Fisher's exact test ($p = 0.0081$), Spearman's correlation coefficient was insignificant at 0.34 ($p = 0.15$).

Discussion

In our study, AVM patients were treated with Radionics XKnife LINAC-based radiosurgery. Both Spearman's correlation coefficient and Fisher's exact test showed a statistically significant association between RSG and excellent outcomes. However, SMG inconsistently predicted excellent outcomes as indicated by the Spearman's correlation coefficient of 0.34 ($p = 0.15$). Because of the small population of patients studied, these data should be interpreted with some caution. Nevertheless, our results in conjunction with the University of Pittsburgh/Mayo Clinic's data offer evidence of the RSG's validity. This certainly warrants additional clinical research to further clarify the application of the RSG to AVM patients.

Because the SMG is insensitive to AVM volume and location, Pollock and Flickinger developed a three-variable RSG to more accurately predict outcomes after radiosurgery [7–9]. This formula was initially tested on 136 patients treated with Gamma Knife radiosurgery. There results showed a highly significant correlation between RSG and excellent patient outcomes ($p = 0.0001$). Patients had $>$95, 80, 70, 60, 50, and $<$40% excellent outcomes with RSG $<$1.0, 1.25, 1.5, 1.75, 2.0, and $>$2.0, respectively. SMG did not significantly predict AVM obliteration ($p = 0.15$) or excellent patient outcomes ($p = 0.13$) on univariate analysis.

The original publication by Pollock and Flickinger only analyzed patients with post-radiosurgery angiographic follow-up [7]. In our study, only three patients (15%) had angiograms after radiosurgery. Instead, the remaining patients had documented obliteration confirmed by magnetic resonance angiography (MRA). The authors believe MRA may possibly be an acceptable alternative for AVM evaluation after radiosurgery as MR imaging has been shown to be accurate for detecting AVM obliteration and assessing the progress of nidus reduction [16–18]. Pollock et al. [16] evaluated 140 AVM patients treated with radiosurgery. All patients were followed with MR imaging and subsequent cerebral angiography as a control at a median of 24 months post-radiosurgery. MR imaging was 80% sensitive for identifying patent AVMs and 100% specific for angiographic obliteration. Only 16% of patients had false-negative MR images (84% negative predictive value). A similar report from Guo et al. [17] also concluded that AVM regression and obliteration can be accurately verified by MRA for medium- to large-volume AVMs. As a result, we believe the findings of this study should be valid regardless of the imaging method used for follow-up after radiosurgery.

Generally, AVMs with large size/high SMGs are treated with combinations of embolization, radiosurgery, and/or surgery to allow the highest probability of obliteration with acceptable treatment-related side effects [19–24]. Five patients in this study had AVM volumes greater than 6 cm^3. Three patients had unchanged outcomes, 1 fair, and 1 poor. Two patients had embolization prior to radiosurgery, and

3 patients had radiosurgery as their only therapy. Two of the 3 patients treated with radiosurgery alone developed radionecrosis at 14 months and 24 months after treatment. These patients had SMGs 2 and 4, RSGs 1.9 and 1.6, volumes of 7 cm^3 and 6 cm^3, and margin doses of 1,600 and 1,700 cGy. Chang et al. [19] reported results of patients with giant AVM measuring greater than 6 cm at maximum diameter. Nearly all patients were offered multimodality therapy with 9% receiving embolization followed by surgery, 43% with embolization followed by radiosurgery, and 43% with embolization, radiosurgery, and surgery. Despite the large sizes of AVMs, multimodality therapy resulted in 51% excellent outcomes, 28% good, and 6% poor with 15% overall treatment-related morbidity rate. Gobin et al. [20] showed that embolization followed by radiosurgery for mostly SMG III–VI had 65% obliteration, 1.6% mortality, and 12.8% morbidity. In total, the data indicates that radiosurgery alone for large AVMs likely has unacceptable obliteration rates and higher risks of complications, whereas multimodality therapy may provide more excellent outcomes with acceptable treatment-related morbidity.

Conclusion

The RSG accurately predicted patient outcomes, thus validating this grading system and suggesting its applicability to linear accelerator-based radiosurgery for AVMs. This system provides clinicians with another tool to offer informed consent to patients regarding the probability of AVM obliteration and treatment-induced neurological deficits after radiosurgery. Future research for AVMs treated with radiosurgery should now report outcomes using this RSG in order to standardize the data for comparative analysis.

Acknowledgement

The authors wish to thank Janis Yao for the statistical analysis.

References

1 Spetzler RF, Martin NA: A proposed grading system for arteriovenous malformations. J Neurosurg 1986;65:476–483.
2 Heros RC, Korosue K, Diebold PM: Surgical excision of cerebral arteriovenous malformations: late results. Neurosurgery 1990;26:570–577.
3 Zhao J, Wang S, Li J, et al: Clinical characteristics and surgical results of patients with cerebral arteriovenous malformations. Surg Neurol 2005;63:156–161.
4 Pik JHT, Morgan MK: Microsurgery for small arteriovenous malformations of the brain: results in 110 consecutive patients. Neurosurgery 2000;47:571–577.
5 Pikus HJ, Beach ML, Harbaugh RE: Microsurgical treatment of arteriovenous malformations: analysis and comparison with stereotactic radiosurgery. J Neurosurg 1998;88:641–646.

6 Schaller C, Schramm J: Microsurgical results for small arteriovenous malformations accessible for radiosurgical or embolization treatment. Neurosurgery 1997;40:664–674.
7 Pollock BE, Flickinger JC: A proposed radiosurgery-based grading system for arteriovenous malformations. J Neurosurg 2002;96:79–85.
8 Pollock BE, Flickinger JC, Lunsford LD: Factors associated with successful arteriovenous malformation radiosurgery. Neurosurgery 1998;42:1239–1244.
9 Pollock BE, Gorman DA, Coffey RJ: Patient outcomes after arteriovenous malformation radiosurgical management: results based on a 5- to 14-year follow-up study. Neurosurgery 2003;52:1291–1296.
10 Zabel A, Milker-Zabel S, Huber P, et al: Treatment outcome after linac-based radiosurgery in cerebral arteriovenous malformations: retrospective analysis of factors affecting obliteration. Radiother Oncol 2005;77:105–110.
11 Schlienger M, Atlan D, Lefkopoulos D, et al: Linac radiosurgery for cerebral arteriovenous malformations: results in 169 patients. Int J Radiat Oncol Biol Phys 2000;46:1135–1142.
12 Miyawaki L, Dowd C, Wara W, et al: Five year results of LINAC radiosurgery for arteriovenous malformations: outcome for large AVMS. Int J Radiat Oncol Biol Phys 1999;44:1089–1106.
13 Friedman W, Bova F, Mendenhall W: Linear accelerator radiosurgery for arteriovenous malformations: the relationships of size to outcome. J Neurosurg 1995;82:180–189.
14 Colombo F, Pozza F, Chierego G, et al: Linear accelerator radiosurgery for cerebral arteriovenous malformations. An update. Neurosurgery 1994;34:14–21.
15 Betti O, Munari C, Rossler R: Stereotactic radiosurgery with the linear accelerator: treatment of arteriovenous malformations. Neurosurgery 1989;24:311–321.
16 Pollock BE, Kondziolka D, Flickinger JC, et al: Magnetic resonance imaging: an accurate method to evaluate arteriovenous malformations after stereotactic radiosurgery. J Neurosurg 1996;85: 1044–1049.
17 Guo WY, Pan HC, Chung WY, et al: Do we need conventional angiography? The role of magnetic resonance imaging in verifying obliteration of arteriovenous malformations after Gamma Knife surgery. Stereotact Funct Neurosurg 1996;66(suppl 1):71–84.
18 Morikawa M, Numaguchi Y, Rigamonti D, et al: Radiosurgery for cerebral arteriovenous malformations: assessment of early phase magnetic resonance imaging and significance of gadolinium-DTPA enhancement. Int J Radiat Oncol Biol Phys 1996;34:663–675.
19 Chang SD, Marcellus ML, Marks MP, et al: Multimodality treatment of giant intracranial arteriovenous malformations. Neurosurgery 2003;53:1–11.
20 Gobin YP, Laurent A, Merienne L, et al: Treatment of brain arteriovenous malformations by embolization and radiosurgery. J Neurosurg 1996;85:19–28.
21 Mizoi K, Jokura H, Yoshimoto T, et al: Multimodality treatment for large and critically located arteriovenous malformations. Neurol Med Chir 1998;38(suppl 1):186–192.
22 Smith KA, Shetter A, Speiser B, et al: Angiographic follow-up in 37 patients after radiosurgery for cerebral arteriovenous malformations as part of a multimodality treatment approach. Stereotact Funct Neurosurg 1997;69:136–142.
23 Steinberg GK, Chang SD, Levy RP, et al: Surgical resection of large incompletely treated intracranial arteriovenous malformations following stereotactic radiosurgery. J Neurosurg 1996;84:920–928.
24 Guo WY, Wikholm G, Karlsson B, et al: Combined embolization and gamma knife radiosurgery for cerebral arteriovenous malformations. Acta Radiol 1993;34:600–606.

Michael R. Girvigian, MD
Department of Radiation Oncology
Southern California Permanente Medical Group
4950 Sunset Blvd., 2nd Floor
Los Angeles, CA 90027 (USA)
Tel. +1 323 783 2841, Fax +1 323 783 5927
E-Mail michael.r.girvigian@kp.org

Kondziolka D (ed): Radiosurgery. Basel, Karger, 2006, vol 6, pp 229–238

Neurological Deficit Rather than Obliteration Determines Quality of Life in Patients Treated with Radiosurgery for AVMs

Meera Ramani, Yuri M. Andrade-Souza, Deirdre R. Dawson, Daryl Scora, May N. Tsao, Michael L. Schwartz

Division of Neurosurgery and Department of Radiation Oncology, Sunnybrook and Women's College Health Sciences Center, University of Toronto, Toronto, Canada

Abstract

Objective: There is a dearth of literature about the quality of life (QOL) of patients treated for brain arteriovenous malformations (AVMs). This study evaluates the factors that predict the QOL after radiosurgical treatment of patients with AVMs. **Method:** Between 1989 and 2000, 228 patients were treated at the University of Toronto using a LINAC system. One hundred and eighty-one had a complete radiological and clinical follow-up, including 7 who died. Of the 174 remaining patients, it proved possible to notify 113 by telephone that a three-part questionnaire consisting of questions concerning their neurological status before and after treatment and a Medical Outcomes Study questionnaire (SF-36) would be sent. **Results:** Of the 113 forms sent, 66 (58.4%) were adequately completed and returned. There were no significant differences in age, AVM location and volume between patients who returned the questionnaires, patients who did not return the questionnaires, and patients who could not be contacted. However, patients who returned the questionnaires had a higher rate of permanent deficit (10.6 vs. 8.1 and 4.4%) and a lower obliteration rate (54.2 vs. 68.8 and 70.3%) than those who did not return the questionnaires, and those who could not be contacted, respectively. In a multivariate analysis, the most important predictor of QOL was permanent deficit. In order of importance, permanent deficit affected the various aspects of QOL as follows: role physical, physical functioning, social functioning and vitality ($p = 0.000, 0.006, 0.040, 0.049$, respectively). AVM obliteration was not a predictor of QOL, even for the emotional scales. **Conclusion:** Permanent deficits were associated with a lower QOL and this should be considered a strong end-point in the choice among treatment modalities. Surprisingly, AVM obliteration was not a predictor of the QOL for these patients.

Arteriovenous malformations (AVMs) can be treated using a variety of methods including surgery, radiosurgery (LINAC and Gamma Knife) and embolization. Izawa et. al. [1] describe the possible long-term complications of treating AVMs with radiosurgery including hemorrhages, delayed cyst formation and an increase in seizure frequency. However, there is little in the literature about the quality of life (QOL) of patients following radiosurgical treatment for AVMs. While Lai and Lun [2] followed the QOL of patients with cerebral AVMs during the latent period between Gamma Knife radiosurgery and lesion obliteration, our QOL assessment includes patients who had radiosurgical treatment 5–16 years prior to the study as well as the use of a 36-item standardized QOL form. The purpose of our study was to determine the factors that affect the QOL of patients after radiosurgery.

Methods

Between 1989 and 2000, 228 patients underwent radiosurgery for AVMs of varying sizes and locations at the Toronto Sunnybrook Regional Cancer Center (TSRCC). A 6 MV Siemens Linear Accelerator (LINAC) was used with the flattening filter removed [3]. The dynamic rotation method as described by Podgorsak et al. [4] was employed. Out of the 228 patients, 181 had imaging as well as a complete follow-up done, including 7 who died. From the remaining 174 patients, it was possible to contact 113 patients by telephone to inform them that a three-part questionnaire would be sent in the mail. The first questionnaire was created by us (Form A) and inquired about the patient's symptoms and deficits prior to and after radiosurgical treatment. The second form sent was the Dartmouth Primary Care Cooperative Information Project (COOP) charts [5]. The purpose of the charts was to provide a rapid way to assess the health and performance of patients in 9 categories: physical functioning, feelings, daily activities, social activities, pain, change in health, overall health, social support and QOL. The third was an abbreviated 36-item form (SF-36) of the Rand Medical Outcomes Study questionnaire designed to be used as a generic indicator of health status [6]. The SF-36 form contains multi-item scales with a final score in 8 aspects of health: physical functioning, role physical, bodily pain, social functioning, mental health, role emotional, vitality and general health. The scores were calculated as described by The Medical Outcomes Study [1]. Briefly, a score in each section was calculated by using the total raw score and subtracting the lowest possible score and then dividing by the possible raw score range. The result was multiplied by 100 in order to transform the raw score into a scale of 0–100. The data and the answers from the patients were collected on Microsoft Excel and the results were calculated using a multivariate analysis (with SPSS, version 9 for windows).

Results

Sixty-six patients out of the 113 patients (58.4%) that were contacted returned completed questionnaires. Thirty-four patients were women (51.5%)

Table 1. Responses to Form A

Patient no	First symptom related to AVM	Neurological deficit prior to radiosurgery	Experience on day of radiosurgery	New or worse neurological deficit during first week after radiosurgical treatment	New or worse neurological deficit anytime after radiosurgery	Did symptom/ deficit disappear
1	Headache	Motor deficit, visual deficit	Bad	No	Yes (related to radiation)	No (permanent deficit/symptom)
2	Seizure	No deficit	Half and half	No	No	N/A
3	Headache	Motor deficit	Bad	No	No	N/A
4	Headache	No deficit	Good	No	No	N/A
5	Headache	Visual deficit	Good	Yes (during the first 48 h)	Yes (related to radiation)	Yes (more than 6 months after it started)
6	Twitches	Twitches	Good	No	No	N/A
7	Seizure	Extreme headaches	Good	No	Yes (related to hemorrhage)	No (permanent deficit/symptom)
8	Headache	Sensory deficit	Good	No	No	No (permanent deficit/symptom)
9	Seizure	No deficit	Good	No	Yes (related to hemorrhage)	No (permanent deficit/symptom)
10	Headache	No deficit	–	No	Yes (related to radiation)	No (permanent deficit/symptom)
11	Hemorrhage	Visual deficit (mild upper right)	Bad	No	No	N/A
12	Headache	Visual deficit	Okay	Yes (during the first week)	Yes (related to radiation)	Yes (more than 6 months after it started)
13	Hemorrhage	Motor, sensory, visual deficit	Bad	No	No	N/A
14	Headache (vomitting)	Motor, sensory, visual, speech deficit	Same as before radiosurgery	No	No	N/A
15	Limb numbness	No deficit	Good	No	No	N/A

Table 1. (continued)

Patient no	First symptom related to AVM	Neurological deficit prior to radiosurgery	Experience on day of radiosurgery	New or worse neurological deficit during first week after radiosurgical treatment	New or worse neurological deficit anytime after radiosurgery	Did symptom/ deficit disappear
16	Toothache, droopiness on left side of face, loss of balance	No deficit	Good	No	Yes (related to hemorrhage)	Yes (less than 6 months after it started)
17	Headache	Visual deficit	–	No	No	No (permanent deficit/symptom)
18	Other (double vision)	Visual deficit	–	No	No	No (permanent deficit/symptom)
19	Seizure, headache	No deficit	Good	No	No	N/A
20	Headache, dizziness	Motor deficit	– –	Yes (during the first week)	Yes (related to hemorrhage)	No (permanent deficit/symptom)
21	Hemorrhage, headache	Difficulty walking for short time	Good/bad	No	No	N/A
22	Other	Visual deficit	Good	No	No	No (permanent deficit/symptom)
23	Headache	Motor, visual deficit	Good	Yes (during first week)	Yes (related to radiation)	Yes (less than 6 months after it started)
24	Headache	Visual deficit	Bad	No	No	Yes (less than 6 months after it started)
25	Headache	No deficit	Bad	No	No	No (permanent deficit/symptom)
26	Seizure, headache	Motor, visual deficit	Good	Yes (during the first 48 h)	Yes (related to hemorrhage)	No (permanent deficit/symptom)
27	Seizure	No deficit	Good	No	No	N/A
28	Hemorrhage	Short term memory loss	Good	No	No	N/A

29	Seizure	No deficit	Bad	No	No	N/A
30	Hemorrhage	Speech deficit, visual deficit	Bad	No	Yes (related to radiation)	No (permanent deficit/symptom)
31	Seizure	No deficit	Good	No	No	N/A
32	Collapsed while on phone	Motor, sensory, speech, visual deficit	Good	No	–	Yes (less than 6 months after it started)
33	Hemorrhage, headache	No deficit	Bad	No	Yes (related to radiation)	No (permanent deficit/symptom) – improved a little
34	Hemorrhage	Sensory deficit	Good	No	Yes (related to radiation)	No (permanent deficit/symptom)
35	Headache	No deficit	Bad	Yes (during the first week)	Yes (related to radiation)	No (permanent deficit)
36	Headache, other	No deficit	Bad	No	No	Yes (less than 6 months after it started)
37	Headache	No deficit	Bad	–	Yes (related to radiation)	No (permanent deficit/symptom)
38	Headache	Short term memory issues, information processing	Good	No	Yes (related to radiation)	No (permanent deficit)
39	Seizure	No deficit	Good	No	Yes (related to radiation)	No (permanent deficit/symptom)
40	Hemorrhage	Motor, sensory, speech, visual deficit	Bad	No	No	No (permanent deficit)
41	Headache (Dec. 25, 1991)	No deficit	Good	– –	Yes (related to hemorrhage and radiation)	No (permanent deficit/symptom)
42	Other (had stroke)	Other (paralzsed left side)	Good	No	No	No symptoms

Table 1. (continued)

Patient no	First symptom related to AVM	Neurological deficit prior to radiosurgery	Experience on day of radiosurgery	New or worse neurological deficit during first week after radiosurgical treatment	New or worse neurological deficit anytime after radiosurgery	Did symptom/ deficit disappear
43	Hemorrhage	Motor, sensory, speech, visual, auditory deficit	Good	No	No	N/A
44	Seizure, headache	Visual deficit	Good	No	No	N/A
45	Seizure	Visual deficit	Good	Yes (during the first 48 h)	–	No (permanent deficit/symptom)
46	Headache, vomiting	Motor, visual deficit, ataxia right arm, wandering eye	Good	No	No	N/A
47	Incapable of speech	Speech deficit	Good	No	No	Yes (less than 6 months after it started)
48	Headache	Short-term memory loss, cognitive deficits	Good/bad	No	No	N/A
49	Unconscious	No deficit	Good	No	No	No (permanent deficit/symptom)
50	Hemorrhage	Other (minor dizziness)	Good	–	–	No (permanent deficit/symptom)
51	Hemorrhage, headache	No deficit	Good	No	No	N/A
52	Hemorrhage, headache	Motor, sensory deficit	Bad	No	No	N/A
53	Seizure	No deficit	–	No	No	N/A

54	Numb on right side	Motor, sensory, speech, visual deficit	Good	No	No	No (permanent deficit/symptom)
55	Hemorrhage	Visual deficit after	Bad	Yes (during the first 48 h)	No	No (permanent deficit/symptom)
56	Headache	Motor, sensory, speech, visual deficit	Bad	No	No	Yes (less than 6 months after it started)
57	Headache	Motor, sensory, speech deficit	Good	No	Yes (related to radiation)	No (permanent deficit/symptom)
58	Dizziness, seizure, headache	Speech deficit	–	No	Yes (related to hemorrhage)	No (permanent deficit/symptom) – improved
59	Seizure	Motor, sensory, speech, visual deficit	Good	Yes (during the first 48 h)	Yes (related to radiation)	No (permanent deficit)
60	Seizure	No deficit	–	No	No	N/A
61	Doctor did head X-ray	Depression	Bad	–	Yes (related to radiation)	–
62	TIA from chiropractic neck adjustment	Sensory, speech, visual deficit, dizziness	Bad	Yes (during the first 48 h)	Yes (related to radiation)	Yes (less than 6 months after it started)
63	Seizure, minor tingle of tongue	No deficit	Bad	No	No	N/A
64	Peripheral vision	Visual deficit	Bad	No	Yes	No (permanent deficit/symptom)
65	Seizure	–	Good	No	No	N/A
66	Seizure	No deficit	Bad	No	No	N/A

Table 2. Transformed scores from the SF-36 form

Patient no	Physical functioning	Role-physical	Bodily pain	General health	Vitality	Social functioning	Role-emotional	Mental health
1	0	0	100	20	15	0	33.3	56
2	90	100	100	62	90	100	100	52
3	40	0	61	27	25	100	0	48
4	95	100	100	90	90	100	100	92
5	100	100	100	82	60	75	33.3	52
6	100	100	100	52	90	100	100	100
7	50	50	52	77	55	100	100	76
8	60	0	41	62	35	50	0	56
9	15	0	22	72	45	50	33.3	72
10	20	50	31	52	30	37.5	100	52
11	100	100	100	100	65	12.5	100	24
12	90	100	84	77	85	100	100	96
13	15	50	62	52	75	75	100	72
14	45	25	100	40	30	62.5	66.7	56
15	50	100	100	87	70	100	100	88
16	95	100	100	97	100	100	100	100
17	85	100	72	92	95	100	100	100
18	35	0	41	20	30	50	66.7	76
19	70	75	62	62	45	62.5	33.3	60
20	5	100	51	67	50	50	66.7	48
21	95	100	62	87	85	100	100	80
22	35	0	0	82	60	25	0	40
23	20	25	41	25	25	50	33.3	40
24	50	100	62	62	55	87.5	66.7	76
25	80	25	41	32	25	75	0	32
26	30	0	52	57	30	37.5	100	88
27	90	75	100	57	55	75	100	72
28	95	100	100	72	60	37.5	100	48
29	65	100	32	40	45	25	0	60
30	90	100	100	87	85	87.5	100	84
31	90	50	72	52	65	87.5	100	52
32	35	0	31	25	35	25	0	64
33	75	75	41	37	30	50	0	48
34	85	50	52	67	70	87.5	100	72
35	45	50	41	10	10	62.5	100	40
36	100	100	100	100	95	100	100	100
37	90	50	22	25	25	62.5	100	32
38	80	50	100	97	65	100	100	92
39	95	100	100	95	65	100	100	80
40	0	25	100	37	30	0	66.7	20
41	65	75	52	40	5	0	0	32

Table 2. (continued)

Patient no	Physical functioning	Role-physical	Bodily pain	General health	Vitality	Social functioning	Role-emotional	Mental health
42	90	75	100	60	20	100	100	92
43	35	0	74	85	70	87.5	100	88
44	60	0	74	40	35	12.5	0	52
45	95	100	100	72	75	100	100	80
46	100	100	100	85	65	100	100	64
47	80	0	52	80	40	50	0	44
48	10	100	100	62	45	100	33.3	68
49	65	50	100	62	45	62.5	66.7	52
50	5	0	100	77	60	87.5	0	80
51	100	100	100	100	100	100	100	100
52	0	25	51	30	15	25	100	64
53	100	100	84	97	80	100	100	80
54	30	25	62	60	70	100	66.7	80
55	100	75	80	77	70	12.5	100	76
56	100	25	100	77	80	62.5	33.3	52
57	65	75	41	47	35	62.5	100	84
58	75	100	84	82	60	100	100	96
59	35	0	74	35	45	100	100	88
60	90	100	84	72	80	100	100	96
61	50	25	31	10	30	37.5	66.7	28
62	70	100	41	57	50	50	100	68
63	95	100	100	77	65	100	100	80
64	15	25	41	25	15	50	0	40
65	80	100	72	77	70	100	100	92
66	100	100	100	100	80	100	100	92

and 32 were men (48.5%) with a mean age of 46.1 (range, 15–80). The 66 patients were more likely to have deficits (10.6%) and residual AVMs (45.8%) than those who did not return the questionnaire (8.1 and 31.2%) and the group that could not be contacted (4.4 and 29.1%). In order of importance, permanent deficit affected the various aspects of QOL as follows: role physical ($p = 0.000$), physical functioning ($p = 0.006$), social functioning ($p = 0.400$) and vitality ($p = 0.460$). AVM obliteration was not an indicator for QOL including the emotional scales ($p > 0.05$ for all scales). Fourteen patients (21.2%) were unaware whether their AVM was obliterated or not. The COOP charts provided no correlation with permanent deficit or obliteration. Table 1 contains the information the patients provided in Form A and table 2 contains the transformed scores for each patient from the SF-36 form.

Discussion

The results from the SF-36 form demonstrated a correlation with QOL and permanent deficit rather than obliteration. Successful obliteration did not improve and failure to obliterate did not worsen the scores on the emotional scales. Surprisingly, 21.2% of the patients were unaware of the condition of their AVM. A higher percentage of patients from the group that returned the questionnaires had a permanent deficit than those who did not. We speculate that they wanted to inform us about their reduced QOL. There was no relationship between the COOP charts and permanent deficit or obliteration most likely due to the brief nature of the charts which only had one question per scale.

Conclusion

While obliteration has been the focus of treatment in the past, we suggest more careful planning when choosing a treatment modality as permanent deficit diminishes the QOL of patients.

References

1 Izawa M, Hayashi M, Chernov M, et al: Long-term complications after gamma knife surgery for arteriovenous malformations. J Neurosurg 2005;102:34–37.
2 Lai EH, Lun SL: Impact on the quality of life of patients with arteriovenous malformations during the latent interval between gamma knife radiosurgery and lesion obliteration. J Neurosurg 2002;97:471–473.
3 O'Brien PF, Gillies BA, Schwartz M, et al: Radiosurgery with unflattened 6-MV photon beams. Med Phys 1991;18:519–521.
4 Podgorsak EB, Olivier A, Pla M, et al: Dynamic stereotactic radiosurgery. Int J Radiat Oncol Biol Phys 1988;4:115–126.
5 Nelson EC, Wasson JH, Kirk J, Keller A, Clark D, Dietrich A, Stewart A, Zubkoff M: Assessment of function in routine clinical practice: description of the COOP chart method and preliminary findings. J Chronic Dis 1987;40:555–635.
6 Ware JE Jr, Snow KK, Kosinski M, et al: SF-36 Health Survey: manual and interpretation guide. Boston, Massachusetts, The Health Institute, New England Medical Center, 1993.
7 Medical Outcomes Trust: How to Score the SF-36 Short-Form Health Survey. Boston, Massachusetts, The Medical Outcomes Trust, 1992.

Michael L. Schwartz
Division of Neurosurgery and Department of Radiation Oncology
Sunnybrook and Women's College Health Sciences Center
University of Toronto
2075 Bayview Ave, A-129
Toronto, Ont. M4N 3M5 (Canada)
Tel. +1 416 480 4738, Fax +1 416 480 6085
E-Mail m.schwartz@utoronto.ca

Kondziolka D (ed): Radiosurgery. Basel, Karger, 2006, vol 6, pp 239–248

Radiosurgery of Cavernous Malformations with Intractable Seizures

Yoshihisa Kida, Masayuki Yoshimoto, Toshinori Hasegawa

Department of Neurosurgery, Komaki City Hospital, Komaki City, Japan

Abstract

Cavernous malformations are known as essentially benign and silent disease. However, they become symptomatic with hemorrhage, seizure or neurological signs. In the cases with supratentorial lesions, seizures are so often intractable and resistant to anticonvulsants. We have experienced 25 cases with such intractable seizures and treated with radiosurgery. There are 13 males and 12 females, ages ranging from 13 to 49 (mean: 31.2 years). Seizure patterns are classified as generalized in 12, complex partial in 6, simple partial in 6, simple partial plus generalized in 1. Most of the lesions are located either in frontal or temporal lobe. At radiosurgery, cavernous malformations, with a mean diameter of 15.9 mm were treated with the maximum and marginal dose of 31.9 and 17.5 Gy respectively. In the mean follow-up period of 45.6 months, MRI showed CR in 1, PR in 9, MR in 2 and NC in 13, indicating the response rate 10/25 (40%). In contrast, the response of seizures are Engel Class I in 9, Class II in 5, Class III in 5 and Class IV in 6, indicating 9/25 (36%) of seizure-free and excellent control 14/25 (56%). Perifocal edema occurred often, but rarely symptomatic. In conclusion, radiosurgery demonstrated a moderate seizure control, but not perfect. The lesionectomy alone with radiosurgery does not always solve the problem, and precise localization of seizure discharge should be searched.

With the advents of MRI, cavernous malformations (CMs) are easily detected. In CMs are clinically silent, but sometimes they become symptomatic with hemorrhage, seizures, or repetitive neurological deficits [1–3]. Seizures associated with CM are consistent and so often intractable [4]. Current treatments are surgical resection of CM lesions with or without resection of seizure focus. Although a significant seizure control have been reported, seizures are

Table 1. Characteristics of 25 patients with cavernous malformations, who are associated with intractable seizures

Gender, male/female	13/12
Age, years	13–49 (mean 31.2)
Seizure pattern	
Generalized (G)	12
Complex partial (CPS)	6
Simple partial (SPS)	6
SPS + G	1
Location of the lesion	
Frontal lobe	10
Temporal lobe	10
Parietal lobe	4
Occipital lobe	1

Table 2. Radiosurgery of cavernous malformations with intractable seizures (25 cases)

Cases	Range	Mean
Age, years	13–49	31.2
Lesion size	6–27 mm	15.9 mm (2.78 ml)
Maximum dose	22–44 Gy	31.9 Gy
Marginal dose	11.3–25.2 Gy	17.5 Gy

still remained after the surgical resection in some cases [5, 6]. From the very first trial [7] radiosurgery for CMs has been always controversial. However, stimulated by the hemorrhage control for CM with radiosurgery [8–11], seizure case were also treated with Gamma Knife in order to achieve seizure control.

Materials and Methods

We have experienced 25 cases with such intractable seizures and treated with radiosurgery. There are 13 males and 12 females, ages ranging from 13 to 49 (mean: 31.2 years). Seizure patterns are classified as generalized in 12, complex partial in 7, simple partial in 6, simple partial plus generalized in 1 (table 1). Most of the lesions are located either in frontal (10 cases) or temporal lobe (10 cases). At radiosurgery, CMs, with a mean diameter of 15.9 mm (range: 6–27 mm) were treated with the mean maximum and marginal dose of 31.9 and 17.5 Gy respectively (table 2).

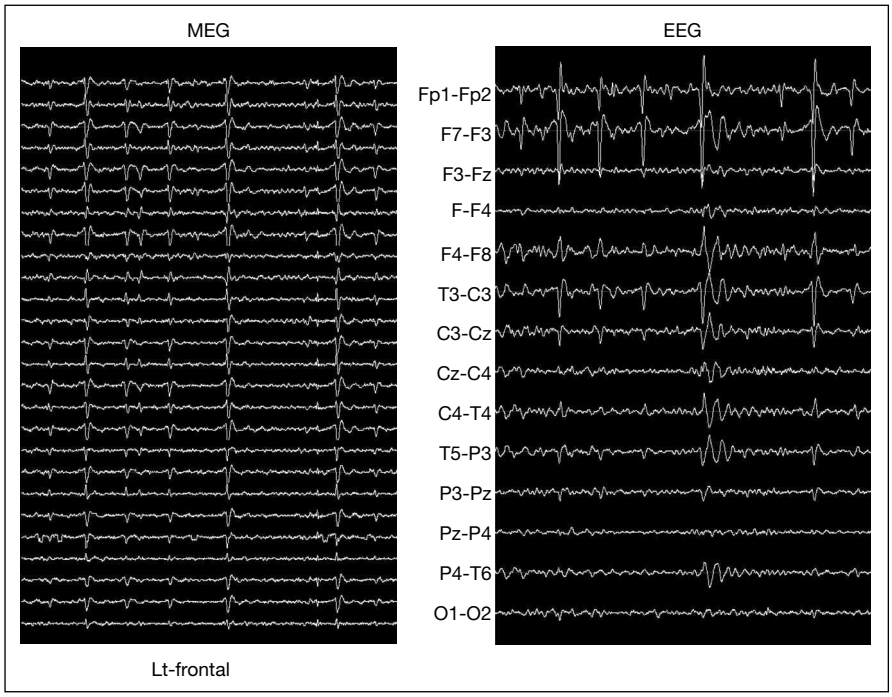

Fig. 1. MEG and EEG findings of a case with intractable seizures.

After the radiosurgery, follow-up studies with neurological signs, MRI, EEG were taken every 3 months in the first year, then 6 months intervals. With the follow-up MRIs, lesion size were compared with the ones at radiosurgery and evaluated in terms of CR, PR, MR, NC and PG. Seizure outcomes were evaluated with Engel's classification, and also compared with the ones before radiosurgery. In recent cases, magnetoencephalography (MEG) was performed before and after radiosurgery to see the seizure focus and the serial changes of seizure dipoles.

Results

EEG and MEG Studies

EEG and MEG showed frequent spikes in majority of cases. Clusters of seizure dipoles were not seen inside the CMs, but in surrounding brain. The exact locations of seizure dipoles are usually unpredictable, some are concentrated and the others are scattered in distribution (figs. 1, 4b).

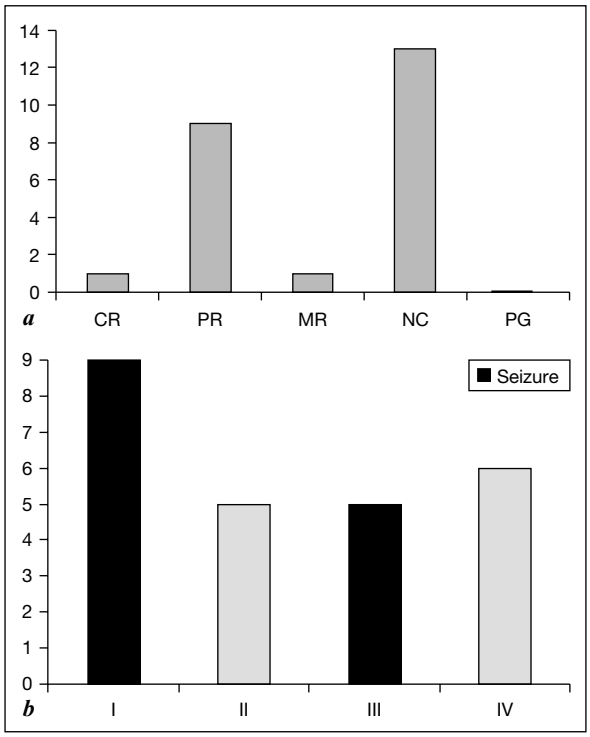

Fig. 2. Radiological (***a***) and seizure outcomes (***b***). I–IV = Engel's classification.

Radiological Changes of Cavernous Malformations

In the mean follow-up of 45.6 months, almost a half lesions showed some shrinkage of the lesion and another half demonstrated no obvious changes. No one showed a progression of the lesions (fig. 2).

Seizure Control

After the radiosurgery, seizures are gradually decreased in some of the cases, but not in all. Depending upon the Engel's classification, seizure-free in 9, far decreased in 5, minor decrease in 5, and unchanged in 6 in the mean follow-up period of 45.6 months (fig. 2). Accordingly to the locations, CMs in frontal lobe showed a good response, in contrast the temporal lesions demonstrated relatively poor seizure control (fig. 3). Accordingly to the seizure patterns, complex partial seizures were less responsive when compared with frontal lobe CMs. Generalized seizures were more favorably, responded than others (fig. 3). Timing of seizure control is unpredictable, some were within a

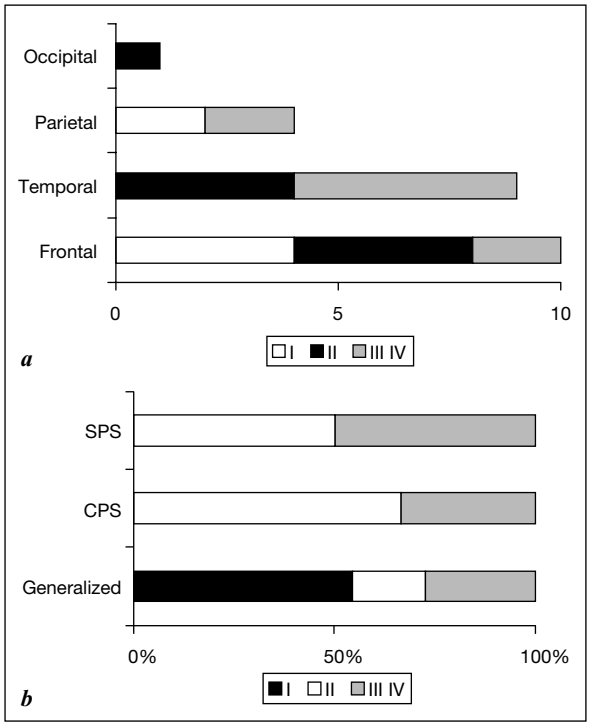

Fig. 3. Seizure control of cavernous malformation depending on locations (***a***) and on seizure patterns (***b***). CPS = Complex partial seizure; SPS = simple partial seizure. I–IV = Engel's classification.

week, and others are by 1 or 2 years. At the last follow-up, 15 cases still have medication of anticonvulsants, another 4 cases discontinued, and 6 were unknown.

Illustrative Cases

Case 1: 13-year-old boy has been suffering from headache and frequent seizures with generalized convulsion or motion arrests. There are two lesions of CM, one in left frontal, the other in occipital lobe (fig. 4a). Both EEG and MEG showed a frequent spikes in left frontal lobe (fig. 4b). Lesionectomy of this CM with Gamma Knife (maximum dose: 40 Gy, Marginal dose: 20 Gy) was performed. Seizures subsided very fast and almost disappeared within a few weeks. However, his EEG and MEG 6 months after radiosurgery showed frequent spikes just same as preradiosurgical study. A careful follow-up study is required for the future.

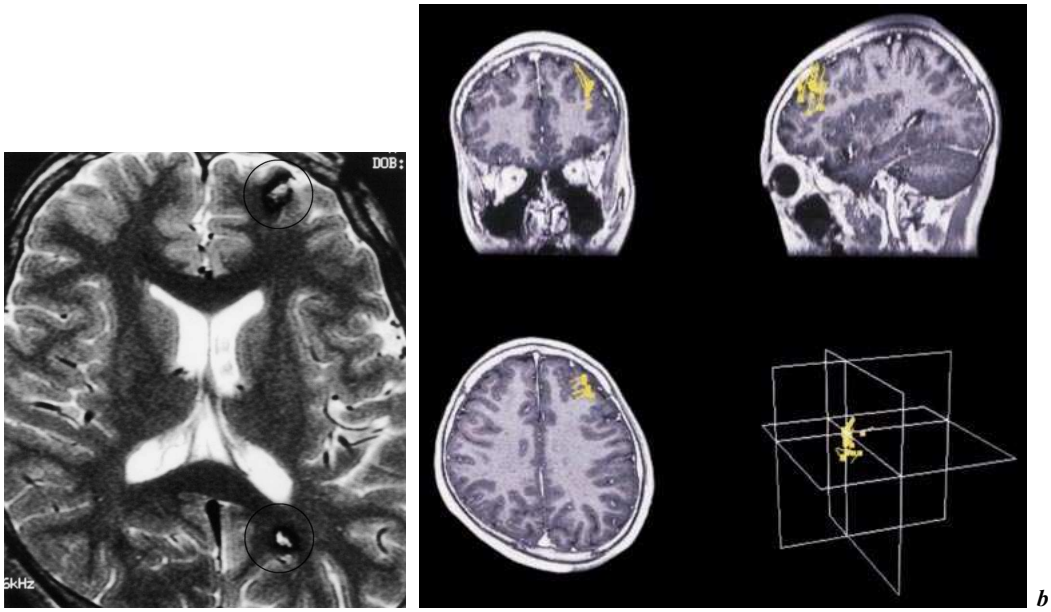

a *b*

Fig. 4. Illustrative case with cavernous malformation, frequent seizures before radiosurgery were completely subsided within a month after radiosurgery. ***a*** MRI, (***b***) seizure dipoles obtained with MEG.

Case 2: CM in right frontal lobe, associated with frequent partial seizures of left hand. After radiosurgery, 18 Gy at the margin (left), the lesion showed a persistent shrinkage (right). Simple partial seizures were gradually subsided and ceathed within 2 years (fig. 5).

Complications

Perifocal edema was seen in many cases, mostly within a year after radiosurgery, which associated with some neurological signs not frequently. In two cases surgical resection of CM were required because of moderate swelling and neurological deterioration a few months after radiosurgery (table 3).

Discussion

Recently, the natural history of CMs becomes clearer [12–15]. Curling et al. [12] reported that the incidence of hemorrhage and seizure are 0.25%/person-year and 1.51%/person-year respectively. However these incidence are not always reliable since hemorrhagic and seizure attack may occure very often

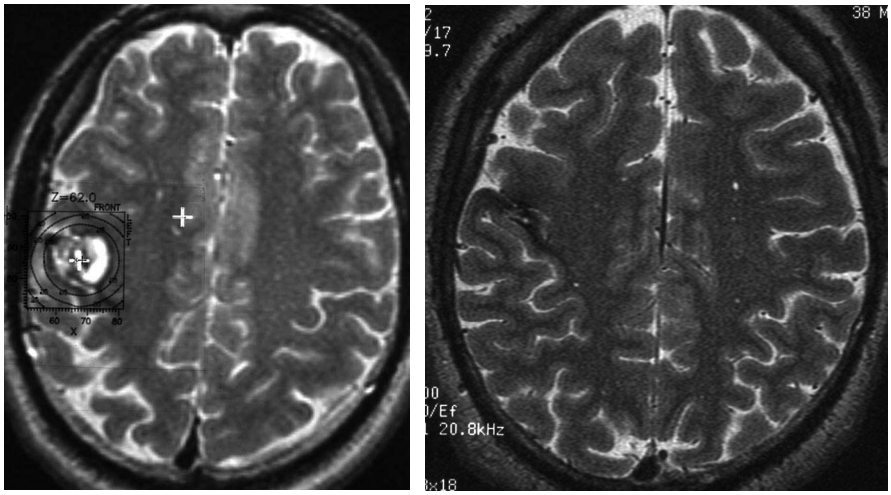

a ***b***

Fig. 5. Cavernous malformation in right frontal lobe, associated with frequent partial seizures of left hand. After radiosurgery, the lesion showed a persistent shrinkage (***a***), 18 Gy at the margin (***b***). Simple partial seizures were gradually subsided and ceathed within 2 years.

Table 3. Adverse effects and complications after radiosurgery

Perifocal edema	11/25 (44%) (+): 3; (++): 8; (–): 14
Operative resection after radiosurgery	2/25 (8%)
Anticonvulsant	
Continued	15
Discontinued	4
Unknown	5

once they become symptomatic, while asymptomatic lesions are always silent [15]. Therefore, it is quite natural that only symptomatic lesions with repeated episodes are indicated for various kinds of treatment like surgical resection or radiosurgery. Surgical resection of CMs associated with hemorrhage has been reported by many investigators [16–20]. It is well known that the seizures associated with supratentorial CMs are very frequent in seizure incidence and resistant to medication of anticonvulsants [4]. Their EEG studies show very consistent spikes in continuous fashion. In our series, seizure discharges are

apparent in EEG as well as MEG in many cases. Clusters of seizure dipoles on MEG are usually concentrated in the surrounding brain just adjacent to CM, but the locations are not predictable and are scattered in some others. Therefore, the extensive search for seizure dipoles on MEG is very important. This is especially true in cases of multiple supratentorial CM, because the symptomatic lesion which is responsible for the attacks should be confirmed.

Operative resection of supratentorial CMs have been carried out either with craniotomy, or by stereotactic techniques [5, 6]. Although the results reported were seemingly favorable, convulsive seizures were not always cured after the operative lesion resections (lesionectomy). In fact convulsive seizures remained after the operation in some cases. Radiosurgery for CMs with intractable seizure has been already reported by Regis et al. [21] that the lesionectomy alone demonstrated a considerable improvement of seizures after the treatment. After the radiosurgery with a mean marginal dose of 19 Gy, 53% of patients were seizure free (Engel's Class I) and another 20% achieved a significant seizure decrease.

In this study only the lesionectomy of CM with radiosurgery was attempted. The results are promising since seizure are either ceathed or decreased in almost a half of the cases after the radiosurgery, with the marginal dose less than 20 Gy. In fact very frequent seizures so often subsided within several weeks after the radiosurgery. Experimental studies have already indicated that the seizure control was achieved dependent on the dose and a good control was obtained with the marginal dose around 20 Gy [22]. Our clinical results indicate two important things. One is that CMs do respond to lesionectomy with radiosurgery at least in half of the cases. The other thing is that the responses are incomplete and the seizure remained in the other half of the cases. Electrophysiological studies with EEG and MEG clearly demonstrate the possible distribution of seizure foci in the surrounding brain. Therefore, these information should be taken into account when CMs associated with intractable seizure are treated. Lesionectomy alone is not always curative with surgery as well as radiosurgery. Seizure foci in the surrounding brain should be considered in order to control and stop the seizure, because the seizure foci created with CMs are so consistent. Therefore, our study directs to do radiosurgery against CMs as well as to the seizure foci at the same time.

Conclusion

Results of radiosurgery for CMs with intractable seizure were reported. After the radiosurgery, seizures were either improved or disappeared in more than half of the cases. Supratentorial CMs associated with convulsive seizure can be successfully treated with radiosurgery.

References

1 Duffau H, Sichez CJP, Faillot T, Bitar A, Arthuis F, Effenterre RV, Fohanno D: Early radiologically proven rebleeding from intracranial cavernous angiomas: report of 6 cases and review of the literature. Acta Neurochir (Wien) 1997;139:914–922.

2 Lobato RD, Perez C, Rivas JJ, Cordobes F: Clinical, radiological, and pathological spectrum of angiographically occult intracranial vascular malformations. Analysis of 21 cases and review of the literature. J Neurosurg 1988;68:518–531.

3 Maraire JN, Awad IA: Intracranial cavernous malformations: lesion behavior and management strategies. Neurosurgery 1995;37:591–605.

4 Awad IA, Robinson JR: Cavernous malformations and epilepsy; in Awad IA, Barrow DL (eds): Cavernous Malformations. Park Ridge, III, American Association of Neurological Surgeons, 1991, pp 49–63.

5 Casazza M, Broggi G, Franzini A, Avanzini G, Spreafico R, Brocchi M, Valentini MC: Supratentorial cavernous angiomas and epileptic seizure: preoperative course and postoperative outcome. Neurosurgery 1996;39;26–34.

6 Cohen DS, Zubay GP, Goodman RR: Seizure outcome after lesionectomy for cavernous malformations. J Neurosurg 1995;83:237–242.

7 Weil S, Tew JM, Steiner L: Comparison of radiosurgery and microsurgery for treatment of cavernous malformations of the brain stem. J Neurosurg 1990;72:336A (Abstract).

8 Amin-Hanjani S, Ogilvy CS, Candia GJ, Lyons S, Chapman PH: Stereotactic radiosurgery for cavernous malformations: Kjellberg's experience with proton beam therapy in 98 cases at the Harvard cyclotron. Neurosurgery 1998;42:1229–1238.

9 Chang SD, Levy RP, Adler JR, Martin DP, Krakovitz PR, Steinberg GK: Stereotactic radiosurgery of angiographically occult vascular malformations: 14-year experience. Neurosurgery 1998;43: 213–221.

10 Kondziolka D, Lunsford LD, Coffey RJ, Bissonette DJ, Flickinger JC: Stereotactic radiosurgery of angiographically occult vascular malformations: indications and preliminary experience. Neurosurgery 1990;27:892–900.

11 Kondziolka D, Lunsford D, Flickinger JC, Kestle JRW: Reduction of hemorrhage risk after stereotactic radiosurgery for cavernous malformations. J Neurosurg 1995;83:825–831.

12 Curling OD, Kelly DL, Elster AD, et al: An analysis of the natural history of cavernous angioma. J Neurosurg 1991;75:702–708.

13 Robinson JR, Awad IA, Little JR: Natural history of the cavernous angioma. J Neurosurg 1991;75:709–714.

14 Zabramski JM, Wascher TM, Spetzler RF, et al: The natural history of familial cavernous malformations: results of an ongoing study. J Neurosurg 1994;80:422–432.

15 Kondziolka D, Lunsford LD, Kestle JRW: The natural history of cerebral cavernous malformations. J Neurosurg 1995;83:820–824.

16 Amin-Hanjani S, Ogilvy CS, Ojemann RG, Crowell RM: Risks of surgical management for cavernous malformations of the nervous system. Neurosurgery 1998;42:1220–1228.

17 Cantore G, Missori P, Santoro A: Cavernous angiomas of the brainstem. Intra-axial anatomical pitfalls and surgical strategies. Surg Neurol 1999;52:84–94.

18 Porter RW, Detwiler PW, Spetzler RF, Lawton MT, Baskin JJ, Derksen PT, Zabranski JM: Cavernous malformations of the brainstem: experience with 100 patients. J Neurosurg 1999;90: 50–58.

19 Wang CW, Liu AL, Zhang J, Sun B, Zhao Y: Surgical management of brainstem cavernous malformations: report of 137 cases. Surg Neurol 2003;59:444–454.

20 Mathiesen T, Edner G, Kihlstrom L: Deep and braistem cavernomas: a consecutive 8-year series. J Neurosurg 2003;99:31–37.

21 Regis J, Bartolomei F, Kida Y, Kobayashi T, Vladyka V, Liscak R, et al: Radiosurgery for epilepsy associated with cavernous malformation: retrospective study in 49 patients. Neurosurgery 2003;47: 1091–1097.

22 Kondziolka D, Mori Y, Blazer J, Thulborn K: Stereotactic radiosurgery for the treatment of epilepsy evaluated in the rat kainic acid model. Presented at the 8th International Leksell Gamma Knife Society meeting, Marseilles, France, June 22–25, 1997.

Dr. Yoshihisa Kida
Department of Neurosurgery, Komaki City Hospital
20, Jhobusi
Komaki City, Aichi Prefecture 485–8520 (Japan)
Tel. +81 568 76 4131, Fax +81 568 76 4145
E-Mail yoshi9@go2.enjoy.ne.jp

Kondziolka D (ed): Radiosurgery. Basel, Karger, 2006, vol 6, pp 249–259

Gamma Knife Radiosurgery as the Primary Intervention for Trigeminal Neuralgia

John Y.K. Lee[a], *Jae Gon Moon*[b], *Douglas Kondziolka*[b], *John C. Flickinger*[b], *L. Dade Lunsford*[b]

[a]Department of Neurological Surgery, University of Pennsylvania, Philadelphia, Pa., and [b]Department of Neurological Surgery, University of Pittsburgh, Pa., USA

Abstract

Introduction: Stereotactic radiosurgery is the least invasive surgical option for patients with trigeminal neuralgia. It has been mainly used for patients who have failed other procedures. To determine the effect of radiosurgery as the primary surgical management for patients with intractable trigeminal neuralgia, we studied those patients who had radiosurgery without any prior surgical treatments (microvascular decompression or percutaneous rhizotomy). **Methods:** Over a nine-year period, 480 patients underwent Gamma Knife radiosurgery for intractable trigeminal neuralgia at the University of Pittsburgh. Two hundred and eleven patients had radiosurgery as first-line treatment. One hundred and forty-nine of the 211 patients had over 6 months of follow-up. Gamma Knife radiosurgery was performed using a single 4-mm isocenter targeted to the trigeminal nerve, just proximal to its entry into the brainstem. A median maximum dose of 80 Gy was prescribed (70–90 Gy). The mean follow-up was 37 months (6–109 months). Pain relief was classified into three categories: pain-free with or without medications, partial pain relief (>50%), and little or no relief (<50%). **Results:** Three months after Gamma Knife radiosurgery, 87% of 149 patients described themselves as being pain-free. At final follow-up (mean = 37 months after Gamma Knife radiosurgery), 63% of 149 patients described themselves as being pain-free. Eleven percent (23 of 211) of patients developed numbness in the trigeminal distribution. Three percent (6 of 211) of patients developed paresthesia or dysesthesias. No patient developed corneal abrasion or keratitis. **Conclusion:** Gamma Knife radiosurgery is a minimally invasive surgical option for patients with trigeminal neuralgia that can be used as a primary surgery for medically refractory patients.

Although the first Gamma Knife radiosurgical lesion for the treatment of trigeminal neuralgia was proposed in 1951 [1], it is only in the last decade with

the widespread availability of the Gamma Knife and magnetic resonance imaging (MRI) has there been a veritable explosion in the use of Gamma Knife radiosurgery as a lesioning device in the treatment of patients with trigeminal neuralgia. At first, Gamma Knife radiosurgery was reserved for patients who had failed prior procedures or who were considered too old and medically unfit for a microvascular decompression or a percutaneous procedure [2]; however, with the increasing demonstration of radiosurgical efficacy and safety, an increasing number of surgeons have offered radiosurgery as a primary treatment. In addition, as patients have learned the benefits of radiosurgery, they have increasingly requested Gamma Knife as a first line treatment for relief of their pain. This chapter presents the results of Gamma Knife radiosurgery at the University of Pittsburgh as a primary treatment for trigeminal neuralgia.

Clinical Materials and Methods

Patient Population

Between December 1992 and December 2003, 480 patients with trigeminal neuralgia underwent Gamma Knife stereotactic radiosurgery. A subset of these patients had no prior procedure, primary Gamma Knife radiosurgery, in 211 patients. Of this cohort of 211 patients, a minimum of 6-month follow-up via phone calls, chart records, or physician visit was available in 149 patients.

The median age of this cohort was 68.7 years (range, 21–91). Sixty percent of patients were female, 63% of the patients had trigeminal neuralgia on the right side of the face, and the majority of patients had pain in the distribution of the V2 and V3 branches of the trigeminal nerve. The etiology of the patient's pain was idiopathic in the majority of patients (n = 137); however, a minority of patients had multiple sclerosis (n = 5), prior stroke (n = 1), acoustic neuroma (n = 1), cerebellar cavernous hemangioma (n = 1), and brainstem glioma (n = 1). In addition, three patients had a greater percentage of constant burning pain than the classic, episodic, lancinating pain of typical trigeminal neuralgia and were classified as having atypical trigeminal neuralgia.

Radiosurgical Technique

All patients underwent application of a Leksell Model G stereotactic frame (Elekta Instruments, Atlanta, Ga., USA) after local anesthetic injection. Supplemental intravenous sedation (50 mg Fentanyl, 1 mg midazolam) was provided to some patients. A high resolution, contrast-enhanced, MR volume-acquisition protocol with 1 or 1.5 mm slices provided detailed graphic, three-dimensional visualization of the brainstem and exiting nerve root. To achieve high-resolution volume acquisition scans, we used a 512 × 256 mm matrix and two excitations. In some patients, nerve recognition was enhanced by use of inversion recovery sequences. Six patients underwent computerized tomography (half of these patients also had intrathecal contrast) as they had indwelling pacemakers and were thus considered unsuitable for MRI. The images were transferred to a dose-planning computer, and computerized dose-planning was performed initially on a Micro-VAX II work station (Digital Equipment

Corporation, Westminster, Mass., USA) and later on a Hewlett-Packard work station, using GammaPlan® software (Elekta Instruments, Atlanta, Ga., USA). The maximum radiation dose, isodose, and margin dose delivered were determined by consultation between the neurosurgeon, radiation oncologist, and medical physicist. Radiosurgery was performed using a 201-source cobalt-60 Leksell Gamma Knife Model U, Model B, or Model C unit (Elekta Instruments). At the time of completion of radiosurgery, each patient received a single intravenous 40-mg dose of methylprednisolone.

A single 4-mm isocenter was used in 132 patients (88.6%) and two 4-mm isocenters were used in 17 patients (11.4%). With a single isocenter, the target was 2–4 mm anterior from the junction of the trigeminal nerve and pons so that the brainstem edge was irradiated usually at no more than the 30% isodose line. When two isocenters were used to create an oval dose plan, a longer nerve segment extending more anteriorly was irradiated [3]. We administered maximum doses of 70 (14.8%), 75 (15.4%), 80 (65.8%) or 85 Gy (4%). A team consisting of the neurosurgeon, radiation oncologist, and medical physicist performed dose selection and planning. All patients were discharged within 24 h after Gamma Knife stereotactic radiosurgery.

Follow-Up and Statistical Analysis

All follow-up information was obtained from one of three sources: direct clinical examination by the treating neurosurgeon, direct telephone call follow-up, or indirect communication with the referring physician. Specific questions included the degree of pain relief, latency interval to pain relief, need for further surgical procedures, use of medication, and complications. Criteria for improvement included reduction in both the frequency and severity of trigeminal neuralgia attacks. The median follow-up period was 27 months (range, 6–109 months) after radiosurgery.

Outcome was classified into the following categories: excellent (pain free and completely off medications); good (pain free with either the same or reduced medications); fair (reduced pain (>50%) with either the same or reduced medications); failure (no pain relief or <50% pain relief). A successful outcome was defined as those patients in the excellent and good categories, e.g. patients with complete pain relief regardless of medication usage. Patients with fair outcomes as well as those with <50% pain relief and those with no pain relief were all considered as failures of Gamma Knife radiosurgery. Patients were classified as having a recurrence if they were initially pain-free (regardless of medication status) but then later lapsed and developed any type of trigeminal neuralgia, e.g. >50, <50%, or absolutely no pain relief.

Statistical methods using Kaplan-Meier analysis was performed with SPSS software.

Results

Pain Relief

Initial response was defined as the time at which Gamma Knife radiosurgery resulted in complete pain relief. Of the total 149 patients, 129 patients (86.5%) were classified as completely pain-free at some time after the Gamma Knife radiosurgery procedure. Seventy-one (47.7%) of the 149 patients described that at some early time period after Gamma Knife radiosurgery they

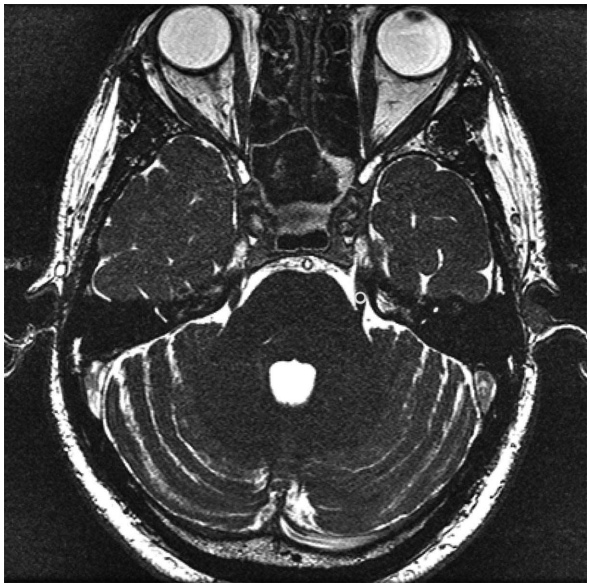

Fig. 1. Axial MRI scan utilizing Fast Imaging Employing Steady state Acquisition scan to demonstrate the left trigeminal nerve and the position of the 4 mm collimator 50% isodose line over the root entry zone of the nerve.

were pain free and off of all medications, 28 (18.8%) patients were pain free with reduced medication, and 30 (20.1%) patients were pain free but still continuing full doses of their medications. The actuarial median time to develop this initial response was 0.8 ± 0.2 months (range, 1 day–14 months). The actuarial response rate at 14 months (time point at which the last patient derived benefit from Gamma Knife radiosurgery) was 87.3 ± 2.8% (fig. 1).

Although the majority of patients derived a significant degree of pain relief and described themselves as completely pain-free after the Gamma Knife radiosurgery procedure, there was a small minority of patients that derived minimal or no benefit from radiosurgery. Sixteen patients (10.7%) had no response or <50% reduction in pain, and four patients (2.7%) had between 50 and 99% relief of pain (fig. 1).

Of those patients who did achieve complete pain relief after the Gamma Knife radiosurgery procedure, a percentage of patients maintained benefit at later time points. At last follow-up (median = 27 months, range, 6–109 months), a total of 88 patients were completely pain free: 43 (28.9%) were completely pain free off medications and 45 (30.2%) were pain free but still continuing some medications (fig. 2). Using actuarial methods, the median duration of

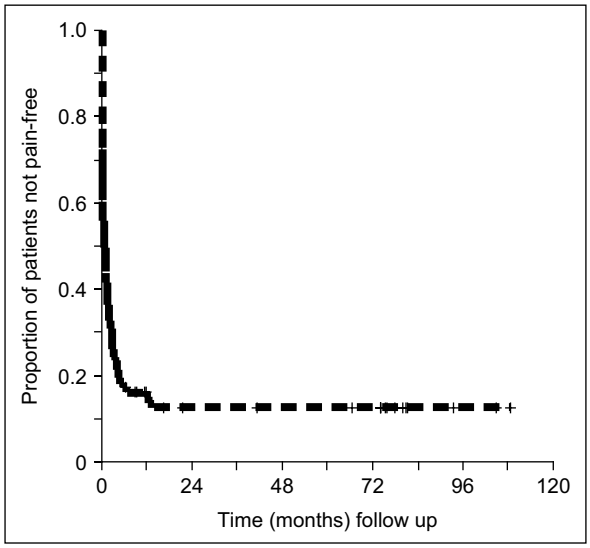

Fig. 2. Actuarial initial response of patients to Gamma Knife radiosurgery. Y-axis represents the proportion of patients who are not completely pain-free, and X-axis represents the amount of time after radiosurgery. 87.3 ± 2.8% of patients are completely pain-free at 14 months, but the median time to complete pain relief was 0.8 ± 0.2 months.

complete relief from the time of the response was 77.4 ± 7.5 months. Hence, if a patient achieved complete pain relief after Gamma Knife radiosurgery, half of the patients could be expected to be pain-free 77.4 ± 7.5 months after the time at which they achieved complete pain relief. The actuarial complete pain free rate at 77 months and beyond was 40.5 ± 11.8% with only four patients pain free beyond 79 months (fig. 3).

At last follow-up, 29 patients had required additional procedures to control their pain. Seventeen patients underwent a second Gamma Knife radiosurgical procedure, eight patients underwent a glycerol rhizotomy, three patients underwent microvascular decompression, and one underwent a balloon microcompression rhizotomy.

Complications

The majority of complications with Gamma Knife radiosurgery were temporary (14%). Permanent complications developed in only 5% of patients. Both temporary and permanent complications developed at a median of 13 months (range, 7 days–50 months) after radiosurgery.

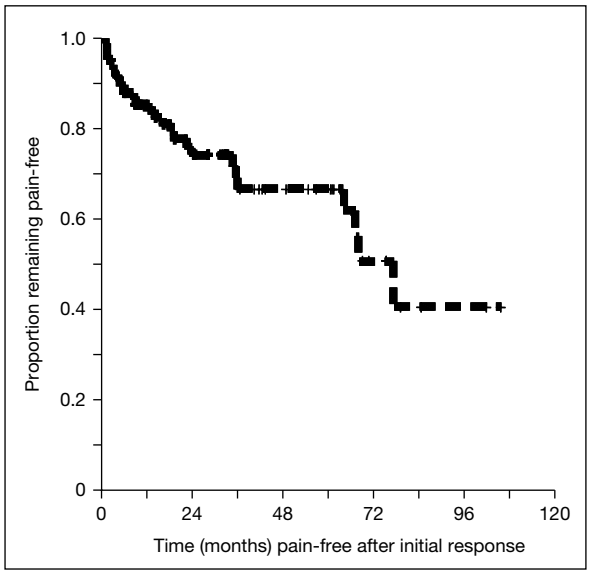

Fig. 3. Actuarial analysis of all 129 patients who initially achieved complete pain relief after Gamma Knife radiosurgery. The median duration of complete pain relief was 77.4 ± 7.5 months.

Permanent complications were seen in eight patients. The rate of permanent facial numbness was 4% (n = 6). The rate of permanent, uncomfortable dysesthesias was 0.6% (n = 1), and the rate of permanent, uncomfortable, pruritus of the eye was 0.6% (n = 1).

Temporary complications were seen in twenty-one patients. Temporary complications included an 11% rate of facial numbness (n = 17), a 1% rate of paresthesias (n = 2), and a 1% rate of dysesthesias (n = 2). These temporary complications usually resolved with a short course of oral steroids, or with time.

Discussion

Radiosurgical ablative therapy for the treatment of trigeminal neuralgia began with the use of orthovoltage X-rays to treat two patients with trigeminal neuralgia in Stockholm [4]. Capitalizing on this initial success, Dr. Leksell and Dr. Hakanson hoped to use the recently created Gamma Knife to ablate the gasserian ganglion. Because of the difficulty of targeting the ganglion solely on skull X-rays alone, Dr. Hakanson injected tantalum dust with glycerol into the

gasserian ganglion with the goal of performing a trans-foramen ovale cisternogram, which ultimately led to the fortuitous discovery of glycerol as a mild neurolytic agent [5]. Although this technique of both visualization and radiosurgical lesioning met with some early success, it was not until the widespread use of MRI and the ability to target the root entry zone did the technique of Gamma Knife radiosurgery flourish [2, 6]. Indeed, the pioneering work of Dr. Jannetta in concentrating attention to the root entry zone as the pathophysiologic pain generator allowed surgeons to direct their efforts at the junction of the peripheral and central myelin in an effort to treat patients with trigeminal neuralgia in both an invasive microsurgical fashion and a less-invasive radiosurgical manner [7, 8].

Prior to the performance of any procedure for the treatment of patient pain, proper patient selection is of utmost importance. The majority of patients treated in this series had the classical features of lancinating, usually unilateral, intermittent, sharp, lightning-like pain in the distribution of the trigeminal nerve. Only a minority of patients described a $<50\%$ component of their pain as being constant, dull or burning pain. These patients were classified as having atypical trigeminal neuralgia. Recently, Burchiel [9] described a new classification scheme of facial pain which provides a mechanistic and clinical framework for decision-making. This classification scheme may prove beneficial in the future as a means of selecting patients and predicting their success rate; however, it has not yet been universally adopted. Nevertheless, as emphasized by Zakrzewska et al. [10, 11] uniformity of diagnostic criteria will allow significant advances in the treatment of patients with trigeminal neuralgia. We continue to use this classic definition of trigeminal neuralgia but are constantly vigilant for an improved diagnostic method that will allow his to stratify patients and to predict treatment success.

The efficacy of Gamma Knife radiosurgery compares quite favorably to other established techniques such as percutaneous radiofrequency rhizotomy, balloon compression, glycerol rhizotomy, and microvascular decompression. In our series of patients, we demonstrated an actuarial complete pain-free initial response rate of $87.3 \pm 2.8\%$ at the last time point at which any patient responded to radiosurgery – 14 months. Hence, 87% of all patients treated with radiosurgery prior to any other procedure can expect to become pain-free, on or off medications. This response is not immediate but rather occurs at a median time point of 0.8 ± 0.2 months after the radiosurgery procedure. This finding is quite similar to other reports of Gamma Knife radiosurgery for trigeminal neuralgia, where the maximal level of pain relief is usually achieved within one month and is seen in approximately 80–90% of patients [3, 12–15].

The delay in benefit of radiosurgery is an important consideration in patient selection. For those patients who are in excruciating pain and demand immediate pain-relief, a percutaneous procedure may be of greater instantaneous benefit

than radiosurgery. For these patients, we may admit them from the office and perform a percutaneous glycerol rhizotomy [16].

The durability of complete pain relief for patients who are treated with primary radiosurgery is quite effective. Of the patients who derived complete pain relief from Gamma Knife radiosurgery, the median duration of complete relief from the time of initial response was 77.4 ± 7.5 months using Kaplan-Meier actuarial analysis. Hence, of the 87% of patients that achieve complete pain relief, half of those patients can expect to remain pain-free for approximately six years. The actuarial complete pain free rate at 77 months and beyond was 40.5 ± 11.8% with only four patients pain free beyond 79 months. This finding demonstrates the durability of pain relief in trigeminal neuralgia and confirms the data in previous reports of the improved beneficial effect of Gamma Knife in patients who have not had prior destructive or non-destructive procedures. For example, in an earlier publication from our group, Maesawa et al. [12] demonstrated a 3 year actuarial complete pain-free rate of 49% in patients who had prior procedures vs. 70% in patients who had primary radiosurgery. Similarly, Pollock et al. [13] demonstrated a 3 year actuarial complete pain-free rate of 45% in patients who had prior procedures vs. 55% in patients who had primary radiosurgery. Hence, patients who underwent radiosurgery as their first procedure appear to achieve longer-lasting pain relief than those patients who underwent prior ablative or microvascular decompression. This conclusion has multiple caveats, of course. These comparisons are not randomized, and there is thus a significant amount of sampling bias, the median follow-up in our study was only 27 months, and methodological concerns can be raised to argue against this conclusion. Nevertheless, our data suggest that radiosurgery can provide durable pain relief for select patients.

For some patients, an important goal of surgical intervention is to eliminate their dependency on drugs and their concomitant side-effects. In this series approximately half of the patients who remained pain-free were completely off their medications, whereas approximately half of the patients remained dependent on some level of medication despite being pain-free. Some of these patients refused to stop their medications for fear of provoking an attack, and hence a true estimate of drug dependency cannot be determined from this study. Perhaps in future prospective studies, a drug reduction protocol could be instituted to address this issue systematically. Some authors have suggested that complete pain relief without medications should be the only marker of success for any procedure [4, 11]. It is argued that this would allow for direct comparisons across studies with equivalent outcome measures, and although we agree with the principle of this argument, we find that patients are happy to be pain-free, even if it requires the continuation of some of their medications.

Nevertheless, in counseling the patient, the surgeon should encourage patients to adopt reasonable expectations. If complete elimination of drugs is

the primary goal of the patient, perhaps a microvascular decompression could be offered [17].

Facial sensory loss is an important side effect of all neuroablative techniques used in the treatment of trigeminal neuralgia. Permanent facial sensory loss can be seen in approximately two thirds of patients treated with radiofrequency rhizotomy [18, 19], and a substantial percentage of these patients report diminished quality of life attributable to this numbness [17, 19]. In addition, Pollock et al. [21] have demonstrated a higher rate of trigeminal nerve dysfunction, including facial numbness in patients who were treated at a dose of 90 Gy as compared to those who were treated at a dose of 70 Gy (54 vs. 15%, $p = 0.003$). Bothersome dysesthesias occurred in 13 high-dose (90 Gy) patients (32%), whereas only 1 low-dose (70 Gy) patient had this complication ($p = 0.01$). In addition, three high-dose patients (8%) developed corneal numbness after radiosurgery. Hence, our median dose (80 Gy) lies between these two doses, and we would thus expect a rate of trigeminal dysfunction to be between these two rates. The rate of both temporary and permanent trigeminal dysfunction in this series was 19.5% ($n = 29$), of which permanent complications were seen in eight patients and temporary complications were seen in 21 patients. This rate of trigeminal dysfunction appears to be an acceptable risk for patients with trigeminal neuralgia, but careful counseling must be provided.

Other complications that appear with significant frequency in patients treated with other percutaneous techniques are generally avoided using Gamma Knife radiosurgery. For example balloon compression can result in a significant percentage of patients with masseter weakness [22]. This complication was not seen in this series and is rarely ever seen in Gamma Knife series. In addition, other complications such as meningitis and neurovascular injury and death have been reported after other percutaneous techniques [23–27]. These, however, are extremely unusual after radiosurgery. It is perhaps for this reason – the extremely low complication rate – after Gamma Knife radiosurgery that patients occasionally come to the clinic asking to be treated with radiosurgery even despite their being candidates for microvascular decompression. Trigeminal sensory dysfunction is the main complication of radiosurgery, and the rate of corneal anesthesia is low [28], and subsequent keratitis remains unreported. By virtue of its noninvasiveness and its low side effect profile, Gamma Knife radiosurgery has emerged as the minimally-invasive option of choice for a majority of patients.

Conclusion

Gamma Knife radiosurgery has emerged as an attractive treatment option for patients with trigeminal neuralgia. Its role as the first line surgical intervention

continues to evolve, and the experience at the University of Pittsburgh demonstrates its effect to be powerful and durable. Our data show that of the 87% of patients that achieve complete pain relief after primary radiosurgery, half of those patients can expect to remain pain-free for approximately six years. Permanent side effects are seen in 5% of patients and mostly consist of trigeminal sensory loss, which is generally tolerable.

References

1 Leksell L: The stereotaxic method and radiosurgery of the brain. Acta Chir Scand 1951;102:316–319.
2 Kondziolka D, Lunsford LD, Flickinger JC, et al: Stereotactic radiosurgery for trigeminal neuralgia: a multiinstitutional study using the gamma unit. J Neurosurg 1996;84:940–945.
3 Flickinger JC, Pollock BE, Kondziolka D, et al: Does increased nerve length within the treatment volume improve trigeminal neuralgia radiosurgery? A prospective double-blind, randomized study. Int J Radiat Oncol Biol Phys 2001;51:449–454.
4 Sheehan J, Pan HC, Stroila M, et al: Gamma knife surgery for trigeminal neuralgia: outcomes and prognostic factors. J Neurosurg 2005;102:434–441.
5 Hakanson S: Trigeminal neuralgia treated by the injection of glycerol into the trigeminal cistern. Neurosurgery 1981;9:638–646.
6 Rand RW, Jacques DB, Melbye RW, et al: Leksell Gamma Knife treatment of tic douloureux. Stereotact Funct Neurosurg 1993;61(suppl 1):93–102.
7 Jannetta PJ: Arterial compression of the trigeminal nerve at the pons in patients with trigeminal neuralgia. J Neurosurg 1967;26(suppl):159–162.
8 Kondziolka D, Flickinger JC, Lunsford LD, et al: Trigeminal neuralgia radiosurgery: the University of Pittsburgh experience. Stereotact Funct Neurosurg 1996;66(suppl 1):343–348.
9 Burchiel KJ: A new classification for facial pain. Neurosurgery 2003;53:1164–1166; discussion 1166–1167.
10 Lopez BC, Hamlyn PJ, Zakrzewska JM: Stereotactic radiosurgery for primary trigeminal neuralgia: state of the evidence and recommendations for future reports. J Neurol Neurosurg Psychiatry 2004;75:1019–1024.
11 Zakrzewska JM, Lopez BC: Quality of reporting in evaluations of surgical treatment of trigeminal neuralgia: recommendations for future reports. Neurosurgery 2003;53:110–120; discussion 112–120.
12 Maesawa S, Salame C, Flickinger JC, et al: Clinical outcomes after stereotactic radiosurgery for idiopathic trigeminal neuralgia. J Neurosurg 2001;94:14–20.
13 Pollock BE, Phuong LK, Gorman DA, et al: Stereotactic radiosurgery for idiopathic trigeminal neuralgia. J Neurosurg 2002;97:347–353.
14 Rogers CL, Shetter AG, Fiedler JA, et al: Gamma knife radiosurgery for trigeminal neuralgia: the initial experience of The Barrow Neurological Institute. Int J Radiat Oncol Biol Phys 2000;47: 1013–1019.
15 Young RF, Vermulen S, Posewitz A: Gamma knife radiosurgery for the treatment of trigeminal neuralgia. Stereotact Funct Neurosurg 1998;70(suppl 1):192–199.
16 Lunsford LD, Bennett MH: Percutaneous retrogasserian glycerol rhizotomy for tic douloureux: Part 1. Technique and results in 112 patients. Neurosurgery 1984;14:424–430.
17 Barker FG 2nd, Jannetta PJ, Babu RP, et al: Long-term outcome after operation for trigeminal neuralgia in patients with posterior fossa tumors. J Neurosurg 1996;84:818–825.
18 Salar G, Mingrino S, Iob I: Alterations of facial sensitivity induced by percutaneous thermocoagulation for trigeminal neuralgia. Surg Neurol 1983;19:126–130.
19 Zakrzewska JM, Jassim S, Bulman JS: A prospective, longitudinal study on patients with trigeminal neuralgia who underwent radiofrequency thermocoagulation of the Gasserian ganglion. Pain 1999;79:51–58.

20 Siegfried J: Percutaneous controlled thermocoagulation of Gasserian ganglion in trigeminal neuralgia. Experiences with 1000 cases; in Samii MJ (ed): The Cranial Nerves. Berlin, Heidelberg and New York, Springer-Verlag, 1981, pp 322–330.
21 Pollock BE, Phuong LK, Foote RL, et al: High-dose trigeminal neuralgia radiosurgery associated with increased risk of trigeminal nerve dysfunction. Neurosurgery 2001;49:58–62; discussion 62–54.
22 Lobato RD, Rivas JJ, Sarabia R, et al: Percutaneous microcompression of the gasserian ganglion for trigeminal neuralgia. J Neurosurg 1990;72:546–553.
23 Abdennebi B, Mahfouf L, Nedjahi T: Long-term results of percutaneous compression of the gasserian ganglion in trigeminal neuralgia (series of 200 patients). Stereotact Funct Neurosurg 1997;68:190–195.
24 Jho HD, Lunsford LD: Percutaneous retrogasserian glycerol rhizotomy. Current technique and results. Neurosurg Clin N Am 1997;8:63–74.
25 Kanpolat Y, Savas A, Bekar A, et al: Percutaneous controlled radiofrequency trigeminal rhizotomy for the treatment of idiopathic trigeminal neuralgia: 25-year experience with 1,600 patients. Neurosurgery 2001;48:524–532; discussion 532–524.
26 Meglio M, Cioni B, d'Annunzio V: Percutaneous microcompression of the gasserian ganglion: personal experience. Acta Neurochir Suppl (Wien) 1987;39:142–143.
27 Nugent GR: Radiofrequency treatment of trigeminal neuralgia using a cordotomy-type electrode. A method. Neurosurg Clin N Am 1997;8:41–52.
28 Matsuda S, Serizawa T, Sato M, et al: Gamma knife radiosurgery for trigeminal neuralgia: the dry-eye complication. J Neurosurg 2002;97:525–528.

L. Dade Lunsford
Department of Neurological Surgery, Suite B-400
University of Pittsburgh Medical Center
200 Lothrop Street
Pittsburgh, PA 15213 (USA)
Tel. +1 412 647 6250, Fax +1 412 647 6483
E-Mail lunsfordld@upmc.edu

Kondziolka D (ed): Radiosurgery. Basel, Karger, 2006, vol 6, pp 260–267

Gamma Knife Surgery for Essential Trigeminal Neuralgia: Advantages in New Treatment Strategy with Robotized Micro-Radiosurgery

M. Hayashi[a–d], *T. Ochiai*[a,c,d], *N. Murata*[a,d], *K. Nakaya*[a], *M. Izawa*[a], *M. Chernov*[a,c], *T. Hori*[a], *J. Régis*[b,d], *K. Takakura*[a,b]

[a]Department of Neurosurgery, Neurological Institute, Tokyo Women's Medical University, Tokyo, [b]Graduate School of Medicine, Institute of Advanced Biomedical Technology & Science, Tokyo Women's Medical University, Tokyo, [c]Saitama Gamma Knife Center, Sanai Hospital, Saitama, Japan; [d]Service de Neurochirurgie Fonctionnale et Stereotaxique, CHU La Timone, Marseille, France

Abstract

Gamma Knife surgery (GKS) is a minimally invasive treatment for brain diseases, and is currently used for functional disorders. Moreover, a revised version of Gamma Knife system, 'Model C-APS (automatic positioning system)' started to be installed in Japan since 2001. This latest model enables us to adjust coordinates by every 0.1 mm, and treat the patient automatically. We have completed a retrospective study of 222 patients suffering from essential trigeminal neuralgia treated with GKS in which the target was localized at the retro-gasserian portion of the nerve (We have treated 179 patients with essential trigeminal neuralgia by 'Model C-APS'). Among the patients, 147 were followed up more than 12 months, and we evaluated a cause-and-effect relationship between the technical development and the clinical results. We categorized patients into three groups based on the term mentioned as follows: first are the patients treated by Model B without completed fusion images in between 1999 and 2001, second are the patients treated by Model B with completed fusion images in 2002, and third are those treated by model C-APS with completed fusion images since 2003. Clinical result, initial pain free was observed in 62.9% (first group), 85.7% (second group), 98.1% (third group), complete recurrence was observed in 12, 8.3, 1.9% for each groups, and postoperative complication was observed in 22.2, 28.6, and 23.6% respectively. We believe that precise dose planning, so-called 'Robotized Micro Radiosurgery', is the key to have a successful GKS.

Gamma Knife surgery (GKS) has become one of the most advanced neurosurgical treatments available. It is well known to be a minimally invasive surgical procedure that can control tumor growth, and moreover, it is efficacious and safe for control of functional disorders without craniotomy.

Recently, we have focused on the management of intractable pain, particularly trigeminal neuralgia (TGN) that has become a functional disease commonly treated by GKS worldwide. Many clinical reports have demonstrated that GKS can provide satisfactory results for patients without serious complications. In this chapter, we will present our institutional experience of GKS treatment for TGN.

Treatment Options for TGN in General

In treating patients with TGN, we normally administer carbamazepine. When the effect is insufficient, we must consider surgical procedures such as glycerol rhizotomy, thermocoagulation, micro-balloon compression, and micro-vascular decompression. The initial pain free rate is reportedly 74–94% and the recurrence rate 16–45% [1–3]. Recently, GKS has been regarded as an alternative treatment for TGN. For the elderly patients in whom surgery has failed and who suffer from possible risks associated with general anesthesia, GKS (the least invasive treatment) is particularly recommended.

Treatment Concept for TGN in GKS

In GKS for TGN, we normally use only 1 isocenter with a 4 mm collimator, and place it at the trigeminal nerve on the affected side. There are two different means of nerve target positioning. One target is exclusively the root entry zone (REZ), which is 2–4 mm from the brain stem and the neuroanatomical border between oligodendrocytes and schwan cells. This strategy is favored by the Pittsburgh group. Another target is the retro gasserian region (RGR), which is located at the trigeminal incisula. This is the approach of the Marseille group. At our institute, we have employed the RGR method for two main reasons:

(1) *Efficacy and safety*: The RGR target is adequately far from the brain stem for an optimal dose (90 Gy at maximum) to the nerve. To date, we have achieved greater effectiveness while avoiding damage to the brain stem that could occur with high dose irradiation.
(2) *Efficacy and accuracy*: we can correct the MRI distortion precisely by using CT/MRI fusion images, because RGR targeting requires a bone landmark; the trigeminal incisula at the top of the petrous bone. On the contrary, it is impossible to directly correct MRI distortion with REZ targeting.

Table 1. The list of treatment indications and diagnostic criteria for essential TGN

Electric discharge
Unique topography (no bilateral)
No neurological deficit (no sensory abnormality of face, no corneal hyporeflex)
No other type of pain (no atypical pain)
Trigger (touch and face washing/tooth brushing/mastication/speech/etc., swallowing)
Initial effect of Carbamazepine

Patient Eligibility

In the field of functional radiosurgery, appropriate patient selection is critical. TGN should be regarded as apparent TGN, to be confirmed clinically. Table 1 presents the features of six subjects with a tentative diagnosis of TGN. Before concluding that GKS can be done, all subjects must be fully informed. Our treatment aim is to prevent or reduce 'electric discharge'.

GKS Procedure for TGN

With frame fixation of the head, the frame must be placed parallel to the trigeminal nerve. Anatomical information regarding the nerve should also be confirmed. Next, we consider MRI sequence selection. Our aim is good visualization of the nerve in the cerebello-pontine cistern. Therefore, we normally use ultra-thin sliced (0.5 mm) 3D heavily T2 WI and thin sliced (1.0 mm) axial CT bone images. Before dose planning, we obtain MRI/CT fusion images. We use RGR targeting, and an irradiation dose of 90 Gy, at maximum, considering the cerebello-pontine cistern space. If the cistern is narrow, however, we use a beam plugging technique to modify the 20% isodose line (18 Gy area), making it parallel to the surface of the brain stem, thus avoiding excessive radiation of the brain stem. We assess the existence of MRI distortion using the MRI/CT fusion images and if any is detected, the amount of distortion is calculated precisely. After confirming the degree of distortion between CT and MRI images, we can correctly and precisely adjust it using an automatic positioning system (APS) by 0.1 mm level (fig. 1). The most important aspect of TGN is radiosurgery that delivers sufficient energy to the nerve with the smallest possible collimator. This means that the isocenter should fall precisely on the center of the true trigeminal nerve. We can achieve this precision by using 3D images (fig. 2) in the final stage of dose planning.

1

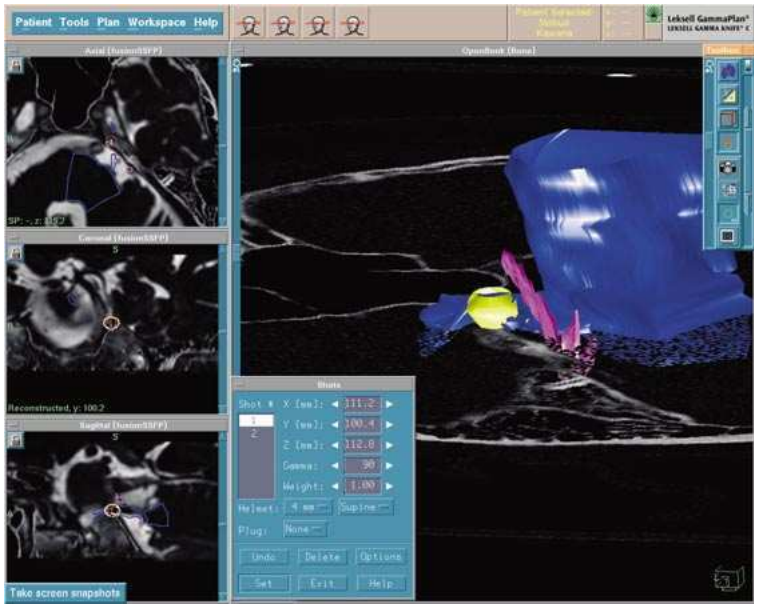

2

Figs. 1, 2. Irradiation planning for TGN (GammaPlan). ***1*** Demonstrates 2D image and ***2*** shows 3D image. Both figures display the anatomical relationships including the trigeminal nerve and surrounding vital structures. The artery obviously conflicts the trigeminal nerve located on trigeminal incisula, and the never is properly covered by the 50% isodose area of 4 mm isocenter.

Efficacy and Clinical Outcome

We have treated 222 patients with TGN (including two underwent second GKS) by Gamma Knife using RGR targeting. Among them, 147 followed up for more than 12 months were clinically evaluated. Initial pain reduction was observed in 98.6% (145/147), complete relief of 'electric discharge' was completed in 91.1% (134/147). Significant effects were ranged from 1 to 90 (mean 26.4) days. True recurrence was observed in 2.9% (4/137). Delayed recurrence was detected at 6–24 months. Postoperative complications (hypoesthesia and dysesthesia) developed in 23.8% (35/147), and 6.8% (10/147) of the patients complained bothersome. However, there were no mortalities. In those who received GKS only once, this rate was 22.4% (33/147). We also investigated clinical outcome according to the following treatment factors:

(1) *First generation group (1998–2001)*: treatment using model B without completely fusion images: 29 cases (27 cases with follow-up).
(2) *Second generation group (2002)*: treatment using model B with completely fusion images: 14 cases (all with follow-up).
(3) *Third generation group (2003–2004)*: treatment using model C-APS with completely fusion images: 179 cases (106 cases with follow-up).

Initial significant pain reduction was observed in 92.6% (25/27) of the first group, 100% of the second (14/14) and 99.1% of the third (105/106). The respective pain free (= complete relief of electric discharge) rate was 63% (17/27), 85.7% (12/14), and 98.1% (104/106). Those with true recurrence were 12% (3/25), 8.3% (1/12) and 1.9% (2/104). Postoperative complication rates were 22.2% (6/27), 28.6% (4/14) and 23.6% (25/105). Both third group cases that developed postoperative dysesthesia underwent GKS twice. Although the follow-up of the third group is yet insufficient, the results are clearly the best among the three.

At our institution, no significant predictive parameter has been identified from our clinical results, age, gender, affected side, topology, carbamazepine dose, delay of onset, previous intervention, cistern space, nerve atrophy, etc.

Discussion

Optimal Targeting

TGN is the most common functional disease that can be controlled well by GKS. This has already been established as single isocenter irradiation with a 4 mm collimator. However, clinical outcomes differ markedly from one institution to another.

Régis et al. [3] (Marseille group) reported the clinical outcomes of 110 patients with RGR targeting in their prospective study. The initial pain free rate

was observed in 97.2% (104/107), and delay of effects was seen at 26.2 days on average (1 day – 6 months). True recurrence was observed in 14.4% (15/104), postoperative complications in 4.5% (5/107). On the other hand, Kondziolka et al. [4] and Maesawa et al. [5] (Pittsburgh group) reported their clinical experience with 220 patients in whom the initial pain free rate was 70.3%, that of true recurrence 13.6%, and postoperative complications were seen in 10.2%.

Fukuoka [6] evaluated treatment data (1,145 cases) and clinical outcomes from multiple Japanese facilities and found that targeting position varies among institutions. REZ targeting was more widely used in Japan (69.4%) than RGR targeting (20.4%). MRI/CT fusion images were not used in all institutions. Significant pain reduction was observed in 85% (973/1145) of cases, approximately 70% (800/1145) of whom had initial pain relief, and the delay of effect was 30 days on average (1–120 days). True recurrence was observed in 9.5% (109/1145), and delayed recurrence at 6.4 months on average (0–48 months). Postoperative complications developed in 12.3% (141/1,145), including 1.4% (16/1,145) with severe complaints. Clinical outcomes at our institution, particularly for the third group (model C-APS with MRI/CT fusion images) were close to those of the Marseille group [7].

So far, we have regarded RGR targeting as more advantageous than REZ targeting in terms of both efficacy and safety. The reasons are: (1) possible to irradiate with optimal dose (90 Gy) with care to protect brain stem, (2) more accurate treatment with availability of MRI/CT fusion images.

Indications for Elderly Patients with Intractable TGN

In order to confirm GKS indications for elderly patients (more than 65 years old) suffering from intractable TGN, Hayashi [8] investigated 69 elderly subjects from the Marseille prospective study of 110 patients. Three issues were considered:

(1) *Comparison of clinical outcomes between elderly and younger groups*: Initial pain relief was observed in 95.7% of the elderly group (vs. 100% in younger group), true recurrence in 16.7% (vs. 10.5% in younger group), and postoperative complications in 2.9% (vs. 5.4% in younger group). As to the response of TGN for GKS, the younger group had slightly more favorable results than the elderly group. However, results are apparently acceptable for elderly patients.

(2) *Comparison of clinical outcome in between previous surgical intervention (PSI) and no previous surgical intervention (NPSI) group*: Initial pain relief was observed in 92.6% (PSI) and 97.6% (NPSI), true recurrence in 20% (PSI) and 24.4% (NPSI), and postoperative complications in 12% (PSI) and 9.8% (NPSI), respectively. The NPI group had better results than the PI group, indicating that elderly patients with TGN should undergo GKS as the critical procedure before surgical intervention.

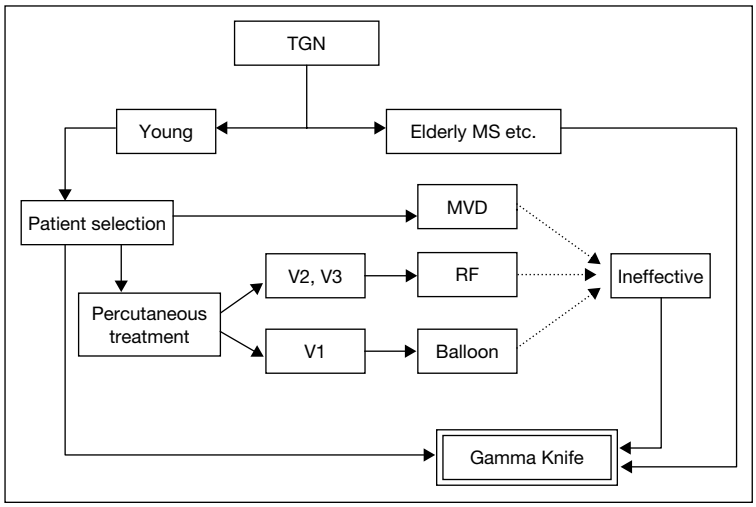

Fig. 3. Clinical indication for essential TGN. MS = Multiple sclerosis; MVD = micro vascular decompression; RF = radiofrequency; TGN = trigeminal neuralgia.

(3) *Comparison of clinical outcomes between 90 Gy and lower dose groups*: Initial pain relief was observed in 96.8% of 90 Gy group (vs. 94.7% in lower dose group), true recurrence in 12.9% (vs. 27.8% in lower dose group), and postoperative complications in 3.2% (vs. 2.6% in lower dose group). Notably, the rate of true recurrence was significant higher in the lower dose group ($p < 0.05$). On the other hand, the rate of postoperative complication did not differ significantly. Thus, 90 Gy appears to be an optimal dose for elderly patients.

In treating elderly patients with TGN, we recommend using the optimal radiosurgical dose (90 Gy at maximum) before any surgical intervention.

Overall Management and Treatment Indications for TGN

If the patient is relatively younger, we recommend surgical intervention first, because the long-term effects of radiosurgery for TGN are yet unknown. Surgical procedures should be selected according to localization of the pain, severity of vessel involvement and patient choice (fig. 3). If surgical procedures fail or the effect is inadequate, we recommend GKS. If the patient is older, we recommend GKS as the first treatment for TGN prior to surgical procedures (fig. 3). Likewise, in young patients, if surgery fails or its effect is inadequate, we recommend a second GKS or other surgical procedures as necessitated by the patient's condition.

Conclusions

Overall, 15,000 cases suffering from TGN have been treated by GKS worldwide. In addition, many published reports on clinical results and strategies have emphasized that GKS provides satisfactory results to most patients with few severe complications. To date, TGN has been widely accepted as an indication for GKS in the functional disease field. However, its mechanism of action has not yet been elucidated. If GKS produces destructive change in the nerve itself, patients will have sensory loss affecting half of the face. A 90 Gy dose appears to be sufficient to produce a functional effect, termed the 'Biological Differential Effect', on the normal nerve/CNS without tissue ablation. This concept is expected to play an important role in treating other functional diseases. Epilepsy and cancer pain have been managed with pituitary radiosurgery. Therefore, both basic and clinical studies are needed to confirm the efficacy and safety of GK radiosurgery for functional diseases. Of course, it goes without saying that we need much longer follow-up after treatment to make an evaluation if GKS is an appropriate treatment for patients with TGN.

References

1 Mullan S, Lichtor T: Percutaneous microcompression of the trigeminal ganglion for trigeminal neuralgia. J Neurosurg 1983;59:1007–1012.
2 Barker FG, Janetta PG, Bissonette DJ, et al: The longterm outcome of microvascular decompression for trigeminal neuralgia. N Engl J Med 1996;334:1077–1083.
3 Régis J, Bartolomei F, Metellus P, et al: Radiosurgery for trigeminal neuralgia and epilepsy. Application of radiosurgery. Neurosurg Clin N Am 1999;10:359–377.
4 Kondziolka D, Lunsford D, Flickinger JC, et al: Stereotactic radiosurgery for trigeminal neuralgia: a multi-institutional study using the gamma unit. J Neurosurg 1996;84:940–945.
5 Maesawa S, Salame C, Flickinger JC, et al: Clinical outcomes after stereotactic radiosurgery for idiopathic trigeminal neuralgia. J Neurosurg 2001;94:14–18.
6 Fukuoka S: Gamma knife radiosurgery for trigeminal neuralgia – multi-institute study of 1,145 cases in Japan. Presented at 12th Leksell International Conference of Gamma Knife Society, Vienna, Austria, 2004.
7 Hayashi M, Ochiai T, Chernov M, et al: Gamma Knife surgery for essential trigeminal neuralgia: new treatment strategy with robotized micro-radiosurgery; in International proceeding of 14th WSSFN; Rome, Mario Meglio, MEDIMOND, 2005; 231–238.
8 Hayashi M: Current Gamma knife surgery for intractable pain [in Japanese]. Pain Clin 2003;24: 213–231.

Motohiro Hayashi
Department of Neurosurgery, Neurological Institute
Tokyo Women's Medical University
8–1 Kawada-cho, Shinjuku-ku
Tokyo 162–8666 (Japan)
Tel. +81 3 3341 6878, Fax +81 3 3341 6878
E-Mail GKRmoto@aol.com

Kondziolka D (ed): Radiosurgery. Basel, Karger, 2006, vol 6, pp 268–276

Gamma Knife Pituitary Radiosurgery for Thalamic Pain Syndrome: New Treatment Trial in Our Institutional Experience

M. Hayashi[a,b,d], *T. Taira*[a], *T. Ochiai*[a,d], *M. Chernov*[a], *K. Nakaya*[a,d], *M. Izawa*[a], *N. Kouyama*[c], *Y. Katayama*[c], *Y. Kawakami*[c], *T. Hori*[a], *K. Takakura*[a,b]

[a]Department of Neurosurgery, Neurological Institute, [b]Graduate School of Medicine, Institute of Advanced Biomedical Technology & Science, [c]Department of Physiology, Tokyo Women's Medical University, Tokyo; [d]Saitama Gamma Knife Center, Sanai Hospital, Saitama, Japan

Abstract

Rationale: Currently, one of represented severe pain, cancer pain related to bone metastasis, has been able to be controlled well using Gamma Knife pituitary radiosurgery (GKPR) without any significant complication. According to the literature, one clinical report found out, that central pain, such as thalamic pain syndrome, had also been controlled with chemical hypophysectomy even though accompanied with transiently diabetes insipidus. This historical evidence also prompted us to perform GKPR for control of thalamic pain syndrome with development of the treatment concept of cancer pain. **Material and Method:** In our institutional experience, we have treated 27 patients who were suffered from central pain with GKPR, and among them, 22 patients who were suffered from thalamic pain syndrome. The target was the just pituitary gland involving the border in between the pituitary stalk and gland. Prescribed maximum dose was 140–180 Gy. We could follow up 20 patients with thalamic pain syndrome more than 6 months. **Results:** Initial significant pain reduction was observed in 75.0% (15/17). Most effective cases experienced pain reduction within 48 h later. Long-term effective (>1 year) was observed in 33.3% (5/15). In the other cases, rapidly recurrence (<3 months) was observed in 33.3% (5/15). No any significant post-operative complication was observed excluding only two patient who developed transiently diabetes insipidus. **Conclusions:** Our clinical study protocol is not mandatory. Much more investigation for clinical results of GKPR in the patients with thalamic pain syndrome is needed to optimize this treatment protocol. However, some efficacy and safety have been shown in all our cases. We suppose that GKPR has a potential to control for this kind of intractable central

pain, and, in the nearest future, will play an important role in the field of the management of intractable pain.

Post-stroke thalamic pain syndrome is one of represented intractable pain, which has been hardly to be cured. This intractable pain has been tried to be controlled with various protocols such as medication and functional neurosurgery, but no sufficient pain control has been observed.

Before three or four decades, intractable pain had been tried to be controlled with hypophsectomy. In 1953, Luft and Olivecrona [1] reported first experience of control of cancer pain with surgical hypophysectomy for the patients with breast cancer and the surgical hypophysectomy had been performed for pain control [2–4]. Subsequently, chemical hypophysectomy which was directly pituitary ablation using alcohol injection had been developed as an alternative lesser invasive treatment [5–8]. So far, the overall clinical results of surgical/chemical hypophysectomy achieved in 64.4% of complete pain relief in 1,101 reported cases who suffered from cancer pain [1–7]. However, majority of patients had developed into significant post-operative complication such as, panhypopituitarism, severe diabetes insipidus, meningitis, visual dysfunction, and hypothalamic insult.

In order to integrate surgical/chemical hypophysectomy to be safer treatment using Gamma Knife surgery (GKS), Backlund et al. [9, 10], in 1972, had tried to treat cancer pain with GKS, targeted to the pituitary gland with 200–250 Gy as a method of pituitary ablation. This report was the first series of pituitary ablation by GKS to show the efficacy and safer than hypophysectomy. Subsequently, Hayashi et al. have reported that 'Gamma Knife pituitary radiosurgery' (GKPR) with highly resolution of MRI/CT using relatively lower irradiation dose (160 Gy) under the concept of no ablation of pituitary gland, could also control well cancer pain [11–18]. Additionally, no any significant adverse effect was observed within limited follow-up (1–24 months). So far, GKPR has been recognized as effective and safer treatment for control of intractable pain, even though action mechanism has not been elucidated.

In 1983, Levin et al. [19] had applied chemical hypophysectomy to thalamic pain syndrome and reported their experience of 3 patients' clinical results. All cases had experienced significant pain reduction within 48 h, and finally 2 of them presented complete pain relief and another one presented much significant pain reduction (>80%). All cases had been accompanied with temporally secondary effect, panhypopituitarism and diabetes insipidus. The efficacy had been lasting within 19–58 months.

Therefore, we just established and have tried to control thalamic pain syndrome with GKPR due to both historical and our own clinical evidence. In this article, we would like to report our initial experience and clinical results, and to demonstrate the potential of GKPR for thalamic pain syndrome.

Materials and Methods

An indication of thalamic pain syndrome in GKPR is as follows: (1) The pain should be post-stroke thalamic pain syndrome, (2) no any other effective treatment prior to GKS, (3) high risk patient: impossible to be treated under general anesthesia, (4) main complaint is 'pain', not 'numbness'.

Patient eligibility was critically performed. Among all, the most important subject is that main complaint is 'pain', not 'numbness'. In our limited experience, no clinical improvement of numbness was observed after GKPR. At the time of pre-operative evaluation, we had to confirm all patients as a normal visual and endocrinological function.

Leksell frame was applied on the head with parallel to the optic pathway. We performed MRI (T1WI axial 1.0 mm slices/T2WI coronal 2.0 mm slices/3D heavily T2WI axial 0.5 mm slices) and CT (plain axial 1.0 mm slices/bone 1.0 mm slices). We were using Gamma Plan (ELEKTA Instrument AB) to make dose planning for this treatment. A center of the isocenter should be located on the pituitary gland. Additionally, 50% isodose area (8 mm collimator) should involve the border of between the pituitary gland and lower part of the pituitary stalk. We were normally using 140–180 Gy at maximum dose. Subsequently, we should take into account for the delivered irradiation dose to the optic pathway to be kept less than 10 Gy at maximum dose. If the length of pituitary stalk is too short, we will have to move the isocenter to be lower in order to reduce the excessive irradiation dose to the optic pathway. We had better to modify gamma angle from 90 degrees to 75–85 degrees to make the 10 Gy isodose line parallel to the optic pathway. And we should use beam plugging technique to modify the shape of 10 Gy line to reduce the delivered dose to the optic pathway, without modification of 50% isodose line.

Finally, we have to check it up using three dimensional images to confirm the relationship between the target (50% isodose line) and the surround vital structures on the display of Gamma Plan (fig. 1), and to know the relationship between 10 Gy line and the optic pathway (fig. 2).

In our institutional experience, we treated 22 patients with post-stroke thalamic pain syndrome. 20 cases were available to be followed up more than 6 months (3–24 months).

Results

Clinical Data and Dose/Energy Calculation in Patients with Thalamic Pain Syndrome

We have treated 22 patients with thalamic pain syndrome, the average age was 64.7 years old, and 14 men and 8 women. All cases had suffered from cerebral vascular disease; 16 thalamic hemorrhage, 5 thalamic infarction, and 1 malignant lymphoma which was treated by radiosurgery. The mean duration between onset and treatment was 91.2 months.

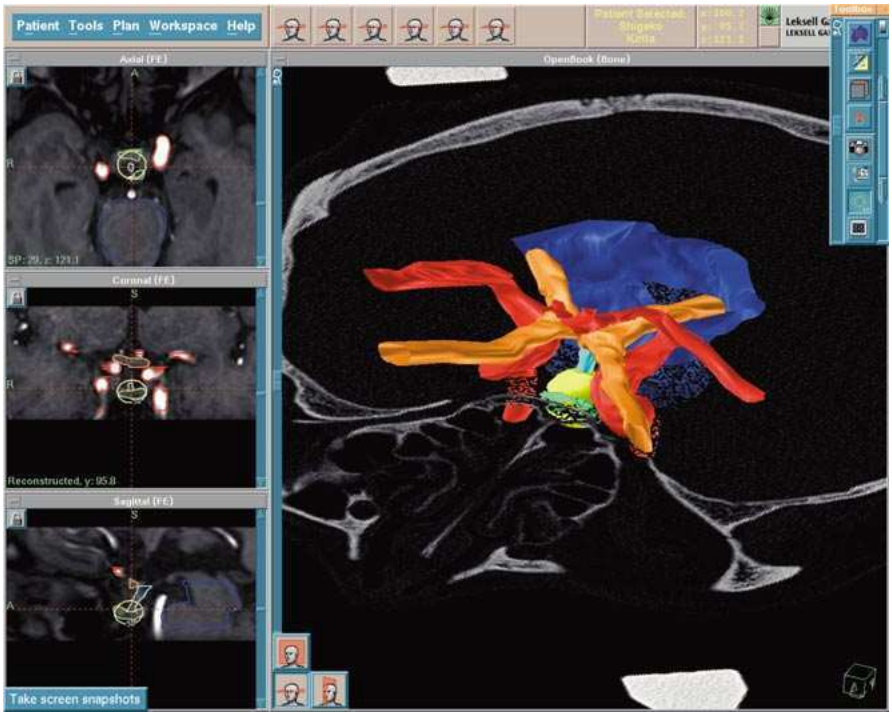

Fig. 1. Dose planning on 3D image (50% isodose): This figure showed the target, which was 50% isodose area (80 Gy) and the anatomical relationship between the target and the optic pathway, carotid artery, pituitary gland, stalk, and brain stem.

We did check dose/energy calculation in every patient, mean length of the pituitary stalk was 9.1 mm, mean maximum and average dose of the pituitary stalk were 136.2 Gy and 45.9 Gy. Mean unit energy, which is energy (mJ) per volume (cm^3), of the pituitary stalk was 29.4 mJ/cm^3. Mean maximum and average dose of the pituitary gland were 146.2 and 110.2 Gy. Mean unit energy of the pituitary gland was 111.7 mJ/cm^3.

Clinical Results of Patients with Thalamic Pain Syndrome after GKPR

Almost all cases have both symptoms of severe pain and numbness at the time of pre-operative evaluation. Initially, pain reduction was observed in 75.0% (15/20) within 48 h after GKPR. Long-term effective (more than 1 year) was observed in 33.3% (5/15). However, 33.3% (5/15) was only within 3 moths effective (rapidly recurrence) and the other 33.3% (5/15) was within 6 months

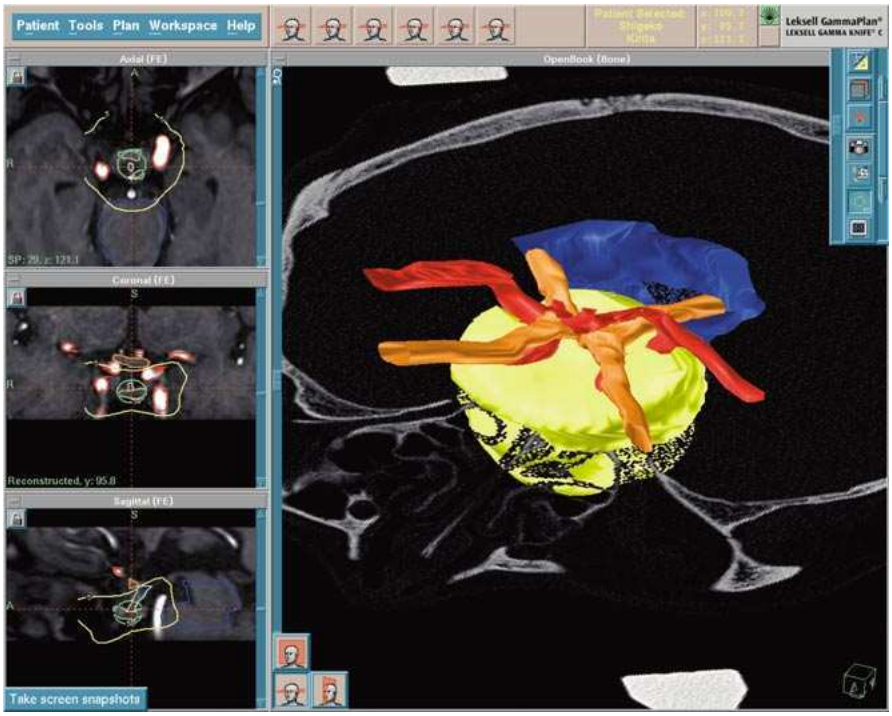

Fig. 2. Dose planning on 3D image (5% isodose): This figure showed the 5% isodose area (8 Gy) to know the anatomical relationship between the area and the optic pathway. We have to avoid excessive irradiated dose to the optic pathway.

effective. Severe numbness has never improved since GKPR. One patient felt worsening after GKPR, because the severity of numbness got worsen in spite of significant pain reduction. No secondary effect of hormonal insufficiency was observed excluding two transiently slight DI. No patient developed visual dysfunction. No any morphological change on MRI was demonstrated within limited follow-up (fig. 3).

Discussion

Hypophysectomy and β*-Endorphin*

The action mechanism that hypophysectomy caused in complete pain relief was not yet elucidated. Majority of the patients with cancer pain have been treated by morphine and have experienced reduction of pain. Therefore,

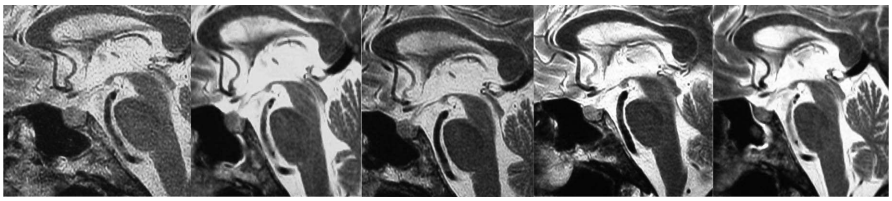

Fig. 3. No morphological change of the pituitary gland on T2 sagittal images after Gamma knife surgery.

one of the action mechanisms was supposed as that hypophysectomy might have triggered an intrinsic morphine like effect. β-endorphin, whose pre-cursor (pre-pro-opiomelanocortin: PPOMC) was existed in the pituitary gland and the arcuate nucleus in the hypothalamus, is known very well to control this kind of severe pain like morphine. There were several reports, the level of β-endorphin increased after hypophysectomy in both blood and cerebrospinal fluid of the patients. Hypophysectomy, ablation of the pituitary gland and stalk, was supposed to trigger to release excessive quantity of PPOMC into the blood and cerebrospinal fluid. On the other hand, even though GKPR did not make apparently damage to the pituitary gland/stalk, endocrinological and morphological point of view. We suppose that β-endorphin should be one of contribution in this action mechanism to reduce the pain severity.

What Is the Action Mechanism of GKPR for Thalamic Pain Syndrome?

Lately, pituitary gland-stalk irradiation with Gamma Knife has been applied as a new alternative treatment option for control of cancer pain. GKPR has provided surprisingly and satisfactory clinical results; immediately, completely, and long lasting clinical effect in control of cancer pain without any significant secondary effects, although we did use extremely highly irradiation average dose and unit energy as 110.2 Gy and 117.2 mJ/cm^3, comparing with those of tumor/vascular anomaly radiosurgery (20–30 mJ/cm^3). We could summarize the effect of GKPR according to our clinical experience as follows; (1) There was no evidence of destructive changes: no dysfunction of endocrinological status and no morphological change of MRI findings [11, 12, 14, 16, 17], and (2) Clinical symptoms showed hyperfunction of the hypothalamus after GKPR: rapidly recovering appetite loss and general condition [11, 12]. GKPR has provided pain reduction as same as hypophysectomy, however severe secondary effect was never seen in the cases of GKPR [11, 12]. Therefore, we strongly supposed, the action mechanism due to GKPR might have provided something of new ‘biological differential

effect' to the hypothalamus-thalamus instead of our expected 'destructive effect' to the pituitary gland/stalk as a hypophysectomy. That should be new 'neuromodulating effect' to the central nervous system by Gamma knife radiosurgery [10–17]. We supposed that this kind of biological differential effect might have also provided efficacy to thalamic pain syndrome. We have just started to investigate MR Spectroscopy in the area of hypothalamus and thalamus to try to show biological differential effect as hyperfunction of the hypothalamus-thalamus, especially the level of NAA/Cr ratio, which is related to the activity of neuron cells.

Rationale and Future Work of GKPR for Thalamic Pain Syndrome

Levin's experience prompted us to establish one sophisticated idea that thalamic pain syndrome could be also controlled with GKPR like cancer pain treatment. In 2002, we developed new treatment protocol for thalamic pain syndrome according to our experience of cancer pain [13–17]. We defined the maximum dose as 140 Gy which was smaller than 160 Gy for cancer pain, because we had to take into account for the risk of secondary effect for these patients who were expected to alive longer. According to the initial clinical results of 8 cases, 7 cases (87.5%) experienced initial pain reduction, however majority of cases (71.4%) presented real recurrence within 6 months without any secondary effect. Even if GKPR provide temporally efficacy, but this biological phenomenon prompt us to develop the new treatment indication. The only remaining problem was the duration of effect. Lately, we suppose, the maximum dose should be shifted from 140 to 160–180 Gy as equal to the treatment protocol for cancer pain with GKPR [13–17]. Much more experience and longer duration of follow-up are necessary to evaluate the efficacy and safety. However, GKPR has been shown to provide significant pain reduction to majority of the patients without any secondary effect. We strongly suppose, GKPR has a possibility to control this kind of medically refractory severe pain in the nearest future.

Conclusions

In our institutional experience, we have treated 39 consecutive patients with intractable (12 patients with cancer pain related to the bone metastasis and 27 patients with intractable central pain). Both two subgroups had a good indication of the treatment with GKS targeted to the pituitary gland/stalk (GKPR), and were treated safely. Majority of the patients experienced significant pain reduction.

So far, our experience is still limited. Moreover, some modification is needed, especially for patients with thalamic pain syndrome. However, the efficacy and the safety were shown in majority of the patients. We believe that this treatment has a potential to manage the control of the intractable severe pain, and GKPR will play a much important role in the field of pain control. Before final evaluation, we have to have much more experience and make an optimal protocol to evaluate which parameters is the most important, to know what treatment strategy is the best, to crucially prove the efficacy and the safety, and to develop this treatment.

References

1 Luft R, Olivecrona H: Experiences with hypophysectomy. J Neurosurg 1953;10:301–316.
2 Forrest APM, Blair DW, Peebles Brown AD: Radioactive implantation of the pituitary. Br J Surg 1959;47:61–70.
3 Hardy J: Transsphenoidal hypophysectomy. J Neurosurg 1971;34:582–594.
4 Zervas N: Stereotaxic radio-frequency surgery of the normal and abnormal pituitary gland. Semin Med Beth Isr Hosp 1969;280:429–437.
5 Greco T, Sbaragli, Cammili L: L alcoolizatione della ipofisi per via transdenoidale nalla terapia di particoleri tumori malgni. Settim Med 1957;45:355–356.
6 Katz J, Levin AB: Treatment of diffuse metastatic cancer pain by instillation of alcohol into the sella turcica. Anesthesiology 1977;46:115–121.
7 Lipton S, Miles J, Williams N, et al: Pituitary injection of alcohol for widespread cancer pain. Pain 1978;5:73–82.
8 Morrica G: Chemical hypophysectomy for cancer pain; in Bonica JJ (ed): Advances in Neurology. Pain. New York, Raven Press, 1974, vol 4, pp 707–714.
9 Backlund EO, Rahn T, Sarby B, et al: Closed stereotaxic hypophysectomy by means of ^{60}Co gamma radiation. Acta Radiol Ther Phys Biol 1972;11:545–555.
10 Backlund EO: Gamma hypophysectomy. J Neurosurg 2004;100:1133–1134; author reply by Hayashi M in p 1134.
11 Hayashi M, Nakaya K, Ochiai T, et al: Gamma knife radiosurgery for cancer pain – new trial method for gamma knife radiosurgical pituitary stalk ablation – (Jpn). Stereotact Radiother 2000;4:1–12.
12 Hayashi M, Taira T, Chernov M, et al: Gamma knife surgery for cancer pain – pituitary gland-stalk ablation: a multicenter prospective protocol since 2002. J Neurosurg 2002;97(suppl 5): 433–437.
13 Hayashi M: Current strategy of gamma knife surgery for intractable pain (Jpn). Pain Clinic 2003;24: 213–231.
14 Hayashi M, Taira T, Chernov M, et al: The role of pituitary radiosurgery for the management of intractable pain and potential future applications. Stereotact Funct Neurosurg 2003;81: 75–83.
15 Hayashi M, Taira T, Chernov M, et al: The role of pituitary gamma knife surgery for management of intractable pain and potential for future work; in Kondziolka D (ed): Radiosurgery. Basel, Karger, 2004, vol 5, pp 161–170.
16 Hayashi M: Current strategy of gamma knife surgery for intractable pain (Jpn). No To Shinkei. 2004;56:458–473.
17 Hayashi M, Taira T, Ochiai T, Chernov M, Takasu Y, Izawa M, Kouyama N, Tomida M, Tokumaru O, Katayama Y, Kawakami Y, Hori T, Takakura K: Gamma knife surgery of the pituitary: new treatment for thalamic pain syndrome. J Neurosurg 2005;102(suppl):38–41.

18 Liscak R, Vladyka V: Radiosurgical hypophysectomy in painful bone metastasis from breast cancer, Cas Lék. Ces 1998;137:154–157.
19 Levin AB, Ramirez LF, Katz J: The use of stereotaxic chemical hypophysectomy in the treatment of thalamic pain syndrome. J Neurosurg 1983;59:1002–1006.

Motohiro Hayashi
Department of Neurosurgery, Neurological Institute
Tokyo Women's Medical University
8–1 Kawada-cho, Shinjuku-ku
Tokyo 162–8666 (Japan)
Tel. +81 3 3353 8111, Fax +81 3 5269 7438
E-Mail GKRmoto@aol.com

Author Index

Subject Index